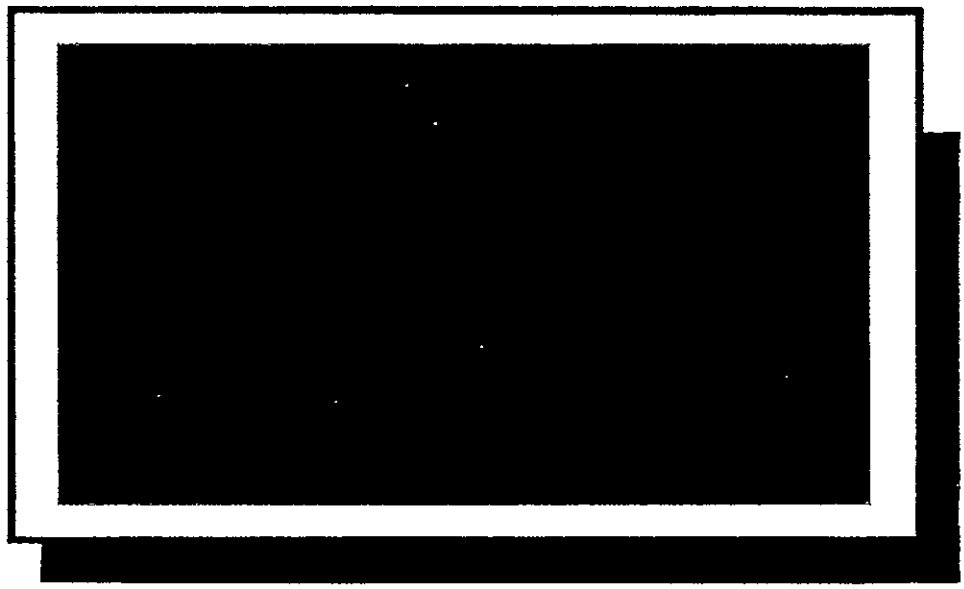

CENTER FOR SPACE RESEARCH

MASSACHUSETTS INSTITUTE OF TECHNOLOGY

Explorer 33 and Explorer 35 Plasma Observations of the Interaction Region Between the Solar Wind and the Magnetic Field of the Earth*

by

Herbert Charles Howe, Jr.

NGR-22-009-372

CSR-TR-71-1

* Submitted to the Physics Department on May 7, 1971 in partial fulfillment of the requirements for the degree of Doctor of Philosophy.

ABSTRACT

Title. Explorer 33 and Explorer 35 Plasma Observations of the Interaction Region Between the Solar Wind and the Magnetic Field of the Earth

Author Herbert Charles Howe, Jr.

Submitted to the Department of Physics on May 7, 1971 in partial fulfillment of the requirements for the degree of Doctor of Philosophy.

The magnetopause, magnetosheath, and bow shock are studied using data from the M I.T plasma experiments on the earth-orbiting Explorer 33 and the lunar-orbiting Explorer 35 The bow shock shape is determined between the sub-solar point and X_{SE}= -115 R_E The shock crossings at X_{SE}= -115 R_E indicate the bow shock is still well defined, though weak, at this distance. The magnetopause shape is determined between the sub-solar point and X_{SE}= -80 R_E Discrepancies are noted between the observed shape and shapes previously calculated using hydrodynamic theory The magnetotail boundary between X_{SE}= -40 R_E and X_{SE}= -80 R_E is rotationally symmetric about an axis aligned with the average solar wind flow direction.

Dual satellite observations of bow shock and magnetopause motion show that, in the examples studied, the motion is often directly related to measured changes in solar wind direction and/or dynamic pressure One example, however, shows frequent motion of the magnetotail boundary in the presence of a steady, non-fluctuating solar wind A statistical study of this transverse random motion at lunar distance indicates the motion consists of two superimposed components with characteristic time scales of $\sim$15 minutes and $\sim$1 hour. A model of the boundary motion indicates the second motion has an amplitude 2-3 times as large as the first motion. Also, the total boundary motion amplitude on the dawn side is $\sim$2 times larger than on the dusk side A boundary layer is observed adjacent to the magnetotail boundary at lunar distance. The results of the model fitting indicate this layer has a thickness of $\sim$ 2 R_E.

The magnetosheath flow between X_{SE}= -20 R_E and X_{SE}= -60 R_E is mapped using dual satellite observations to separate temporal and spacial variations. The overall flow pattern is found to agree well with the predictions of hydrodynamic theory The explicit dependence of the measured ratio of magnetosheath to solar wind densities on the measured upstream Mach number is shown This density ratio is consistently observed to be less than unity adjacent to the magnetotail boundary and this is shown to reflect the irreversible nature of the flow across the bow shock

Thesis Supervisor: Joseph H Binsack

Title Associate Head, Laboratory for Space Experiments

ACKNOWLEDGMENT

I would like to thank Dr J Binsack for his supervision of this thesis and for his effort in preparing the Explorer data for study Throughout the study and especially during the investigation of magnetosheath flow, Dr V M. Vasyliunas made many important suggestions, for which I am indebted to him Dr. G Siscoe and I worked together during the Explorer 35 boundary motion study and I would like to express my appreciation for his assistance and guidance. Finally, thanks are due Dr. H Bridge for his critical and helpful reading of the text and to Dr. S. Olbert and Dr. A. Lazarus and my fellow graduate students and other co-workers for many helpful discussions

I would like to express my appreciation to the National Science Foundation for its support of me as a National Science Foundation Fellow during the first four years of my graduate studies.

Finally, I would like to thank my wife for her encouragement and patience throughout the duration of this study.

TABLE OF CONTENTS

CHAPTER 1

HISTORICAL INTRODUCTION

A. Pre-satellite Observations

The current concept of the interaction between the interplanetary medium and the geomagnetic field was first introduced by Chapman and Ferraro (1930). The entire Chapman-Ferraro model is discussed in detail by Chapman (1964). Chapman and Ferraro proposed that magnetic storms were caused by streams of ionized gas emitted from solar flares Since such a gas would be highly conducting, they argued that the flow would compress the geomagnetic field into a cavity, from which the flow itself would be excluded. The sudden commencement of a magnetic storm, they suggested, was caused by the field compression and the main phase was caused by the subsequent development of ring currents within the cavity. This basic concept has been enlarged and refined, but the Chapman-Ferraro model has become basic to our understanding of the solar wind-geomagnetic field interaction.

From observations of the acceleration of irregularities in comet tails, Biermann (1951, 1961) argued that the streaming plasma proposed by Chapman and Ferraro was continuously present and did not occur only in individual streamers Theoretical justification for a continuous solar wind was presented by Parker (1958b,1963). This suggested that the geomagnetic cavity might be present at all times and not only during magnetic storms

The intensity of the solar wind and the resultant size of the geomagnetic cavity were uncertain, prior to actual solar wind observations. From energy considerations, Chapman and Ferraro (1930) estimated that if the velocity of the gas was $\sim$1000 km/sec, then the density was $\sim$60 H^+/cm^3. Biermann (1961), using the observed acceleration of comet tails and assuming charge exchange as the primary acceleration mechanism, determined a

solar wind flux of 10^{11} cm^{-2} sec^{-1}, which yields a density of 10^{3} cm^{-3} for a flow velocity of 1000 km/sec The theory of Parker predicted densities of $\sim$100 cm^{-3} at the distance of the earth These early estimates of the density of the solar wind were, in the light of subsequent observations, too high by one or two orders of magnitude. Consequently, the size of the geomagnetic cavity calculated on the basis of a pressure balance between the geomagnetic field and the incident plasma was smaller than the cavity size which was later observed. Beard (1960) estimated the distance to the boundary of the magnetospheric cavity in the solar direction to be $\sim$7.5 R_E, while Parker (1958a)argued that the cavity might approach as close as $\sim$2 R_E during intense magnetic sub-storms. Thus, prior to spacecraft observations, the existence of the solar wind and of the geomagnetic boundary were suspected, but the quantitative nature of these phenomena were known only very approximately

B. Early Satellite Observations Through IMP-1

The first observation of the termination of the geomagnetic field in the sunward direction came with the single passage of Pioneer 1 along the earth-sun line in 1958 As the spacecraft proceeded out, the onboard search-coil magnetometer first detected the characteristic dipole field After a data gap between 7 R_E and 12 3 R_E, the field became irregular and, at 13.8 R_E, dropped in strength and variability. This drop was interpreted as the termination of the geomagnetic field (Sonett et al , 1960), although hindsight indicates it was probably the bow shock. These observations confirmed the presence of a geomagnetic field termination in the solar direction, while demonstrating the complexity of the boundary region.

The next observation of the geomagnetic boundary was made near the dusk meridian with the search coil magnetometer on Pioneer 5 (Coleman et al.,

1960, Smith et al , 1960, Coleman, 1964). A disturbed region, indicative of the boundary observed by Pioneer 1, was observed between 7 R_E and 13 R_E The interplanetary region was observed when the spacecraft was further from the earth, although the field measured was incorrectly interpreted at first (Coleman, 1964). These results tended to confirm the Pioneer 1 observations

The next observations of the field boundary were made by Explorer 10, which was launched on March 25, 1961. In addition to a magnetic field experiment (Heppner et al., 1962, 1963), this spacecraft carried a plasma experiment (Bridge et al , 1962, Bonetti et al., 1963). The trajectory of the spacecraft lay in the anti-solar direction on the dusk side of the earth-sun line and below the ecliptic Data were gathered only for the outbound segment of the first orbit Between the earth and 20 R_E in the anti-solar direction, the magnetic field experiment saw the dipole field gradually distorted into a field roughly parallel to the earth-sun line. During this time, no measurable positive ion fluxes were detected. Between 20 R_E and 40 R_E in the anti-solar direction, the measurements from both experiments indicated that the spacecraft made many transitions between two distinct regions The signals from the first region were similar to those closer to the earth, with radial magnetic fields and no detectable plasma In the second region, however, the plasma detector measured a plasma streaming from the general direction of the sun with a mean energy of several hundred electron volts. At the same time, the magnetic field became much more variable in magnitude and direction It was concluded that the spacecraft passed many times between the anti-solar extension of the geomagnetic cavity and the exterior streaming plasma region

The Explorer 10 results marked the first conclusive detection of the streaming solar plasma Further, the results confirmed the predictions of

Chapman-Ferraro and others that the streaming interplanetary plasma is excluded from the geomagnetic cavity. The observations of the boundary at 40 R_E, as well as the observed radial magnetic field, tended to support the suggestion first made by Johnson (1960) that the downstream geomagnetic field might open into an elongated tail. Kellogg (1962) proposed that the alternate appearance and disappearance of flux was due to motion of the tail boundary. The nature of the tail boundary was also discussed by Axford (1962).

The Explorer 10 measurements indicated that the streaming plasma was supersonic This confirmed one prediction of the Parker model and led Kellogg (1962) to propose the existence of a standing shock ahead of the geomagnetic field boundary. From a calculation of the shape of this shock, Kellogg argued that the Explorer 10 observations were probably made behind the shock and thus did not represent the interplanetary solar wind. The observed rapid variations of the magnetic field in the plasma streaming region were also attributed by Kellogg to turbulence generated as the plasma traversed the shock. In a further discussion, Axford (1962) argued that Pioneer 1 and Pioneer 5 had actually observed the shock, as well as the magnetopause.

The launch of Explorer 12 on August 15, 1961 provided the opportunity for the first repeated magnetic field observations of the magnetopause in the solar direction (Cahill and Amazeen, 1963). The fields just inside the magnetopause were found to be approximately twice the undistorted dipole field, confirming a prediction of the Chapman-Ferraro model The forward magnetopause was observed between 8 and 11 R_E and Kellogg (1962) found this distance to be consistent with a solar wind density of 5 cm^{-3} and a velocity of 300 km/sec This density is lower than the densities predicted by the

Parker model. From estimates of the standoff distance of the proposed bow shock, Kellogg suggested that Explorer 12 might penetrate the shock on occasion. The subsequent detection of the shock by the Explorer 12 electron experiment (Freeman, 1964) marked the first observation of the bow shock

The repeated observation of the forward magnetopause by Explorer 12 indicated that the geomagnetic field termination, and hence the solar wind, were permanent features of the interplanetary medium. This was first confirmed by direct measurement by Mariner 2 (Snyder and Neugebauer, 1962, Neugebauer and Snyder, 1966) These measurements showed that the supersonic solar wind is a permanent, though variable, feature of the interplanetary medium, as predicted by the Parker theory.

The first repeated plasma and magnetic field observations of the forward boundary region on the dawn side of the sun-earth line were made by experiments onboard IMP-1, which was launched on November 27, 1963 The apogee of this spacecraft was $\sim$30 R_E and lay initially in the solar direction, thus during the first months of observation, the satellite orbit covered the entire magnetosheath on the dawn side between the sub-solar point and $\sim$20 R_E downstream from the earth From the magnetic field experiment and both plasma experiments, the existence of the bow shock was established (_____, I G. Bull., 1964) The shape of the magnetopause from the sub-solar point to 20 R_E downstream and the shape of the bow shock from the sub-solar point to 10 R_E downstream were mapped by the magnetic field and plasma experiments (_____, I G Bull , 1964; Ness et al., 1964, 1966, Wolfe et al., 1966, Lyon, 1966, Olbert, 1968) The theoretical shapes of these boundaries, calculated using hydrodynamic theory (Spreiter and Jones, 1963), were found to agree well with the observations, although Ness et al.

(1964) noted that the observed magnetopause flared our more than the theoretical magnetopause at the dawn meridian.

The excess magnetopause flaring was interpreted by Ness et al (1964) as indicating that the boundary did not close in the downstream direction but extended into a long tail, as observed by Explorer 10. The nature of the tail was discussed by Axford et al (1965) and by Dessler and Juday (1965) and the actual tail, with the associated stretched field lines and embedded neutral sheet, was observed in the IMP-1 magnetic field data (Ness, 1965).

The conditions of flow in the magnetosheath were also examined by the experiments on IMP-1. The magnetosheath magnetic field was found to be much more variable than the interplanetary field and this change in variability upon crossing the shock was often the most notable feature of the measured magnetic fields (Ness et al., 1964) The plasma flow in the magnetosheath appeared to be slower and hotter than the interplanetary flow (Wolfe et al , 1966, Olbert, 1968). In addition, the measured flow angles were found to be consistent with the deflection of the solar wind around the magnetopause (Olbert, 1968) The magnetosheath flow was also compressed, as evidenced by the higher measured magnetosheath densities (Olbert, 1968). These plasma observations were in qualitative agreement with the flow of the shocked magnetosheath gas around the magnetopause, as derived by Spreiter et al (1966).

In summary, the IMP-1 observations resulted in the following basic understanding of the interaction between the solar wind and the earth's magnetic field. The compression of the field into a cavity by the highly conducting solar wind, as proposed by the basic Chapman-Ferraro model, was well documented Further, the existence of the bow shock, which had been sus-

pected for the high Mach number solar wind flow, was proven. The shapes of the forward magnetopause and bow shock were found to agree with theoretical shape calculations based on hydrodynamics This agreement confirmed the fluid approach to the flow interaction problem The question of why the collisionless solar wind behaves as a fluid, though still unanswered, is discussed by Levy et al (1964) and Axford (1965). Also from IMP-1 observations, the qualitative nature of the flow in the magnetosheath was understood and was found to agree qualitatively with what was expected for flow behind a shock. Finally, the existence of the geomagnetic tail was confirmed, although the length of the tail and role of the tail in observed geomagnetic phenomena were still not known

Theoretical and experimental work subsequent to IMP-1 tended to concentrate on the refinement of various aspects of the basic solar wind-geomagnetic field interaction. Therefore, rather than proceeding with a chronological description of results, we will now review the results of previous work done on each topic which is discussed in the present thesis In the review of each topic, we will explain what new understanding of the topic we hope to gain and how this understanding will fit in with and extend previous results.

C. Satellite Observations Since IMP-1

1. Boundary Shapes

After the initial mapping of the forward boundaries by IMP-1, the next major observations of the boundaries were made by the twin satellites Vela 2A and Vela 2B (Gosling et al., 1967) These satellites, launched into circular orbits at 17 R_E, made repeated observations of both boundaries at 17 R_E and extended previous observations to higher ecliptic latitudes Both boundaries were found to be tilted 2° -4° with respect to the

sun-earth line This tilt was in the ecliptic plane and was clockwise when viewed from the north. Since the solar wind direction is aberrated 3° -4° (with respect to the solar direction) by the orbital motion of the earth, then this result showed that the boundaries tend to be aligned with respect to the incident wind Vela observations at high latitudes also showed that the boundaries were axisymmetric about the incident solar wind direction, although the possibility of a slight flattening of the magnetopause at the poles was noted. Comparing the Vela results with the predictions of Spreiter and Jones (1963), Gosling et al. (1967) found that the magnetopause at $\sim$10 R_E downstream from the earth tended to flare out more than predicted.

The mapping of the forward boundaries was repeated by experiments on OGO 1 (Heppner et al., 1967, Holzer et al , 1966; Wolfe, et al., 1966) and IMP-2 (Binsack, 1966) and the shapes determined were found to agree well with the IMP-1 boundaries and with the predicted shapes of Spreiter and Jones (1963)

Observations of the magnetopause and bow shock were extended to 80 R_E and 50 R_E downstream of the earth, respectively, by the magnetic field experiment on Explorer 33 (Behannon, 1968) The magnetopause was found to be well defined at these distances, although the boundary appeared to be constantly in motion. An elongation of the magnetotail boundary in the north-south direction was also noted Spreiter and Alksne (1969a) extended the previous theoretical boundary shapes of Spreiter et al (1966) to include the magnetotail and found general agreement between the observed and predicted shapes of the downstream magnetopause

The distant magnetotail was observed at 1000 R_E downstream of the earth by Pioneer 7 (Ness et al , 1967, Wolfe et al , 1967; Fairfield, 1968) and at 500 R_E by Pioneer 8 (Intriligator et al , 1969, Siscoe et al , 1970,

Mariani and Ness, 1969). At these distances, the magnetotail region was characterized by depressed plasma flux and magnetic field and the boundary was no longer a well defined structure Thus, while these distant downstream regions are still perturbed by the presence of the earth, the plasma is probably no longer excluded from the magnetotail and what was observed was most likely the remnants of the near-earth geomagnetic tail

A recent mapping of the forward boundaries has been reported (Egidi et al., 1970) from the plasma experiment on HEOS-1 Comparison of these shapes with the shapes obtained by IMP-1 showed that the average boundary positions lie further from the earth during solai maximum than during solar minimum. This difference may indicate a difference in the average solar wind flux between solar maximum and solar minimum

In the current study, we map the bow shock and magnetopause using three years of Explorer 33 plasma data The total number of boundary observations used represents a significant increase over previous work and the boundary shapes determined are therefore more statistically meaningful. The cylindrical symmetry of the tail boundary is discussed Discrepancies between the observed magnetopause boundary shape and the model of Spreiter and Alksne (1969a) are examined and the limitations of the model which lead to the discrepancies are discussed.

2. Boundary Motion

In this thesis, we study the motion of the magnetopause at lunar distance in detail Thus, we review here primarily previous observations and theories of magnetopause motion.

Motion of the magnetopause has been evident since the first observations of the boundary. Explorers 10, 12, and 18 all observed boundary motion, as discussed in the references for these spacecraft above Observa-

tions of the motion have been of three primary types 1) compression of the magnetopause associated with magnetic storms, 2) periodic or wave motion of the boundary which is uncorrelated with solar wind pressure and direction changes and which is usually attributed to intrinsic boundary instability, and 3) steady inward magnetopause motion prior to substorms which is probably related to magnetic field line reconnection at the boundary.

Observations of boundary compression coincident with observed solar wind flux increases and/or magnetic storm sudden commencements have been reported by several authors. The effect on the boundaries of shocks propagating in the solar wind was observed by the plasma and magnetic field experiments on Explorer 14. The event observed by the plasma experiment (Wolfe and Silva, 1965) was a compression of both the magnetopause and the bow shock across the spacecraft. The solar wind flux increase which caused the compression was observed several hours earlier by Mariner 2. A magnetic storm sudden commencement was also observed coincident with the compression A similar event was observed by the magnetic field experiment on Explorer 14 (Cahill, 1964), when a flux increase observed by Mariner 2 caused both a magnetopause compression past the spacecraft and a sudden commencement on the ground. These two events gave early support to the Chapman-Ferraro model of the sudden commencement of geomagnetic storms

Gosling et al. (1967) reported both magnetopause and bow shock compressions observed by Vela 2A at the beginning of a magnetic storm. Large flux increases were seen by the Vela 2A plasma experiment just prior to the compression A compression of the magnetopause to the position of ATS 1 at 6.6 R_E has been studied by several different experiments (Cummings and Coleman, 1968, Freeman et al , 1968) Observations from Vela 3A (Bame et al , 1968) showed a large increase in the solar wind pressure coincident

with the compression Both Vela 3A and 3B (Bame et al , 1968) also observed boundary crossings due to this compression In the case of Vela 3B, the magnetopause was also crossed during the main phase of the ensuing geomagnetic storm at an unusually large distance from the earth, suggesting that the boundary was inflated by the increased ring current This event was also observed by the magnetometer on OGO 3 (Russell et al., 1968), data from which showed compression of both boundaries over the spacecraft. A similar compression event has been recently observed at 6.6 R_E by ATS 5 (Skillman and Sugiura, 1971)

A direct relation between boundary motion and solar wind flux changes was shown most conclusively by Binsack and Vasyliunas (1968), using simultaneous data from IMP-2 and OGO-1. Using one spacecraft as a solar wind monitor and the other as a boundary observer, they showed how the observed motion of the bow shock across the boundary-observing spacecraft including and subsequent to a large bow shock compression could be explained directly by solar wind dynamic pressure increases observed by the other spacecraft

Siscoe et al (1968) studied the relation between solar wind pressure increases observed by Pioneer 6 and the corresponding sudden impulses recorded on the ground Their results supported the view that sudden impulses are caused by the compression of the magnetopause due to increases in solar wind dynamic pressure. However, the observed magnitudes of the sudden impulses were only half as large as expected on the basis of simple cavity compression This difference was attributed to the diamagnetic properties of the magnetospheric particle population The observations of Siscoe et al. (1968) were confirmed from a study of Explorer 34 data by Burlaga et al (1968).

An example of magnetopause inward motion preceeding a substorm has recently been reported from the magnetic field experiment on OGO 5 (Aubry et al , 1970). This inward motion was not accompanied by a corresponding geomagnetic field compression and seemed to be related to a change in the interplanetary field direction in the presence of a constant solar wind plasma flux. The inward motion was attributed to increased friction at the boundary, due perhaps to field line merging, which erroded magnetic flux from the forward magnetosphere into the geomagnetic tail. This view is supported by the work of Meng (1970), who found a negative correlation between the size of the geomagnetic cavity, as measured by IMP-2, and the substorm activity index AE. This type of boundary motion was not envisioned by the Chapman-Ferraro model and may be a major contributor to geomagnetic substorms.

The intrinsic stability of the boundary has been studied by several authors. Talwar (1964), Sen (1965), Fejer (1964) and, most recently and comprehensively, Southwood (1968) have examined the stability of the boundary to the Kelvin-Helmholtz instability. Using a hydromagnetic approach, these authors have determined that the boundary may be unstable, especially in the downstream region However, Lerche (1966) has pointed out that these theories all predict the largest growth rates for instability at the shortest wavelengths, where the hydromagnetic approach becomes invalid due to the finite gyroradius of the plasma particles. The stability of the boundary in the presence of the ensuing charge separation has been discussed by Parker (1967a, b), Lerche (1967), Davies (1968, 1969), and Karlson '1970). These authors disagree on the stability of the boundary; thus the question is still open. In any event, none of these authors are able to predict the final nature of any instability; thus it is unclear whether observable waves or a thin turbulent layer will result

Characteristic frequencies of the entire magnetotail have been calculated by McClay and Radoski (1967), Siscoe (1969), and McKenzie (1970) The latter two authors find that characteristic periods in the tail, which should also be reflected in tail boundary motion, are on the order of 10-20 minutes. Possible driving mechanisms for these resonant oscillations are solar wind changes and intrinsic boundary instabilities

The most definitive observations of forward magnetopause wave or random motion have been made by Anderson et al. (1968) with experiments on the IMP-2 satellite They found that the motion of the boundary consisted of one component with a characteristic time of $\sim$10 minutes and a second component with a characteristic time on the order of one hour. The first motion was attributed to intrinsic boundary instability, while the second was attributed to changes in the solar wind On a much shorter time scale, observations of boundary motion made during the single outbound pass of Mariner 5 (Smith and Davis, 1970) showed a characteristic time of $\sim$2 minutes. Other observations of oscillitory motion of the forward boundary have been made on OGO 1 (Heppner et al., 1967), and Explorer 12 (Kaufmann and Konradi, 1969; Freeman et al , 1967).

Observations of oscillatory motion of the geomagnetic tail boundary have been made by the magnetic field experiment on Explorer 35 (Mihalov et al , 1970). These observations show that the tail boundary is almost always in motion. From an analysis of the motion of boundary normals, the authors conclude that the motion is primarily a fluting of the tail boundary induced by the Kelvin-Helmholtz instability.

In the current study, we will use Explorer 35 plasma observations of magnetopause motion at lunar distance to gain a quantitative understanding of the nature of the boundary motion The characteristic times and

amplitudes of the motion will be investigated by modeling the motion Using simultaneous observations from Explorer 33 and Explorer 35, the relation between the motion and external solar wind conditions will also be investigated.

3. Magnetopause Structure

Axford (1964) calculated the thickness of the boundary inferred from the magnetospheric convection model of Axford and Hines (1961). This calculation was enlarged upon by Dryer and Heckman (1967). The structure of a charge-separation layer at the boundary was discussed by Lerche (1967). Eviatar and Wolf (1968) argued that the tangential drag on the boundary was caused by the diffusion of particles across the boundary by magnetic irregularities Recently, Coleman (1970) proposed unipolar induction as a possible agent responsible for the drag. Faye-Peterson and Heckman (1968) and Cassen and Szabo (1970) have calculated contours of magnetic field and plasma flux for a viscous boundary layer Specific results of the above theoretical work will be discussed in more detail in conjunction with the results of the present study of boundary structure

Many observations have been made of the plasma and magnetic field structure of the boundary. Using Explorer 12 data, Sonnerup and Cahill (1967, 1968) showed that the boundary is a tangential discontinuity during quiet times and tends to become a rotational discontinuity during disturbed times. Heppner et al (1967), using OGO I data, found that the magnetic field usually changed smoothly across the boundary over a time of one minute Several examples were noted, however, where the magnetosheath field on the dawn flank was actually larger than the magnetospheric field. Heppner et al (1967) argued that this structure causes the dawn boundary to be highly unstable

The structure of the compressed forward magnetopause was examined by Freeman et al (1968) using data from ATS-1 These authors found evidence for the return tailward flow just inside the magnetopause, as envisioned by the Axford-Hines model The same event gave no evidence for magnetic merging in the forward boundary region, in spite of the strong compression (Cummings and Coleman, 1968) Aubry et al (1971) also observed the structure of the compressed boundary with the magnetic field experiment on OGO 5 Although these authors were able to rule out the possibility that the boundary was a rotational discontinuity, they were unable to determine the boundary structure conclusively due to the complexity of the measured fields

Mihalov et al (1970) have studied the magnetopause structure at lunar distance using magnetic field data from Explorer 35 On several occasions, they found the magnetic field direction changed much more rapidly than the field magnitude as the boundary moved past the spacecraft. On the basis of several crossings, a boundary thickness of 10^3 km was estimated

In summary, a poor theoretical understanding of the boundary structure exists, due primarily to the shortcomings of the hydrodynamic equations in treating problems where large plasma and magnetic field gradients are present Results of magnetic field observations indicate that the boundary is a tangential discontinuity, but other possibilities are not excluded Preliminary boundary thicknesses have also been derived on the basis of magnetic field data. Plasma observations of the boundary are limited primarily to the ATS observations and indicate the presence of a return flow of plasma just inside the boundary.

The present study will examine the first evidence for a magnetosheath boundary layer adjacent to the magnetopause The average thickness of the layer will be derived from a statistical model of the data The derived

thickness will then be compared with the theoretical predictions of the various authors mentioned above.

4. Magnetosheath Flow

The flow of plasma within the magnetosheath has been studied most extensively adjacent to the bow shock, where the observed plasma jumps and the jumps calculated on the basis of the Rankine-Hugoniot relations have been compared. Such comparisons have been made from plasma data taken on IMP-1 (Olbert, 1968), Vela 2 (Gosling et al., 1967), Vela 3 (Argo et al., 1967), Pioneer 6 (Howe, 1970, Spreiter and Alksne, 1968), Vela 4 (Montgomery et al , 1970, Dryer, 1971), Explorer 34 (Burlaga and Ogilvie, 1968), and from combined plasma and magnetic field measurements taken on Pioneer 6 (Mihalov et al., 1969) Greenstadt et al (1968) and Neugebauer (1970) have also studied the detailed structure of the shock, using high resolution plasma and magnetic field data These authors have found general agreement between the observed and theoretical plasma jumps at the shock, while the actual shock structure has been found to be quite complex.

Calculations of the magnetosheath flow patterns have been made by Spreiter et al (1966) and by Dryer and Heckman (1967) and Dryer (1971). Few observations of the flow pattern have been made, due to the difficulty most plasma instruments have observing the heated, fluctuating magnetosheath plasma While the observations of flow directly behind the shock (see the references cited above) are in general agreement with the calculation of Spreiter et al (1966), the only detailed measurement of the flow pattern (i.e., velocity, density direction, and temperature) within the magnetosheath away from the boundaries was made by the plasma instruments on Pioneer 6 Although this spacecraft crossed the magnetosheath only once, the crossing occurred during a period of unusually steady solar wind conditions,

allowing a measurement of the spacial variations of the magnetosheath flow Comparison between the measurements and the calculations of Spreiter et al (1966) confirmed the validity of the hydrodynamic calculations of the magnetosheath flow (Wolfe et al , 1968, Spreiter and Alksne, 1968, Howe, 1970)

Simultaneous flow direction measurements in the dawn and dusk flanks of the magnetosheath were made by the twin Vela 3 satellites (Hundhausen et al , 1969) A dawn-dusk flow asymmetry was noted which seemed to support the predictions of Walters (1964), who suggested that the differing orientation of the interplanetary magnetic field at various positions along the bow shock should result in a larger deviation of the flow at the dusk shock than at the dawn shock

Magnetic field measurements made in the magnetosheath are in agreement with the predicted convection of the field around the magnetopause by the solar wind Using simultaneous magnetic field data from IMP-1 and IMP-2, Fairfield (1967) showed that the average magnetic field orientation in the magnetosheath was in accord with the convected field pattern as calculated by Spreiter et al (1966) Further evidence for the convection of the field by the magnetosheath flow was provided by Fairfield (1968) using data from Pioneer 7, Explorer 28, and Explorer 33 By calculating the velocity of observed magnetic irregularities between the forward and distant downstream flow regions, Fairfield concluded that the field is carried downstream at approximately the observed flow velocity

In the present study, we use 369 hours of simultaneous Explorer 33 and Explorer 35 plasma data to map the magnetosheath flow between 20 R_E and 60 R_E downstream of the earth These measurements are also compared with a flow calculation similar to the calculation of Spreiter et al (1966) From the comparison, we gain a greater understanding of the downstream magneto-

sheath flow and of the relation between the flow and the upstream solar wind Mach number

CHAPTER 2

EXPERIMENT, DATA, AND BOUNDARY CROSSINGS

The data used in the studies undertaken for this thesis were gathered by modulated Faraday cup plasma detectors flown on Explorer 33 and Explorer 35 In this chapter, we will first discuss the instruments and the nature of the raw and reduced data We will then discuss the orbits and the times of operation of the two spacecraft in order to define the total spacial and temporal extent of the observations Finally, by looking at samples of data, we will examine the nature of magnetopause and bow shock crossings

A Experimental Description

1 Instrument

The basic method of operation of a modulated Faraday cup plasma detector has been presented by Bridge et al (1960) and Bonetti et al. (1963) A review of some spurious effects of this type of instrument, along with a comparison of the Faraday cup with other types of plasma detectors, has recently been presented by Vasyliunas (1971) The specific instruments flown on Explorer 33 and Explorer 35 are discussed by Lyon et al (1968) Therefore, we will only briefly discuss these instruments here

The Explorer 33 and Explorer 35 instruments measured fluxes of positive ions and electrons in the energy range between 100 ev and 4 kev The instrument normal was perpendicular to the spacecraft spin axis and thus scanned the spacecraft equatorial plane each spin period The angular acceptance of the cup was 40 degrees wide in the equatorial plane and 120 degrees wide in the spin axis-cup normal plane

One measurement of the plasma was initiated by a complete equatorial scan with the instrument set to accept all particles with energies normal

to the cup between 100 ev and 4 kev During this integral scan, the direction, with respect to the sun direction, and magnitude of the peak flux were noted On the eight subsequent revolutions of the spacecraft, the flux in each of eight narrow, contiguous energy ranges was measured at the peak direction This provided a differential energy spectrum of the plasma in the peak direction The sequence required 25 seconds to complete and was initiated every 82 seconds A complete sample of the plasma consisted of four such sequences During the first and third, the sum of the positive ion current from the two collection plates in the instrument was measured, while during the second, the difference of the positive ion current was measured and on the fourth, the sum of the electron current was measured The complete sample required 328 seconds to complete

2 Plasma Parameters

Plasma parameters (bulk velocity, density, thermal speed, and flow direction) were derived from each pair of sum and difference positive ion measurements Thus, one set of parameters was derived each 164 seconds Temporal variations in the plasma on a time scale less than 164 seconds, such as a boundary traversal of the type studied for this thesis, could have led to incorrect parameters; thus parameters derived from data taken in the boundary region were considered to be unreliable and the actual measured currents were used to determine the times of boundary traversals The time of a crossing was uncertain by the time between summed integral flux measurements, which was 164 seconds or approximately 2 5 minutes

3. Spin Axis Orientation

The relation between spacecraft and solar ecliptic coordinates was important in determining boundary crossings from the measured currents. The relation is illustrated in figure 1 The orientation of the spin axis

in solar ecliptic coordinates is given by the longitude and latitude of the spin axis, and this direction defines the spacecraft equatorial plane As the spacecraft spins, the instrument normal sweeps around in the equatorial plane When the cup points nearest the incident plasma flow direction, the collection plate below (above) the spacecraft equatorial plane receives more (less) than half the total flux if the incident plasma comes from above (below) the equatorial plane The plates above and below the plane are called plate A and plate B, respectively, and by noting whether the current on plate A is less than or greater than the current on plate B, the incident direction of the plasma with respect to the equatorial plane may be determined directly from the measured currents As we will see, this point is important in determining boundary crossings from the unreduced data

4 Coverage in Space and Time

Explorer 33 was launched on July 1, 1966 in an attempt to gain lunar orbit Due to the overperformance of the launch vehicle, this attempt failed and the spacecraft was placed instead into a large earth orbit with apogee and perigee of approximately 80 R_E and 10 R_E, respectively The spin axis of the spacecraft was in the solar ecliptic plane (latitude less than 5 degrees in magnitude) and made one complete revolution per year with respect to the earth-sun line Since the instrument normal was perpendicular to the spin axis, the cup could not see the solar wind during periods of the year when the spin axis- earth-sun line angle was less than 30 degrees Thus, useful data were gathered during two four month periods of each year The times during which observations were made are given in table 1

TABLE 1

EXPLORER 33 PERIODS OF OBSERVATION

From	To
July 2, 1966	October 6, 1966
December 10, 1966	March 14, 1967
June 25, 1967	October 2, 1967
December 13, 1967	April 14, 1968
July 1, 1968	October 17, 1968
January 11, 1969	April 22, 1969

On January 19-20, 1969, Explorer 33 made a close encounter with the moon which shifted the spacecraft into a larger orbit with apogee and perigee of 120 R_E and 20 R_E. Several of the large orbits were made before the end of the observation period used for this thesis, April 22, 1969 In figures 15a and 15b, all orbits during which useful observations were made are shown in solar wind coordinates (see page 36), where the abscissa is the X_{SW} axis and the ordinate is the perpendicular distance from the axis As may be seen in figure 15, the orbit of this spacecraft was especially suited for study of the bow shock and magnetopause behind the dawn-dusk meridian

Explorer 35 was launched on July 19, 1967, and achieved lunar orbit on July 22, 1967 Data were taken continuously until July 14, 1968, when the instrument failed During this period, the spacecraft made 11 complete traversals of the tailward magnetosphere and magnetosheath, including numerous magnetopause and bow shock crossings at a radial distance of approximately 60 R_E from the earth The spin axis of the spacecraft was perpendicular to the solar ecliptic plane (latitude approximately -90 degrees), thus data were taken continuously except during periods of lunar shadow, when the spacecraft was shadowed from the sun by the moon, and during periods of radio shadow, when the spacecraft was shadowed from the earth by the moon, thereby precluding transmission of data The period of the spacecraft about the moon was approximately 11 5 hours and the lunar and optical shadow each lasted about 1 hour, thus data were gathered for approximately 80% of each day.

5 Data Format

Referring to figure 3, we will now explain the format of the data used to determine boundary traversals The horizontal axis of the plots

represents universal time, in decimal day and hour Also plotted on the horizontal axis is the sequence number One sequence is 81 seconds and one measurement of the plasma occurred each sequence.

In figure 3a, the top trace represents the angle between the sun direction and the peak current direction, taken positive in the direction of satellite rotation The next trace tells, for the difference integral proton measurement, which plate receives the most current The third trace from the top is the integral current measurement, where the height of the top of each vertical line represents the peak current and the height of the bottom of the line represents the current measured at approximately 45 degrees to the peak current direction The bottom trace is the average electron current in the direction away from the sun

In figure 3b are plotted the differential current measurements corresponding to the integral current measurements in figure 3a. The lowest energy channel is at the bottom and the highest is at the top of the plot For each energy channel, the sum proton measurements are represented by the trace with a small S on it, while the difference proton measurements are represented by the trace with the small D The sum trace is usually above the difference trace. It must be emphasized that the measurements are made at discrete times and are shown as continuous traces only for each of illustration

Before turning to examples of boundary crossings, let us review what may be learned about the state of the plasma from the measured currents and angles Whether the bulk flow velocity normal to the collection plates is large or small may be inferred from the position of the largest current in the differential measurements. The spread of currents in the differential channels, as well as the integral current measured at 45 degrees to the

peak flux direction, reflect the thermal spread of the plasma.

The angle of flow of the plasma may be inferred from the measurements in one of two ways, depending on which spacecraft is under consideration In the case of Explorer 35, the spin axis was perpendicular to the solar ecliptic plane, thus the measured angle between the sun and peak flux direction is the angle of flow in the ecliptic plane The sign of the angle of flow out of the ecliptic plane is given by the relative current on the two half collector plates and the magnitude of the angle may be estimated by noting the difference between the sum and difference integral currents For flow in the ecliptic plane, both plates receive equal currents and the difference is much less than the sum, while for flow at a large angle to the plane, most of the current is collected on one plate and the sum and difference currents are almost equal

In the case of Explorer 33, the spin axis lay approximately in the ecliptic plane, thus the spacecraft equatorial plane was perpendicular to the ecliptic The angle between the sun and peak flux direction gives the angle of flow out of the ecliptic plane directly The angle of flow in the solar ecliptic plane is inferred from the angle of flow out of the satellite equatorial plane In practice, only changes in this angle, as shown by changes in the difference between the sum and difference integral currents, were considered and the way this was done is best illustrated by the examples discussed in the next two sections

B. Bow Shock Traversals

As the solar wind crosses the bow shock, there is a conversion of directed motion to random motion The streaming velocity decreases and changes direction and the thermal velocity increases. This may be verified theoretically from the conservation of mass, momentum, and energy (see

chapter 4) and has also been observed experimentally (Argo et al , 1967) We will now examine several examples of Explorer 33 and Explorer 35 data to see how these changes in the plasma manifest themselves in the data

1 July 28, 1966 Crossing

At the time of the bow shock traversal shown in figures 3a and 3b, Explorer 33 was located at X_{SE}=-5 R_E, Y_{SE}=-27 R_E, Z_{SE}=-7 R_E, proceeding in the positive X_{SE} direction toward perigee This is location S1 in figure 2 The spacecraft spin axis longitude was 103 degrees, thus the instrument normal made an angle of 13 degrees with the sun direction when the normal was in the ecliptic plane For nearly radial solar wind flow, more current should have been collected on plate A and, prior to the shock traversal at 1052 UT, we see in figure 3a that this was the case The small difference between the sum and difference integral currents was consistent with a flow as large as 13 degrees from the spacecraft normal The roll angle indicated that the spacecraft rolled approximately 5 degrees after seeing the sun before the peak flux was measured This 5 degree roll indicates that the solar wind flow had a slight northward component The differential channels show the largest flux occurred in channel 4, which is typical for a solar wind measurement, and that smaller currents were evident in the other channels

At the time of the shock traversal, the solar wind was deviated both in and out of the ecliptic plane The phase trace changed to indicate that more current was measured on plate B; thus the wind was deflected to flow at least 13 degrees from the radial direction The roll angle indicated that the flow was also deflected from northward to southward flow by at least 10 degrees The southward deflection is consistent with the location of the spacecraft 7 R_E below the ecliptic at the time of the crossings,

since the shock deflects the wind primarily in the solar wind direction - spacecraft plane The largest differential flux was measured in channel 3 after the shock crossing, indicating that the flow was slowed as well as deviated Thermal heating is evident both in the larger spread of currents in the differential energy channels and by the appearance of flux in the sum integral measurements at 45 degrees to the peak direction Some electron heating is also evident from the electron measurements

2. July 27, 1966 Crossings

The data shown in figures 4a and 4b represent a multiple bow shock traversal The data were taken on the day prior to the time of the previous example; thus the spin axis orientation given there applies here also The spacecraft was located at position S2 in figure 2 Prior to 1108, Explorer 33 was in the solar wind At 1108, the spacecraft crossed the shock into the magnetosheath and at 1120, crossed the shock again back into the solar wind The occurrence of the crossings is indicated in much the same way as was the single traversal in the previous example The difference integral current went almost to threshold, indicating that the flow was deflected almost directly into the cup The roll angle indicates that the flow experienced an additional southward deflection The differential measurements indicate thermal heating by an increase in the spread of measured currents and electron heating is also evident

3. February 1, 1967 Crossing

The Explorer 33 bow shock crossing shown in figures 5a and 5b is typical of the strong shock crossings observed forward of the dawn-dusk meridian At the time of the shock traversal, the spacecraft was located at X_{SE}= 10.8 R_E, Y_{SE}= 13 7 R_E, Z_{SE}= 1 17 R_E, proceeding inbound toward perigee This is position S3 in figure 2 The longitude of the spin axis was 275 8

degrees Prior to the shock crossing, more current was measured on plate B than on plate A, in agreement with the spin axis orientation, and the largest differential current was measured in channel 3 After the spacecraft crossed the shock, the difference between the sum and difference integral measurements decreased, indicating the deflection of the flow in the positive Y_{SE} direction The deflection caused the plasma to enter the cup at a large angle to the normal This, and the slowing of the flow across the shock, caused a decrease in the total measured current and a shift of the largest differential current into the lower two channels Heating of the protons is evident in the integral measurements at 45 degrees to the peak direction

The bow shock is strong in the subsolar region because the flow meets the shock at a small angle to the shock normal For this reason, shock crossings such as the one above are easily identified in the data We will now discuss two examples of crossings of the shock further downstream of the earth, where the shock begins to approach the Mach angle and is consequently much weaker

4 September 1, 1967 Crossing

At the time of the bow shock crossing at 1249 UT, day 243.0, 1967, shown in figures 6a and 6b, Explorer 33 was located at X_{SE}= -41 2 R_E, Y_{SE}= 52.5 R_E, Z_{SE}= -8 5 R_E and the longitude of the spin axis was 73 2 degrees The spacecraft location is position S4 in figure 2. The largest current was measured on plate B in the solar wind and the largest change in the data as the spacecraft crossed the bow shock was the flow deflection, which caused the largest current to change to plate A The differential spectrum changed only slightly away from the peak and no slowing or heating of the flow is clearly seen Electron heating is also absent This is all con-

sistent with the weakness of the shock downstream from the earth Shock crossings such as this, though not nearly as obvious as that in the previous example, are still clearly defined in the data

5. March 23, 1969 Crossings

The bow shock traversals shown in figure 7a to 7d occurred when Explorer 33 was located at X_{SE}= -116 1 R_E, Y_{SE}= -10 9 R_E, Z_{SE}= -64 4 R_E (position S5 in figure 2) The spin axis longitude was 242 4 degrees These crossings are among the most distant observations of the bow shock that have ever been made and, due to the weakness of the shock at this distance, the crossings are marked by subtle changes in the data To make the identification of the shock crossings more definite, the reduced plasma parameters have been included (figures 7c and 7d)

Prior to the shock crossings, the spacecraft was in the magnetosheath proceeding away from the earth-sun line toward apogee The observations occurred 82 degrees below the ecliptic plane, measured counterclockwise about the earth-sun line as seen from the sun Therefore, any deflection of the plasma by the bow shock should have been primarily in the north-south direction and would have appeared as a change in the roll angle of the peak flux direction Since the wind should have been deflected southward upon crossing the shock, then for the spin axis orientation given above, the roll angle should have been more positive in the magnetosheath than in the solar wind Referring to figure 7a, we see that the roll angle did change suddenly between an average positive value of 2 to 5 degrees and an average negative value of -5 to -7 degrees. At the beginning of the data in figure 7a, the angle was slightly positive and continued positive until the data gap at sequence 95420 When the data resumed at sequence 95436, the angle was negative This change is interpreted to mean

that the spacecraft crossed the bow shock during the data gap from the magnetosheath into the solar wind Four more traversals occurred at sequences 95446, 95478, 95491, and in the data gap between sequences 95523 and 95542 These crossings are marked by the symbol BS in figure 7d and the region (I for solar wind, II for magnetosheath) in which the spacecraft was located between crossings is also indicated After sequence 95615, the data became spotty and no more definitive crossings could be identified

The differential measurements shown in figure 7b are also consistent with the above identification of the shock crossings During the times when the spacecraft was in region I, the current in channel 2 was lower than during the times when the spacecraft was in region II Since this is the energy channel below the channel in which the largest current was measured, this means the energy spectrum narrowed in region I Thus, the plasma was heated upon crossing the shock, producing a slightly wider energy spectrum in region II. Plasma heating is a characteristic change across the shock and the heating observed here lends further support to the interpretation of these changes as being bow shock crossings

In figure 7d, the actual derived thermal speed of the plasma is given by the bottom plot In region II, the thermal speed was approximately 50 km/sec, while those thermal speeds which were measured in region I average around 20 to 30 km/sec The spectra which could not be analyzed by the program (denoted by the heavy black circles on the thermal speed plot in figure 7d) had thermal speeds too low for the analysis program to analyze These spectra were all taken in region I The thermal speed plot therefore confirms the interpretation of the energy spectra in figure 7b and lends further evidence to the existence of the shock crossings

The derived plasma densities are shown in the bottom plot of figure 7c During the region II portions of the plot, the density was approxi-

mately 10 cm^{-3}, while during the region I portion, it was slightly less, at about 8 cm^{-3} This change is also consistent with the bow shock identifications, since it indicates the plasma was compressed slightly upon crossing the shock

When we examine the average shape of the bow shock in the next chapter, we will see that the above shock crossings occurred closer to the earth-sun line than an average crossing would be observed. The derived plasma parameters are consistent with this discrepancy in two ways First, from the plot of the solar ecliptic latitude of the direction from which the flow was coming, it is seen that the solar wind plasma was flowing to the north approximately 5 degrees Assuming that the boundaries line up with the incident flow direction, this means that, below the ecliptic where the observations were made, the shock would be closer to the earth-sun line than normal. Second, the low solar wind thermal speed means the incident Mach number was large Thus, the Mach angle was smaller than usual, making the shock closer to the boundary symmetry axis than normal. Both of these effects are consistent with the observation of the shock closer to the earth-sun line than usual.

In summary, we see that the plasma was deflected, compressed, and heated in the magnetosheath behind the shock Also, the unusual position of the shock is consistent with the external solar wind conditions at the time of observations Therefore, the observed changes in the measured currents and derived parameters indicate with a fair amount of certainty that the bow shock identifications made above are correct This example of shock crossings shows how even a weak shock may be identified in the data when all available evidence is brought to bear on the identification

6 August 24, 1967 Crossing

The data taken during a bow shock crossing by Explorer 35 are shown in figures 8a and 8b Because Explorer 35 always crossed the shock at approximately the same radial distance from the earth, the shock crossings all appear in a similar way in the data; therefore only one example of an Explorer 35 shock crossing is presented The crossing occurred at 1112 UT on day 235 0, 1967 when the spacecraft was located at X_{SE}= -41 7 R_E, Y_{SE}= -47 8 R_E, Z_{SE}= -1 0 R_E, (position S6 in figure 2) Prior to the crossing, the spacecraft was in the magnetosheath. Since the spacecraft spin axis was perpendicular to the ecliptic plane, the roll angle gave the ecliptic flow angle of the plasma directly. In the magnetosheath, the flow was deflected 10 to 15 degrees from the radial direction in the negative Y_{SE} direction, which is consistent with the dawn side location of the spacecraft. The flow was warm, as evidenced by the wide differential current spread and the measurable integral flux at 45 degrees to the peak flux direction

As the spacecraft crossed the shock, the direction of the flow changed abruptly to the characteristic aberrated solar wind flow direction Simultaneously, the upper and lower differential currents decreased, indicating a decrease in the plasma thermal speed, while the total integral flux decreased, indicating a decrease in the plasma density. This shock traversal is well defined, as are most shock traversals observed by Explorer 35, and this is consistent with the location of these shock traversals in a region where the shock is still fairly strong

C Magnetopause Traversals

1 Explorer 33 Examples

The magnetopause is the boundary which excludes the shocked solar wind flow from the region of space containing the earth's magnetic field

Thus, a traversal of this boundary is characterized by the disappearance of measurable positive ion flux We will now examine measurements made during several Explorer 33 magnetopause traversals to see how these traversals appear in the data

a) July 29, 1966 Crossing

The magnetopause traversals shown in the data in figures 9a and 9b occurred when the spacecraft was located at X_{SE}= 7.2 R_E, Y_{SE}= -7 6 R_E, Z_{SE}= -4 0 R_E (position M1 in figure 2) This location is approximately 45 degrees from the sub-solar point and is well below the ecliptic plane The proximity to the sub-solar point is reflected in the magnetosheath data prior to the final magnetopause crossing at 0620 UT The largest differential current was measured in the lowest energy channel, indicating flow with a very low velocity The roll angle indicates that the flow was deflected out of the ecliptic plane 20 to 40 degrees from the sun direction and the sense of the deflectior is southward, which is consistent with the -4 0 R_E position of the spacecraft below the ecliptic plane The temperature of the plasma was high, as evidenced by the wide differential energy spread and by the large currents measured in the integral proton channels at 45 degrees to the peak direction

At 0542 UT, the integral flux dipped momentarily and at 0620 UT, disappeared completely The complete disappearance of measurable flux indicates that the spacecraft crossed the magnetopause into the magnetosphere, while the multiple crossings are indicative of boundary motion.

b) August 3, 1966 Crossings

A typical example of multiple magnetopause crossings as observed by Explorer 33 downstream of the earth is shown in figures 10a and 10b. At the time of observation, Explorer 33 was located at X_{SE}= -67 8 R_E, Y_{SE}=

$-16.3\ R_E$, $Z_{SE} = 5.6\ R_E$ (position M2 in figure 2) and the longitude of the spin axis was 98.0 degrees. The magnetosheath flow was typical, with plate A receiving more than half the total current in agreement with the spin axis orientation. The roll angle indicates the flow had a slight northward component, in agreement with the location of the spacecraft above the ecliptic plane. The magnetopause crossings are evident by the disappearance or reappearance of integral proton flux. The magnetopause was clearly in motion at the time of these observations and, from the many observations of the downstream magnetopause by Explorer 33 and Explorer 35, it is evident that this motion is almost always present. The motion is discussed in detail in chapter 3.

2. Explorer 35 Examples

a) Explorer 35 Crossing Parameters

The magnetopause crossings observed by Explorer 35 are studied in some detail in chapter 3. For this study, it was necessary to characterize each traversal by 1) when it occurred, 2) where it occurred, and 3) the time required to cross the boundary. We will now see what criteria were used to determine the above quantities and will examine several examples of Explorer 35 magnetopause crossings.

The time of a boundary crossing was taken to be the time of the first (last) measurable integral flux for a region III to region II (region II to region III) traversal. The position of the crossing was defined to be the position of the moon at the time of the crossing. The time and position of each crossing were determined for those crossings which did not occur in data gaps or shadow.

Not all cases allowed a determination of the time required to cross the boundary. For this time to be defined, several criteria had to be

satisfied First, at least five sets of plasma parameters had to be available adjacent to the crossing This criterion ruled out closely spaced multiple crossings and crossings for which no plasma parameters were available Second, no data gaps were allowed during the boundary traversal This ruled out crossings which extended into either the optical or radio shadow of the moon Third, the magnetosheath plasma velocity had to decrease or stay relatively constant adjacent to the crossing This ruled out several cases where the velocity increased, probably due to solar wind changes For crossings which satisfied the above criteria, the time to cross the boundary was defined to be the time between the time of the first measurable flux and the time of the last significant velocity change, for a region III to region II traversal If the velocity remained constant, the crossing time was defined to be the time between the first measurable flux and the first velocity measurement We will now examine several examples to see how these criteria were applied in practice

b) June 13, 1968 Crossing

The Explorer 35 magnetopause traversal shown in figures 11a to 11d is a typical example of a crossing requiring a finite time The time of the crossing was the time of the first measurable flux at sequence 362467, or 0721 UT, and the position of the moon at this time was X_{SE}= -47 4 R_E, Y_{SE}= -32 2 R_E, Z_{SE}= -5 0 R_E (position M3 in figure 2) and solar ecliptic longitude 214 2 degrees No data gaps occurred and more than five plasma velocities (figure 11c) were available adjacent to the crossing; thus the time to cross the boundary was also determined Since the last significant velocity increase occurred at sequence 362475, the crossing occurred in 8 sequences, or 11 minutes

c) February 14, 1968 Crossing

The magnetopause crossing shown in figures 12a to 12d is typical of those crossings which occurred in a time less than the time between measurements The first measurable flux was detected at sequence 237064, or 1341 UT, when the moon was located as X_{SE}= -55.9 R_E, Y_{SE}= -16 8 R_E, Z_{SE}= 3 2 R_E (position M4 in figure 2) and solar ecliptic longitude 196 8 degrees The criteria to determine a time to cross the boundary were met Since the first velocity measurement occurred at the same time as the first measurable flux and since the velocity did not increase after the first measurement, the time to cross the boundary was defined to be zero minutes

d) August 17, 1967 Crossings

An example of multiple magnetopause traversals observed by Explorer 35 is shown in figures 13a to 13d The spacecraft was located along location M5 in figure 2 Although a time and position were determined for each traversal, at no time was the spacecraft in the magnetosheath long enough for five velocity measurements to be made Therefore, the time required to cross the boundary could not be determined for any of these crossings The motion of the boundary which is evident from the occurrence of these multiple crossings is studied in detail in chapter 3

CHAPTER 3

Boundary Observations

A Boundary Shapes

In this section, we discuss the shapes of the bow shock and magnetopause as observed by Explorer 33 and Explorer 35 First, we will introduce the coordinate system which is most appropriate to the discussion and which we call solar wind coordinates Next, we will use magnetopause position observations made by the lunar orbiting Explorer 35 to calculate the angle in the solar ecliptic plane between the sun-earth line and the (assumed) rotational symmetry axis of the magnetopause Using Explorer 33 observations, we will then show that the magnetotail boundary is, in fact, rotationally symmetric about this assumed rotational symmetry axis Finally, the shapes of the magnetopause and bow shock will be derived from the boundary positions observed by Explorer 33

1 Coordinate System

Two coordinate systems widely used in studies of the solar wind-earth's magnetic field interaction are solar ecliptic coordinates and solar magnetospheric coordinates In solar ecliptic coordinates, the X axis points from the earth toward the sun, the Z axis points from the earth toward the north ecliptic pole and the Y axis completes a right handed system In solar magnetospheric coordinates, the X axis points from the earth toward the sun, the Y axis is perpendicular to the X axis and to the earth's magnetic dipole and points in the direction opposite to planetary motion, and the Z axis completes a right handed system

We now wish to introduce a third coordinate which is most appropriate for the topics studied in this thesis and which we call solar wind coordi-

nates In this geocentric coordinate system, the X_{SW} axis points from the earth into the solar wind direction, the Y_{SW} axis is perpendicular to the X_{SW} axis and to the earth's magnetic dipole and points in the direction opposite to planetary motion, and the Z_{SW} axis forms a right handed system For solar wind flow along the earth-sun line, solar wind coordinates reduce to solar magnetospheric coordinates The transformation from solar ecliptic to solar wind coordinates is presented in appendix A

A primary purpose for using solar wind coordinates in this chapter is to take into account the aberration of the solar wind due to the earth's orbital motion The average solar wind velocity measured over a period of eleven months by Explorer 35 is $\sim$400 km/sec For radial solar wind flow with a velocity of 400 km/sec, the 30 km/sec orbital motion of the earth causes the apparent direction of the flow to come from $\sim 4°$ west of the sun Accordingly, the X_{SW} axis is rotated 4° about the Z_{SE} axis in a clockwise direction as viewed from the north The choice of this value for the rotation angle is justified further in the next section The average flow direction, and hence the X_{SW} axis, are assumed to lie in the ecliptic plane This fixed orientation of the X_{SW} axis is used in all discussions in this section

2 Symmetry of the Magnetopause

a) Alignment with Solar Wind

Let us assume for the moment that the magnetopause is rotationally symmetric about some axis This assumption is verified in the next section We further assume this symmetry axis lies in the solar ecliptic plane In this section, we determine the angle between the assumed symmetry axis and the earth-sun line

The inclination of the (assumed) magnetopause symmetry axis to the earth-sun line at lunar distance may be calculated from the positions of the magnetopause crossings observed by the lunar orbiting Explorer 35 During the total Explorer 35 observational period, the spacecraft made eleven complete traversals of the magnetotail at the rate of approximately one traversal per month Therefore, eleven estimates of the symmetry axis inclination are obtained From these eleven values, the average inclination may be calculated, along with a measure of the variability of the inclination

Each estimate of the symmetry axis inclination is obtained from the average dawn and dusk magnetopause positions The average position of the dawn or dusk magnetopause for a complete traversal of the magnetopause region is defined to be the average of the positions of all crossings observed during the traversal Thus, for each magnetotail passage, one average dawn and one average dusk magnetopause position is obtained By averaging the longitudes of these two magnetopause locations, the symmetry axis inclination in the ecliptic plane is derived

Since the positions of the dawn and dusk magnetotail boundaries are not measured simultaneously by Explorer 35, several effects which cause magnetopause motion act to blur the average magnetopause positions. Changes in the external solar wind, as well as changes in the internal structure of the magnetotail, may cause magnetopause motion Also, we shall see later in this chapter that the magnetopause has an intrinsic motion, probably due to an instability or to a magnetotail resonance These effects all limit the accuracy with which the average magnetopause positions, and hence the magnetopause symmetry axis, may be defined

Since a traversal of either the dawn or dusk magnetopause region requires approximately a day to complete, then fluctuations of the magnetopause on a time scale much less than a day are averaged out These fluctuations include the intrinsic motion, which we will show has a time scale of one hour or less, and those fluctuations due to changes in external conditions on a time scale of several hours or less The spread in the average positions of the symmetry axis is therefore due primarily to 1) the statistical sampling error in determining the average magnetopause positions, 2) changes in external conditions and internal magnetotail structure on a time scale between one day, the time to cross a magnetopause region, and several days, the time between measurements of the dawn and dusk magnetotail boundaries, and 3) changes in the average solar wind direction and velocity from one magnetotail traversal to the next which cause the actual position of the symmetry axis to change

The derived average magnetopause longitudes and symmetry axis inclinations are given in table 2 of section C-2 The average solar ecliptic longitude of the assumed rotational symmetry axis is -2 7°, with a standard deviation of 1 9° The average solar ecliptic longitude of the direction from which the wind flowed as measured by Explorer 35 during the solar wind portions of the eleven months of observations is -4 5°, with a standard deviation of 3 7° Since the experimental error in this angle is estimated to be ± 1 5°, then some of this deviation is due to real fluctuations in the direction of the flow in the ecliptic Within the errors of both the direction measurement and the symmetry axis determination, we conclude that the (assumed) rotational symmetry axis of the magnetopause is aligned with the aberrated solar wind direction

The inclination of the assumed symmetry axis derived from the magnetic field observations on Explorer 33 and Explorer 35 agree with our result. Behannon (1970), using the magnetotail boundary locations observed by both Explorers, derived an inclination of 3 1°. Also, Behannon used the observed internal magnetotail field directions to calculate an inclination of 2 7° Substantially the same results were derived by Mihalov et al (1970) Possible reasons for the small difference between the observed symmetry axis inclination and the expected direction of an aberrated, radially-flowing solar wind are discussed by Behannon (1970) He notes that the difference is consistent with a small, non-radial, corotating component of the solar wind flow

b) Cylindrical Symmetry of the Magnetopause

Having discussed the alignment of the (assumed) magnetopause symmetry axis in the ecliptic plane, we will now discuss the cross sectional shape of the magnetotail boundary in the plane perpendicular to the symmetry axis The question to be answered by this discussion is whether the magnetotail boundary is rotationally symmetric with respect to the ecliptic symmetry axis or whether there exists a pronounced north-south or east-west elongation or flattening which results in an elliptical or other non-circular cross-section

In figure 14 is shown the Y_{SW}-Z_{SW} projection of the portions of all Explorer 33 orbits in the range $-100\ R_E < X_{SW} < -40\ R_E$ The solar wind coordinates, described above, are used with an ecliptic rotation of 4° to align the system with the average measured solar wind direction. Thus, the X_{SW} axis is the (assumed) rotational symmetry axis of the magnetotail boundary The oscillatory nature of the orbits is due to the diurnal motion of the earth's dipole, which causes the Y_{SW}-Z_{SW} plane to oscillate with a

period of one day The heavy portions of the orbits represent times when Explorer 33 was in the magnetotail, while the light portions represent the magnetosheath parts of the orbits The heavy black circle is centered on the origin and has a radius of 28 R_E

We will assume that the average cross-section of the magnetotail boundary in any given Y_{SW}-Z_{SW} plane is stationary in time This is a plausible assumption primarily because the effect of the diurnal motion of the earth's magnetic dipole on the magnetotail orientation has been removed by using solar wind coordinates The small seasonal displacement of the neutral sheet, and hence of the entire magnetotail, from the X_{SW} - Y_{SW} plane has been ignored Since the magnetopause cross-section is assumed to be stationary in the Y_{SW} - Z_{SW} plot of figure 14, a non-circular cross-section would be evidenced in two possible ways First, the magnetotail portions of the orbits will extend to different radial distances from the X_{SW} axis at different parts of the magnetopause Second, the diurnal motion of the earth's dipole will carry the apparent position of the spacecraft in and out across protruding parts of the magnetopause This will result in the positive swings of the orbit oscillations being the opposite shading of the negative swings in the region of the non-uniform portion of the magnetopause

The magnetotail boundary beyond X_{SW} = -40 R_E is approximately parallel to the X_{SW} axis, as we will see below; thus we assume the projection of this boundary onto the Y_{SW} - Z_{SW} plane may be represented by a single contour This contour is the cross section of the boundary We saw in figure 14 that the heavy circle separates the magnetotail and magnetosheath portions of the orbits fairly well Furthermore, the diurnal oscillations of the orbits do not display the second effect described above The mixtures of magnetotail and magnetosheath portions of the individual orbits

can be explained in terms of transverse motion of the magnetopause. This motion is discussed in sections B and C of this chapter. We conclude that the cross-section of the magnetotail is approximately circular and does not have any pronounced elongation or flattening Due to the uneven spacial distribution of magnetotail boundary observations (see figure 14), this result applies only to the parts of the magnetopause below the ecliptic plane

The observation of rotational symmetry of the magnetotail boundary by Explorer 33 agrees with some previous observations Gosling et al (1967), using Vela 2 observations, studied the magnetopause rotational symmetry at a constant distance of 17 R_E from the earth This corresponds to a magnetopause distance crossing at approximately $X_{SW} = -10\ R_E$ which is at the beginning of the magnetotail. The Vela observations extended to ± 60° solar ecliptic latitude Gosling et al (1967) concluded that 1) the magnetopause symmetry axis is tilted 2° - 4° to the west of the sun, in agreement with the expected aberration angle, and 2) the minimum value of the ratio of the vertical to horizontal diameters of the boundary in solar magnetospheric coordinates is 81 This amount of flattening was stated to be conservative, and Gosling et al. (1967) concluded that, within the scatter of the observations, the boundary is rotationally symmetric.

The distant magnetotail boundary has also been mapped by Behannon (1968), using one year of magnetic field data from Explorer 33 From the locations of observed boundary crossings in solar magnetospheric coordinates, Behannon concluded that the tail boundary is elongated in the Z_{SM} direction such that the vertical diameter is 2 to 3 times the horizontal diameter Our observations do not support this conclusion and we feel there are two possible explanations for this discrepancy First, Behannon used only one

year of observations, while our conclusion is based on three years of observations. From the figures in Behannon (1968) compared to our figure 14, it is clear that our coverage of the tail magnetopause is much more complete; thus the magnetic field observations may have been influenced by statistical variations. Second, the effect of aberration on the tail boundary was not removed. Thus, the magnetopause appears closer to the X_{SM} axis in the negative Y_{SM} direction than it actually was. Since observations in the positive Y_{SM} direction were limited, then the apparent closeness of the boundary to the supposed symmetry axis in the horizontal direction may have been due to aberration, rather than to cylindrical asymmetry. If all magnetic field data now available were used and if solar wind coordinates were used to account for the effects of aberration, we feel that the conclusions derived from the magnetic field observations would agree with our conclusions regarding the rotational symmetry of the magnetotail boundary.

3 Magnetopause and Bow Shock Profiles

We will now discuss the X_{SW} dependence of the perpendicular distance of the bow shock and magnetopause from the X_{SW} axis. As we have seen, the magnetopause is approximately circular in cross-section about a line which is parallel to the average solar wind direction. The distance to the magnetopause perpendicular to the X_{SW} axis is therefore independent of the angle about the X_{SW} axis. Accordingly, to map the shapes of the magnetopause and bow shock, each crossing has been plotted at the distance $D = \sqrt{Y_{SW}^2 + Z_{SW}^2}$ from the X_{SW} axis. This procedure effectively rotates all crossings about the X_{SW} axis into a common plane.

The spacial extent of the observations is shown in figure 15a, where all portions of the orbits of Explorer 33 between July 1, 1966 and January 16, 1969, during which useful data were taken, are shown. The exact periods

of observation are given in table 1, chapter 2 The average boundary shapes, as described below, are also shown in figure 15a From the figure, we see that extensive observations of the bow shock and magnetopause extend from the upstream beginning of these boundaries to $X_{SW} = -50\ R_E$ and $X_{SW} = -80\ R_E$, respectively In figure 15b, the portions of the orbits between January 16, 1969 and April 22, 1969 during which data were taken are shown The larger orbits result from a close encounter between the spacecraft and the moon. These orbits extend the observations of the bow shock to $X_{SW} = -115\ R_E$ The positions of all the magnetopause and bow shock crossings which occurred between July 1, 1966 and April 22, 1969 are plotted in figures 16 and 17. The heavy lines which extend through the crossings are subjectively determined average shapes of the boundaries These average shapes are functions which are used in the following sections The function used for the average magnetopause shape is

$$D = 23\ 9 \tan^{-1} \sqrt{\frac{10.0 - X_{SW}}{15\ 9}}$$

while the average-shock function is

$$D = 56\ 7 \sqrt{\left(\frac{191\ 2 - X_{SW}}{177\ 7}\right)^2 - 1}$$

The average-magnetopause function has a radius of $D = 28\ R_E$ at $X_{SW} = -80\ R_E$ and goes asymptotically to a constant radius boundary of $D = 37\ 5\ R_E$ The shock function is a hyperbola whose asymptote makes an angle of 17.7° with the X_{SW} axis

4. Comparison Between Observed and Theoretical Magnetopause Profiles

The shape of the magnetopause from the nose region to well into the

tail has been computed by Spreiter and Alksne (1969a) Separate solutions were obtained for the forward magnetopause and for the tail and the two solutions were joined resulting in one continuous boundary shape We will now review the nature of the solutions and compare a typical calculated boundary shape with the shape derived from the observed crossings

The forward solution was obtained by equating the magnetosheath plasma pressure on one side of the boundary to the magnetosphere magnetic field pressure on the other side of the boundary The magnetosheath plasma pressure was assumed to be given by the Newtonian approximation, $P_{II} = P_{\infty} + P_d \cos^2\psi$, where P_{∞} is the thermal pressure in the incident flow, P_d is the pressure at the stagnation point of the boundary, and ψ is the angle between boundary normal and the incident solar wind direction The magnetosphere magnetic field pressure was approximated by assuming the magnetic field was twice the unperturbed, equatorial dipole field, thus $P_{III} = (2B)^2/8\pi$, where $B = B_s/r^3$ Here, B_s is the field at the earth's equator (B_s = 312 gauss) and r is the distance to the boundary, in earth radii By letting $P_{II} = P_{III}$, a differential equation resulted which was solved numerically to give the equatorial shape of the forward magnetopause

The tail solution was derived by assuming that tail currents caused the tail field to be stretched out approximately parallel or antiparallel to the incident flow direction The magnitude of the field was assumed to be H^* at a distance X^* into the tail from the earth and the tail radius at X^* was assumed to be R^* The field B at a further distance X, where the radius was R, was derived by demanding conservation of magnetic flux, thus $B = H^* (\frac{R^*}{R})^2$ Pressure balance was again used, where the magnetosheath pressure was given by the Newtonian approximation and the tail pressure was given above The resulting differential equation was solved numerically to

give the tail shape The two solutions were matched by picking X^*, R^* and H^* so that H^* matched twice the magnetosphere dipole field at the position X^*, R^* on the boundary The primary purpose of the tail calculation was to allow the tail boundary to flare out a certain amount with increasing distance into the tail

The theoretical solution for an incident Mach number of $M_\infty = 8$, a magnetic field at the beginning of the tail of $H^* = 20\gamma$ and a distance to the stagnation point of 10 R_E is shown superimposed on the observed boundary crossings in figure 17 As may be seen, the calculated shape results in a smaller tail radius than is indicated by the data The Mach number, magnetic field and nose distance are all typical and varying them within reasonable limits does not appreciably improve the fit between the calculation and the data The calculated tail boundary agrees in shape, however, with the observed tail boundary and is only offset in the D direction by ~ 5 R_E The primary discrepancy between the calculation and the observations is in the region $X_{SE} \sim 0$; thus the discrepancy stems from the forward magnetopause solution If this solution resulted in a boundary which was wider at the flanks, then the tail solution would lie along the observed crossings of the magnetotail boundary and the general fit between the calculation and the data would be much closer

A disagreement between the forward magnetopause calculations of Spreiter et al (1966) and the observed boundary shape in the region $X_{SE} \leq 0$ has been observed previously This discrepancy was first noticed by Ness et al (1964) Also, Wolfe et al (1966) compared the locations of IMP-1 magnetopause crossings with the calculations of Spreiter et al (1966) and, from figure 15, of Wolfe et al (1966), it was concluded that the agreement between the calculation and the observations was good. However, the projec-

tion of the IMP-1 crossings onto the ecliptic plane was used for the comparison (Wolfe et al (1966), figure 15). Many of the IMP-1 crossings occurred at higher solar ecliptic latitudes and a simple projection of these crossings onto the ecliptic plane, rather than a rotation, results in the apparent crossing locations being closer to the earth-sun line then they actually were When the crossings are rotated about the earth-sun line (Wolfe et al (1966), figure 16), the crossings in the flank fall further from the earth-sun line than the calculations of Spreiter et al (1966) predict Gosling et al. (1967) also noticed that the magnetopause position at the Vela distance was outside the Spreiter boundary The map of the rotated crossings of IMP-1 agrees well with the locations of the crossings of Explorer 33 for $X_{SE} > 0$ Thus, both previous observations and the observations of Explorer 33 indicate that the magnetopause flares out more on the flanks than predicted by the calculations of Spreiter et al (1966).

An additional magnetosphere pressure is necessary to cause the calculated boundary to extend further into the incident flow Because the calculation and the observations agree near the sub-solar point and diverge in the flank region, this pressure must act primarily in the flanks In the calculation, the effect of the pressure of the magnetospheric plasma was ignored Vasyliunas (1968a, 1968b) has shown that the pressure of the plasma sheet electrons is approximately equivalent to a magnetic field of 20 γ and that this plasma extends to the magnetopause over the entire forward boundary. This constant pressure term on the boundary is negligible compared to the magnetic pressure in the sub-solar region, but becomes progressively more important further away from the sub-solar point until, in the region $X_{SE} \sim -10\ R_E$, where $H \sim 20\ \gamma$, the plasma pressure becomes comparable to the magnetic field pressure Therefore, this pressure should

produce exactly the type of flaring which is observed Although other reasons may be advanced for the flaring, such as failure of the Newtonian approximation or failure of the magnetosphere field approximation, the magnetospheric plasma pressure seems to be a reasonable explanation for the discrepancy between the calculated and observed boundary shapes in the flanks

In summary, the discrepancy between the calculated and observed boundary shapes is primarily in the region $X_{SE} \sim 0$ and this discrepancy might be removed by inclusion of the magnetospheric plasma pressure in the theoretical model The calculated shape of the tail boundary agrees well with the observed shape and adequately explains the observed amount of tail flaring for $X_{SE} < -10\ R_E$ We may note that since the tail portion of the solution assumes conservation of magnetic flux, this agreement implies that the amount of magnetic field which merges or closes in the tail between $X_{SE} = -10\ R_E$ and $X_{SE} = -80\ R_E$ is no more than a small fraction of the total field

B. Dual Satellite Boundary Motion Observations

From the plot of the locations of observed magnetopause crossings (figure 17), it is evident that the magnetopause position is variable This implies motion of the boundary, which may be due either to changes in the incident solar wind, changes in the internal magnetospheric structure, or to intrinsic boundary instability or waves The effect on the boundary position of changes in the incident solar wind is examined in this section using simultaneous observations from Explorer 33 and Explorer 35

1 Theoretical Considerations

The primary properties of the solar wind which may affect the magnetopause and bow shock positions are 1) the solar wind dynamic pressure,

ρv^2, 2) the solar wind direction, 3) the interplanetary magnetic field direction and magnitude, 4) the solar wind Mach number, and 5) the solar wind thermal pressure

A basic concept of the Chapman-Ferraro model is that the solar wind dynamic pressure determines the overall size of the magnetopause At the sub-solar point, the distance of the magnetopause from the earth is determined by a balance of magnetospheric magnetic field pressure and magnetosheath plasma pressure Since, to good approximation, the magnetospheric magnetic field terminates at the magnetopause, then the effect of (Chapman-Ferraro) boundary currents is to add a magnetic field equal to and opposite in direction to the unperturbed dipole field just outside the magnetopause These currents, therefore, add a field equal in direction and magnitude to the dipole field just inside the boundary The magnetic field pressure at the sub-solar point (P_B) is thus calculated from a field twice the unperturbed dipole field If B_e is the field at the earth's equator and D is the distance to the sub-solar point in earth radii, then

$$P_B = \frac{1}{8\pi}\left[\frac{2B_e}{D^3}\right]^2$$

The magnetosheath plasma pressure at the sub-solar point, P_s, results from the solar wind plasma which crosses the bow shock and then comes to rest at the sub-solar, or stagnation, point The value of this pressure is derived in chapter 4, section A3, and is given by

$$P_s = K \rho_\infty v_\infty^2$$

where ρ_∞, v_∞ are the incident solar wind density and velocity and, for $M_\infty >> 1$,

$$K \cong .881 - .336/M_\infty^2$$

This approximation for K is also given by Spreiter et al (1966). The pressure balance condition at the sub-solar point is $P_s = P_B$ and the resulting distance to the sub-solar point is

$$D = \left[\frac{B_e^2}{2\pi} \frac{1}{K \rho_\infty v_\infty^2} \right]^{1/6} \qquad (1)$$

The entire size of the magnetopause scales with this distance as the inverse sixth power of the solar wind dynamic pressure

From the previous discussion of the magnetopause symmetry axis, we saw that the average magnetopause position is aligned with the average solar wind direction This result should reasonably be expected to apply to the instantaneous boundary position on a time scale longer than the time required for the wind to travel the dimensions of the boundary

Olbert (1968) has shown that the bow shock shape conforms to the magnetopause shape Therefore, the effects of solar wind pressure and direction changes on the magnetopause are reflected also on the shock Two observations of shock motion due to changes in solar wind dynamic pressure have recently been presented by Binsack and Vasyliunas (1968)

The effect of the interplanetary magnetic field on boundary shapes is manifested in several ways The Mach number of the solar wind is a function of the magnetic field As we have seen, the sub-solar distance is a weak function of the Mach number; thus the magnetic field plays a small role in determining the magnetopause size The asymptotic Mach angle of the shock, as well as the standoff distance between the shock and the magnetopause at the sub-solar point, depend on the Mach number; thus the Mach number affects the shock position, especially downstream of the dawn-dusk meridian The dependence on Mach number has been ignored because the magnetic field data

are not used in the study Walters (1964) argued that the different orientation of the magnetic field with respect to the shock normal on the dawn and dusk sides of the shock should result in a dawn-dusk asymmetry in the magnetosheath flow pattern This flow asymmetry has been recently observed near the dawn-dusk meridian (Hundhausen et al , 1969) The asymmetry might, therefore, be present even further downstream in the magnetosheath and could result in an asymmetric magnetotail boundary We have seen, however, that the tail boundary is approximately symmetric; thus the effect proposed by Walters has a small effect on the downstream boundary.

The amount of flaring of the tail boundary is influenced by the solar wind thermal and magnetic field pressure The sum of these pressures, in addition to the tangential drag on the boundary, act to contain the magnetotail field far back in the tail Since the tangential drag is poorly understood and, again, since the magnetic field data are not utilized in this study, the effects related to tail flaring are not included in the current study

Changes in the internal structure of the magnetosphere may also affect the magnetopause position The enhancement of the ring current during magnetic storms may inflate the forward magnetosphere Increased tangential drag on the boundary preceeding substorms may carry magnetic flux from the region near the sub-solar point into the magnetotail, causing an inflation of the tail boundary (Aubry et al , 1970) Also, the tail may contract preceeding a substorm as increased merging carries magnetic field and the attached plasma closer to the earth Finally, the tilt of the earth's dipole causes a diurnal motion of the magnetotail in the north-south direction These effects have all been neglected in the current study.

2. Method of Analysis

The method used to examine the effect of changes in the solar wind

dynamic pressure and direction on the boundary positions is illustrated in figure 18 Times were chosen when one spacecraft, called the monitor, was in the solar wind and the other spacecraft, called the observer, was in the boundary region Thirty minute averages of the solar wind direction and dynamic pressure were calculated, using data from the monitor spacecraft For each thirty minute period, the expected positions of the boundaries were then derived by rotating and scaling the average boundaries which were derived above from the study of the Explorer 33 boundary crossings For the rotation and scaling, solar wind coordinates were used, as follows First, the coordinate system was rotated until the X_{SW} axis was aligned with the measured average solar wind direction Using the measured average solar wind dynamic pressure, the distance D to the sub-solar magnetopause was derived, using equation 1 The Mach number dependence of D was ignored, i e , K was assumed to be 881. The positions of the boundaries were then derived in solar wind coordinates so that the magnetopause nose was a distance D from the origin (see figure 18) This last procedure scaled the-size of the boundaries to the solar wind dynamic pressure

For $X_{SW} < 0$, a line was then drawn perpendicular to the X_{SW} axis through the position of the observing spacecraft For $X_{SW} > 0$, the line was drawn radially from the origin The distances along this line to the bow shock, magnetopause, and observing spacecraft (DBS, DMP, S, respectively, in figure 18) were then compared to predict in which region of space the observing craft should have been The region the observer was actually in was defined to he the regior in which the spacecraft spent the most time during the 30 minutes for which the average monitor data were taken

An example of the result of this procedure is shown in figure 20 Here, DBS, DMS, and S are plotted as a function of time The upper broken

line is DIP, and the series of symbols represents S The smooth curve is described below The symbols denote which region the observer was actually in during each 30 minute time interval, where the symbols ◇, ✳ and □ denote the magnetosphere, magnetosheath, and solar wind, respectively If perfect agreement between the predicted and observed regions obtained, then the observer positions marked with a ✳ would lie between the upper and lower broken-line boundary traces and the positions marked by a ◇ and a □ would lie below and above the lower and upper traces, respectively

Before examining the agreement between the predicted and observed observer locations, several explanatory comments are in order Since the distances indicated are measured in solar wind coordinates, then for $X_{SW} < 0$, where most observations were made, changes in the solar wind dynamic pressure are reflected by changes in the distances to the boundaries, as the boundaries contract and expand Changes in the solar wind flow direction, however, are evidenced primarily by changes in the distance to the observer as the solar wind coordinate system moves with respect to the observer A change in solar wind direction may also appear as a change in the distance to the boundaries, since such a solar wind change affects the X_{SW} coordinate of the observer This effect is more important for the bow shock, which has a stronger dependence of shape on the X_{SW} coordinate than does the magnetopause Superimposed on these fluctuations are longer term changes due to the motion of the observer in its orbit This motion changes the distance to the spacecraft and to the boundaries, as the spacecraft moves into regions where the boundaries are closer to or further from the X_{SW} axis The smooth line parallel to the observer-location trace is the location the observer would have for a constant solar wind direction 4° from the west of the sun in the ecliptic Depatures of the actual observer location from

the smooth curve therefore represent departures of the measured solar wind direction from the average, aberrated solar wind direction.

A thirty minute averaging period was picked for several reasons First, an averaging period of approximately 30 minutes or longer smooths the monitor plasma data, which may have small point to point variations due to data quantization More important, the time required for the solar wind to flow from the monitor to the observer spacecraft may be as long as 30 minutes; thus any study of the boundary motion on a time scale less than this must include a model of the dynamic response of the boundaries to rapid solar wind changes Since the present study ignored the time delay and did not include a dynamic model, then the study can only be concerned with time scales longer than 30 minutes Finally, we will see in the next section that the magnetotail boundary possesses an intrinsic motion at lunar distance with a time scale on the order of 15 minutes This motion is partially averaged out of the present study by using an averaging interval of 30 minutes

3. Shock Motion Examples

We will now examine two examples of bow shock crossings and three examples of magnetopause crossings as observed simultaneously by both spacecraft

a) Example 1

The bow shock crossing shown in figure 20 was observed by Explorer 35 on September 13, 1967 (decimal day 255 0) Between the first and last times shown in figure 20, Explorer 35 (the observer) moved along the line marked 'S1 Observer' in figure 19 Simultaneously, Explorer 33 (the monitor) moved along the line marked 'S1 Monitor' in figure 19 Prior to the shock crossing, which occurred during the lunar shadow gap centered on hour 8, September 13,

the solar wind was observed by Explorer 33 to be coming from approximately the average aberrated direction with a dynamic pressure which compressed the nose to a calculated distance of about 8 to 9 R_E At hour 4, an interplanetary shock was observed in the solar wind. The increase in dynamic pressure associated with the shock compressed the calculated nose distance to 7 5 R_E A world wide sudden commencement of a magnetic storm occurred at 0346 UT The next several days of data indicate that this was the beginning of a high velocity stream.

Before the bow shock crossing, Explorer 35 was 20 R_E away from the predicted shock location During the lunar shadow, the solar wind direction changed from $\sim 4°$ west of the sun to $\sim 13°$ west of the sun This change caused the apparent distance of the monitor spacecraft from the X_{SW} axis to decrease At the same time, the dynamic pressure of the wind decreased, allowing the calculated distance to the nose to expand to ~ 8.5 R_E This expansion is evident from the increased distance to the shock after the lunar shadow gap

As indicated in figure 20, these two changes caused the bow shock to be moved close to the observer During the gap, the observer spacecraft also crossed the bow shock Thus, we conclude that the bow shock crossing was caused by a change in the solar wind dynamic pressure and direction which moved the bow shock across the observer.

From figure 20, it is evident that the effect of the solar wind pressure and angle change was to move the shock only into the region of the observer and not entirely past the observer. However, since multiple shock crossings are not evident even on the finest time scale of the data, the actual shock distance was probably further away from the X_{SW} axis than the distance calculated from the model The reason for the discrepancy is most

likely the neglect in the model of the influence of the solar wind Mach number on the bow shock position During the lunar shadow gap during which the shock crossing occurred, the measured solar wind thermal speed increased from $\sim$30 km/sec to $\sim$60 km/sec This lowered the solar wind Mach number The lower Mach number resulted in an increased stand-off distance of the bow shock from the magnetopause nose, as well as an increase in the Mach angle Both of these increases would move the bow shock further from the X_{SW} axis than is indicated in figure 20

b) Example 2

The bow shock crossing shown in figure 21 occurred at 2000 UT, February 17, 1968. The monitor and observer were Explorer 33 and Explorer 35, respectively, and the trajectories of these spacecraft during the times plotted in figure 21 are denoted by 'S2 Monitor' and 'S2 Observer' in figure 19 Prior to the crossing, the solar wind came almost directly from the sun direction and the solar wind dynamic pressure was somewhat larger than average, compressing the calculated nose distance to $\sim$9 R_E At 2000 UT, the dynamic pressure increased so that the calculated nose distance was decreased to $\sim$8 R_E This compression moved the calculated shock position in past the observer spacecraft and a shock crossing was seen by the observer A small shift in the solar wind direction at 2030 UT also moved the shock further past the observer We conclude that this shock crossing was caused primarily by compression of the shock over the spacecraft due to an increase in the dynamic pressure of the solar wind

4. Magnetopause Motion Examples

We will now discuss three examples of magnetopause motion. The first example shows motion induced by a change in solar wind direction, the second example shows motion induced by changes in the solar wind dynamic pressure

and the third case, which is most typical of dual satellite observations, shows multiple crossings in the presence of a constant, steady solar wind

a) Example 1

The magnetopause crossings shown in figure 23 were observed by Explorer 35 on February 11 (decimal day 41.0) and February 12 (decimal day 42 0), 1968 The monitor and observer trajectories for the times plotted in figure 23 are marked as 'M1 Monitor' and 'M1 Observer' in figure 22. All three crossings, at 1430 UT and 2030 UT, February 11, and 1230 UT, February 12, were associated with sudden changes in solar wind direction Prior to the first crossing, the solar wind came from $\sim 2°$ west of the sun. Starting at 1100 UT, February 11, the wind direction shifted over a period of 3 hours to a final direction of $\sim 10°$ west of the sun This direction change moved the boundary into the region of the observer, as evidenced by the apparent displacement of the observer, and, at 1430 UT, the observer spacecraft crossed into the magnetosphere. The time delay between the solar wind direction change and the observed boundary crossing is discussed below. At 2000 UT, the wind direction shifted abruptly to $\sim 2°$ east of the sun and within 30 minutes, the observer crossed back into the magnetosheath The spacecraft then moved along its orbit until at 1230 UT, February 12, a small change in solar wind direction (at 1130 UT) carried the boundary over the observer again, leaving the observer finally in the magnetosphere

In all three crossings, it is evident that the change in the solar wind direction preceeded the crossing by 30 minutes to 2 hours, and there are three possible reasons for this. First, the crossings may not have been caused by the direction changes In the case of the crossing at 1230 UT, February 12, a decrease in the solar wind pressure caused the boundary to expand at the same time as the boundary crossing Examination of the fine

scale data indicates that the crossing actually occurred 15 minutes after the solar wind pressure decrease We will see below that this time delay is somewhat less than the time delay expected from the time required by the solar wind to flow from the monitor to the observer However, the possibility that this crossing was caused by the pressure decrease cannot be discounted. The second explanation is that the time delay represents the response time of the boundary to solar wind direction changes. It is difficult to examine this possibility in detail because there exists no dependable dynamic model of the boundary response.

The third and most likely explanation is that the time delay represents the time required by the solar wind to flow from the monitor to the observer. The solar wind velocity at the time of the crossings was $\sim$400 km/sec and the spacecraft separation in the X_{SW} direction was $\sim$110 R_E For the wind to flow this distance at this velocity requires 29 minutes This time is a lower limit for the delay time, since the actual flow is slowed upon crossing the bow shock and therefore requires longer than 29 minutes to flow to tne downstream boundary. The delay times are therefore consistent in order of magnitude with the flow delay time

The delay time for the crossing at 1430 UT, February 11, is appreciably longer than the delay for the other two subsequent crossings and the following explanation, although unverifiable without the magnetic field data, seems reasonable The solar wind direction change associated with the first boundary crossing at 1430 UT, February 11, was smooth while the direction changes associated with the other two crossings were discontinuous The detailed data suggest these two last changes were tangential discontinuities. Turner (1971) has found that tangential discontinuities tend to line up with the average interplanetary spiral field direction, which makes an angle of

$\phi_{SE} = -45°$ (field points toward the sun) or $\phi_{SE} = 135°$ (field points away from the sun) with the X_{SE} axis. Referring to the locations of the monitor and observer in figure 22, we see that a discontinuity aligned along the average spiral field direction would reach both spacecraft almost simultaneously. Thus, the observed delay time for the two crossings observed after the discontinuous direction changes may be a measure of the response time of the boundary to direction changes of the solar wind. The longer time delay observed after the continuous solar wind direction change may then be a sum of the flow delay time and the response time. This would indicate that the flow delay time and response time are both on the order of one hour. It must be emphasized that this is not a conclusion, but rather a reasonable explanation for the observed delay times.

b) Example 2

The magnetopause crossings shown in figure 24 were observed by Explorer 35 on February 15 (decimal day 45.0) and February 16 (decimal day 46.0), 1968. The positions of the monitor (Explorer 33) and the observer (Explorer 35) for the times plotted in figure 24 are denoted in figure 22 as 'M2 Monitor' and 'M2 Observer', respectively. Prior to the magnetopause crossings, Explorer 35 was proceeding outbound from the magnetosphere to the magnetosheath. The solar wind was coming from near the average aberration direction of 4° west of the sun, as is evidenced by the nearness of the observer trace to the smooth line in figure 24, and the dynamic pressure indicated a distance to the nose of $\sim$8.5 R_E.

The spacecraft orbital motion carried the spacecraft into the region of the boundary near the middle of February 15 and multiple crossings began to be observed, indicating the beginning of a typical boundary region crossing into the magnetosheath. However, at 1530 UT, February 15, the solar

wind dynamic pressure decreased and allowed the calculated distance to the nose to increase to $\sim 10\ R_E$ This boundary expansion moved the calculated boundary position well outside the observer position and the spacecraft was again in the magnetosphere Between 1530 UT, February 15 and 0430 UT, February 16 the spacecraft continued to move relentlessly outward toward the boundary, but the solar wind direction and dynamic pressure continued to change slightly so as to keep the boundary outside the observer location At 0400 UT, February 16 a small increase in solar wind dynamic pressure compressed the boundary inward, resulting in the observer finally crossing into the magnetosheath Only two more multiple crossings were observed (at hour 1800 UT, February 16) and these were apparently unrelated to solar wind pressure or direction changes. From this example, we see that changes in the solar wind dynamic pressure as well as in the solar wind direction may cause magnetopause motion.

c) Example 3

Finally, we will now examine dual satellite observations of a set of multiple crossings near lunar distance to see the relation of these crossings to changes in the solar wind. In the next section, we will discuss the multiple magnetopause crossings which are almost always observed by Explorer 35 when it crosses the boundary at lunar distance

The crossings plotted in figure 25 were observed by Explorer 33 on September 5, 1967. The position of the monitor (Explorer 35) and the observer (Explorer 33) are shown as 'M3 Monitor' and 'M3 Observer' in figure 22, for the time plotted in figure 25. During the pass of Explorer 33 through the boundary region, the calculated distance to the nose fluctuated between 10.8 R_E and 11.5 R_E and the solar wind direction fluctuated between 3° and 8° west of the sun As is evident from figure 25, the observer moved

between the magnetosheath and the magnetosphere several times during the transition of the boundary region Furthermore, these crossings do not appear to be related to changes in the solar wind direction or dynamic pressure, both of which were relatively constant during the transition This example shows that the boundary motion typically observed during crossings of the magnetotail boundary are not necessarily related to solar wind pressure or direction changes

5. Summary of Dual Satellite Observations

Three types of boundary motion appear in the examples presented in this section The first type of motion is related to changes in the solar wind flow direction, where the boundaries move much as a solar wind sock to align themselves with the incident flow direction The second type of motion is due to compression and expansion of the boundaries as the solar wind dynamic pressure increases and decreases We have seen how these two types of motion combine to produce several of the boundary traversals observed by Explorer 33 and Explorer 35 The traversals due to this type of motion, however, were large scale phenomena That is, these traversals were due to relatively large changes in the solar wind direction and pressure. Also, any multiple crossings which were associated with external changes occurred on the order of 12 hours or longer apart.

Superimposed on the above two motions were multiple crossings on a time scale of a few hours or less which were not clearly related to solar wind changes These multiple crossings appear in several of the examples and the third magnetopause crossing example (figure 25) consists entirely of such multiple crossings in the presence of a quiet solar wind. From figure 17, it is clear that multiple crossings of the tail boundary for X_{SW} <-30 R_E are common The nature of the short-time-scale multiple crossings is examined in detail in the next section.

C Explorer 35 Magnetopause Observations

1 Introduction

In the last section, dual satellite observations were used to study individual cases of magnetopause and bow shock motion on a time scale of several hours or more In this section, we examine the motion of the magnetopause at lunar distance on a time scale between two minutes and one hour The study utilizes all magnetopause observations made by Explorer 35, and, instead of examining individual cases, we derive the average temporal and spatial characteristics of the boundary motion and structure. This is accomplished by a study of histograms of magnetopause crossing positions, times between crossings, and times required to cross the boundaries. The dawn and dusk magnetopause crossings are studied separately because clear dawn-dusk differences in the motion are evident from the data After presenting the data, we attempt to parameterize the motion and structure of the boundaries through the use of a model The temporal and spacial characteristics of the boundary motion and structure are then related to various theories of the magnetotail and to previous observations

2 Data and Derived Parameters

In the study we used 267 individual magnetopause crossings observed during the eleven Explorer 35 magnetotail traversals which occurred between August 1967 and June 1968. Each crossing was characterized by 1) where it occurred, 2) when it occurred, and 3) the time required to cross the boundary These three parameters were defined and several examples given in chapter 2

The above parameters for each magnetopause crossing were used to construct histograms as follows. For each complete magnetopause region traversal, we determined the average and standard deviation of the individual

crossing location longitudes The angle between each crossing and the average boundary position longitude for the complete boundary region traversal in which the crossing occurred was determined Histograms of the resulting angles for the dawn and dusk magnetopause are shown in figure 26 Table 2 shows the number of crossings, average longitudes, and standard deviation for each of the 22 complete boundary region traversals

A clear dawn-dusk asymmetry is evident in figure 26 The total number of dawn and dusk magnetopause traversals observed during the eleven months of data used here are 183 and 84, respectively, or a dawn to dusk number ratio of 2 2 Also, the standard deviations of the dawn and dusk histograms are 4 7 ° and 2.7°, respectively. Thus, the dawn magnetopause appears to be more disturbed than the dusk magnetopause and several possible reasons for this are discussed later

TABLE 2

Number of Crossings (N), Average ($<\phi>$) and Standard Deviation (σ_ϕ) of Crossing Longitudes and Longitude of Symmetry Axis (Φ_S) for Each Complete Boundary Region Traversal

		DAWN SIDE			DUSK SIDE			
YR	MONTH	N	$<\phi>$	σ_ϕ	N	$<\phi>$	σ_ϕ	Φ_S
67	AUG	11	203 2	0.9	21	152.4	3 7	2.2
	SEPT	25	197 5	4 1	10	152.7	1.9	4.9
	OCT	11	202 8	1 5	1	153.0	-	2.1
	NOV	7	203 7	1 7	8	149.9	1.1	3 2
	DEC	4	198.3	2.3	2	154 0	5 1	3 8
68	JAN	12	198 8	4 2	1	148 2	-	6 5
	FEB	38	199.9	6.7	8	152.5	4.4	3.8
	MAR	15	205 8	3 1	7	151 4	0.6	1.4
	APR	19	204 0	3.1	4	154 4	3 3	0.8
	MAY	19	203 8	2 0	3	157.6	0.2	-0.7
	JUN	21	206 1	2.7	19	151.2	1.8	1.3

$<\Phi_S> = 2\ 7$

$\sigma_{\Phi_S} = 1.9$

A measure of the time scale of magnetopause motion is obtained by studying the times between the multiple crossings seen on each complete boundary region traversal We refer to the time between one arrival of the boundary at the spacecraft and the next arrival as the interarrival time For example, if crossings were observed at 1110 UT and 1130 UT, the interarrival time would be 20 minutes and for any set of N sequential crossings, a set of N-1 interarrival times could be determined. The determination of interarrival times for all the crossings used in this study was subject to two constraints. First, the crossings observed on any particular magnetopause region traversal were kept separate from those crossings observed on the previous and subsequent magnetopause region traversals This was done so that the time required by the spacecraft to travel from the dusk to the dawn magnetopause did not count as an interarrival time Second, the time between two crossings was not used if a long data gap occurred between the two crossings This constraint assured that no unobserved magnetopause crossings occurred in the middle of an interarrival interval. Since the spacecraft entered radio shadow approximately twice a day, this also limited the maximum measurable interarrival time to 11 hours. The minimum detectable interarrival time was approximately 2 minutes.

The dawn and dusk histograms of interarrival times are shown in figures 27a and 27b For both histograms, the number of observed interarrival times decreases approximately exponentially with increasing interarrival time Furthermore, the dawn histogram shows a break at $\sim$40 minutes and the decrease in the number of observed times with increasing interarrival time is more gradual for times greater than 40 minutes The break is not apparent in the dusk histogram, but we will see that this is probably due to the lessernumber of observed dusk crossings The exponential decrease

suggests that it is meaningful to determine characteristic interarrival times (t_o) from the histograms by performing a least-squares-fit to the function $f(t)=Ke^{-t/t_o}$ For the dawn histogram, this fit was performed twice, once for the points with $t < 40$ min and again for the points with $t > 40$ min. The times thereby determined from figure 27a are t_s = 16.7 minutes and t_L = 63 3 minutes, respectively We deduce from these two times that the dawn interarrival times are governed by two superimposed motions, one with an apparent time scale of ~ 17 minutes and the other with an apparent time scale of ~63 minutes These two components of magnetopause motion we label the small and large scale motions, respectively. Since the dusk histogram does not have an apparent break, only one fit is performed for points with $t < 60$ minutes The resulting time is t_o = 22.8 minutes, which suggests that these interarrival times are the result of the small scale motion.

To parameterize the relative importance of the small and large scale motions on the dawn histogram, we use the ratio of the total number of crossings due to the large and small scale motions as inferred from the fitted functions. The assumed distribution of small and large scale induced interarrival times is

$$n_S(t) = \frac{N_S}{t_S} e^{-t/t_S} \qquad 0 < t < 40 \text{ min.}$$

$$n_L(t) = \frac{N_L}{t_L} e^{-t/t_L} \qquad t > 40 \text{ min.}$$

respectively, where N_S, N_L and t_S, t_L are the total number of interarrival times and the characteristic times of the small and large scale motions We have assumed for simplicity that the contribution of the small (large) scale

motion to the large (small) scale motion portion of the histogram is negligible If A_S, A_L are the intercepts of the small and large scale fitted lines with the t = 0 axis and Δ is the histogram bin size, then

$$A_{(S)} = N_{(S)} \left[2 \sinh\left(\frac{\Delta}{t_{(S)}}\right) \right]$$

and the ratio A' of the number of small to large scale interarrival times is

$$A' = \frac{N_S}{N_L} = \frac{A_S}{A_L} \left[\sinh\left(\frac{\Delta}{2t_L}\right) / \sinh\left(\frac{\Delta}{2t_S}\right) \right]$$

This parameter is a direct measure of the relative importance of the large and small scale motions and is used in the modeling procedure described below The value of A' as deduced from the dawn histogram is A' = 1.48

We next consider the boundary layer crossing times The time required for the spacecraft to cross the boundary is given by

$$\tau = \frac{D}{|V \pm v_n|} \qquad (2)$$

where D is the boundary thickness, V the boundary velocity and v_n the velocity of the spacecraft normal to the boundary. The + and - signs are taken when the spacecraft and boundary are moving in opposite and in the same direction, respectively If the average boundary velocity were much greater than the spacecraft velocity, then

$$\tau \cong \frac{D}{|V|}$$

and the crossing time would be determined solely by the magnetopause thickness and velocity If, on the other hand, the boundary velocity were comparable to the spacecraft velocity, then equation 2 applies and we should see a correlation between the spacecraft velocity and the boundary crossing time To decide which sign to use in equation 2, we note that the observation of multiple boundary crossings in itself indicates that the boundary velocity is somewhat larger than the spacecraft velocity Also, the orbital

motion of the moon insures that the normal velocity of the spacecraft is almost always approximately in the negative Y_{SE} direction. Thus, the + sign in equation 2 applies when the boundary is moving in the opposite direction as the spacecraft, or in the positive Y_{SE} direction, and since the average boundary velocity is somewhat higher than the spacecraft normal velocity, this motion corresponds to outward (magnetosphere to magnetosheath) boundary traversals on the dawn side and inward traversals on the dusk side Similarly, the minus sign in equation 2 applies to inward dawn traversals and outward dusk traversals The data for these two cases are plotted in figure 28. From this figure, we see that the crossing times and the spacecraft velocities are uncorrelated and we therefore conclude that the boundary crossing times are primarily due to motion of the boundary rather than to motion of the spacecraft

The dawn and dusk histograms of boundary crossing times are shown in figures 29a and 29b The dawn crossing times appear to obey an exponential law and from the least squares fit to the histogram as before, the characteristic crossing time is 8 7 minutes The dusk histogram does not show a distinct decrease with increasing crossing time; thus the exponential fit is not meaningful The nature of the dusk histogram is probably due to the small number of points

3 Summary of Empirical Data

Before proceeding to the model used to examine the data, let us summarize the salient features and parameters of the data which any model of magnetopause motion must reproduce The basic features of the data which a model must reproduce in form are:

1) the peaked distribution of crossing locations,

2) the exponential distributions of interarrival times, and

3) the exponential distribution of the boundary crossing times on the dawn side

In particular, the interarrival and crossing times histograms should not be strongly peaked

The parameters which must be matched by a model are

1) the total number of dawn and dusk crossings, N_{DAWN}=183, N_{DUSK}=84,

2) the total widths of the dawn and dusk observation regions $2\sigma_{DAWN}$= 9.4°, $2\sigma_{DUSK}$= 5 4°,

3) the characteristic interarrival times of the small and large scale motions on the dawn side, t_s = 16 7 minutes, t_L = 63 3 minutes,

4) the inferred number ratio of small-to-large-scale-motion induced crossings on the dawn side, A' = 1 48,

5) the characteristic interarrival time on the dusk side, t_o = 22.8 minutes, and

6) the characteristic boundary crossing time on the dawn side, τ_c = 8.7 minutes

4. Boundary Motion Simulation

In this section, we describe a model used to simulate the motion of the boundary at lunar distance From the simulation, histograms similar to those observed are derived and compared with the data The simulation is performed for several reasons Different forms of the assumed boundary motion are tested and from the derived histograms, we gain insight into what general types of motion of the boundary may be present at lunar distance Also, certain types of motion are excluded by the results of the simulation For those types of motion which give reasonable histograms, we may determine if the observed time and amplitude scales of the motion are consistent with

the total number of observed crossings Quantitatively, the simulation allows us to estimate the relative amplitudes of the large and small scale motions Also, the average boundary thickness may be estimated by comparing the derived and observed boundary crossing times histograms.

Before proceeding with the description of the simulation, several comments about the limitations of the method are in order First, the simulation does not uniquely specify the actual motion We will see two different assumed forms of motion which each reproduce the observed form of the data satisfactorily Other forms of the motion undoubtedly exist which also reproduce the data However, it seems likely that such forms differ only in minor ways from the forms used here and that the same conclusions would be drawn Second, the simulation in no way explains the origin of the motion By simulating the motion, we only investigate and characterize the nature of the motion and leave the question of the origin of the motion to the discussion section below.

Figure 30 shows the basic method used to simulate the boundary motion The time history of the displacement of the boundary from its average position is the function f(t), while the orbit of the spacecraft is the line g(t) As we saw above, the observed boundary traversals are independent of the velocity of the spacecraft; thus we assume the orbit of the spacecraft to be well represented by the orbit of the moon. The orbital function g(t) then represents the motion of the moon through the boundary region at a constant velocity of 1 km/sec

The different boundary functions f(t) used in the simulation have several features in common. Since the dawn data indicate that the total boundary motion is the sum of a large and small scale motion, we let f(t) be

the linear sum of two similar functions, L(t) and S(t) The standard deviations of the distributions of large and small scale amplitudes, σ_L and σ_S, cannot be directly fixed from the histograms, but the deviation of the total motion $\sigma_T = \sqrt{\sigma_S^2 + \sigma_L^2}$ can be We may therefore use σ_T and the ratio $R = \sigma_L/\sigma_S$ to characterize the amplitude of the total motion, f(t)

For the dawn simulation, the time scales of the large and small motion are set equal to the time scales derived from the dawn interarrival-time histogram For the dusk simulation, the time scale of the small scale motion, S(t), is set equal to the time derived from the dusk interarrival-time histogram The time scale of the large scale motion on the dusk side is set equal to the observed dawn large scale motion time, by assumption. Although no apparent large scale motion is observed on the dusk side (equivalent in the simulation to R = 0), we will see that by varying R away from zero in the simulation, a qualitative idea may be gained of the amount of large scale motion that may be present

To simulate a single passage of the spacecraft through the boundary region, we sample the difference g(t)-f(t) at the spacecraft resolution frequency of once every two minutes. A boundary crossing occurs whenever the difference changes sign from one sample to the next We record the position, time and boundary velocity $V = \frac{df(t)}{dt}$ for each crossing. For those crossings more than 13 minutes removed from the previous crossing, we compute a boundary traversal time $\tau = \frac{Dm}{V}$ where Dm is an arbitrarily assumed boundary layer thickness The 13 minute separation reproduces the criterion of 5 good plasma measurements adjacent to a boundary crossing, as described in chapter 2 The simulation of optical and radio shadow, during which no usable data were returned by the spacecraft, is accomplished by deleting those crossings which

occur during a one hour interval each 11 5 hours. In this way, we derive a set of boundary crossing positions, interarrival times and boundary crossing times completely analogous to the data from one boundary region traversal.

For a given model function f(t) and assumed value for R, a complete simulation of the dawn or dusk data proceeds as follows 11 complete simulated passes of the spacecraft through the boundary region are made, σ_T being set equal to each of the eleven dawn or dusk values of σ_ϕ in table 2 in turn In complete analogy with the treatment of the actual data, histograms of boundary crossing positions, interarrival times, and boundary crossing times are compiled The parameters defined above which characterize the data are also derived N_{TOTAL} and σ are derived from the position histogram and, using the identical least squares fit as was used for the data, t_L, t_S, and A' are derived from the interarrival times histogram for the dawn simulation and t_o is derived for the dusk simulation. The characteristic time τ_c is also derived from the boundary crossing times histogram for the dawn simulation

A complete test of an assumed model for f(t) proceeds as follows The simulation described above is performed for both the dawn and dusk sides for various values of R to find that value of R which results in the closest fit between the measured and derived parameters, N_{DAWN}, σ_{DAWN}, t_S, t_L, A' on the dawn side and N_{DUSK}, σ_{DUSK}, t_o on the dusk side For all models used, σ_{DAWN}, t_s, t_L and t_o are fairly insensitive to R and agree well with the data, as they should since they were taken directly from the data Therefore, the choice of the best value for R is usually made on the basis of N_{DAWN}, A' on the dawn side and N_{DUSK} on the dusk side. For the optimum R, the form of the actual and derived histograms are compared on each side to

assure that the position histogram shows the peaked nature evident in the data and that the interarrival and dawn boundary crossing times histograms show the exponential nature also evident in the data

For a model which matches the data qualitatively as well as quantitatively, we are able to determine an average boundary layer thickness on the dawn side by the following scaling law Let τ_D, τ_M = characteristic boundary crossing times derived from the data and from the model, respectively, D_M = assumed boundary thickness used in the model to construct the boundary crossing times histogram from the boundary velocities V Since each crossing time τ is determined from

$$\tau = \frac{D_M}{V}$$

then the actual boundary thickness D to be inferred from the model is given by the simple scaling law

$$D = D_M \left(\frac{\tau_D}{\tau_M}\right) \qquad (3)$$

Any f(t) which satisfactorily reproduces the data thus allows a statistical estimate of the average magnetopause thickness at lunar distance.

5. Simulation Results

The boundary motion simulation is performed with three different assumed forms for f(t) We will now present the reasons each model is used, describe the models, and present the results of the simulations

Model 1

The temporal and spacial characteristics of the first model of f(t) are taken directly from the data The temporal nature of the motion is derived from the following considerations Consider the boundary motion in

time to be a square wave oscillating between amplitudes ±A with unequal intervals between amplitude changes. Assume further that the spacecraft is between +A and -A If we assume that the amplitude changes come at completely random times, subject to the constraint that the average time between amplitude changes be a certain value t_o, then it is easily verified that the probability distribution of the time between amplitude changes is Poisson, i e.,

$$P(\Delta t) = \frac{1}{t_o} e^{-\Delta t/t_o} \tag{4}$$

where Δt is the time between changes For a spacecraft located between +A and -A, each amplitude change of the boundary results in a boundary crossing Thus, $P(\Delta t)$ is also the distribution of interarrival times observed by the spacecraft We have seen that the distributions of interarrival times observed by Explorer 35 appear to obey an exponential law. Accordingly, for the first model, we assume that the position of the boundary changes at random times governed by the above distribution $P(\Delta t)$. Further, since the observed histograms of crossing positions are peaked, we assume that the amplitude (d) to which the boundary moves at each amplitude change is also random and governed by a Gaussian distribution,

$$P(d) = \frac{1}{\sqrt{\pi}\,\sigma} e^{-(d/\sigma)^2} \tag{5}$$

Finally, to allow for a finite boundary velocity, we assume the boundary moves uniformly from one distance to another in the time Δt, rather than instantaneously

Both the large and small scale motions are assumed to be governed separately by the above distributions Since the probability that each amplitude change will cause the boundary to cross the origin is $\frac{1}{2}$, then it is necessary that the model's characteristic time be half the apparent interarrival time derived from the histogram of interarrival times Thus, for

the small and large motions on the dawn side, we let t_o be 8 and 35 minutes, respectively, and for the dusk side, we let t_o be 11 minutes for the small scale motion and assume t_o to be 35 minutes for the large scale motion This last assumption is discussed later

For a given ratio R ($= \sigma_L/\sigma_S$) and total amplitude σ_t ($=\sqrt{\sigma_S^2+\sigma_L^2}$), the small and large scale amplitudes used in equation 5 above are

$$\sigma_S = \sigma_T/\sqrt{1+R^2}$$

$$\sigma_L = \sigma_S R$$

where σ_t is to be set equal to measured σ_ϕ (table 2) for each complete simulated boundary region traversal.

The large and small scale motions are linearly combined to give a total motion f(t) = L(t) + S(t) and a complete simulation is performed three times each for values of R between 0 and 5. The predicted total number of crossings (averaged for the three simulations), N_{DAWN} and N_{DUSK}, as well as the average derived value of A', are shown for various values of R in figure 31 The error bars represent the spread of the three simulated values about the average The total number of observed crossings decreases as R increases, for the following reason The small scale motion is more effective than the large scale motion in causing simulated boundary crossings due to the higher frequency of the small scale motion As R increases, however, the large scale motion, with its larger amplitude, moves the boundary away from the spacecraft more often. At the same time, the amplitude of the small scale motion decreases Thus, the spacecraft is exposed less often to the small scale motion and the total number of multiple crossings decreases This also implies that closely spaced multiple crossings should come in groups, separated by periods with no crossings Subjectively,

this actually is the nature of multiple crossings observed by Explorer 35 The dependence of A' on R simply reflects the increased importance of the large scale motion with increasing R

From figure 31, it is evident that the values of R which best reproduce the measured parameters on the dawn and dusk sides are R = 3 and R = 2, respectively If we examine the simulated position and interarrival histograms in figures 32, 33a, and 33b, we see that they strongly resemble the observed histograms In particular, we see that the large scale motion is not clearly evident in the simulated dusk interarrival times histogram, in agreement with the data However, it is evident from the dependence of N_{DUSK} on R (figure 31), that the large scale motion must be present to keep the boundary away from the spacecraft and reduce the total number of crossings to the observed level

We conclude that for this simulation, the large scale motion is ~3 times larger in amplitude than the small scale motion on the dawn side. Furthermore, some large scale motion is probably present on the dusk side and its amplitude is probably greater than the amplitude of the small scale motion. The actual amplitude of the large scale motion on the dusk side cannot be derived because we can only assume a characteristic time for this motion

Since this model successfully simulates the data both qualitatively and quantitatively, and since the simulated crossing times histogram on the dawn side (figure 33a) qualitatively resembles the histogram of measured crossing times, we may estimate the boundary thickness by the scaling law, equation 3 The average derived characteristic crossing time is τ_m = 8.5 minutes and the assumed thickness is $D_m = 2\ R_E$; thus by combining the measured characteristic crossing time τ_0 = 8 7 minutes with the scaling equation,

we see that the average magnetopause boundary thickness predicted by this model is D = 2 R_E

We note that the histogram of simulated dusk boundary crossing times is qualitatively similar to the data That is, the majority of crossing times for both the data and the simulation are less than ~10 sequences Thus, the dusk simulation is at least consistent with a 2 R_E dusk boundary thickness

Model 2

With the second model, we investigate the possibility that the boundary motion may have a basic period For this purpose, we assume that the time between amplitude changes, Δt, is constant rather than random Since the amplitude distribution is still assumed to be governed by a random Gaussian distribution, the assumed times between amplitude charges must be half the observed characteristic times Thus, for the small scale motion, we assume that Δt = 8 minutes and for the large scale motion, $\Delta t'$ = 35 minutes The results of the simulation using this model are the same quantitatively and qualitatively as the results of the previous model Therefore, this model also successfully simulates the data and leads to the same conclusions regarding the relative amplitudes of the large and small scale motions as did the first model Further, we see that the motion is not necessarily purely random in time, as may have been inferred directly from the data.

The boundary crossing times histogram on the dawn side also agree qualitatively with the data The boundary thickness for this model derived from the scaling law is D = 2 R_E

Model 3

The third model tests the possibility that the motion is quasi-periodic in space as well as in time For this purpose, the Gaussian distribution of amplitudes is replaced by a constant amplitude The time between amplitude changes is also constant, as in the second model, thus the assumed form of the motion is a sawtooth wave Since each amplitude change now causes the boundary to cross the origin, then the time between amplitude changes is taken to be approximately the same as the observed characteristic interarrival time

The dawn interarrival times histogram derived from this model for R = 4 is shown in figure 35 As one might expect for truly periodic motion, the interarrival times show several prominent peaks at odd multiples of the small scale motion characteristic time of 16 minutes. Clearly, this is not the nature of the data and this model cannot be used to estimate R or the boundary thickness By comparing the results of the second and third models, we conclude that any periodic motion of the boundary must have random amplitudes in order to produce the observed form of the interarrival times histograms

6 Conclusions

1. The dawn magnetopause is more disturbed than the dusk magnetopause The average observed amplitude of the dawn boundary motion is approximately twice that of the dusk boundary motion From the modeling procedure, we see that the ratio of the number of observed multiple crossings of the dawn boundary to those of the dusk boundary is consistent with the measured amplitudes Thus, the larger number of observed multiple crossings is due to the larger amplitude of the dawn motion, which increases the total time the spacecraft is in the boundary observation region

2. The motion of both the dawn and dusk boundaries appears to consist of two superimposed components On the dawn side, the characteristic times of these two motions derived from the data are ~15 minutes and ~1 hour. From the modeling procedure, the second motion appears to have an amplitude ~ 3 times the amplitude of the first motion On the dusk side, the characteristic time of the short time scale motion is ~ 20 minutes. The amplitude of the longer time scale motion appears, from the modeling procedure, to be at least comparable to the short time scale motion On both sides, the data are not detailed enough to distinguish between models in which the time scales refer to quasi-periodic or purely random motion of the boundary in time

3 The thickness of the plasma boundary layer at the dawn magnetopause obtained from the model fitting is approximately 2 R_E at lunar distance The dusk data are also consistent with a thickness of this order of magnitude.

7 Discussion

The number of observed dawn and dusk magnetopause traversals is 183 and 84, respectively This is consistent with a model in which the dawn magnetopause motion is more disturbed, i e , has a larger average amplitude, than the dusk magnetopause motion This amplitude asymmetry may be due either to different external solar wind conditions at the times of observation or to an intrinsic difference in the variability of the magnetosheath flow on the dawn and dusk flanks of the magnetotail

To examine the possibility that the differences in the boundary motion amplitude may be due to different solar wind conditions, we examine the relation between the measured solar wind magnetosheath velocities and the position of the moon about the earth We divide the lunar orbit into ten degree

sectors in solar ecliptic longitude and, for each sector, average all plasma velocities measured in that sector regardless of the time of the measurement All 70,000 measurements made during the eleven months of observation are used and this represents approximately 3,000 velocities for each 10° sector. Velocity measurements in the solar wind and in the magnetosheath are averaged separately The result is shown in figure 41 If the solar wind velocity were a random quantity which varied on a time scale short compared with the lunar period, then the sector averages would all be approximately equal However, fast and slow streams which appear every 27 days, the solar rotation period, have been repeatedly observed (Neugebauer and Snyder, 1966) and since this period is close to the lunar period, the possibility exists that these streams will occur at the same longitude over several lunar rotations. Referring to figure 41, we see that this is what happens and that two high velocity regions are apparent. The dusk and dawn magnetopause traversals occur at average solar wind velocities of 430 and 480 km/sec, respectively Thus, the average external solar wind conditions are somewhat different for the two sides and may contribute to the observed amplitude asymmetry If this were the case, we would infer that larger solar wind velocities cause larger amplitude magnetopause motions at lunar distance. This inference is consistent with the observed correlation between solar wind speed and geomagnetic activity (Snyder, et al , 1963).

Although the difference in solar wind conditions for dawn and dusk traversals may explain at least in part observed differences we cannot exclude also the possible action of intrinsic differences Fairfield (1967) has investigated the magnetosheath magnetic field orientation using data from IMP-1 and IMP-2. He found that when the interplanetary field was along the spiral

direction, the dusk magnetosheath field was well ordered and, on the average, was in the direction predicted by Spreiter et al (1966), while the dawn magnetosheath field was fairly disordered. This difference between the dawn and dusk fields may be related to the difference in orientation of the interplanetary field with respect to the bow shock on the two sides Thus, the dawn magnetosheath flow may be intrinsically more variable than the dusk flow, resulting in the observed larger amplitude magnetopause motion on the dawn side than on the dusk side

The two observed time scales of magnetopause motion are close to characteristic times of motion which have been calculated for the magnetotail or observed in the magnetosphere and solar wind Siscoe (1969) has calculated eigenperiods of the tail under the assumption that the tail behaves as a fixed-wall wave guide for magneto-acoustic waves. For the antisymmetric mode, where the two sides of the tail move together, Siscoe calculated an eigenperiod of approximately 11 minutes. By treating the tail as a cylindrical vortex sheet immersed in a streaming plasma, McKenzie (1970) matched boundary conditions between the interior magnetotail and the magnetosheath and found that boundary waves with a wavelength of the order of the tail diameter have a period of approximately 13 minutes These times are close to the observed small scale motion characteristic time of ~17 min; thus the small scale motion may be an intrinsic motion of the magnetotail Using data from Mariner 5, Siscoe et al. (1968) found that the characteristic time between discontinuities in the interplanetary magnetic field was approximately one hour, which is close to the characteristic time of 63 min associated with the large scale motion of the dawn side Thus, the large scale motion may be due to small changes in the solar wind These observations

are consistent with the view that the boundary motion consists of a small scale intrinsic motion superimposed on a larger time-scale and amplitude motion which is related to the external magnetosheath or solar wind flow.

Anderson et al (1967) have also observed magnetopause motion from IMP-2 data gathered in the forward magnetopause region. They found that the motion consisted of two modes, one with a time scale of $\sim$8 minutes and another with a larger time scale of 20-60 minutes The short time scale motion was attributed to intrinsic boundary instability, perhaps of the Kelvin-Helmholtz type, while the larger time scale motion was assumed to be the response of the boundary to solar wind changes These observations and their interpretation agree well with ours and indicate that the two component motion of the boundary is not strictly a tail phenomenon but occurs over the entire magnetopause.

Magnetic field variations with time scales of the order of the small scale boundary motion have also been observed in the magnetosphere and on the ground Modulation of energetic electrons in a period range centered around 6 minutes observed on IMP-1 and IMP-2 by Lin and Anderson (1966) was attributed to hydromagnetic waves generated at or beyond the magnetopause. Patel (1966), using magnetosphere magnetic field data from Explorer 14, found low frequency waves with periods between 3 and 30 minutes, with a predominance of periods of approximately 10 minutes In one case, a clear correlation was found between the satellite observations and ground observations on the same field line. Using magnetometer data taken near New York, Herron (1967) calculated a power spectrum of the observed magnetic variations In addition to several peaks in the pc-3 to pc-5 range, he found a broad peak centered at approximately 28 minutes. Atkinson and

Watanabe (1966) concluded from a study of the polarization of magnetic field variations on the ground that such low frequency micropulsations may be caused by waves on the surface of the magnetopause The agreement between the time scales of forward magnetopause motion, magnetotail boundary motion, magnetosphere and ground magnetic field variations, and theoretical magnetotail calculations indicates that the various motions are probably related, although cause and effect cannot be clearly established

Theoretical estimates of the magnetopause boundary layer thickness have been made essentially in two ways Axford (1964) argued that the electric potential observed between the dawn and dusk magnetopause must equal the potential drop across a thin layer at the magnetopause If ϕ is the magnetosphere potential and U, B and δ are the plasma velocity, magnetic field and thickness of the boundary layer, then Axford argued that

$$UB\delta \sim \frac{\phi}{2}$$

and, using typical observed values, derived a thickness of $\delta \sim 400$ km Implicit in this argument is the assumption that the plasma in the boundary layer is accelerated magnetospheric plasma, which has a density of the order of $1 cm^{-3}$ and would therefore not be observable with the instrument on Explorer 35. Thus, this calculation probably does not apply to our results The other method of calculating the boundary layer thickness is that used by Eviatar and Wolf (1968), who calculated the effective viscosity (ν) of a turbulent field mixing region at the boundary They derived an approximate value of $\nu \sim 10^{13}$ cm^2/sec From classical boundary layer theory, the thickness of a boundary layer a distance X from the leading edge of a boundary emmersed in a flow of incident velocity U is $\delta = 0(\frac{\nu x}{U})^{1/2}$. If we take

representative values of X and U for Explorer 35 of X = 50 R_E, U = 400 km/sec, then using the effective viscosity derived by Eviatar and Wolf, we find δ = .2 R_E Faye-Petersen and Heckman (1968) also calculated the effective viscosity in the boundary layer by assuming that the particles are scattered by irregular magnetic fields and derived a thickness of δ = .86 R_E at X_{SE} = -20 R_E Thus, the boundary layer thickness calculated from effective viscosities appear to be consistent within an order of magnitude with, though less than, our observed layer thickness of $\sim$2 R_E

Previous observations of boundary thickness at lunar distance (Mihalov et al., 1970) were made on the basis of only a few boundary crossings and are thus statistically unreliable However, the boundary crossing times used to estimate the thicknesses are significantly shorter than our characteristic crossing time and do indicate that the magnetic boundary may be thinner than the plasma boundary. If this is the case, it is possible that the magnetic field changes occur in a thin boundary region, the magnetopause proper, while the plasma changes occur in the boundary layer adjacent to the boundary This question will be answered only through the comparison of simultaneous field and plasma data

CHAPTER 4

MAGNETOSHEATH FLOW OBSERVATIONS

A. Theory

1 Introduction

The plasma flow characteristics in the magnetosheath have been calculated by Spreiter et al. (1966) and by Dryer and Heckman (1967) and Dryer (1971). For this calculation, the hydrodynamic fluid equations were integrated numerically along the streamlines to give the velocity, direction, density, and temperature of the magnetosheath flow as multiples of the respective quantities in the solar wind The calculations, however, only extend to $X_{sw} = -20\ R_E$ and are for a restricted range of incident solar wind Mach numbers In this chapter, we present measurements of the flow in the magnetosheath as far downstream as $X_{sw} = -60\ R_E$ Also, the measured solar wind Mach numbers corresponding to the plasma measurements are outside the range of Mach numbers for which calculations were made by the above authors. Therefore, we now present calculations which were made to allow us to compare our measurements with the predictions of the hydrodynamic flow equations for magnetosheath flow

Two places in the magnetosheath where the plasma flow parameters may be expressed in closed form as a function of the upstream parameters are just inside the bow shock and along the magnetopause, i e., at the boundaries of the magnetosheath This assumes that the shapes of the boundaries are already known Thus, we assume that the bow shock and magnetopause shapes are well represented by the functions fit to the boundary crossings observed by Explorer 33 (see chapter 3) The values of the magnetosheath flow parameters inside the shock are derived by applying the Rankine-

Hugoniot jump conditions across the shock. The magnetopause values are derived by first using the shock jump conditions at the sub-solar point to find initial values for the flow and then using Bernoulli's equation to follow the flow to the stagnation point. By using Bernoulli's equation, the Newtonian pressure approximation (described below) and the shape of the magnetopause, we then follow the flow from the stagnation point along the stagnation streamline to find the plasma parameters at any point on the magnetopause

To find the plasma parameters at any point (X,D) in the magnetosheath (see figure 36), we first calculate the values of the parameters at the magnetopause (position 1 in figure 36) and at the bow shock (position 2 in figure 36) at the position X We then interpolate linearly along the dashed line in figure 36 to predict the value of the parameters at (X,D)

We will now present the solutions described above for the magnetosheath plasma parameters along the bow shock and magnetopause. Explicit examples of the solutions for an incident Mach number of 10 will also be presented. Finally, we will compare our interpolated magnetosheath flow parameters with the exact calculations of Spreiter et al (1966) at X_{sw} = -10 R_E to examine the accuracy of the extrapolation method.

2 Bow Shock Plasma Parameters

Assume the upstream and downstream values (with respect to the bow shock) of the plasma density, velocity and pressure are (ρ_o, V_o, P_o) and (ρ_1, V_1, P_1), respectively Further, let θ be the angle between the incident flow direction and the shock normal θ is shown in figure 36 on the snock curve Let ϕ be the angle between the upstream and downstream flow directions, as shown in figure 36 ϕ, then, is the angle of deflection of the flow across the shock Assume the equation of state is

$$P = 2nkT = \rho w_o^2$$

where n is the number density, T the temperature and w_o the plasma thermal speed The factor of 2 comes from the assumption of equal electron and proton temperatures and number densities The conservation equations may then be written as

$$\rho_1 v_{n1} = \rho_o v_{no} \qquad \text{Normal Mass Flux}$$

$$P_1 + \rho_1 v_{n1}^2 = P_o + \rho_o v_{no}^2 \qquad \text{Normal Momentum Flux}$$

$$v_{t1} = v_{to} \qquad \text{Tangential Momentum Flux}$$

$$\left(\frac{1}{2}\rho_1 V_1^2 + \frac{\gamma}{\gamma-1} P_1\right) v_{n1} = \left(\frac{1}{2}\rho_o V_o^2 + \frac{\gamma}{\gamma-1} P_o\right) v_{no} \qquad \text{Normal Energy Flux}$$

where the normal and tangential velocities are given by

$$v_{no} = V_o \cos\Theta \qquad v_{to} = V_o \sin\Theta$$

$$v_{n1} = V_1 \cos(\Theta+\phi) \qquad v_{t1} = V_1 \sin(\Theta+\phi)$$

and γ is the specific heat ratio.

If we define the incident Mach number (M_o) to be

$$M_o = V_o / \sqrt{\gamma P_o / \rho_o} \qquad (1)$$

then the jump relations for density, velocity and thermal speed, and the deflection angle ϕ are easily derived to be

$$\frac{\rho_1}{\rho_o} = \frac{(\gamma+1) M_o^2 \cos^2\Theta}{(\gamma-1) M_o^2 \cos^2\Theta + 2} \equiv \frac{1}{\Omega} \qquad \text{Density} \qquad (2)$$

$$\frac{V_1}{V_o} = \sqrt{\Omega^2 \cos^2\Theta + \sin^2\Theta} \qquad \text{Velocity} \qquad (3)$$

$$\frac{w_1}{w_o} = \sqrt{1 + \frac{\gamma-1}{2} M_o^2 \left(1 - \frac{V_1^2}{V_o^2}\right)} \qquad \text{Thermal Speed} \qquad (4)$$

$$\phi = \tan^{-1}\left[\left(\frac{1-\Omega}{\tan^2\theta+\Omega}\right)\tan\theta\right] \qquad \text{Deflection Angle} \qquad (5)$$

The angle between the incident flow direction and the shock normal is derived directly from the shock function derived in chapter 3 and is

$$\theta = \cot^{-1}\left[\left(\frac{b}{a}\right)^2\left(\frac{a+d-x}{y}\right)\right]$$

where $a = 177\ 7\ R_E$

$b = 56\ 7\ R_E$

$d = 13\ 5\ R_E$

and x is the X_{sw} coordinate of the position along the boundary

We will see later that the average solar wind Mach number (as defined in equation 1) measured by Explorer 35 is $M_o = 10$ The equations 2,3 and 5 are plotted in figure 37 for $M_o = 10$ and $\gamma = 5/3$.

3. Magnetopause Plasma Parameters

The values of the plasma parameters along the magnetopause are derived in several steps. The first step is to derive the values of the parameters just downstream of the bow shock at the sub-solar point If (ρ_o,V_o, M_o) are the incident density, velocity and Mach number, then by setting θ = 0 in equations 2 to 4, the values of the density, velocity and thermal speed (ρ_1,V_1,w_1) just behind the shock (see figure 36) are

$$\frac{\rho_1}{\rho_o} = \frac{(\gamma+1)M_o^2}{(\gamma-1)M_o^2+2} \equiv \Omega^{-1}$$

$$\frac{V_1}{V_o} = \Omega$$

$$\frac{\omega_1}{\omega_o} = \sqrt{1+\left(\frac{\gamma-1}{2}\right)M_o^2\left(1-\Omega^2\right)}$$

The next step is to derive the values of the pressure and density at the stagnation point (P_s,ρ_s in figure 36), where the velocity is zero, in terms of the upstream values The flow between the sub-solar bow shock and the stagnation point obeys Bernoulli's equation, which may be written in terms of the stagnation pressure (P_s) and density (ρ_s) as

$$\frac{1}{2}V^2 + \frac{\gamma}{\gamma-1}\frac{P}{\rho} = \frac{\gamma}{\gamma-1}\frac{P_s}{\rho_s} \tag{6}$$

Further, we assume the flow is adiabatic, thus

$$\frac{P}{\rho^\gamma} = \frac{P_s}{\rho_s^\gamma} \tag{7}$$

If for P, ρ and V we take the values P_1,ρ_1, and V_1 just inside the shock (where $P_1 = \rho_1 w_1^2$), then the stagnation pressure and density may be derived and are given by

$$\frac{P_s}{\rho_o V_o^2} = \left(\frac{\gamma+1}{2}\right)^{\frac{\gamma+1}{\gamma-1}} \frac{1}{\gamma\left[\gamma - \frac{\gamma-1}{2M_o^2}\right]^{1/(\gamma-1)}} \tag{8}$$

$$\frac{\rho_s}{\rho_o} = \frac{(\gamma+1)M_o^2}{(\gamma-1)M_o^2+2}\left(\frac{\gamma+1}{2}\right)^{\frac{2}{\gamma-1}}\left(\gamma - \frac{\gamma-1}{2M_o^2}\right)^{-\frac{1}{\gamma-1}} \tag{9}$$

The stagnation pressure and density are plotted for various Mach numbers and $\gamma = 5/3$ in figure 38 For large Mach numbers and $\gamma = 5/3$,

$$\frac{P_s}{\rho_o V_o^2} \simeq 88 + 265/M_o^2$$

$$\frac{\rho_s}{\rho_o} \simeq 4\ 41 - 11\ 9/M_o^2$$

To follow the flow along from the stagnation point downstream along the boundary, we again use equations 6 and 7 Now, however, there are three parameters (ρ,V,w) to be specified and we need one more equation

It has been shown (Spreiter et al , 1966) that the pressure along the boundary is well represented by the Newtonian pressure approximation,

$$P = P_o + K\rho_o V_o^2 \cos^2\theta \tag{10}$$

where (P_o,ρ_o,V_o) are the upstream values of pressure, density and velocity and θ is the angle between the incident flow direction and the boundary normal. θ is illustrated on the magnetopause trace in figure 36. K is chosen so that $P = P_s$ at the stagnation point (θ=0) and $P = P_o$ far downstream where the boundary is parallel to the incident flow direction (θ=90°) From these two conditions and the value of P_s given above, K is given by

$$K = \left(\frac{\gamma+1}{2}\right)^{\frac{\gamma+1}{\gamma-1}} \frac{1}{\gamma\left[\gamma - \frac{\gamma-1}{2M_o^2}\right]^{1/(\gamma-1)}} - \frac{1}{\gamma M_o^2} \tag{11}$$

K is plotted versus M_o for γ = 5/3 in figure 38 For large Mach numbers and γ = 5/3, $K \cong 88 - 335/M_o^2$.

From the boundary function derived in chapter 3, the value of θ at a position $X_{sw} = x$ along the magnetopause is

$$\theta = \cot^{-1}\left[\frac{b}{2a}\left(\frac{1}{1+\frac{10-x}{a}}\right)\frac{1}{\sqrt{\frac{10-x}{a}}}\right] \tag{12}$$

where a = 15.9 R_E, b = 23 88 R_E.

From the Bernoulli equation (equation 6), the adiabatic assumption (equation 7) and the Newtonian pressure approximation (equation 10 and equation 11), the density, velocity, and thermal speed along the magnetopause are given in terms of the upstream parameters by

$$\frac{\rho}{\rho_o} = \frac{(\gamma+1)M_o^2}{(\gamma-1)M_o^2+2}\left\{\left[\frac{\gamma+1}{2}\frac{1}{\left(\gamma M_o^2 - \frac{\gamma-1}{2}\right)}\right]\left[1+\gamma M_o^2 K\cos^2\theta\right]\right\}^{1/\gamma} \tag{13}$$

$$\left(\frac{V}{V_o}\right)^2=\left(\frac{\gamma+1}{\gamma-1}\right)\left(\frac{(\gamma-1)M_o^2+2}{(\gamma+1)M_o^2}\right)\left[1-\frac{2}{(\gamma+1)M_o^2}\left(\frac{2\gamma M_o^2-(\gamma-1)}{\gamma+1}\right)^{1/2}\left(1+\gamma M_o^2 K\cos^2\theta\right)\right] \quad (14)$$

$$\frac{\omega}{V_o}=\left[\frac{P_s}{\rho_o V_o^2}\left(\frac{\rho_o}{\rho}\right)\left(\frac{\rho}{\rho_s}\right)^{\gamma}\right]^{1/2} \quad (15)$$

where K and θ are given by equations 11 and 12, respectively.

The angle between the flow at the magnetopause and the incident flow is

$$\phi=\frac{\pi}{2}-\theta \quad (16)$$

since the flow is assumed to be everywhere parallel to the boundary. In figure 37 are plotted ρ/ρ_o, V/V_o and ϕ for $M_o = 10$ and $\gamma = 5/3$.

4. Comparison with Exact Calculations

As discussed above, the values of the plasma parameters between the boundaries are calculated by interpolating linearly between the values of the parameters calculated on the boundaries using equations 2 - 5 and 13 - 16 To compare this approximate method with the exact calculations of Spreiter et al (1966), let us consider the plasma parameters along the line A-A' in figure 36 This is a line at $X_{sw} = -10\ R_E$ and is in a region where both the Spreiter calculation and our approximate solution are available Spreiter has calculated the magnetosheath flow parameters for $M_o = 8$, $\gamma = 5/3$ From these calculations, the values of the magnetosheath density and velocity, normalized to the incident density and velocity, may be found along the line A-A' These parameters are plotted in figure 39 as a function of the distance from the X_{sw} axis between the magnetopause and shock In figure 39, the boundary distances calculated by Spreiter are

marked as MP SPREITER and SHOCK SPREITER Between these boundaries, the exact calculations show that the velocity is approximately constant and is on the order of 82% of the incident velocity The density rises from a value at the magnetopause of slightly less than the external density to a value about 3.5 times the external density at the bow shock

The positions of the boundaries at $X_{SW} = -10\ R_E$ as derived from the Explorer 33 measurements are shown in figure 39 as MP HOWE and SHOCK HOWE The discrepancy between the Spreiter boundaries and the measured boundaries has been discussed earlier. The values of the normalized density and velocity at the magnetopause calculated from equations 13 and 14 are 1 0 and 80, respectively, and the values at the shock calculated from equations 2 and 3 are 3.5 and .84, respectively

The linear interpolations between these values are shown in figure 39. As is evident from figure 39, the agreement between the exact calculation of Spreiter and the linear approximation is good; thus we are confident that valid comparisons may be made between theory and measurements using the results of the linear approximation method.

B. Explorer 35 Average Map

1. Introduction

During the months of operation of Explorer 35 for which plasma data are available, the spacecraft made 11 complete traversals of both the dawn and dusk magnetosheath at lunar distance. In addition, the spacecraft spent over half of the 11 months in the solar wind; thus the solar wind conditions between the magnetosheath traversals were monitored continuously In this section, the average magnetosheath flow measured by Explorer 35 during the 11 months of operation is compared with the average solar wind flow Where possible, the measured magnetosheath flow is normalized to the

measured average solar wind flow and compared with the linear theory discussed above This comparison gives us a limited understanding of the agreement between theory and measurement as pertains to magnetosheath flow at lunar distance. More importantly, however, the comparison demonstrates the severe limitations of magnetosheath flow study using only one spacecraft, where spacial and temporal variations in the flow cannot be separated.

2 Method of Analysis

To compare the Explorer 35 magnetosheath and solar wind data, the following averaging procedure is used The solar ecliptic plane is divided into 36 ten degree sectors in solar ecliptic longitude with the first sector starting at the X_{SE} axis. A separate average is made of all data taken in each ten degree sector during the eleven months of observations That is, the average velocity measured in each ten degree sector represents the average of 11 distinct sets of observed velocities, where one set is measured each month. Separate averages are made for magnetosheath and solar wind data. This averaging procedure is performed in an attempt to average out temporal variations in the plasma If this attempt is successful, the spacial magnetosheath flow structure may then be studied by comparing the averages from the magnetosheath sectors with each other and with the solar wind sector averages We will now examine the averaged Explorer 35 plasma measurements to see if this procedure successfully separates the temporal and spacial variations of the plasma parameters in the magnetosheath

3 Results

a) Flow Angles

The average flow angles are shown in figure 40 as a function of the solar ecliptic longitude of the sectors The angles plotted are the solar ecliptic longitude (ϕ) and latitude (λ) of the direction from which the

solar wind flows. Thus, ϕ and λ are positive for flow from the east of the sun and from the north, respectively Magnetosheath averages are indicated by the points plotted as open circles. The solar wind averages of both angles have observed standard deviations of ~3°. The magnetosheath standard deviations are ~5°.

For both flow angles, the solar wind averages vary little between sectors, indicating that temporal variations in these angles over the eleven months of observation have been successfully averaged away. The average longitude of the flow is $\phi_{SE} = -4°$, which is the typical aberration angle for radial solar wind flow. The average latitude of the flow is $\lambda_{SE} = 1\ 5°$ and this may be due to a small instrumental bias

The magnetosheath averages of the latitude show that the flow is deflected very little, if at all, from the ecliptic plane. Because the magnetosheath flow is deflected primarily in the solar-wind-direction-spacecraft plane, then the small out-of-the-ecliptic deflection of the flow is consistent with the orbit of the spacecraft, which is within 5° of the ecliptic plane The magnetosheath averages of the longitude show that, on both sides of the magnetotail, the flow is deflected on the order of 15° at the bow shock. The deflection decreases monotonically toward the magnetopause until, adjacent to the boundary, the flow returns to the incident flow direction The heavy line in figure 40 is the deflection calculated by the linear interpolation method described above for $M_o = 10, \gamma = 5/3$. The end points of the lines are the calculated deflections at the points on the average boundaries where the orbit of the moon intercepts the boundaries. The incident flow direction is assumed to be 4° from the west of the sun and both the average boundary locations and the calculated magnetosheath deflection reflect this 4° tilt. As may be seen, the observed and calculated deflections agree fairly well

We conclude that the averaging procedure successfully separates temporal and spatial variations in the plasma flow angles in the magnetosheath Furthermore, the spatial structure of these angles in the magnetosheath agrees well with the predictions of gas dynamic theory

b) Velocity and Density

The average velocities shown in figure 41 vary considerably between solar wind sectors Since the period of the moon and the rotation period of the sun are almost the same, then recurrent high velocity solar wind streams which rotate with the sun appear in the same part of the moon's orbit for several consecutive months. Thus, rather than averaging away, these velocity fluctuations add from one rotation to the next, resulting in the pattern in figure 41 The magnetosheath averages simply follow the general solar wind pattern Clearly, then, the variations of the velocity in the magnetosheath are temporal rather than spatial; thus these data may not be used to study the structure of the magnetosheath velocity pattern

The density averages in figure 42 also show appreciable temporal variations. Thus, the density structure may not be studied using these data. However, one interesting point does appear in figure 42. The solar wind sectors adjacent to the bow shock show unusually high average densities. These sectors are ones where only part of the measured data are from the solar wind and the rest are from the magnetosheath When the solar wind density is high, the boundaries are compressed by the resultant high dynamic pressure. Thus, solar wind density measurements tend to be made in these sectors during high density periods, and magnetosheath measurements tend to be made during lower density periods This effect results in the high observed average solar wind densities in the sectors adjacent to the bow shock The sectors where $120° < \phi_{sc} < 130°$ and $220° < \phi_{sc} < 230°$ show this effect most

strongly This illustrates one more limitation to using single spacecraft data to study magnetosheath flow

The study of Explorer 35 data shows that to map the flow of plasma in the magnetosheath, simultaneous data from the magnetosheath and from the solar wind are necessary to uniquely separate spacial from temporal variations in the flow We now proceed to a mapping of the flow in the magnetosheath using simultaneous data from Explorer 33 and Explorer 35.

C. Dual Satellite Magnetosheath Map

1 Introduction

To map the plasma flow in the magnetosheath, we use 369 hours of simultaneous data taken by both spacecraft when one spacecraft was in the solar wind and the other spacecraft was in the magnetosheath For each hour of data, the average parameters from both spacecraft are first formed Using the average solar wind dynamic pressure and flow direction, the position of the magnetosheath spacecraft with respect to the boundaries is calculated. The average magnetosheath parameters are then normalized to the average solar wind parameters Using the method described below, we are then able to determine the flow characteristics at 369 positions in the magnetosheath, i.e , to map the magnetosheath flow. This observed flow pattern is then compared with the predictions of the linear approximation to the theoretical flow, as described above. This method takes account of the effect of temporal solar wind plasma variations on both the boundary positions and the magnetosheath plasma parameters and allows a meaningful comparison between the observed and calculated magnetosheath flow

2. Method of Analysis

a) Normalization of Magnetosheath to Solar Wind Flow Parameters

In order to simplify the analysis, hourly averages of plasma para-

meters are used This accomplishes the dual purpose of smoothing the data and allowing us to neglect the time delay for flow between the two spacecraft The averages used are subject to several restrictions. First, any hours during which either spacecraft crossed the bow shock are rejected This criterion minimizes any effects of shock motion on the averages Second, to assure the statistical reliability of the averages, only hours which include at least 6 solar wind measurements and 11 magnetosheath measurements are used The maximum possible number of measurements per hour is 21

For hours of data which satisfy these criteria, the average magnetosheath density and velocity are divided by the corresponding average solar wind density and velocity to obtain values of the ratios between these parameters. In the final comparison between the observations and the theory, these ratios are compared directly with the ratios of ρ/ρ_o and V/V_o calculated by the linear approximation method presented above

The deflection of the solar wind is assumed to be entirely in the plane containing the magnetosheath spacecraft and the incident solar wind direction The flow may be deflected out of this plane as it crosses the bow shock, due to the presence of the interplanetary magnetic field, but the magnitude of the out-of-the-plane deflection is of the order of the ratio of the interplanetary magnetic field energy density ($B^2/8\pi$) to the solar wind flow energy density ($1/2\ \rho_o V_o^2$) For typical solar wind parameters, this deflection is on the order of 1°, which is much less than the deflection in the plane. Thus, the deflection angle ϕ is assumed to be simply the angle between the average solar wind and magnetosheath flow directions In the final comparison, this angle is compared directly with the magnetosheath flow angle ϕ calculated in the linear approximation theory.

The thermal speed averages are also available but are not used for two reasons First, the magnetosheath thermal speeds derived from the Explorer data are quite variable and may not be accurate The second reason stems from our assumption that the effect of the interplanetary magnetic field on the magnetosheath flow is second order. The macroscopic flow parameters (density, velocity, and flow angles) are not greatly affected by the presence of the interplanetary field These parameters reflect the directed flow of the plasma and the energy density of this flow is much greater than the energy density of the magnetic field The thermal energy density of the flow, however, is comparable to the field energy density To completely treat the thermal speeds theoretically, therefore, the magnetic field must be included We have not included the field in our calculations because the effect of the field is to render the theoretical treatment of magnetosheath flow intractable in a closed form Thus, we do not study the thermal speed structure in the magnetosheath because we do not have either accurate thermal speed observations or a reliable theoretical treatment of the magnetosheath thermal and magnetic field structure.

b) Location of the Magnetosheath Spacecraft

The location of the magnetosheath spacecraft (called the observer) with respect to the boundaries is determined in much the same way as was the observer position in the dual satellite boundary motion study above. As the solar wind direction and dynamic pressure change, the boundaries move and carry the magnetosheath flow pattern with them This changes the apparent position of the magnetosheath spacecraft with respect to the flow pattern. Other effects which cause the boundaries to move are discussed in conjunction with the dual-satellite boundary motion study above These effects are neglected here

Solar wind coordinates are again employed to determine the observer location The instantaneous X_{sw} axis orientation for each hour is first determined from the average solar wind direction as measured by the solar wind spacecraft (called the monitor). The X_{sw} and D_{sw} coordinates of the observer are then determined by transforming the observer location from solar ecliptic to solar wind coordinates For the dual spacecraft boundary motion study, the boundaries were then scaled to the solar wind dynamic pressure For the magnetosheath flow study, however, the observer position is scaled to the solar wind pressure In figure 43, the X and S coordinates of the observer are given by

$$X = \frac{10}{D_{nose}} X_{sw} \qquad S = \frac{10}{D_{nose}} D_{sw}$$

where D_{nose} is the distance to the sub-solar magnetopause given by equation 1, chapter 3 This procedure gives the coordinates of the observer with respect to boundaries of constant size The distance to the sub-solar magnetopause for these boundaries is 10 R_E Since the theoretical flow pattern maintains a constant relation to the boundaries, then in the (X,S) system of figure 43, the flow pattern is stationary The (X,S) coordinates of the observer therefore enable us to place the measured plasma parameter ratios with respect to the theoretical flow pattern We assume, then, that as the observer position in the (X,S) system changes, due to changes either in solar wind direction or dynamic pressure, the ratios measured are actually indicative of the spacial structure of the magnetosheath flow pattern.

We have seen how spacial changes due to motion of the observer with respect to the magnetosheath flow pattern are separated from temporal changes in the incident solar wind Spacial variations are removed by rotating and scaling the observer position with respect to the average boundaries. Temporal variations are removed by normalizing the magnetosheath data to the

solar wind data Let us now examine the resulting map of magnetosheath flow and compare this map with theory

c) Format of Results

The format used to plot the magnetosheath map is illustrated in figure 43. The X axis is first divided into 10 R_E sections, starting at the origin. For example, the values of X_1 and X_2 shown along the X axis in figure 43 might be -40 R_E and -50 R_E, respectively All plasma parameters ratios calculated for hours when the observer X coordinate is between X_1 and X_2 are then plotted as shown in the bottom drawing of figure 43. In this plot, the ordinate is S, the distance of the observer from the X axis, and the abscissa is one of the plasma parameter ratios A separate plot is made for each parameter As an example, consider a case where the calculated observer position is (X,S), as shown in figure 43. Since $X_1>X>X_2$, then the value of the parameter ratio (α_{ms}/α_{sw}) is plotted in the lower figure at a distance S from the origin Three such plots are made, one each for α = velocity, density and flow angle These plots, then, represent cross-sections of the magnetosheath flow, where each cross-sectional cut is 10 R_E wide.

Theoretical cross-sections of the parameters are calculated using the linear approximation method described above The distance (S) to the bow shock and magnetopause in the center of each 10 R_E section are determined from the average boundary shapes measured by Explorer 33. These positions are marked BS and MP, respectively, on the ordinate of lower figure in figure 43 The values of the velocity, density, and flow angle ratios at these two positions are calculated, using the equations derived previously. For an assumed solar wind Mach number (M_o), the magnetopause and bow shock ratios for each parameter are plotted on the respective ratio plots

at the distance MP and BS These values are then connected by a line, giving the linear interpolation for the values in the magnetosheath This is done for several assumed Mach numbers (M_1, M_2, M_3 in figure 43) The agreement between the observed and calculated flow may then be ascertained by noting the agreement between the plotted and theoretical ratios in the various 10 R_E plots.

d) Spatial Coverage

The spatial coverage of the magnetosheath during the 369 hours of observation is not uniform. The total number of hours of observation in each 10 R_E bin are given in figure 44. The region $-50\ R_E<X<-40\ R_E$ is observed extensively and our results will be derived primarily from studying the data in this region However, good spatial coverage is obtained for all regions for which $-60\ R_E<X<-20\ R_E$ and we will discuss the flow within this entire region. Due to the high thermal speeds of the magnetosheath flow in the forward magnetosheath, the data gathered for $X>-20\ R_E$ are too sparse and unreliable for a comparison between hourly averages and the theory.

3. Interplanetary Magnetic Field

a) Solar Wind Mach Number

The theoretical description of the flow is a function of the solar wind Mach number. In the hydrodynamic theory used here, this number is simply the flow velocity divided by the gas sound speed, $C_s = \sqrt{\frac{\gamma kT}{m}}$ Histograms of solar wind Mach numbers observed by the monitor spacecraft for those hours during which the observer spacecraft was in each 10 R_E bin for $-60\ R_E<X<-20\ R_E$ are shown in figure 44. The Mach numbers tend to occur with greatest frequency between 8 - 10 and range from a low of 5 to a high of 25.

The hydrodynamic Mach number is an upper limit to the actual solar wind Mach number Due to the presence of the interplanetary field, the velocity of a fast wave in the solar wind is usually higher than the gas sound speed, C_s. Thus, the actual Mach number is usually lower than the hydrodynamic Mach number. Since the magnetic fields for the times of observation are not utilized, we can only estimate the Mach numbers which should actually be used in the theory.

In the presence of an interplanetary magnetic field, one speed of propagation of a disturbance is the fast wave velocity, C_f If C_s and C_A are the sound and Alfven speeds, respectively, and if θ_B is the angle between the propagation direction and the magnetic field direction, then

$$C_f = \frac{1}{\sqrt{2}}\left[\left(C_s^2 + C_A^2\right) + \sqrt{\left(C_s^2 + C_A^2\right)^2 - \left(2 C_s C_A\right)^2 \cos^2\theta_B}\right]^{1/2}$$

In the shock jump relations, the relevant Mach number is the solar wind velocity divided by the velocity C_f in the direction normal to the shock Thus, the Mach number is dependent upon the position along the shock contour For the interplanetary field in the average spiral direction, the dawn Mach number is derived for $\theta_B \sim 0$, while the dusk Mach number is derived for $\theta_B \sim \frac{\pi}{2}$. If we let $C_s = C_a$, then these two extreme cases result in the following Mach numbers

Dawn Side $(\theta_B = 0)$ $M_f = M_s$

Dusk Side $(\theta_B = \frac{\pi}{2})$ $M_f = \frac{1}{\sqrt{2}} M_s$

where $M_f = \frac{V}{C_f}$ and $M_s = \frac{V}{C_s}$.

Since the dawn and dusk flow are not separated in the analysis, then this calculation allows us a rough feeling for the difference between the actual Mach numbers (M_f) and the measured Mach numbers (M_s).

b) Method of Estimation of Effect of Magnetic Field

In addition to lowering the Mach number, the magnetic field also affects the jump conditions of the flow at the bow shock Since we assume $\underset{\sim}{B} = 0$ in our analysis, we wish to see how much effect $\underset{\sim}{B}$ might have if it were included. To estimate the effect of the inclusion of the interplanetary magnetic field on the calculated flow we use the complete Rankine-Hugoniot relations to calculate the shock jump conditions along the shock contour derived from the Explorer 33 shock crossings. The complete R-H relations are given by Chao (1970) and will not be repeated here In these relations, we assume $C_A = C_s$ and, further, we assume the field is in the average spiral direction. The jump relations are then calculated for the dawn and dusk sides for various hydrodynamic Mach numbers ($M_s = V/C_s$) and the results are included on the final cross-sectional data plots This procedure allows us insight into how much our results might change if the interplanetary field were included in both the data and theoretical analyses

4. Results

a) Velocity

The velocity cross-sections for $-60\ R_E < X < -20\ R_E$ are shown in figures 45a to 45d. Since the largest number of observations were made for $-50\ R_E < X < -40\ R_E$, we discuss the data plotted in figure 45c in detail. The point marked SW in figure 45c is the average ratio of measured velocities between the two spacecraft for all times during the operation of the Explorer 35 instrument when both spacecraft were in the solar wind The average falls near 1.0, which indicates that there is no significant offset in the velocity measurements between the two spacecraft The error bar represents the standard deviation of the measured ratios, and thus gives the experimental

uncertainty in the measured velocity ratios

The observed velocity ratios plotted in figure 45c indicate that the magnetosheath velocity is typically slightly less than the corresponding solar wind velocity The lines in figure 45c represent the calculated velocity ratios for assumed Mach numbers of 3, 4, 6, and 10. As is evident from the plot, the theory also predicts that the velocity ratio is slightly less than unity. Thus, within the scatter of the observed ratios, we see that the theory and the observation agree

The scatter of observed magnetosheath velocity ratios in figure 45c may be due to several effects First, the scatter is of the order of the solar wind scatter in the velocity ratio (shown by the error bar), thus much of the magnetosheath scatter is probably due to experimental fluctuations Second, the histogram of solar wind Mach numbers (figure 44) which correspond to the observed ratios shows a large spread in Mach number The calculated lines in figure 45c show a small dependence on Mach number, thus some of the observed scatter in the ratio may be due to the variations in the solar wind Mach number Finally, the interplanetary magnetic field may cause variations in the magnetosheath flow. Using the complete Rankine-Hugoniot relations as described above, the velocity ratio at the shock for a Mach number of 10 is shown in figure 45c for both the dawn and dusk sides. The effect of including the magnetic field is to increase the calculated velocity at the dawn shock and to decrease it on the dusk side The difference between the dawn and dusk ratios for $M_o = 10$ is of the order of the observed scatter in the observed magnetosheath ratios Thus, some of the observed scatter may be due to the presence of the interplanetary magnetic field.

The agreement between theory and observation shown in figure 45c is also evident in the cross-sectional plots shown in figures 45a, 45b, and 45d

From these plots, we conclude that the flow velocity in the magnetosheath between X = -20 R_E and X = -60 R_E is, on the average, relatively constant relative to and slightly less than the solar wind velocity

b) Deflection angle

The cross-sectional plots of the angle between the average solar wind and magnetosheath flow directions are shown in figures 46a to 46d The average value of this angle for times when both spacecraft were in the solar wind is marked 'SW AVERAGE' in figure 46c. Since this angle is always greater than zero, then the average solar wind value is a direct measure of the experimental spread in the angle Thus, any scatter on the order of 3° or less may be attributed to experimental fluctuations

Referring to figure 46c, we see that the average magnetosheath deflection is much greater than 3°; thus the deflection plot represents a real deflection of the flow around the magnetosheath As is evident from figure 46c, the deflection is greatest at the bow shock and decreases closer to the magnetopause The theoretical lines indicate that this trend is in complete accordance with hydrodynamic theory

The observed scatter of the deflection angles is due to three possible mechanisms First, the experimental error of 3° is of the order of much of the scatter Second, the scatter is of the order of the calculated change in the deflection angle of the flow for changes in the Mach number between 4 and 16. Third, the inclusion of the magnetic field produces large changes between the dawn and dusk deflection of the flow at the shock. These three effects may combine to produce the observed amount of scatter of the magnetosheath deflection angles

Near the magnetopause, the scatter in the deflection angle is much larger than for the rest of the magnetosheath As we have seen, the mag-

netopause is in motion most of the time and the largest effect this motion should have on the magnetosheath flow adjacent to the boundary is to perturb the flow direction Thus, the large deflections observed near the magnetopause are probably due to wave motion of the boundary

The cross-sectional plots shown in figures 46a, 46b, and 46d show basically the same features as are evident in figure 46c. The boundary motion perturbations adjacent to the magnetopause are particularly evident in figure 46b The plot in figure 46d indicates that the flow is still deflected by 10° - 15° at the bow shock at ~60 R_E downstream from the earth This means the shock is still fairly strong and well defined at this distance

Another feature of the deflection angle evident from a comparison of the four cross-sectional plots is the decrease in average deflection with increased downstream distance from the earth This simply shows the downstream flow returning to the incident solar wind direction To examine whether this decrease agrees with the hydrodynamic theory, we make a plot of the deflection angle as a function of the distance X (figure 43) for those times when the observer is in the middle third of the magnetosheath. This corresponds to observer positions S between the lines S_1 and S_2 in figure 43 Thus, this plot represents a cut through the center of the magnetosheath roughly parallel to the flow. The plot is shown in figure 47

The line in figure 47 is the theoretical deflection midway between the magnetopause and the bow shock for M_o = 10. As is evident, the observed deflection compares well with the calculated deflection between the earth and ~70 R_E downstream

We conclude that, within the experimental uncertainties and the theoretical assumptions, the observed magnetosheath flow direction, between

the earth and 60 R_E downstream of the earth, is well described by the hydrodynamic theory

c) Density

The cross-sectional plots of the observed density ratios are shown in figures 48a to 48d From the solar wind average of the ratio shown in figure 48c, we see that no large density offset exists between the two spacecraft. Also, the scatter of the magnetosheath density ratios is much larger than the experimental fluctuations indicated by the error bar on the solar wind average point

Two characteristics of the observed density ratios are immediately apparent Referring to figure 48c, we see that there is a clear agreement between the observed trend in the density and the calculated trend between the magnetopause and the bow shock That is, both theory and observation indicate that the density rises from less than the solar wind value at the magnetopause to 2-3 times the solar wind density at the bow shock. Second, the scatter of the observed ratios also increases from the magnetopause to the bow shock. Since the theoretical lines for different Mach numbers also diverge between the magnetopause and the bow shock, this strongly suggests that the observed scatter is due to fluctuations in the solar wind Mach number

To examine the dependence of the measured density ratios on the solar wind Mach number, we replot figure 48c in figure 49. In the latter figure, the density ratios plotted as open circles were measured during hours when the observed solar wind Mach number was greater than ten Conversely, the ratios plotted as solid circles were measured during hours when the observed solar wind Mach number was less than ten. From figure 49, we see that there is a separation of the points, with the ratios measured during higher Mach

number periods tending to be larger than the ratios measured during low Mach number periods This is direct evidence for the Mach number dependence of the magnetosheath density predicted by hydrodynamic theory

All the scatter observed in the ratios is not explained by the Mach number dependence The interplanetary magnetic field may also affect the density ratios. This is evident from the dawn and dusk ratios (shown in figure 48c) computed at the bow shock in the presence of a magnetic field. In figure 49, the line of separation for M = 10 is shown, but it appears that the actual line may be slightly below this. From the dawn and dusk shock density ratios for $M_S = M_A = 10$ which are shown in figure 49, it is apparent that the theoretical line would be lower if the magnetic field were included in the calculation Thus, some of the scatter in the observed density ratios may be due to the interplanetary magnetic field.

The other cross-sectional plots (figure 48a, 48b, and 48d) show the same general agreement between the observations and the theoretical calculations as did figure 48c. Thus, we conclude that the magnetosheath density between -20 R_E and -60 R_E downstream of the earth is well explained by the hydrodynamic theory

One important point to notice in the density plots is that the density adjacent to the magnetopause is less than the solar wind density This is due, in the hydrodynamic theory, to the irreversible nature of the flow across the shock The entropy of the gas is given by $S = \ln\left(\frac{P}{\rho^{\gamma}}\right)$, where P is the pressure and ρ is the mass density. Let the solar wind pressure and density be (P_o, ρ_o) and let the value of these parameters well downstream on the stagnation streamline be (P, ρ). Then the change in entropy on the stagnation streamline between the upstream solar wind and the downstream magnetosheath is $\Delta S = \ln\left(P/\rho^{\gamma}\right) - \ln\left(P_o/\rho_o^{\gamma}\right)$.

As the downstream flow returns to the conditions of the upstream flow, then $P \longrightarrow P_o$ to balance transverse pressures in the flow Entropy is conserved everywhere along the stagnation streamline except at the shock Since the flow across the shock is irreversible, then the entropy must increase; thus $\Delta S>0$ Therefore, as $P \longrightarrow P_o$, we must have $\rho<\rho_o$ This is what is actually observed and the observations thus provide an example of the irreversible nature of the flow across the bow shock

CHAPTER 5

Summary and Conclusions

The magnetotail symmetry axis, as determined from the positions of magnetopause crossings observed at lunar distance by Explorer 35, is aligned with the average solar wind direction. Thus, any dawn-dusk asymmetry introduced into the magnetosheath flow by the interplanetary spiral field (Walters, 1964, Hundhausen et al , 1969) does not result in a magnetotail alignment asymmetry of more than the measurement uncertainty of ±2°. The magnetopause below the ecliptic for $-80\ R_E < X_{SE} < -40\ R_E$ is axisymmetric about the X_{SW} axis The observed symmetry was determined from three years of Explorer 33 data and contradicts the asymmetry found by Behannon (1968). The magnetopause profile, determined from the Explorer 33 magnetopause crossing positions, shows general agreement with the fluid calculations of Spreiter and Alksne (1969) However, the observed magnetopause flares out more than the predicted boundary in the dawn-dusk meridian This discrepancy may be due to the magnetospheric particle population, which was neglected in the theoretical calculation

The bow shock profile was obtained to 115 R_E downstream of the earth. The crossings observed at this distance showed that the shock is still well defined in the plasma data at this distance This is in agreement with the recent Pioneer 8 magnetic field observations of the bow shock between 100 R_E and 170 R_E downstream from the earth (Bavassano et al., 1971).

The response of the bow shock to changes in the incident solar wind pressure and direction was examined using dual satellite measurements. The two examples studied indicate that the bow shock moves so as to align with the incident wind direction In addition, the shock expands and contracts

in response to upstream pressure changes These observed responses probably represent motion of the shock in response to changes in the orientation and size of the magnetospheric cavity.

A study of magnetopause motion using dual satellite observations showed several examples of observed magnetotail boundary motion which were caused by observed solar wind pressure and/or direction changes The delay times observed between the solar wind changes and the resulting magnetopause motion indicated that the magnetopause may require as long as an hour to adjust to new solar wind flow conditions An example of magnetopause motion in the presence of a quiet solar wind was also presented.

The average nature of the magnetopause motion at lunar distance was studied further using Explorer 35 data The motion appears to consist of two superimposed components with time scales of $\sim$15 minutes and $\sim$1 hour. The results of a motion simulation indicate that the amplitude of the second motion is $\sim$ 3 times the amplitude of the first The dawn magnetopause motion amplitude is twice that of the dusk motion This may be due to observed temporal velocity differences between the two sides. Alternately, the dawn bow shock may be more effective in producing magnetosheath turbulence and this may be reflected in increased magnetopause motion

The magnetopause motion simulation indicates that a boundary layer thickness of $\sim$2 R_E is consistent with the observed boundary crossing duration times This thickness is of the order of, though larger than, thicknesses calculated using various theoretical assumptions

The flow of plasma in the magnetosheath was examined using average observations from one year of Explorer 35 operation General agreement was found between the measured average magnetosheath flow angles and the predictions of hydrodynamics The velocity and density averages, however, served

only to demonstrate the necessity of dual satellite observations in mapping magnetosheath flow

Dual satellite observations of the flow in the region $-60\ R_E < X_{SE} < -20\ R_E$ show general agreement between the observed velocity, density, and deflection angle, and the predictions of hydrodynamics The possible effect of the interplanetary magnetic field on the results was estimated and was found to be large enough to explain much of the observed data scatter The dependence of the calculated density ratios and deflection angles on the upstream Mach number was also of the order of the scatter and the Mach number dependence of the observed density ratios was demonstrated explicitly The effect of the irreversibility of the flow across the bow shock on the downstream stagnation line density was also shown

The general agreement between the observations and hydrodynamic theory further confirms the applicability of fluid concepts to the magnetosheath flow problem The observed sharpness of the bow shock indicates that the plasma flow has a very small mean free path in the shock region. The results of the above magnetosheath flow study, however, show that the general flow away from the bow shock also has a mean free path short compared to magnetospheric dimensions

Appendix A Direction of solar wind coordinate axes in solar ecliptic coordinates

Let

$\vec{\mu}$ = earth's dipole direction, in solar ecliptic coordinates,

(ϕ_w, λ_w)= solar ecliptic longitude and latitude of the direction from which the solar wind comes,

$(\hat{x}_{sw}, \hat{y}_{sw}, \hat{z}_{sw})$= unit vectors along the three solar wind coordinate directions, expressed in solar ecliptic coordinates,

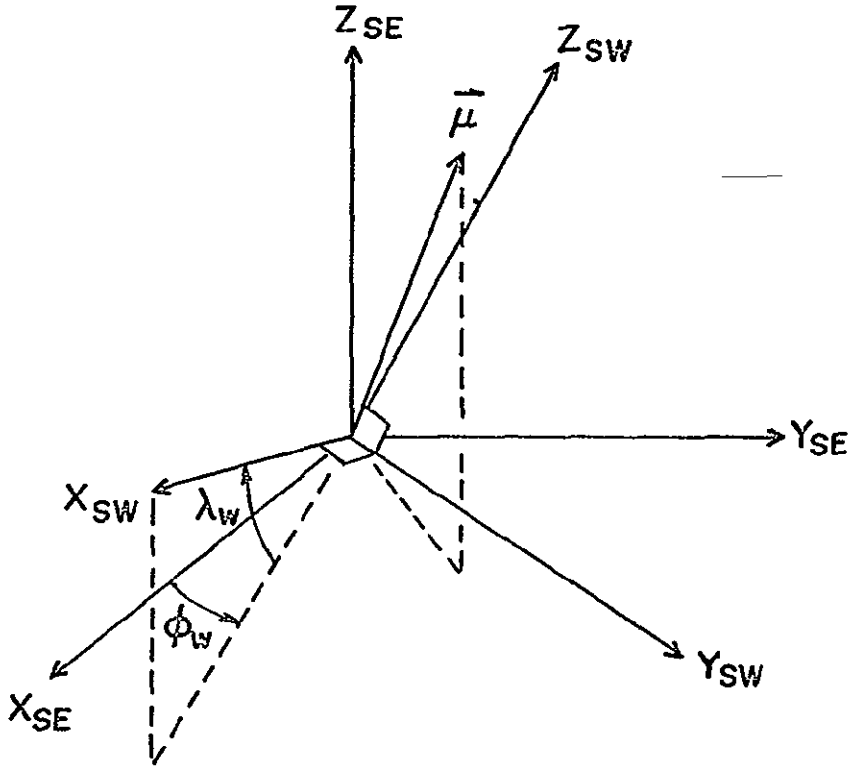

then

$$\hat{x}_{SW} = \cos\lambda_W \cos\phi_W \, \hat{x}_{SE} + \cos\lambda_W \sin\phi_W \, \hat{y}_{SE} + \sin\lambda_W \, \hat{z}_{SE}$$

$$\hat{y}_{SW} = \pm \left| \vec{\mu} \times \hat{x}_{SW} \right| \Big/ \sqrt{1 - (\vec{\mu} \cdot \hat{x}_{SW})^2}$$

$$\hat{z}_{SW} = \hat{x}_{SW} \times \hat{y}_{SW}$$

where the sign of $\hat{y}_{SW}$ is chosen so that $\hat{z}_{SW} \cdot \hat{z}_{SE} > 0$ This assures that the Z_{SW} axis lies in the northern solar ecliptic hemisphere.

If a vector $\vec{R}_{SE}$, such as the spacecraft location, is specified in solar ecliptic coordinates, then the three components of the vector in solar wind coordinates are given by

$$R_{SW\,x} = \vec{R}_{SE} \cdot \hat{x}_{SW}$$

$$R_{SW\,y} = \vec{R}_{SE} \cdot \hat{y}_{SW}$$

$$R_{SW\,z} = \vec{R}_{SE} \cdot \hat{z}_{SW}$$

Dipole direction in solar ecliptic coordinates

The direction $\vec{\mu}$ in solar ecliptic coordinates is most directly derived in celestial coordinates, as shown in the following figure

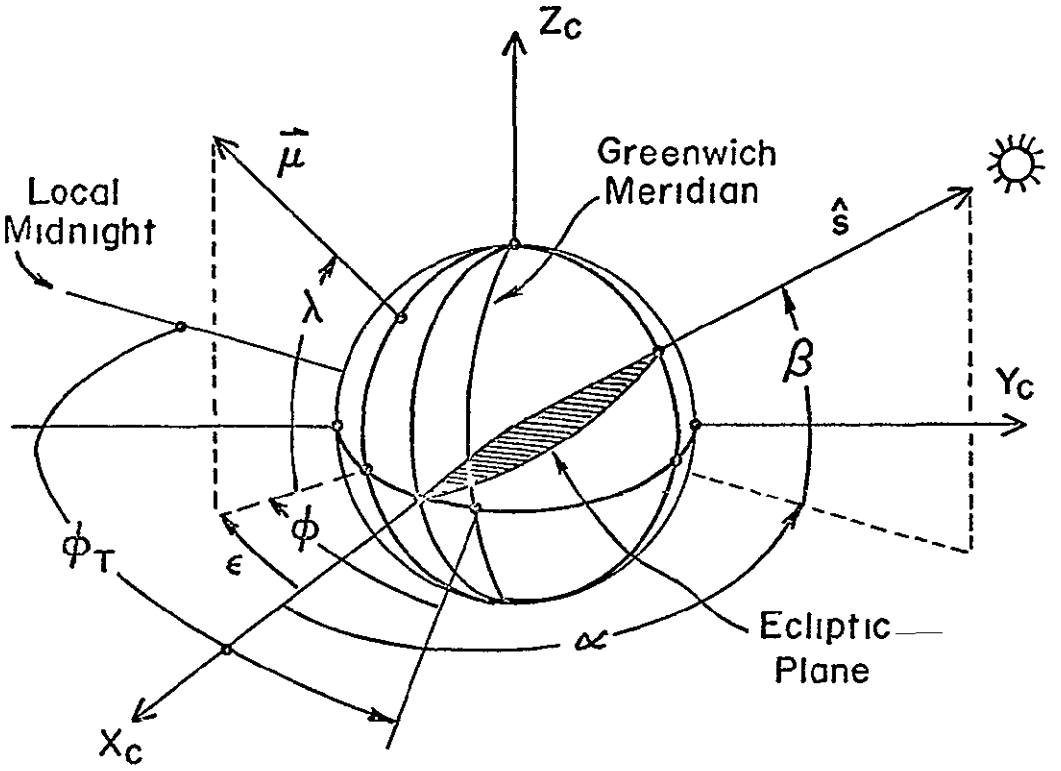

Let

(α, β) = right ascension and declination of the sun at universal time T,

(ϕ, λ) = geographic coordinates of the magnetic dipole,

ϕ_T = degrees of rotation of Greenwich past 0000 UT

Since both the vernal equinox (X_c) and the direction of the sun ($\hat{S}$) lie in the solar ecliptic plane as seen from the earth, then these two vectors define the ecliptic in celestial coordinates If we let

$(\hat{x}_c, \hat{y}_c, \hat{z}_c)$= celestial unit vectors

then the solar ecliptic coordinate unit vectors $(\hat{x}_{SE}, \hat{y}_{SE}, \hat{z}_{SE})$ are given by

$$\hat{x}_{SE} = \hat{S}$$

$$\hat{z}_{SE} = \left(\hat{x}_c \times \hat{S}\right) \Big/ \sqrt{1-(\hat{x}_c \cdot \hat{S})^2}$$

$$\hat{y}_{SE} = \hat{z}_{SE} \times \hat{x}_{SE}$$

where

$$S_x = \cos\beta \cos\alpha$$
$$S_y = \cos\beta \sin\alpha$$
$$S_z = \sin\beta$$

The direction of the dipole in celestial coordinates $(\hat{\mu}_x, \hat{\mu}_y, \hat{\mu}_z)$ is given by

$$\hat{\mu}_x = \cos\lambda \cos\varepsilon$$
$$\hat{\mu}_y = -\cos\lambda \sin\varepsilon$$
$$\hat{\mu}_z = \sin\lambda$$

where $\varepsilon = \pi - (\alpha + \phi_T - \phi)$

The components of the dipole in solar ecliptic coordinates are obtained by dotting $\hat{\mu}$ onto the three solar ecliptic unit vectors, thus

$$\mu_{SE\,x} = \hat{\mu} \cdot \hat{x}_{SE}$$
$$\mu_{SE\,y} = \hat{\mu} \cdot \hat{y}_{SE}$$
$$\mu_{SE\,z} = \hat{\mu} \cdot \hat{z}_{SE}$$

These three components are the ones used in the determination of solar wind unit vectors above The necessary constants are

ϕ = 70.1° W

λ = 78 5° N

Direction of the sun ($\hat{S}$) in celestial coordinates

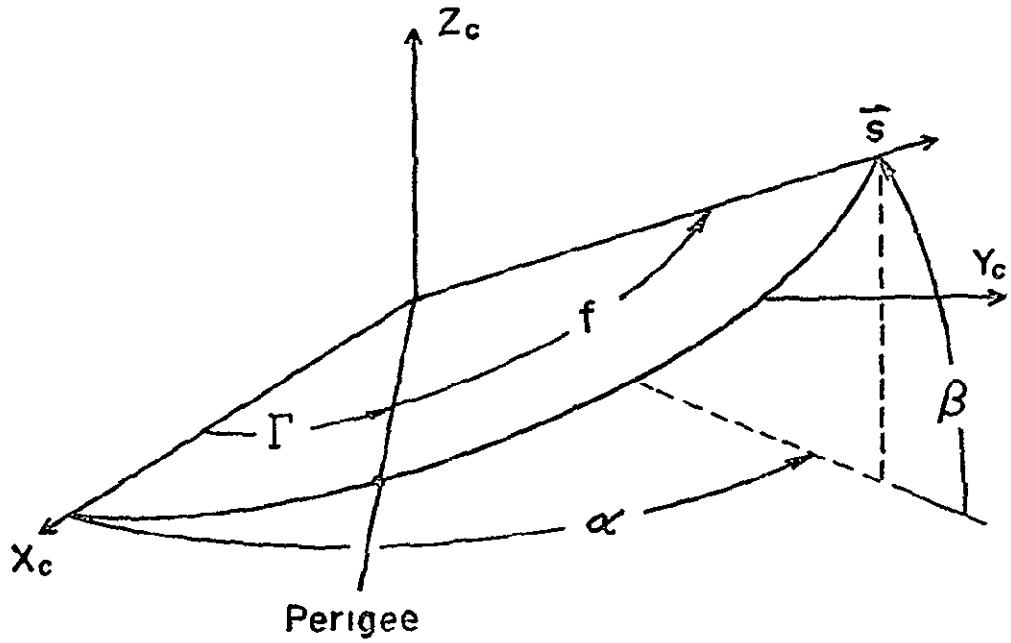

Let

f = sun true anomaly

M = sun mean anomaly ,

t = time

n = mean angular velocity of sun

τ = time of perigee passage

Γ = longitude of perigee

e = eccentricity of sun's orbit

i = inclination of earth's spin axis to the ecliptic

then

$$M = n(t-\tau)$$

$$f \approx M + 2e \sin M$$

$$\tan\alpha = \tan(\Gamma+f)\cos i$$

$$\sin\beta = \sin(\Gamma+f)\sin i$$

FIGURE CAPTIONS

Figure

1 Relation between solar ecliptic coordinates and spacecraft coordinates (ϕ_S, λ_S) are the solar ecliptic longitude and latitude of the spacecraft spin axis β is the roll angle between the "see-sun" direction and the peak plasma flux direction, measured positive in the direction of spacecraft rotation For the case shown, the current on plate B is larger than the current on plate A

2 Locations of Explorer 33 and Explorer 35 at the times of the bow shock (S1-S6) and magnetopause (M1-M5) crossing examples discussed in chapter 2 The abscissa is the solar ecliptic X axis and the ordinate is the cylindrical distance from the X axis

3-13 Examples of plasma data taken during magnetopause and bow shock crossings For all figures, the abscissa is the time, with ten minutes between tic marks For parts a and b of each figure, each hour is labelled with the decimal day and hour For parts c and d, each hour is labelled and the decimal day is given at the bottom of the figure The ordinates of part a to part d are as follows a) from top to bottom angle between solar direction and largest flux measurement (positive in the direction of satellite rotation), phase (denoting which plate received the largest current), integral positive ion current measurement, integral electron measurement, b) differential positive ion current measurements, with the lowest energy channel at the bottom, c) derived plasma flow velocity (V, km/sec) and proton number density (ρ, cm^{-3}), d) derived solar ecliptic longitude and latitude of the direction from which the flow comes (ϕ, λ), and the derived plasma thermal speed (ω_o)

The date, the boundary crossed, and the spacecraft for each figure are as follows

3 July 28, 1966, bow shock; Explorer 33

4 July 27, 1966, bow shock, Explorer 33

5 February 1, 1967, bow shock, Explorer 33

6 September 1, 1967, bow shock, Explorer 33

7 March 23, 1969, bow shock, Explorer 33

8 August 24, 1967, bow shock, Explorer 35

9 July 29, 1966, magnetopause, Explorer 33

10 August 3, 1966, magnetopause, Explorer 33

11 June 13, 1968, magnetopause, Explorer 35

12 February 15, 1968, magnetopause, Explorer 35

13 August 17, 1967, magnetopause, Explorer 35

14 Y_{SW}-Z_{SW} Explorer 33 trajectory for all times between July 1, 1966 and January 16, 1969 when $-100\ R_E < X < -40\ R_E$. The rotation of the X_{SW} axis is -4° in the ecliptic plane. The heavy and light portions of the orbits are the magnetosphere and the magnetosheath portions, respectively. The heavy circle has a radius of 28 R_E

15a The Explorer 33 orbits for all times between July 1, 1966, and January 16, 1969, when the spacecraft region could be determined The abscissa and ordinate are the X_{SW} axis and the $\sqrt{Y^2_{SW}+Z^2_{SW}}$ axis, respectively. The average boundary shapes are also shown

15b Same as figure 15a for all times between January 16, 1969, and April 21, 1969

16 All Explorer 33 bow shock crossings observed between July 1, 1966 and April 21, 1969 The coordinates are identical to those in figure 15 The subjective average shock shape is also shown.

17 All Explorer 33 magnetopause crossings observed between July 1, 1966 and April 21, 1969 The coordinates are identical to those in figure 15 The subjective average shape (labelled AVERAGE) and the theoretical curve of Spreiter and Alksne (1969) (labelled THEORETICAL) are also shown

18 Illustration of the distances used in the dual satellite boundary motion study

19 Locations of the monitor and observer spacecraft during dual satellite observations of bow shock motion.

20 Bow shock motion observed by Explorer 35 on September 13, 1967

21 Bow shock motion observed by Explorer 35 on February 17, 1968.

22 Locations of the monitor and observer spacecraft during dual satellite observations of magnetopause motion.

23 Magnetopause motion observed by Explorer 35 on February 11 and 12, 1968

40 Measured average solar ecliptic longitude (ϕ) and latitude (λ) of the direction from which the solar wind comes versus the solar ecliptic longitude of the moon The points plotted as open circles were measured in the magnetosheath The dashed lines are the theoretical angles.

41 Same as in figure 40 for measured bulk flow velocity.

42 Same as in figure 40 for measured number density

43 Illustration of method used to compile cross-sections of magnetosheath flow parameters

44 Histograms of average solar wind Mach numbers measured during the hours used to compile the flow cross-sections for $-20\ R_E > X_{SW} > -60\ R_E$

45a-d Velocity ratio cross-sections for $-60\ R_E < X < -20\ R_E$ The locations of the magnetopause (MP) and bow shock (BS) are marked on the S axis The results of the linear flow calculation are shown for various Mach numbers. The solar wind average and standard deviation are shown in part c, along with the computed shock jump on the dawn and dusk sides for $M_0 = 10$ The points plotted with the symbols ☐ and ⧖ were measured when the observer was Explorer 33 and Explorer 35, respectively.

46a-d Same as figure 45 for the deflection angle

47 Deflection angle measured in the center third of the magnetosheath versus downstream distance. Theoretical curve for $M_0 = 10$ is also shown.

48a-d Same as figure 45 for the density ratio.

49 Cross-section of the density ratio for $-50\ R_E < X < -40\ R_E$ showing the separation by Mach number.

General Spin Orientation

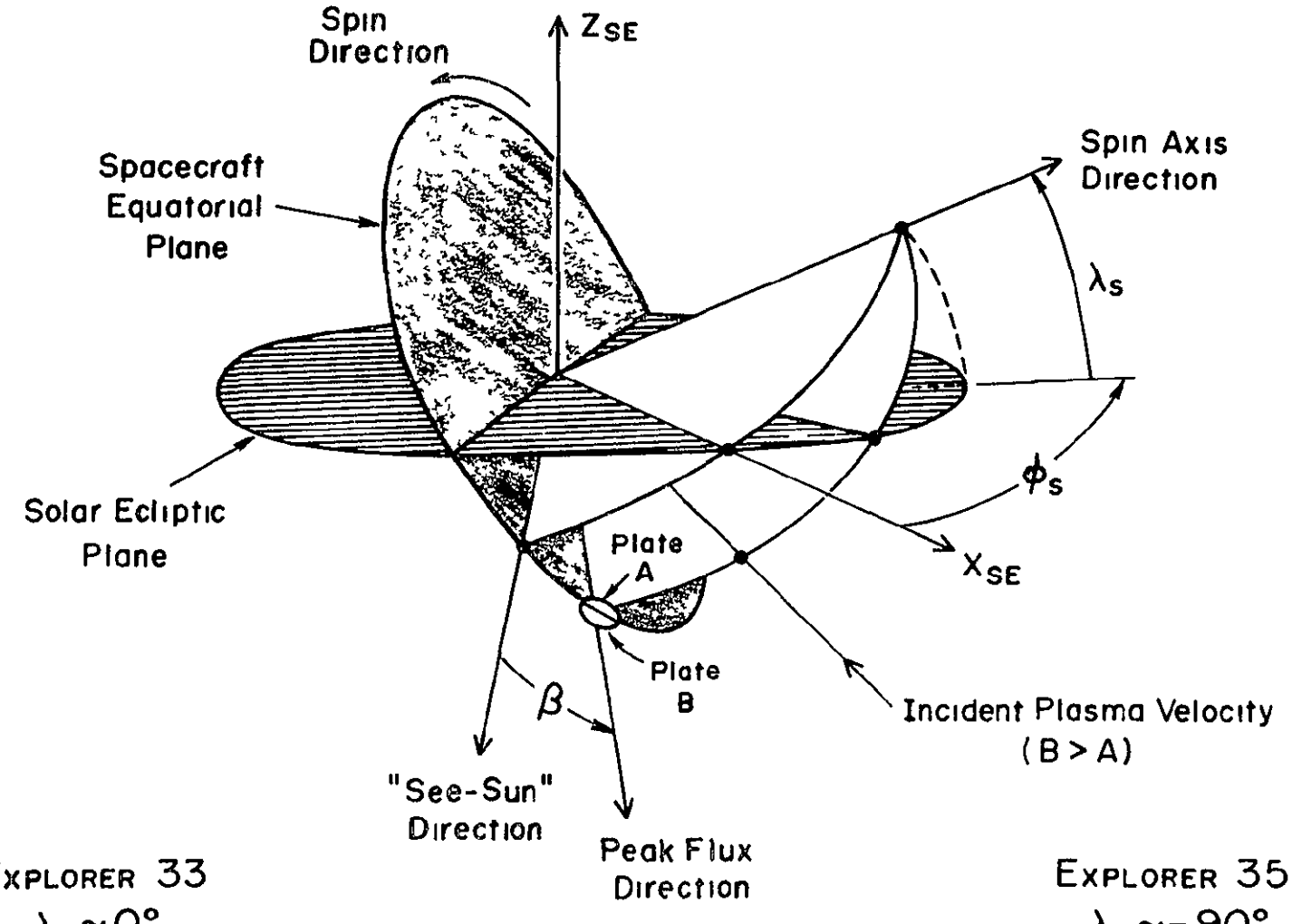

Explorer 33
$\lambda_s \sim 0°$

Figure 1

Explorer 35
$\lambda_s \sim -90°$

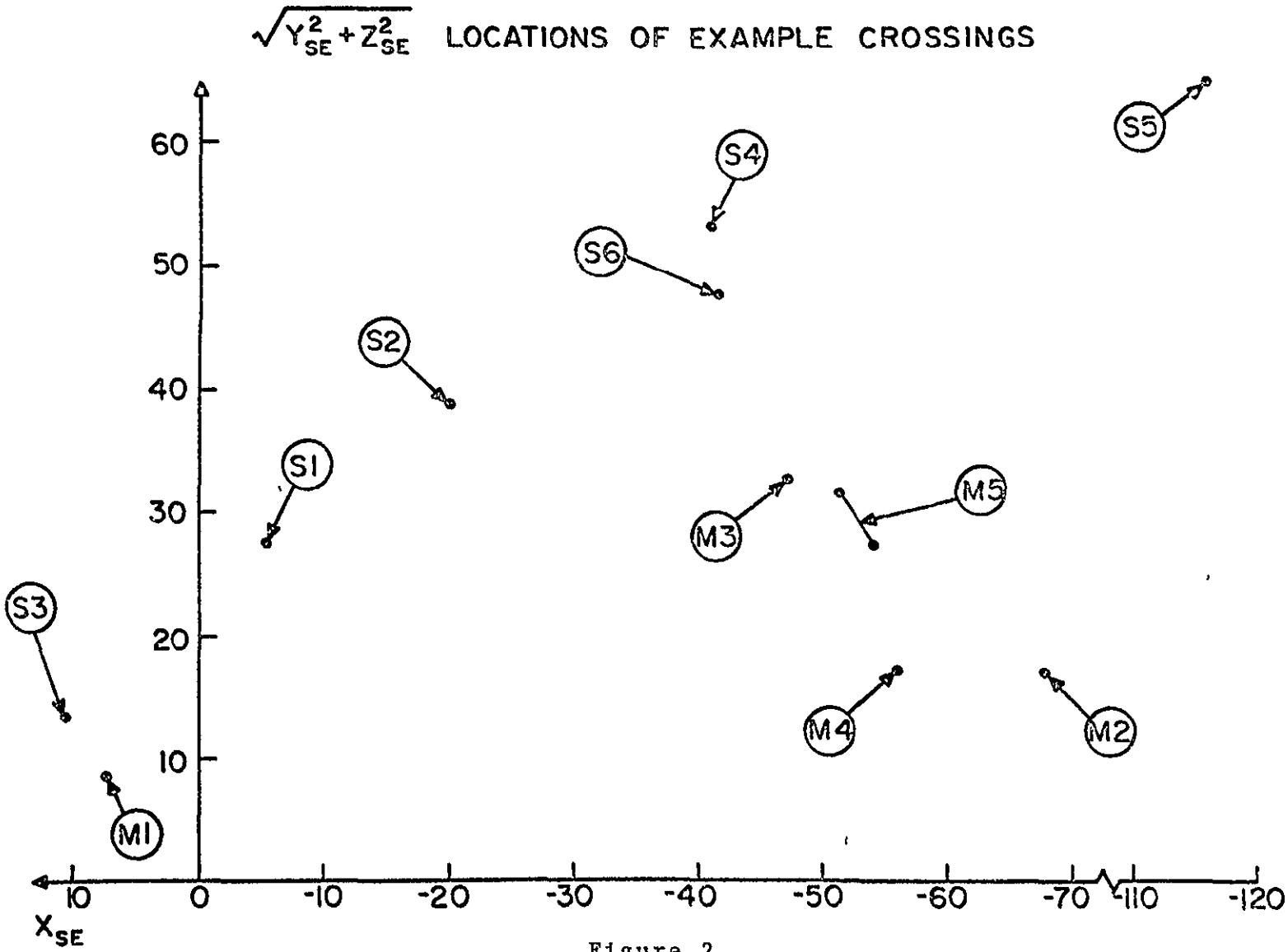
$\sqrt{Y_{SE}^2 + Z_{SE}^2}$ LOCATIONS OF EXAMPLE CROSSINGS
60
50
40
30
20
10
S1
S2
S3
S4
S5
S6
M1
M2
M3
M4
M5
10
0
-10
-20
-30
-40
-50
-60
-70
-110
-120
X_{SE}

Figure 2

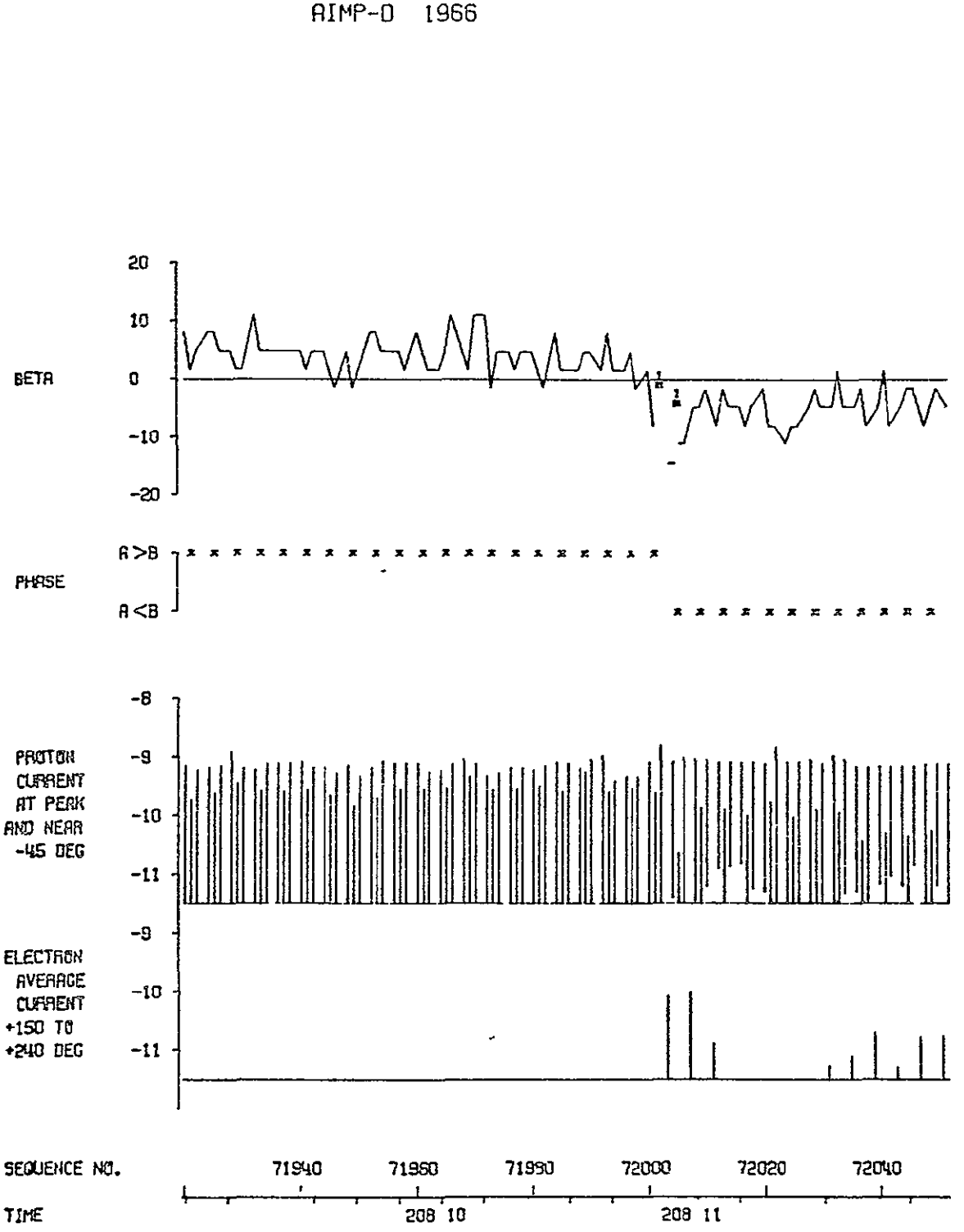
AIMP-D 1966
BETA
20
10
0
-10
-20
PHASE
A>B
A<B
PROTON CURRENT AT PEAK AND NEAR -45 DEG
-8
-9
-10
-11
ELECTRON AVERAGE CURRENT +150 TO +240 DEG
-9
-10
-11
SEQUENCE NO.
71940
71960
71980
72000
72020
72040
TIME
208 10
208 11

Figure 3a

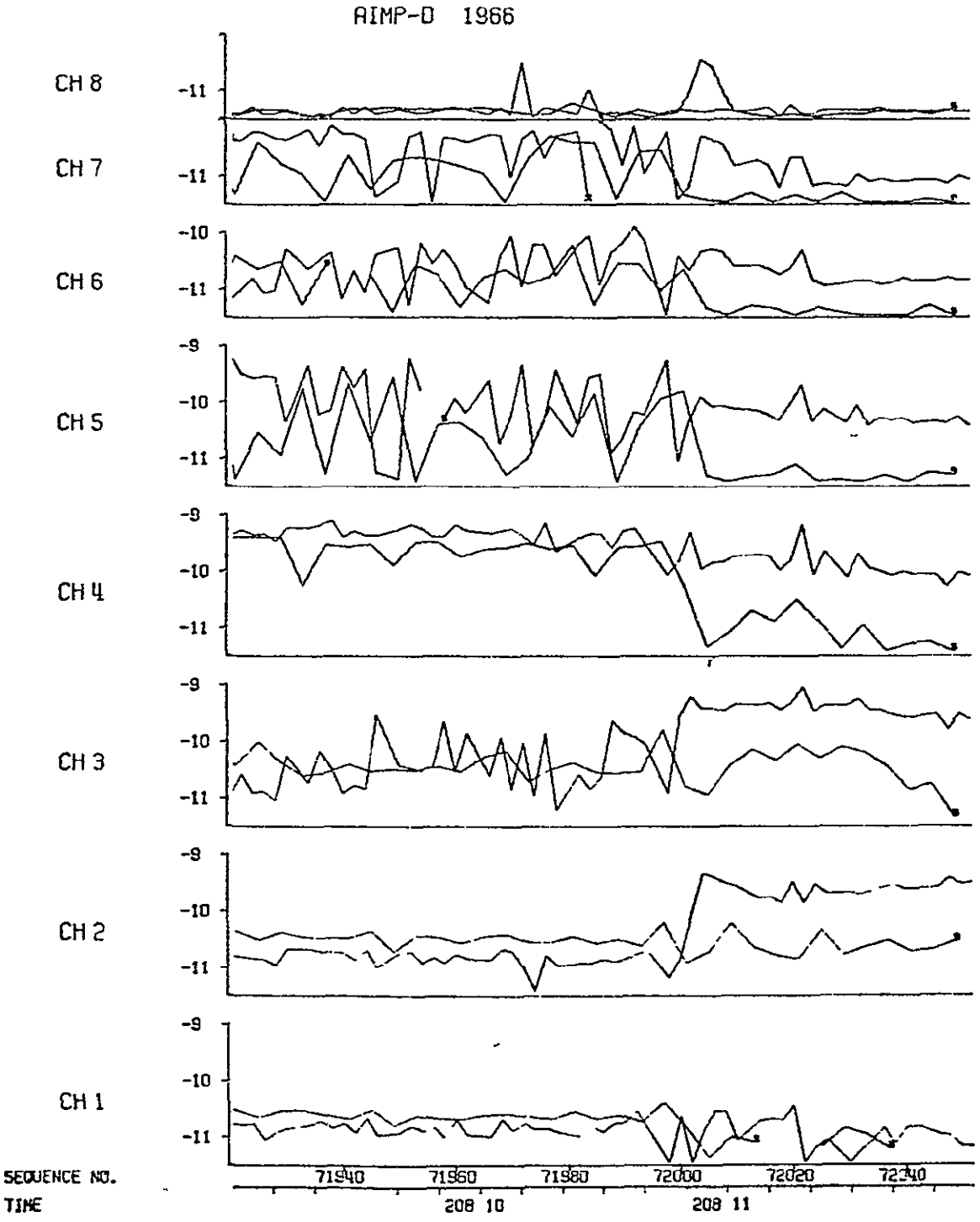
AIMP-D 1966
CH 8
CH 7
CH 6
CH 5
CH 4
CH 3
CH 2
CH 1
-11
-10
-9
SEQUENCE NO.
71940
71960
71980
72000
72020
72240
TIME
208 10
208 11

Figure 3b

AIMP-D 1966

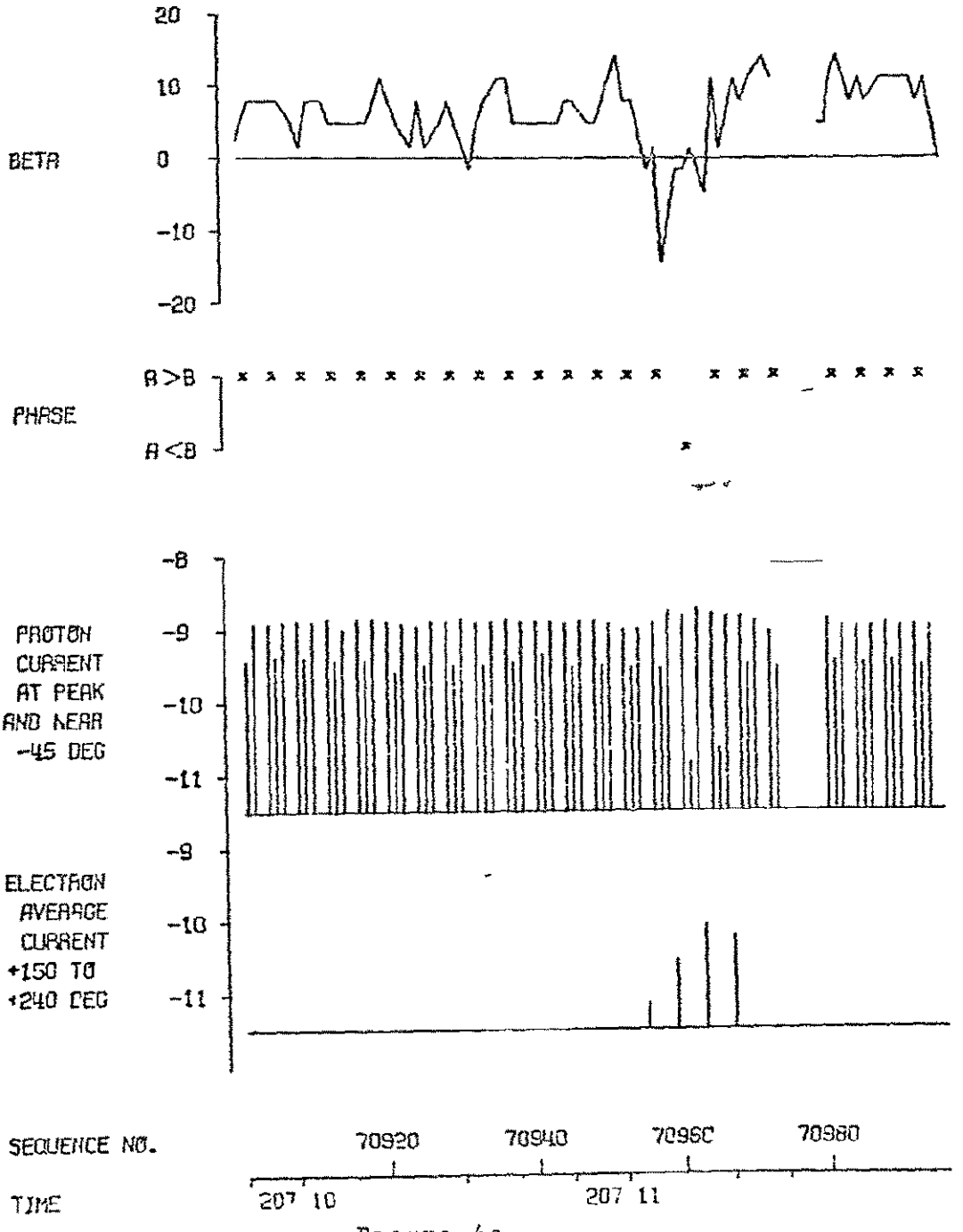

Figure 4a

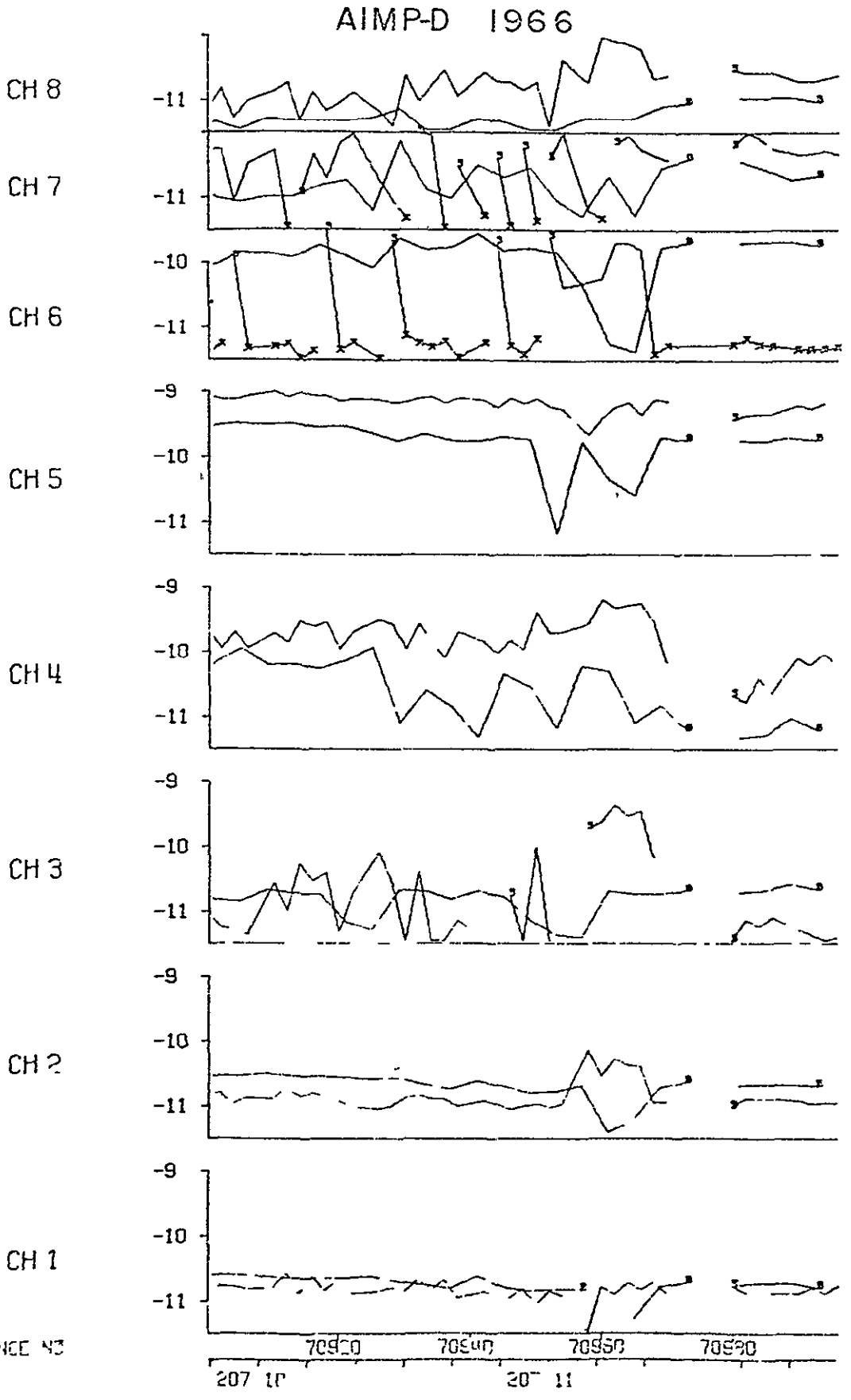
AIMP-D 1966
CH 8
CH 7
CH 6
CH 5
CH 4
CH 3
CH 2
CH 1
-11
-10
-9
SEQUENCE N3
TIME
207 18
20 11

Figure 4b

AIMP-D 1967

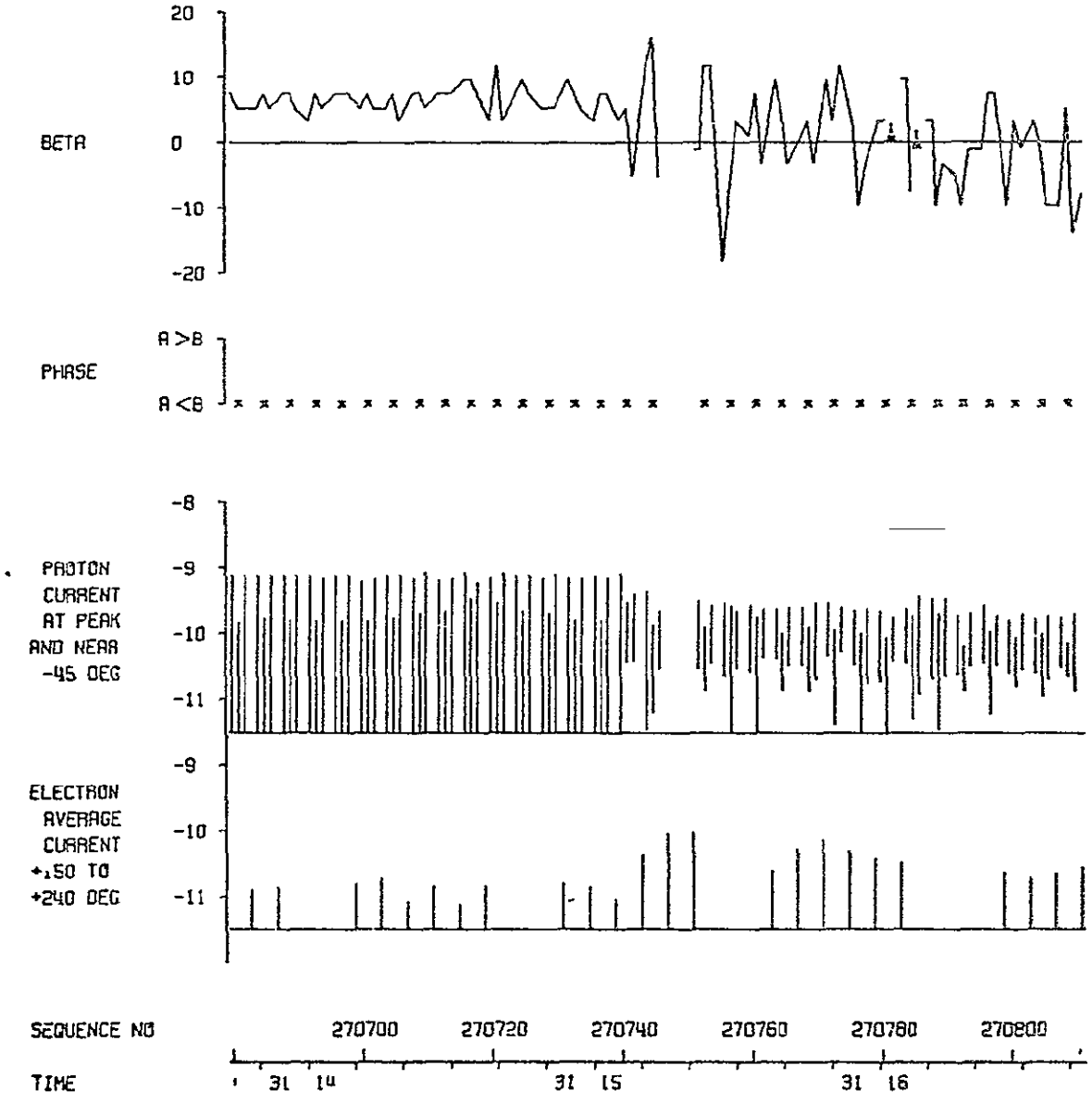

Figure 5a

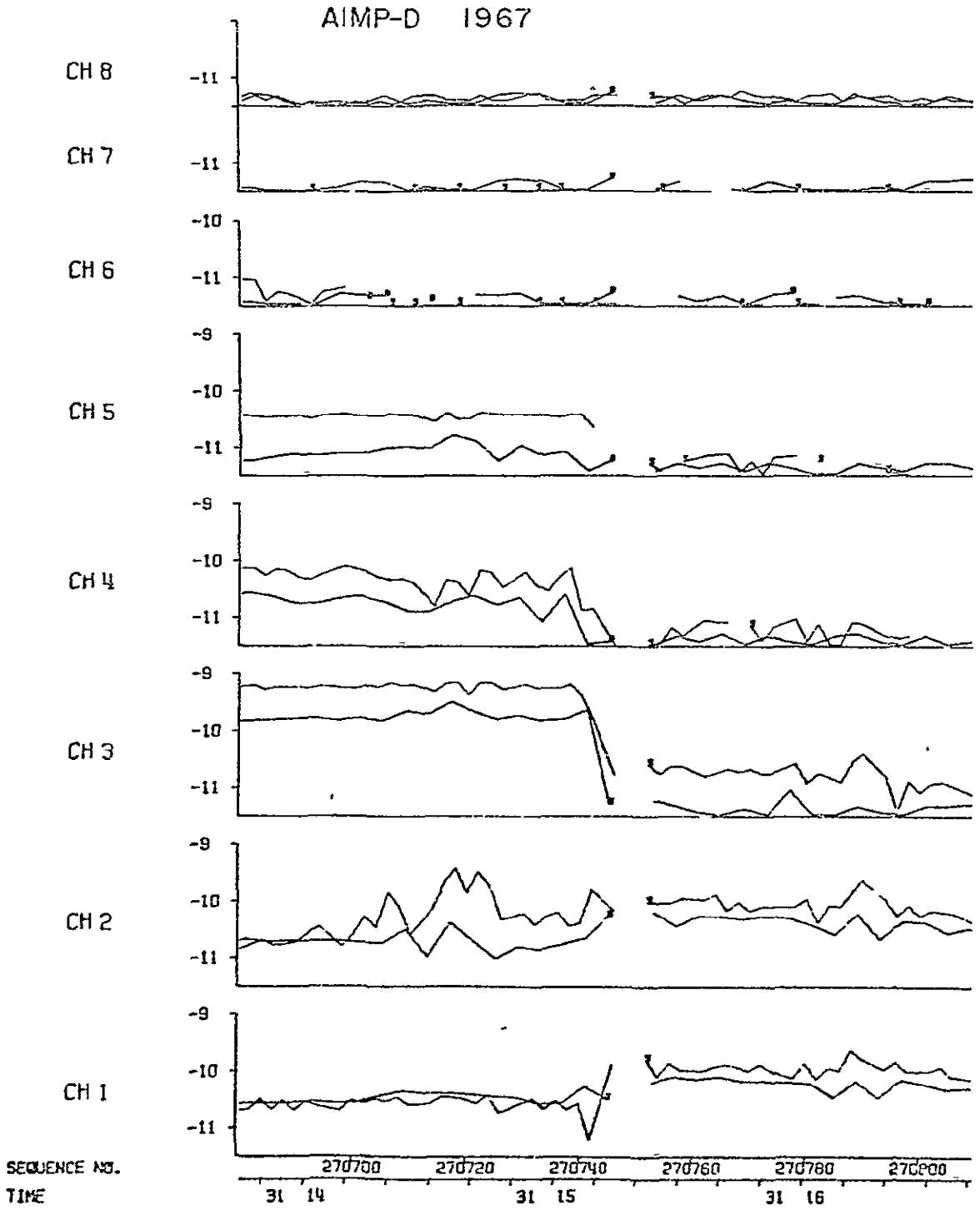
AIMP-D 1967
CH 8
CH 7
CH 6
CH 5
CH 4
CH 3
CH 2
CH 1
-11
-10
-9
SEQUENCE NO.
TIME
27D700
27D720
27D740
27D760
27D780
27D800
31 14
31 15
31 16

Figure 5b

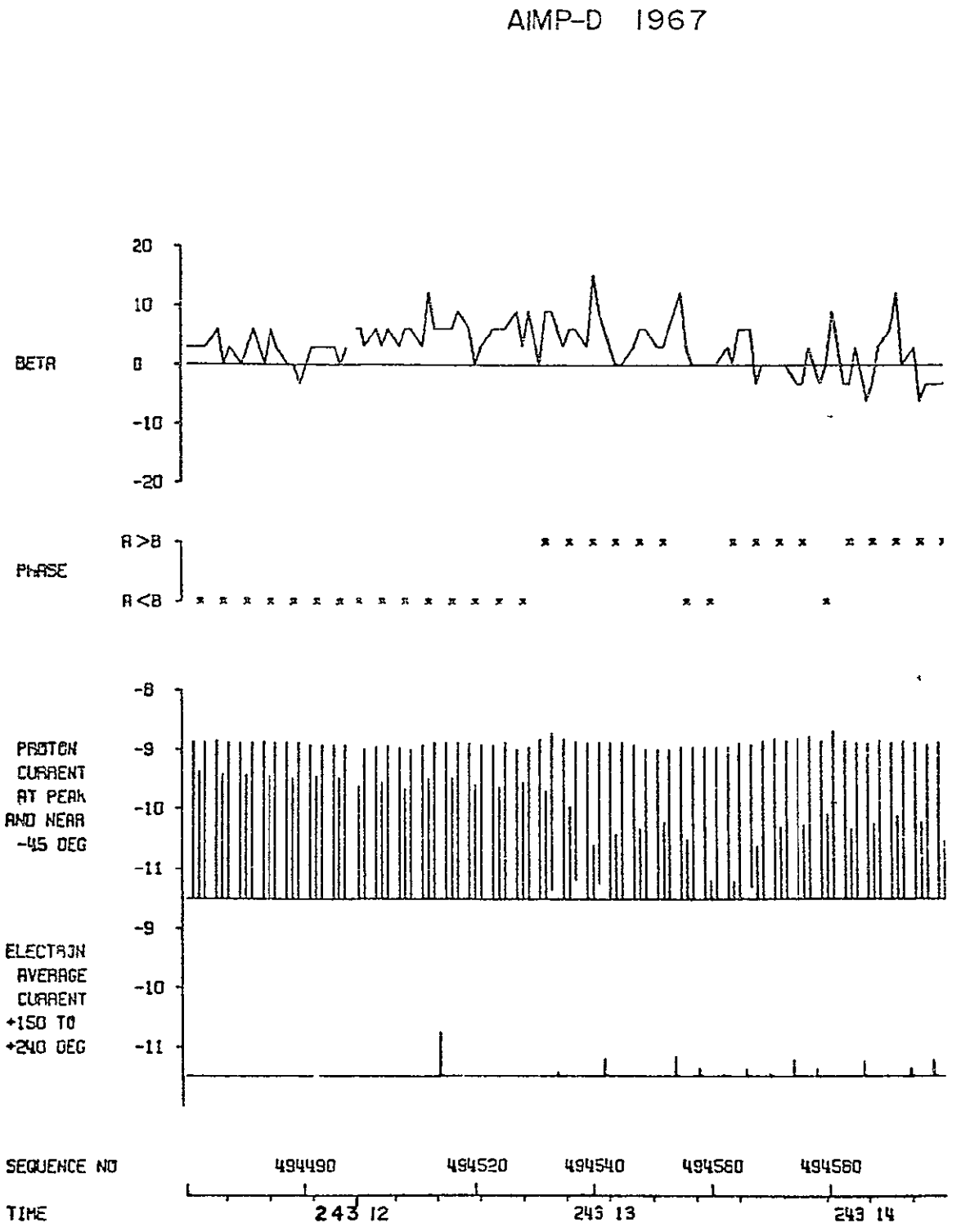
AIMP-D 1967
BETA
20
10
0
-10
-20
PHASE
A>B
A<B
PROTON CURRENT AT PEAK AND NEAR -45 DEG
-8
-9
-10
-11
ELECTRON AVERAGE CURRENT +150 TO +240 DEG
-9
-10
-11
SEQUENCE NO
494490
494520
494540
494560
494580
TIME
243 12
243 13
243 14

Figure 6a

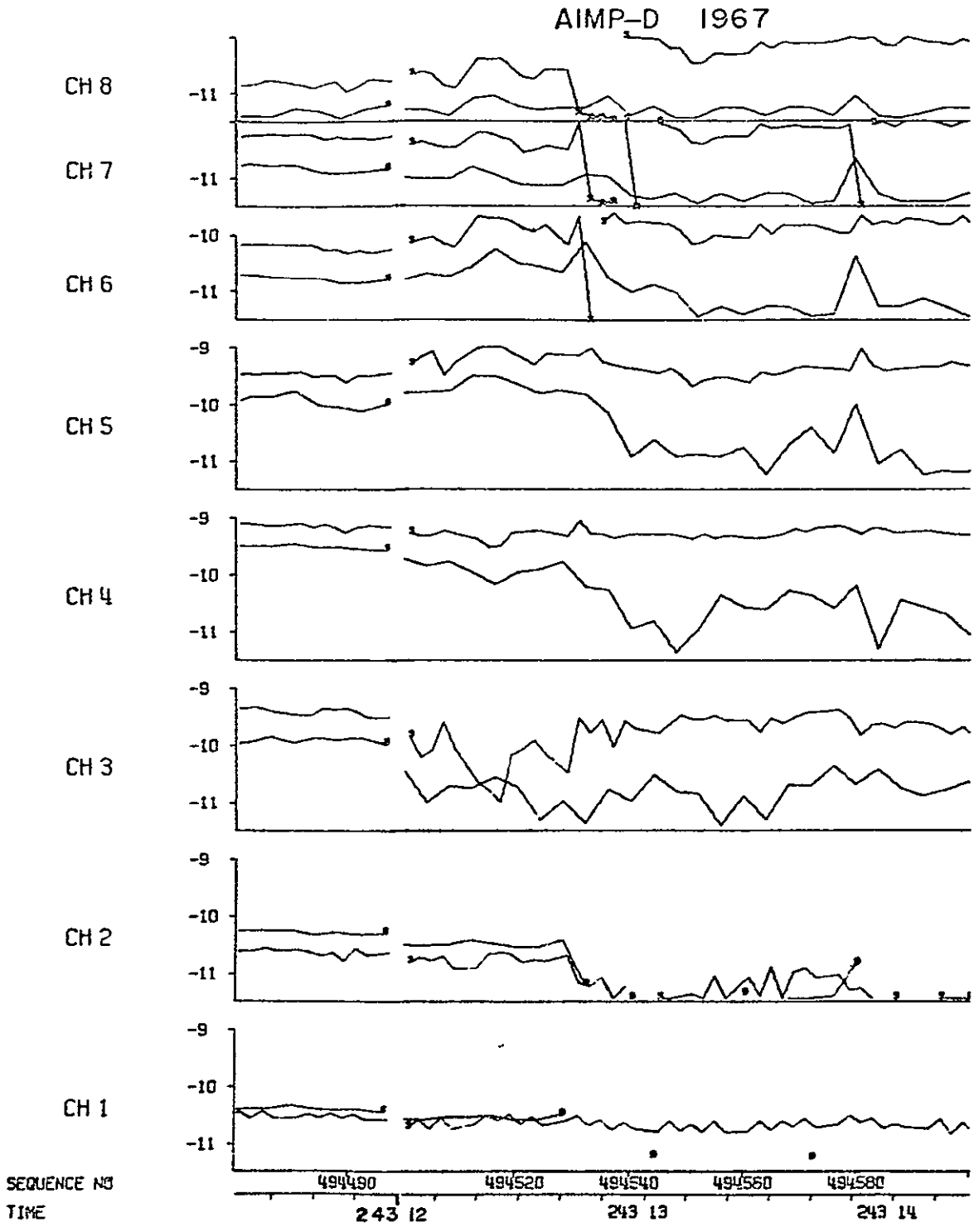
AIMP-D 1967
CH 8
CH 7
CH 6
CH 5
CH 4
CH 3
CH 2
CH 1
-11
-10
-9
SEQUENCE NO
494490
494520
494540
494560
494580
TIME
243 12
243 13
243 14

Figure 6b

AIMP-D 1969

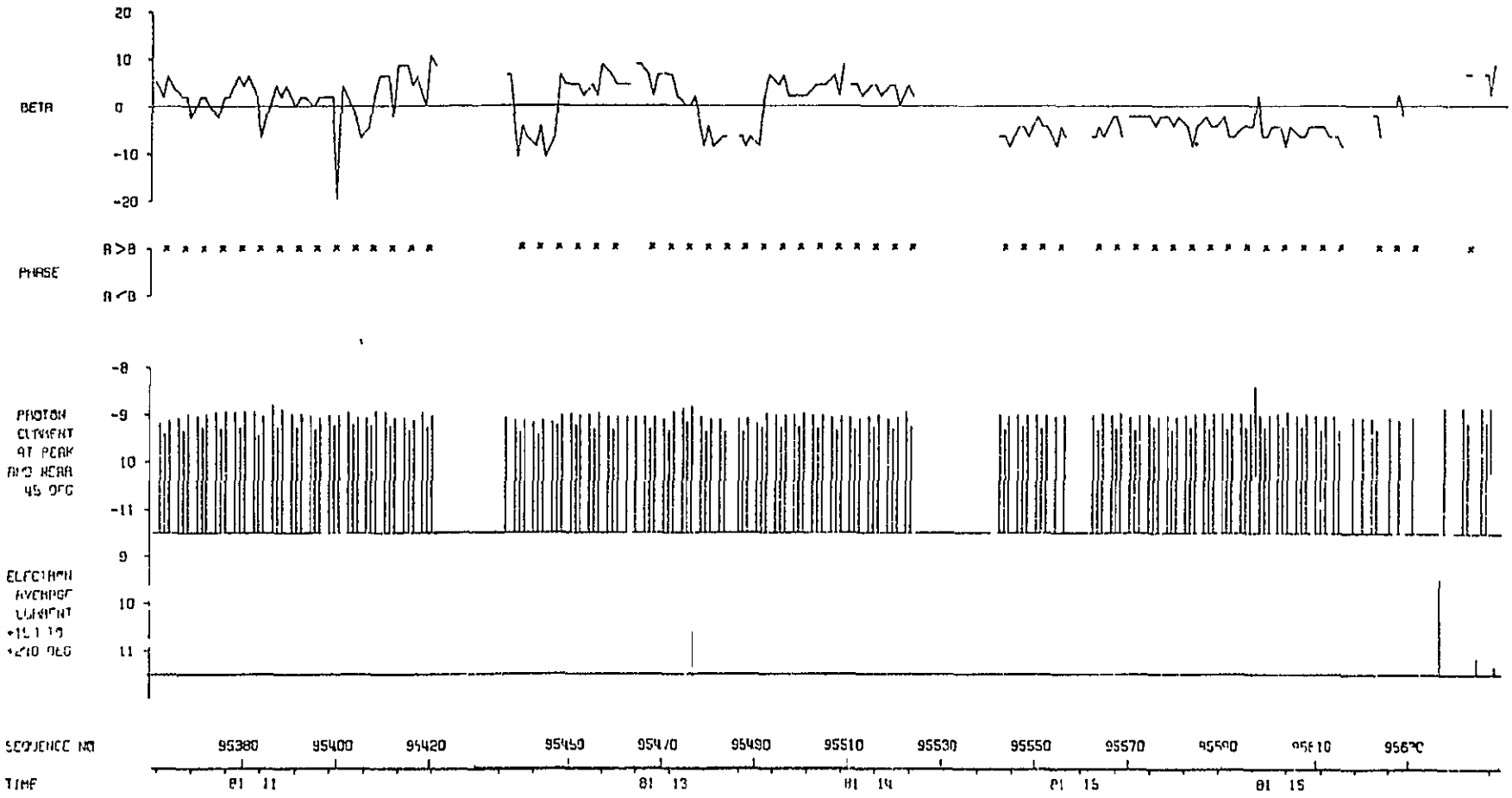

Figure 7a

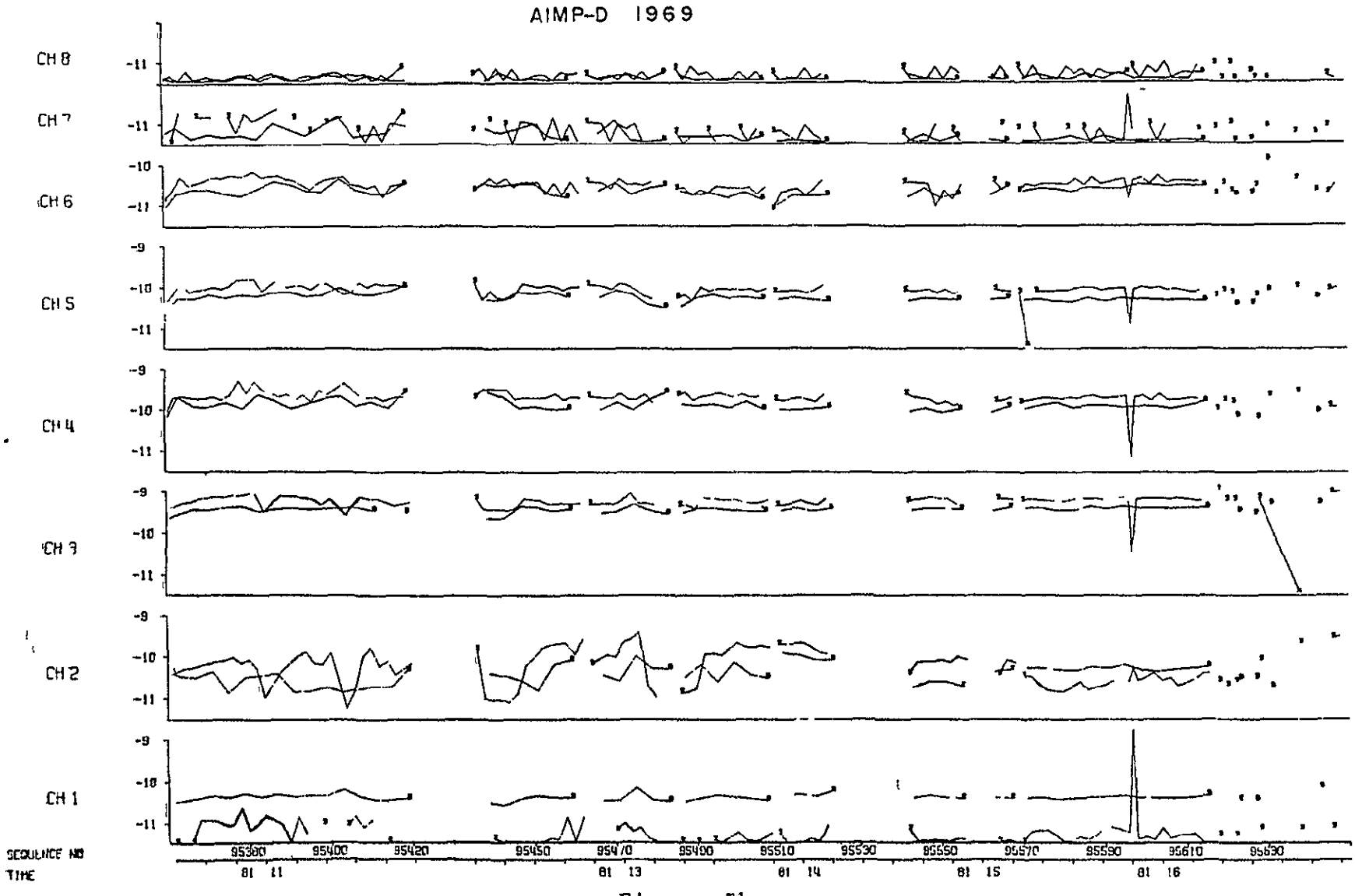
AIMP-D 1969
CH 8
CH 7
CH 6
CH 5
CH 4
CH 3
CH 2
CH 1
-11
-10
-9
SEQUENCE NO
95380
95400
95420
95450
95470
95490
95510
95530
95550
95570
95590
95610
95630
TIME
81 11
81 13
81 14
81 15
81 16

Figure 7b

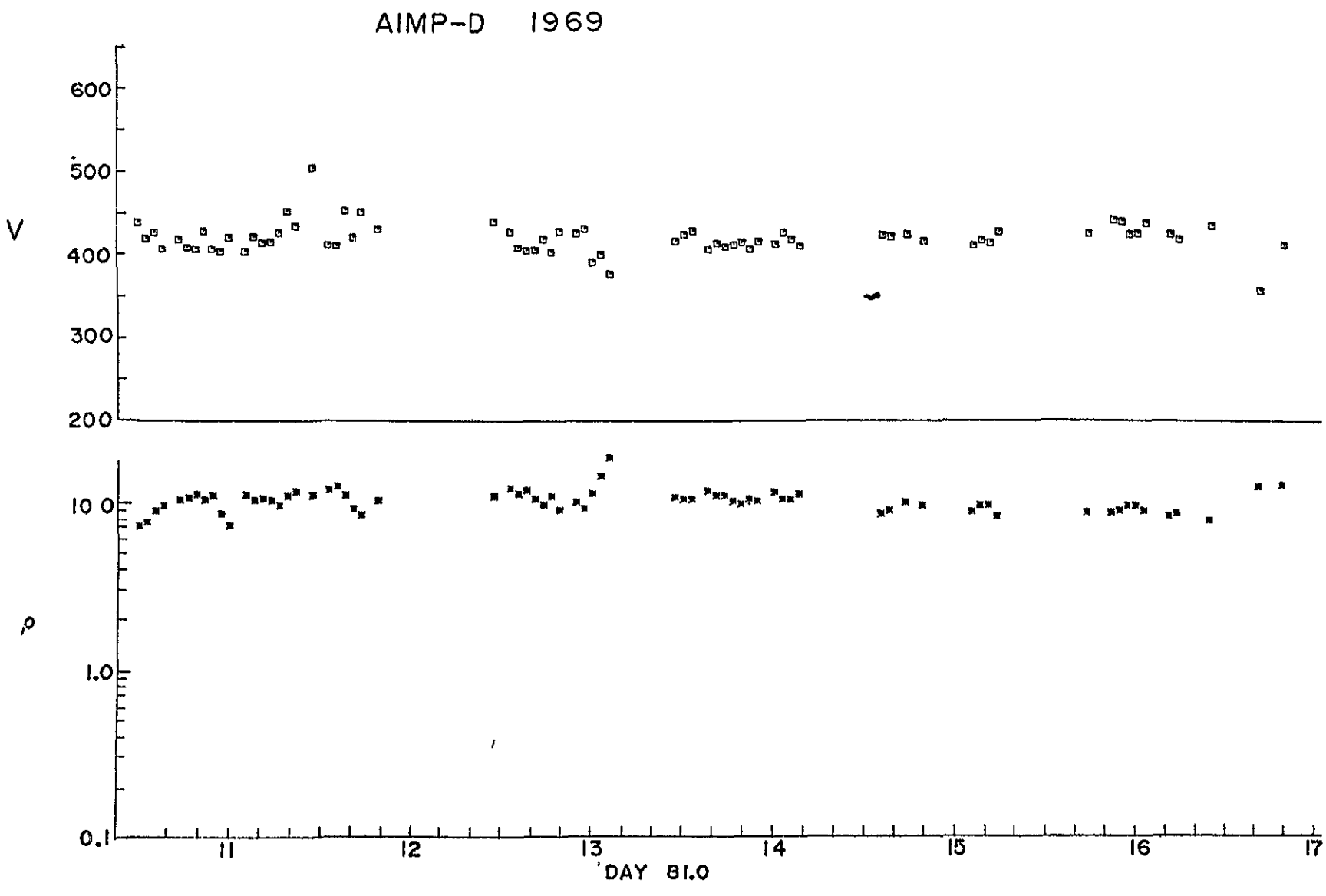
AIMP-D 1969
V
600
500
400
300
200
ρ
10.0
1.0
0.1
11
12
13
14
15
16
17
DAY 81.0

Figure 7c

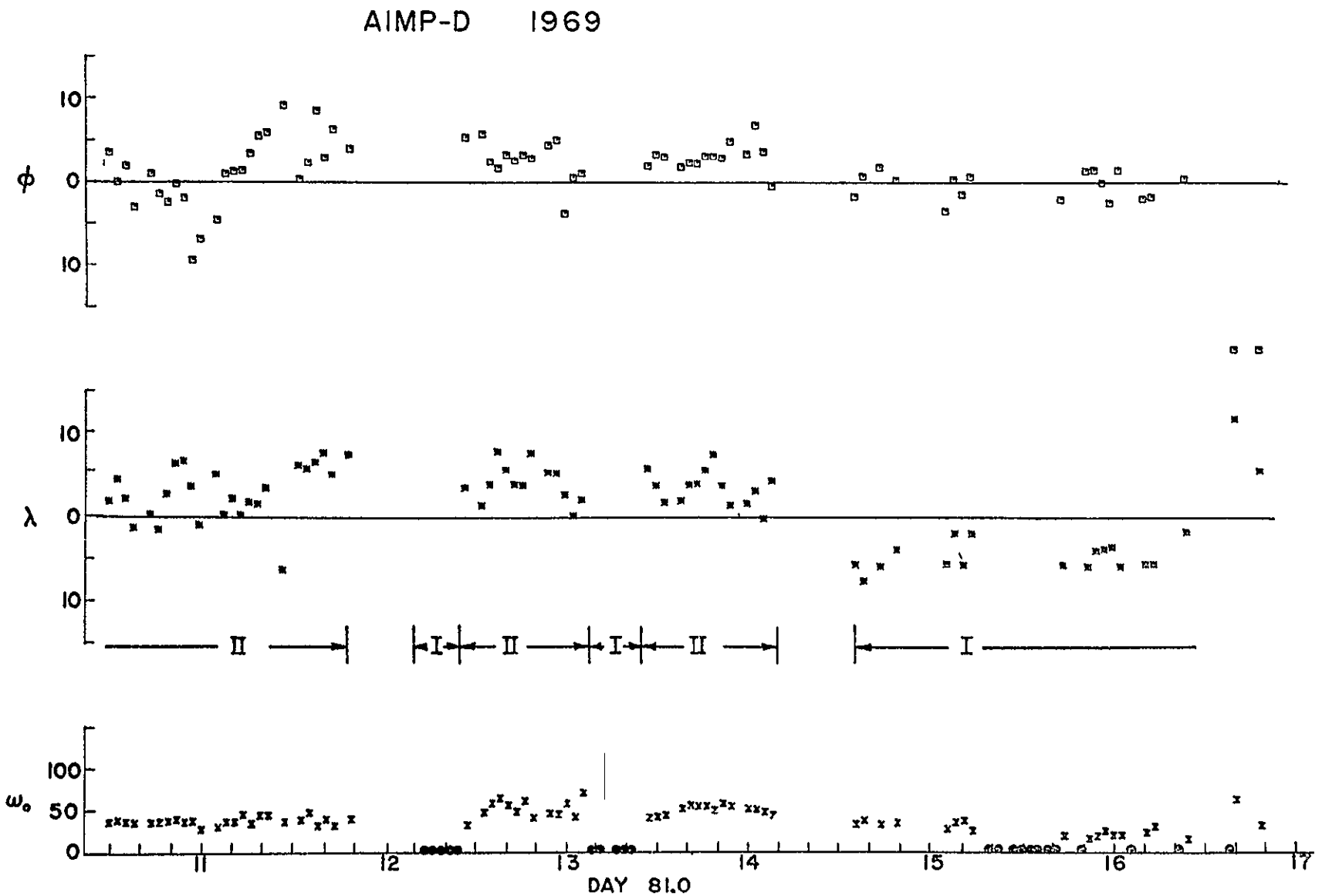
AIMP-D 1969
10
0
10
φ
10
0
10
λ
II
I
II
I
II
I
100
50
0
ω_o
11
12
13
14
15
16
17
DAY 81.0

Figure 7d

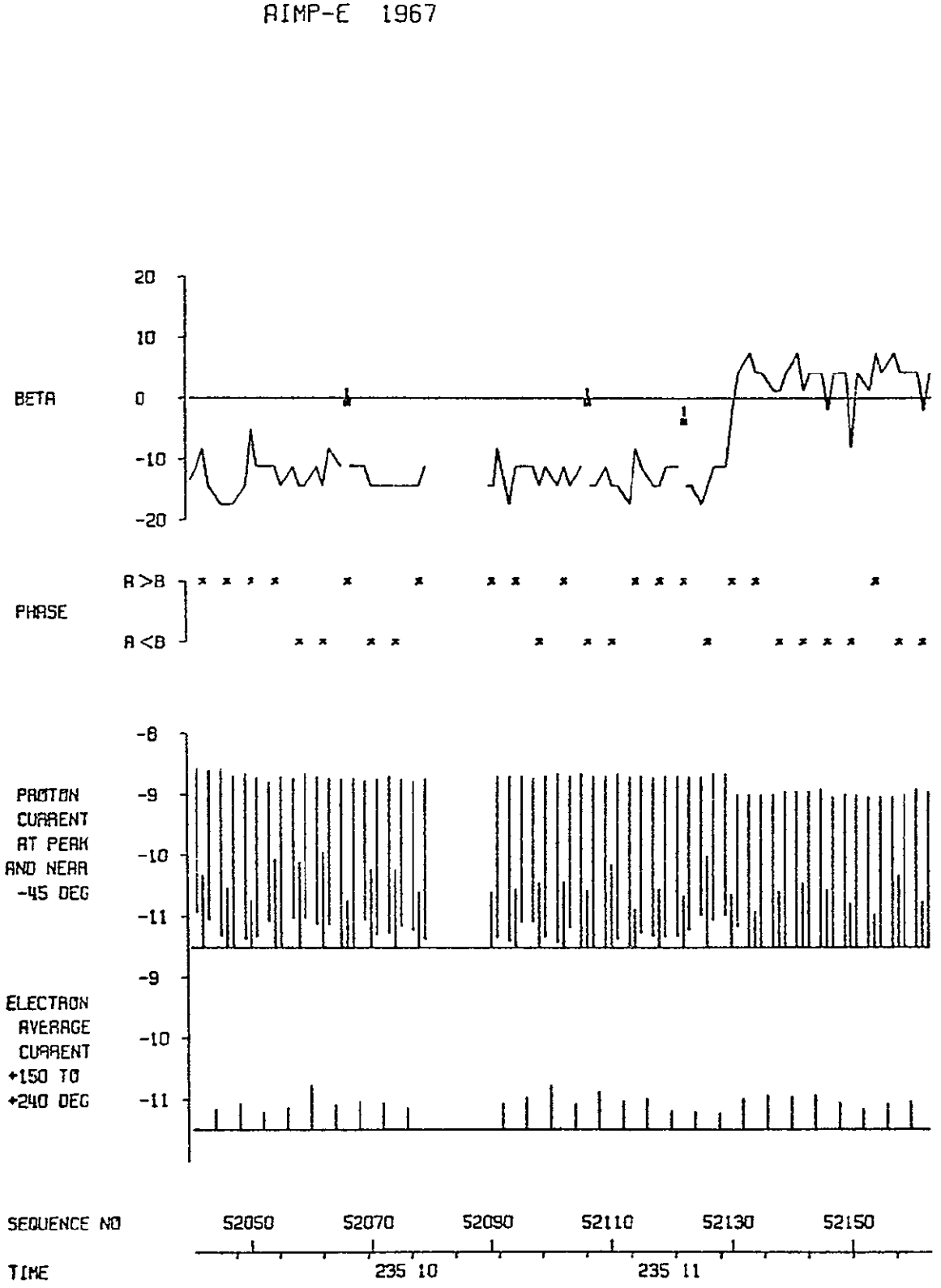
AIMP-E 1967
BETA
20
10
0
-10
-20
PHASE
A>B
A<B
PROTON
CURRENT
AT PEAK
AND NEAR
-45 DEG
-8
-9
-10
-11
ELECTRON
AVERAGE
CURRENT
+150 TO
+240 DEG
-9
-10
-11
SEQUENCE NO
52050
52070
52090
52110
52130
52150
TIME
235 10
235 11

Figure 8a

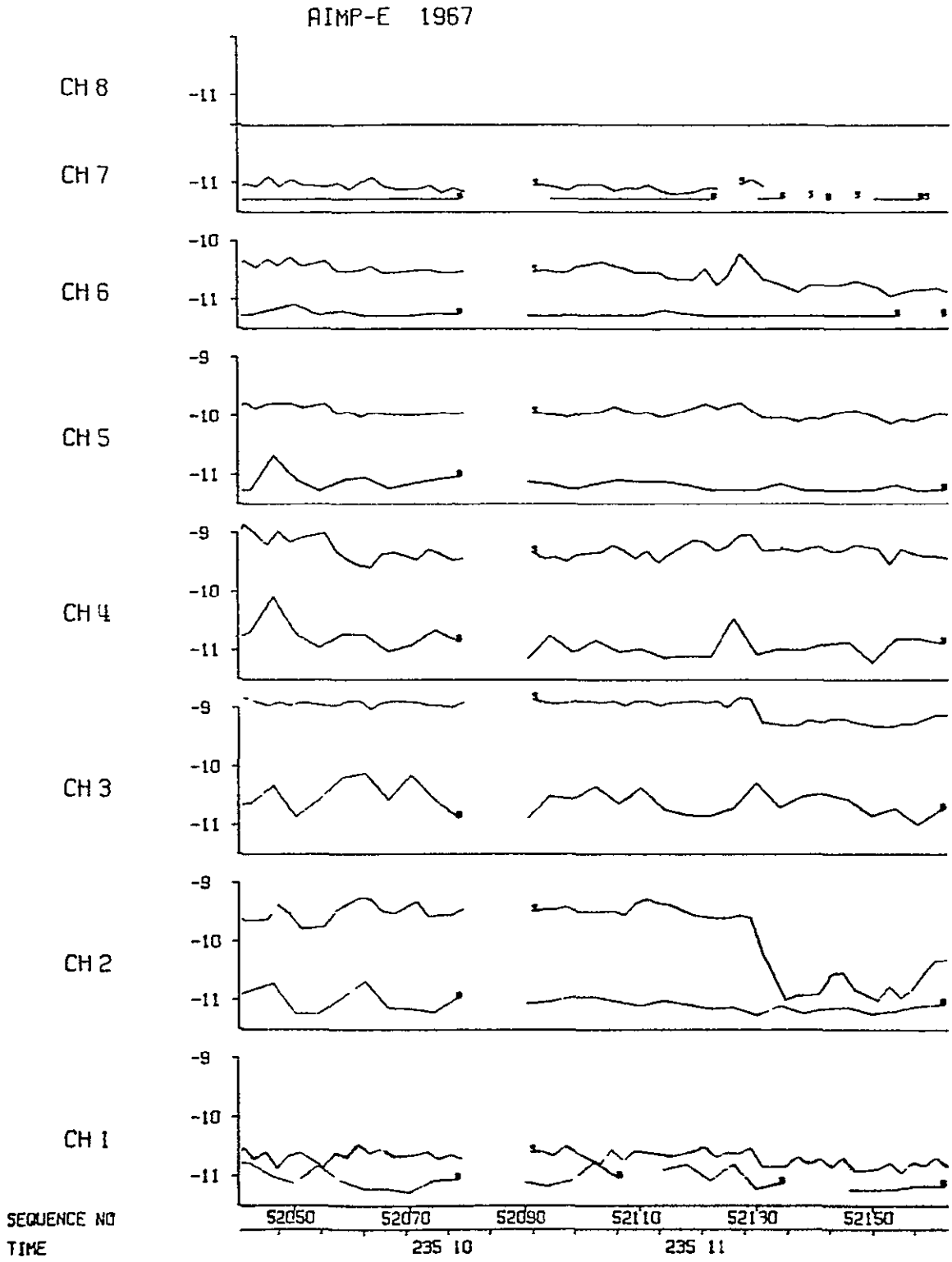
AIMP-E 1967
CH 8
CH 7
CH 6
CH 5
CH 4
CH 3
CH 2
CH 1
-11
-10
-9
SEQUENCE NO
TIME
52050
52070
52090
52110
52130
52150
235 10
235 11

Figure 8b

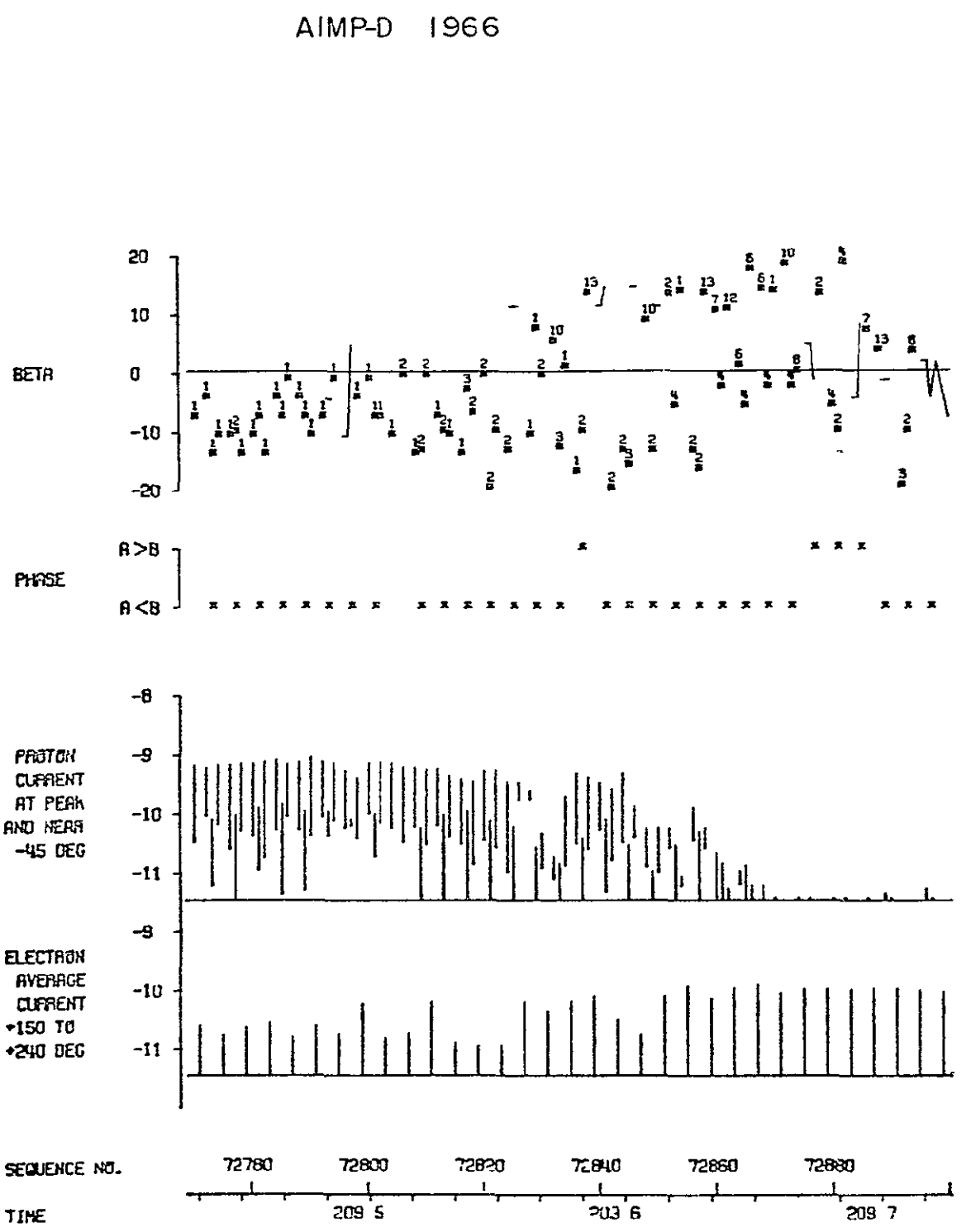
AIMP-D 1966
BETA
20
10
0
-10
-20
PHASE
A>B
A<B
PROTON CURRENT AT PEAK AND NEAR -45 DEG
-8
-9
-10
-11
ELECTRON AVERAGE CURRENT +150 TO +240 DEG
-9
-10
-11
SEQUENCE NO.
72780
72800
72820
72840
72860
72880
TIME
209 5
209 6
209 7

Figure 9a

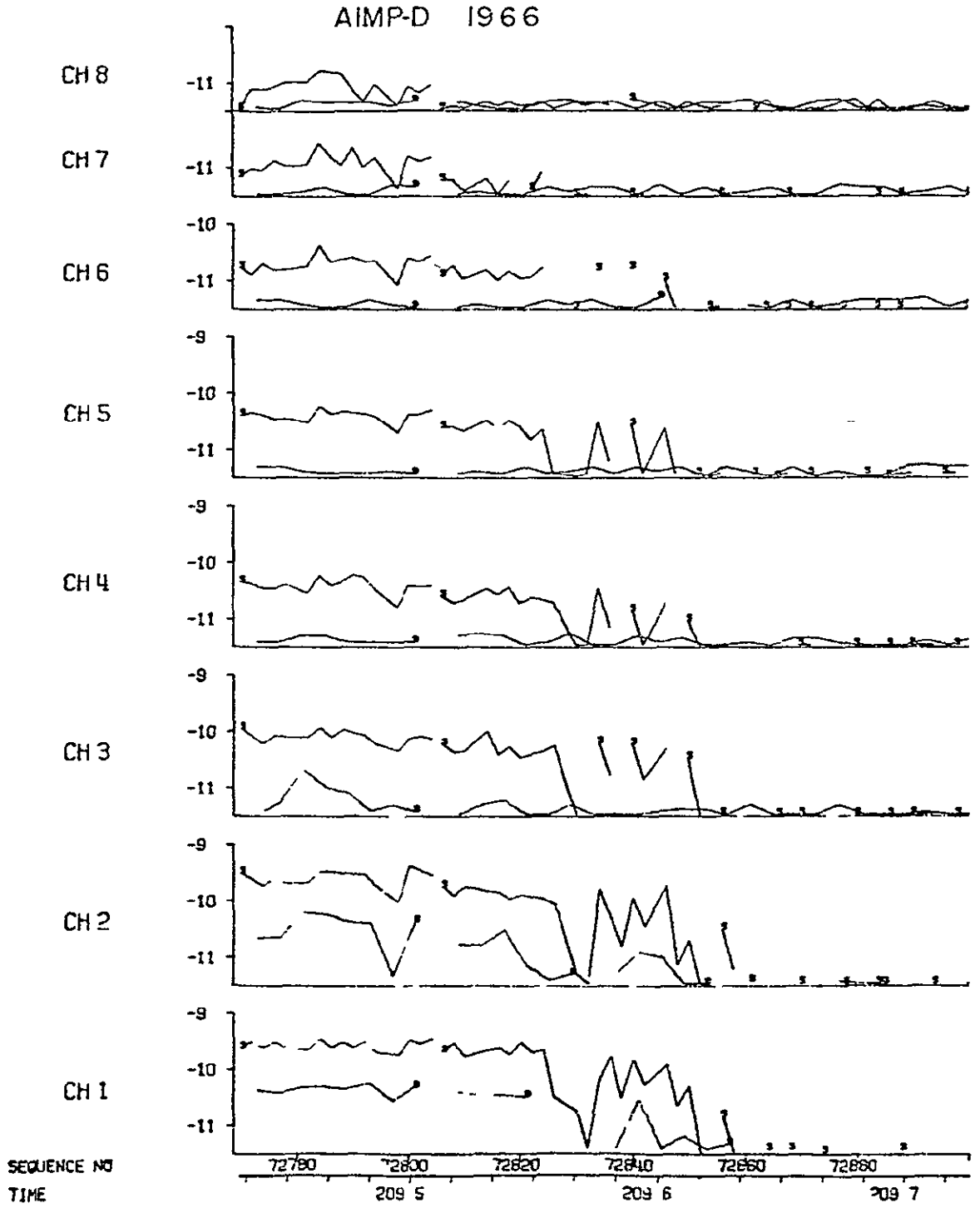
AIMP-D 1966
CH 8
CH 7
CH 6
CH 5
CH 4
CH 3
CH 2
CH 1
-11
-10
-9
SEQUENCE NO
72780
72800
72820
72840
72860
72880
TIME
209 5
209 6
209 7

Figure 9b

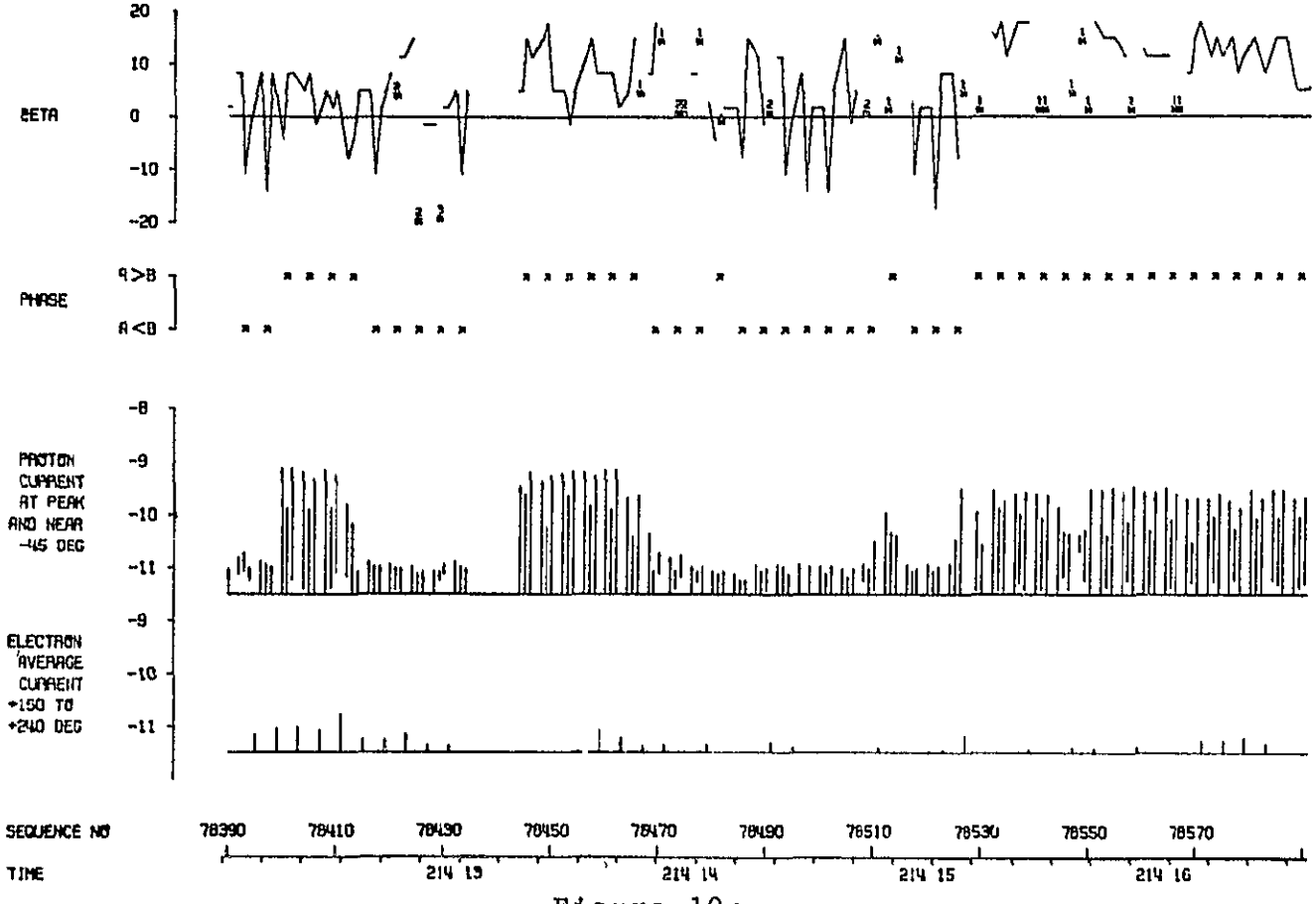
IMP-D 1966
BETA
20
10
0
-10
-20
PHASE
P>B
P<B
PROTON CURRENT AT PEAK AND NEAR -45 DEG
-8
-9
-10
-11
ELECTRON AVERAGE CURRENT +150 TO +240 DEG
-9
-10
-11
SEQUENCE NO
78390
78410
78430
78450
78470
78490
78510
78530
78550
78570
TIME
214 13
214 14
214 15
214 16

Figure 10a

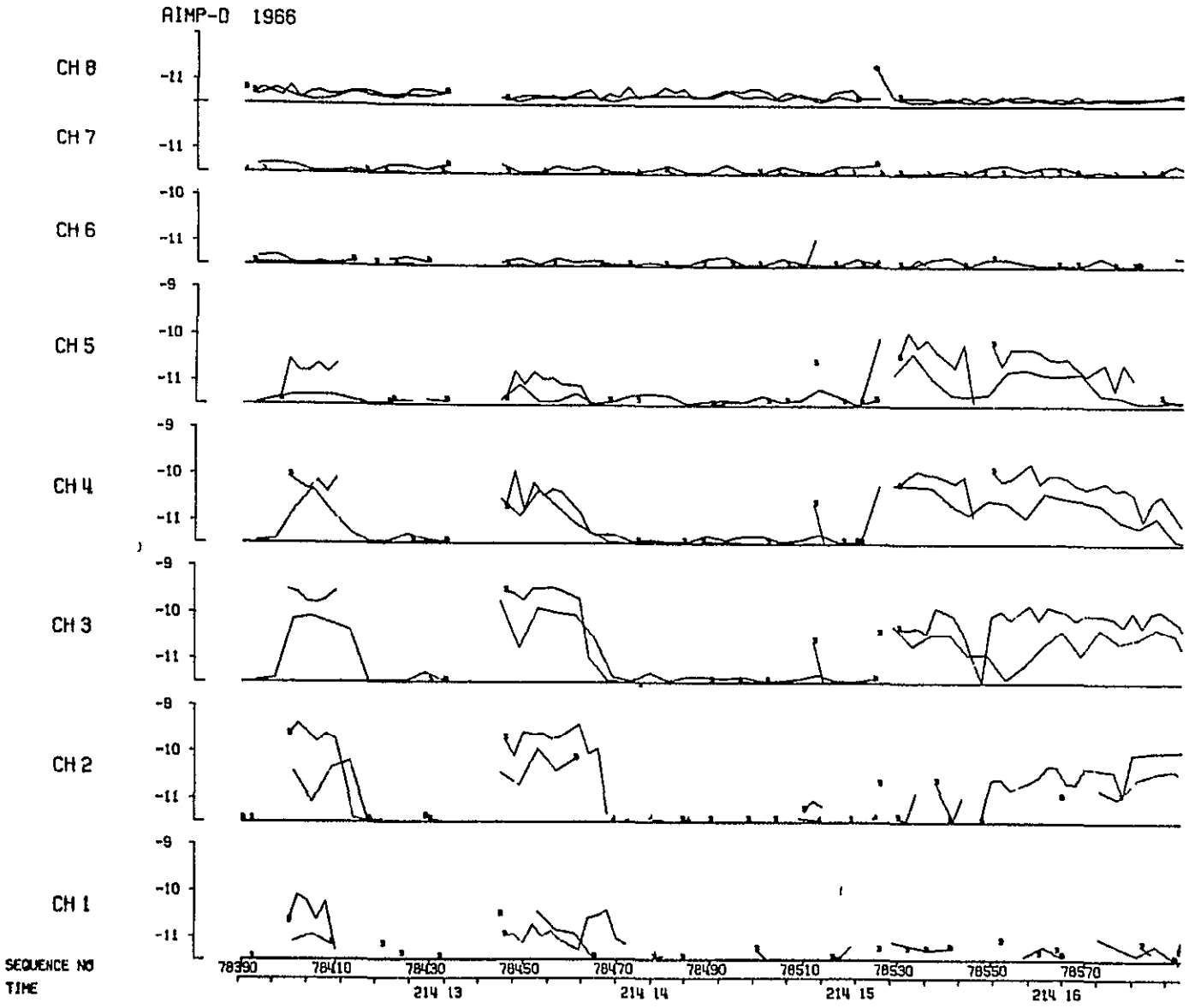
AIMP-D 1966
CH 8
CH 7
CH 6
CH 5
CH 4
CH 3
CH 2
CH 1
-11
-10
-9
SEQUENCE NO
TIME
78390
78410
78430
78450
78470
78490
78510
78530
78550
78570
214 13
214 14
214 15
214 16

Figure 10b

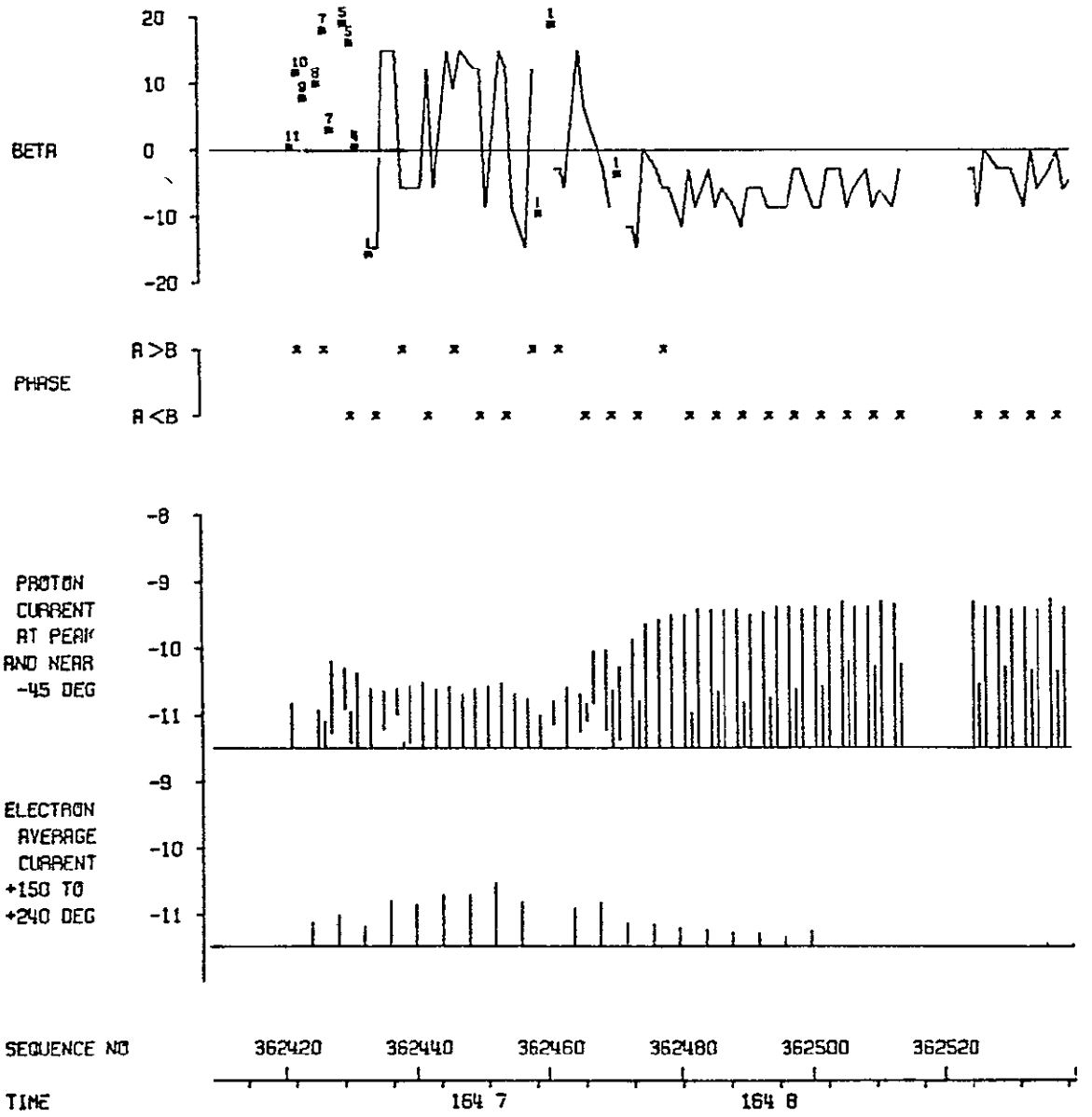
AIMP-E 1968
BETA
20
10
0
-10
-20
PHASE
A>B
A<B
PROTON CURRENT AT PEAK AND NEAR -45 DEG
-8
-9
-10
-11
ELECTRON AVERAGE CURRENT +150 TO +240 DEG
-9
-10
-11
SEQUENCE NO
362420
362440
362460
362480
362500
362520
TIME
164 7
164 8

Figure 11a

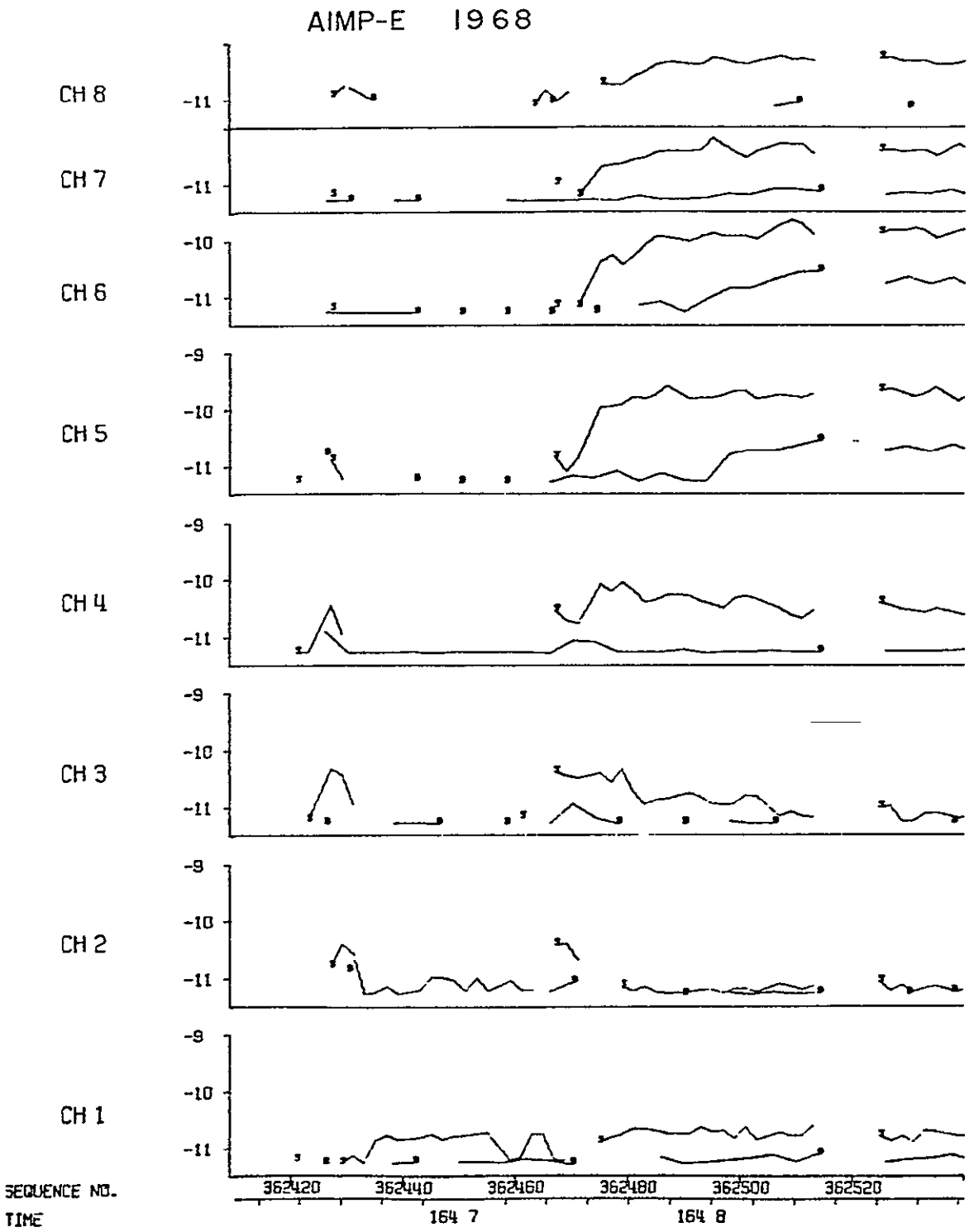
AIMP-E 1968
CH 8
CH 7
CH 6
CH 5
CH 4
CH 3
CH 2
CH 1
-11
-10
-9
SEQUENCE NO.
362420
362440
362460
362480
362500
362520
TIME
164 7
164 8

Figure 11b

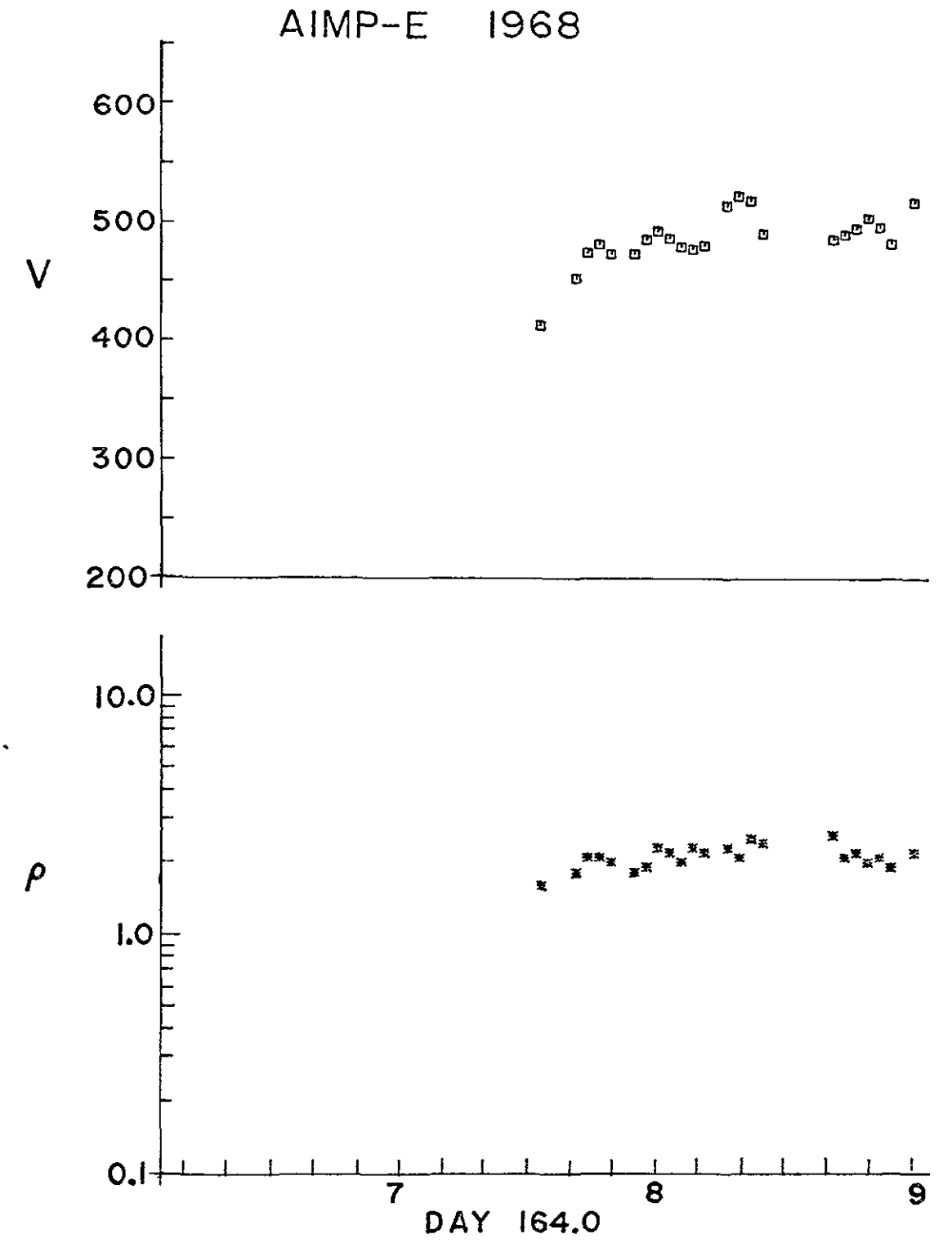

Figure 11c

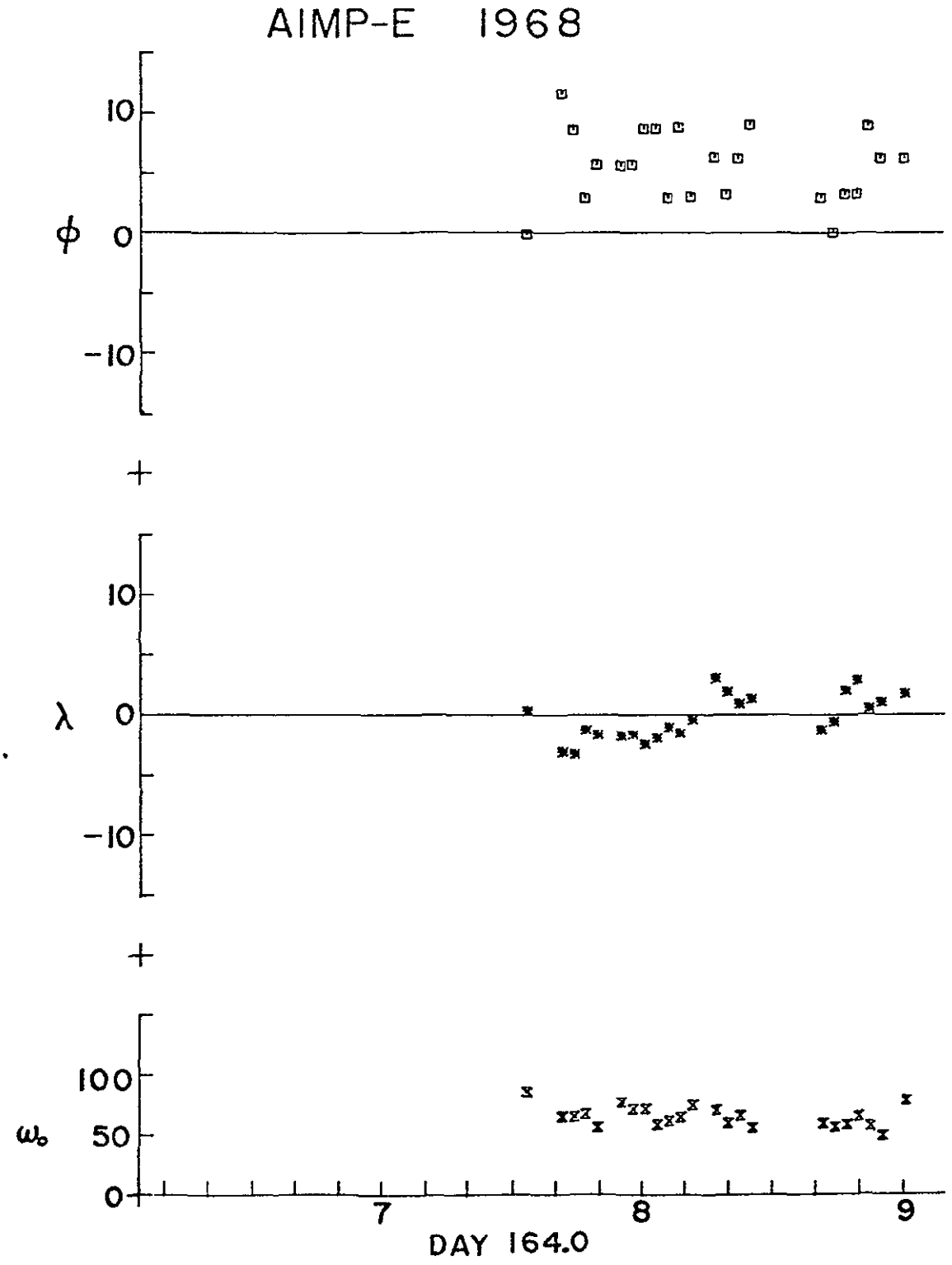

Figure 11d

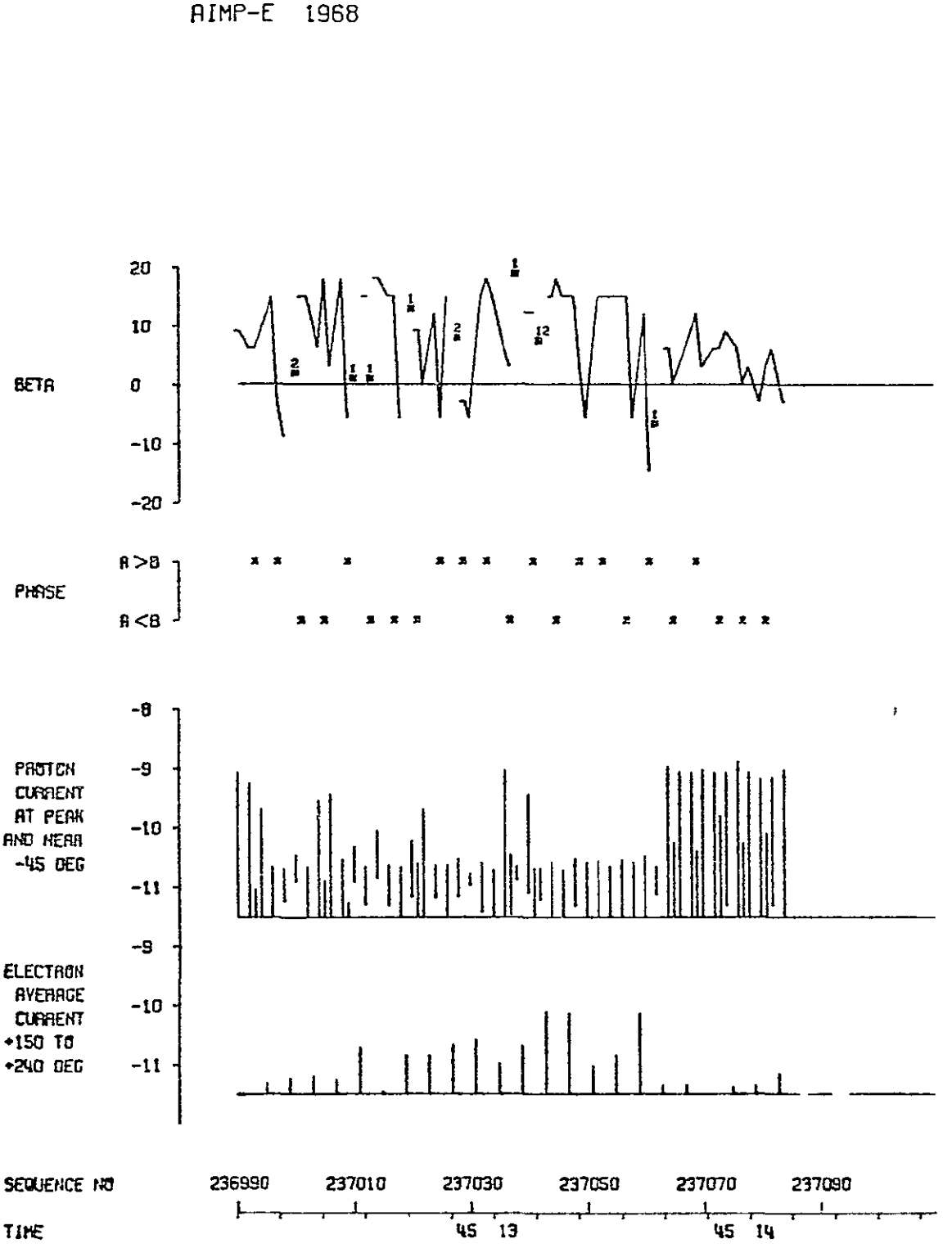
AIMP-E 1968
BETA
20
10
0
-10
-20
PHASE
A>B
A<B
PROTON CURRENT AT PEAK AND NEAR -45 DEG
ELECTRON AVERAGE CURRENT +150 TO +240 DEG
-8
-9
-10
-11
-9
-10
-11
SEQUENCE NO
236990
237010
237030
237050
237070
237090
TIME
45 13
45 14

Figure 12a

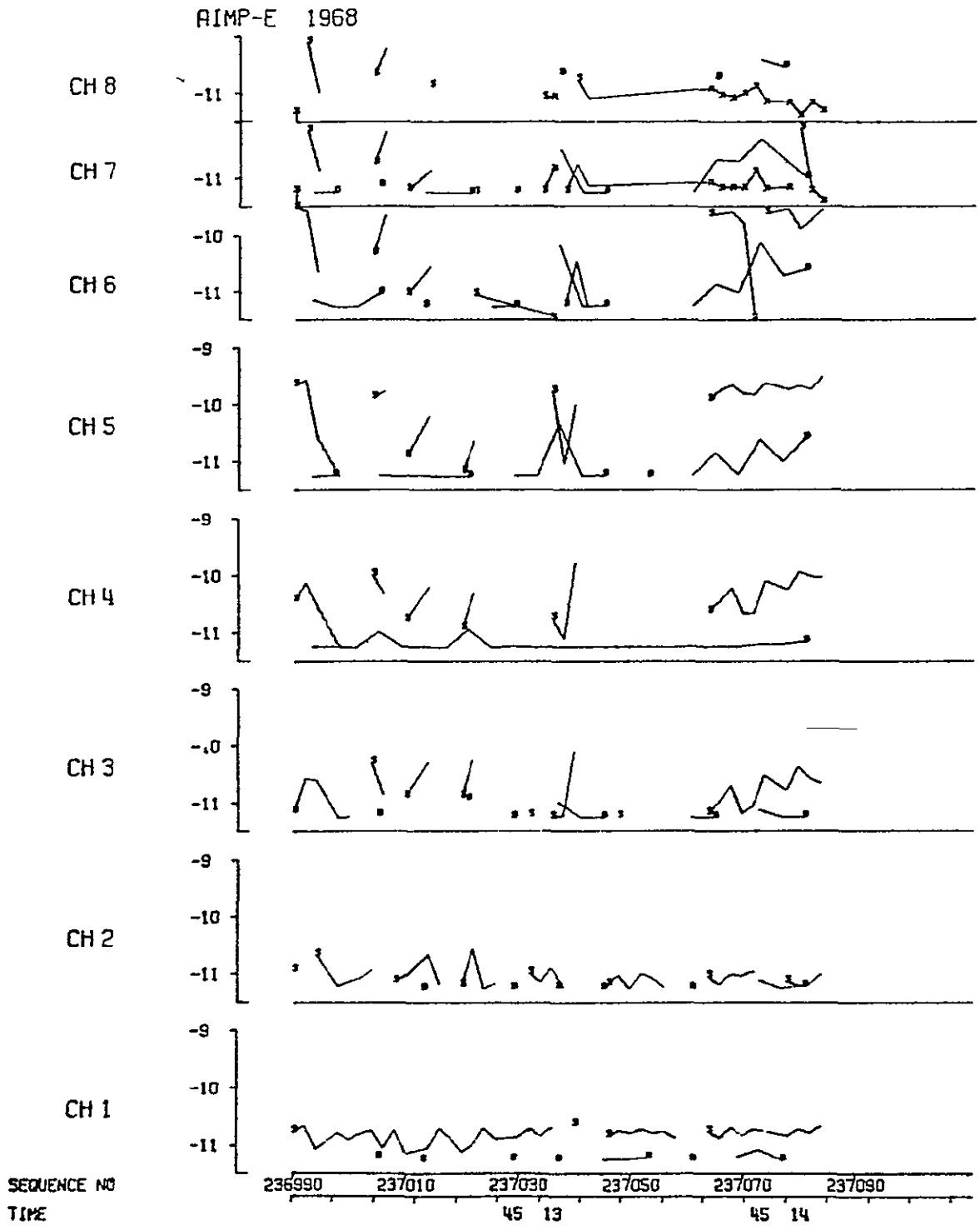
AIMP-E 1968
CH 8
CH 7
CH 6
CH 5
CH 4
CH 3
CH 2
CH 1
-9
-10
-11
SEQUENCE NO
TIME
236990
237010
237030
237050
237070
237090
45 13
45 14

Figure 12b

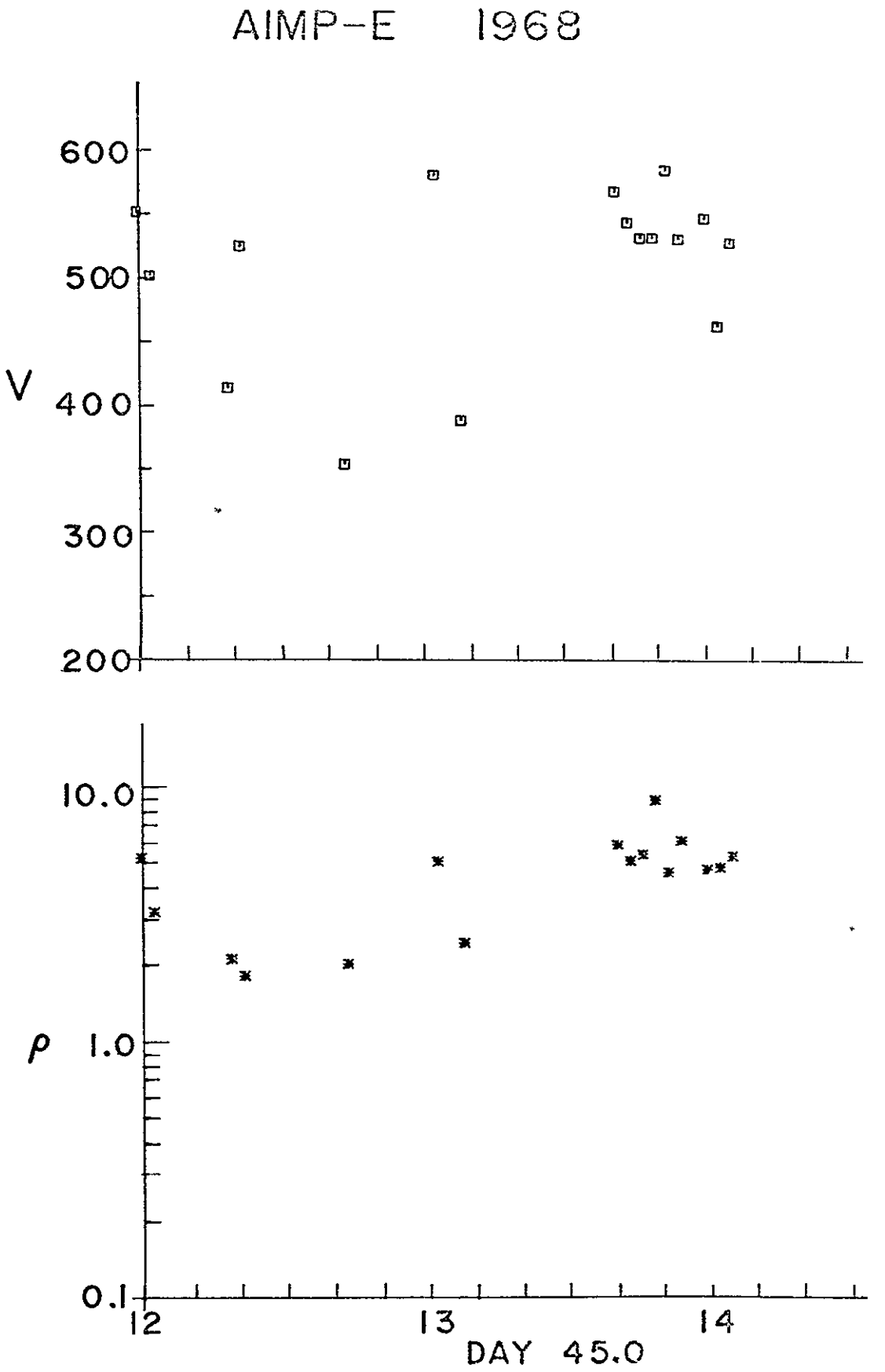

Figure 12c

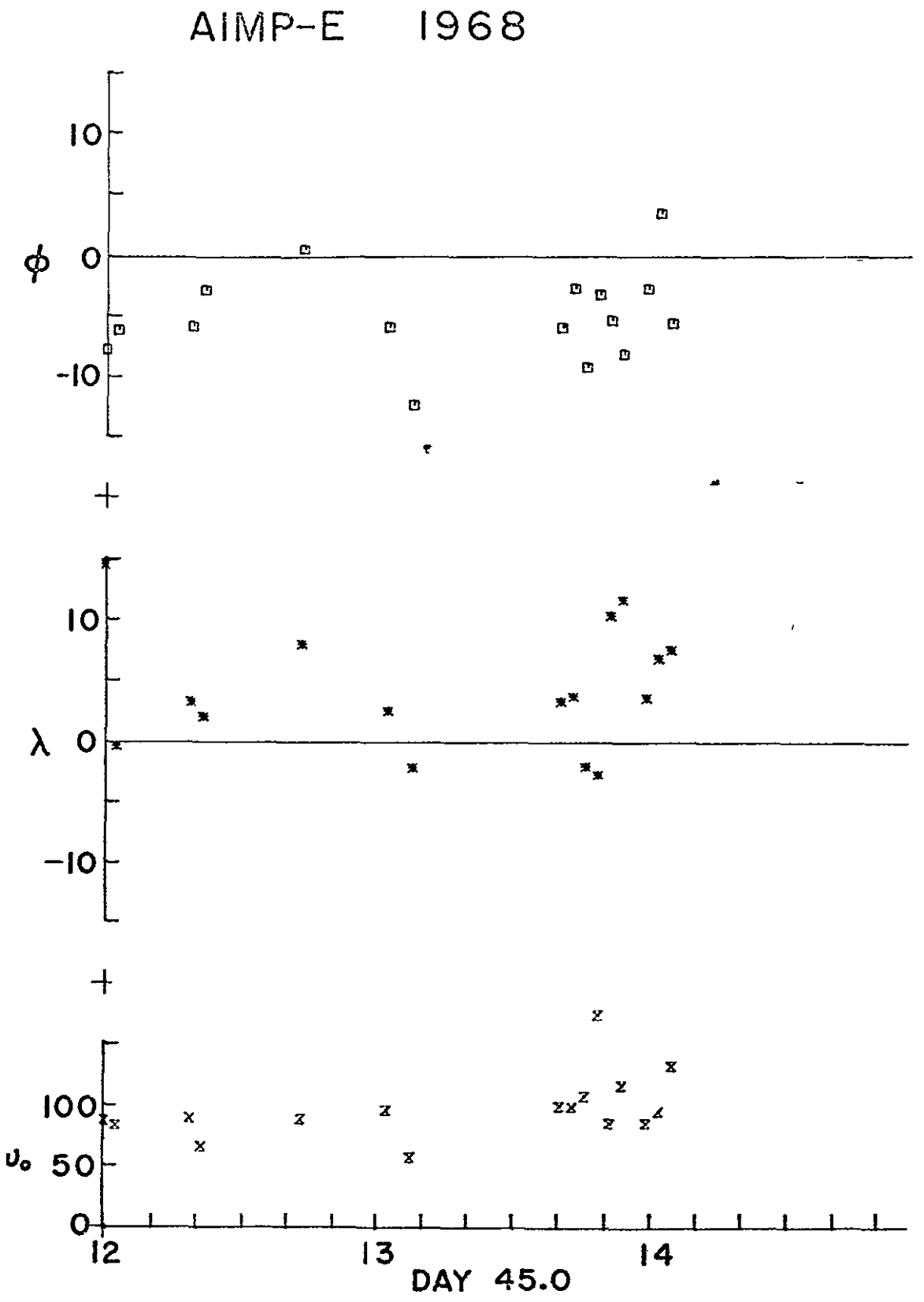

Figure 12d

AIMP-E 1967

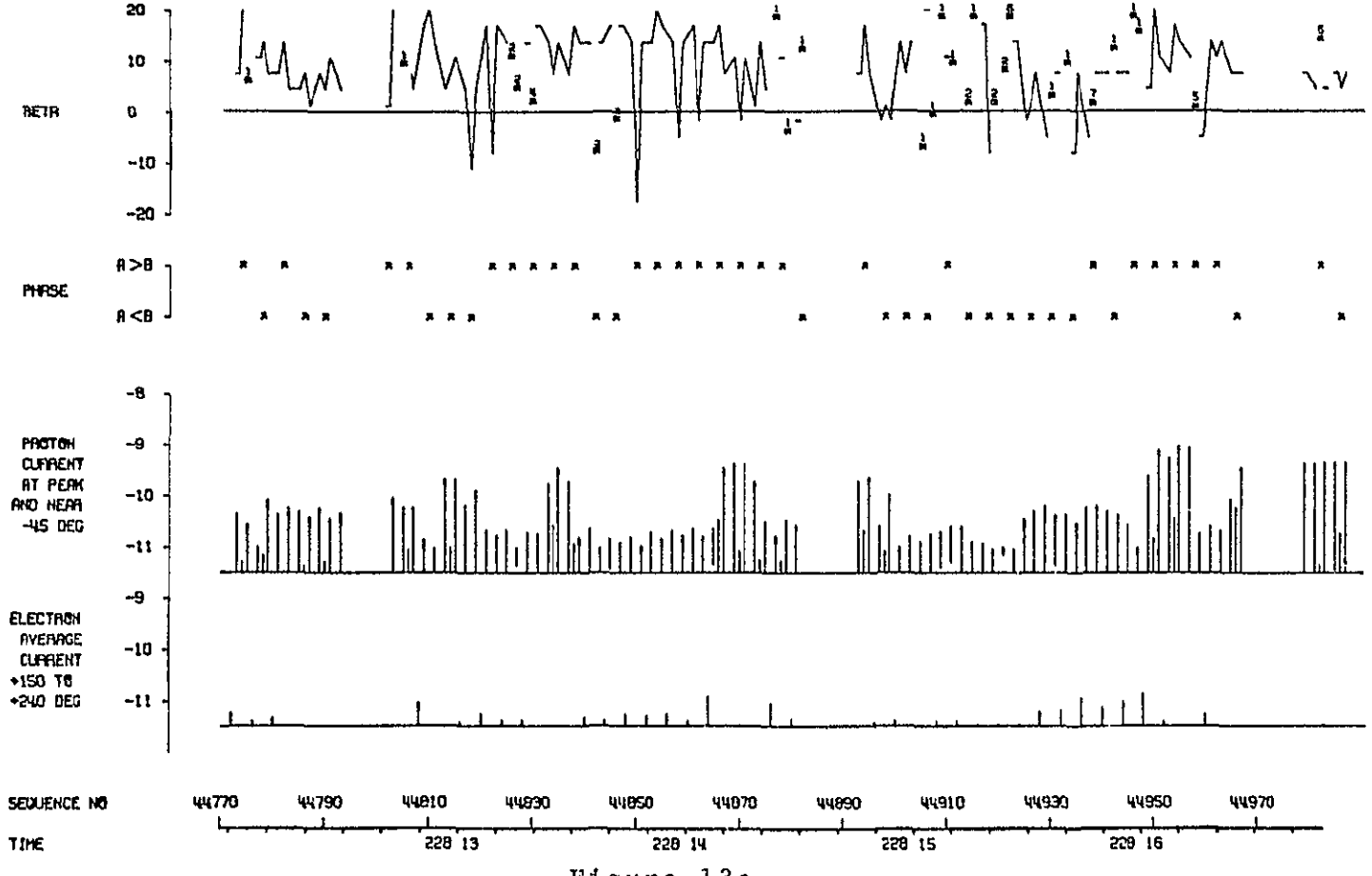

Figure 13a

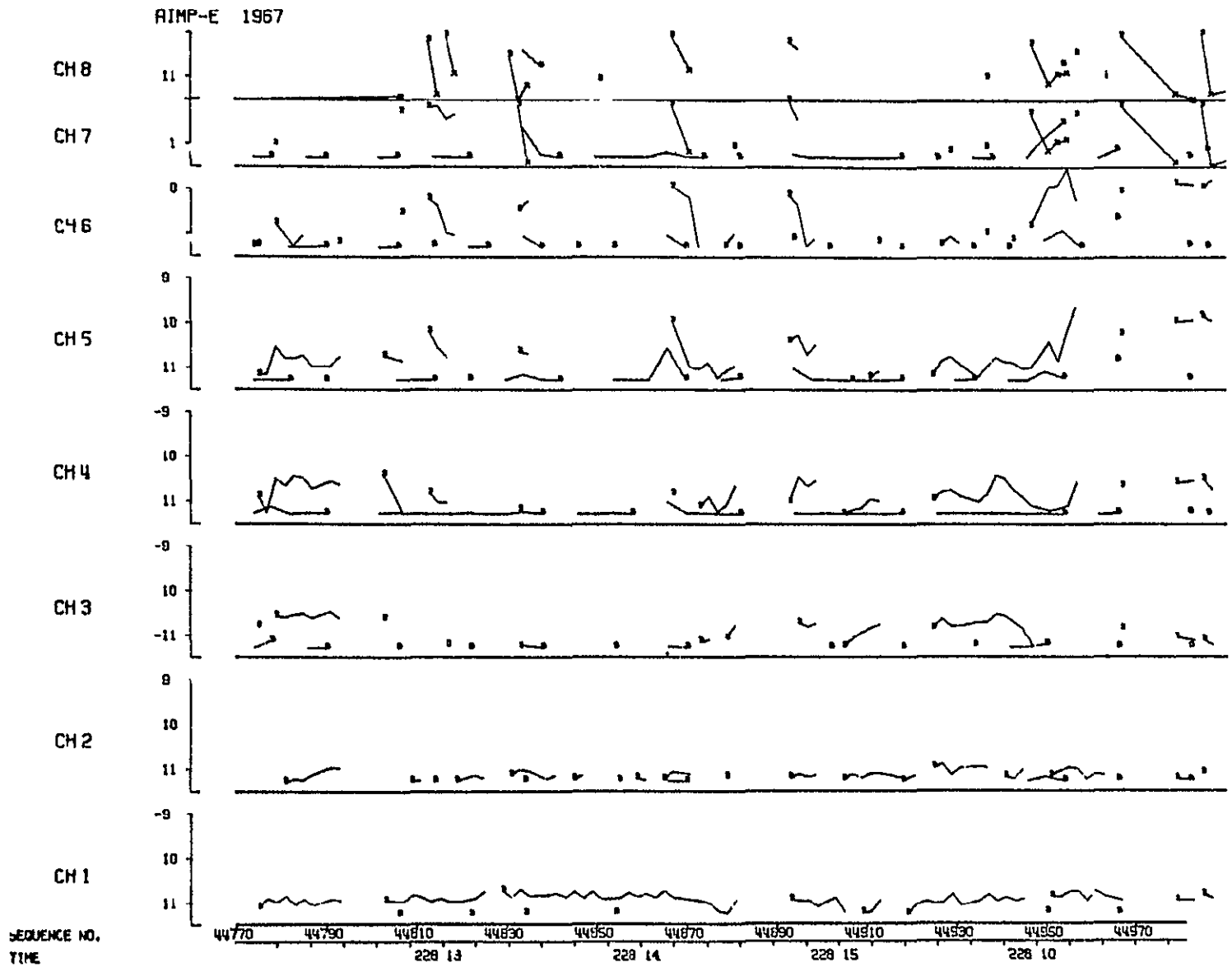
AIMP-E 1967
CH 8
CH 7
CH 6
CH 5
CH 4
CH 3
CH 2
CH 1
SEQUENCE NO.
TIME
44770
44790
44810
44830
44850
44870
44890
44910
44930
44950
44970
228 13
228 14
228 15
228 16

Figure 13b

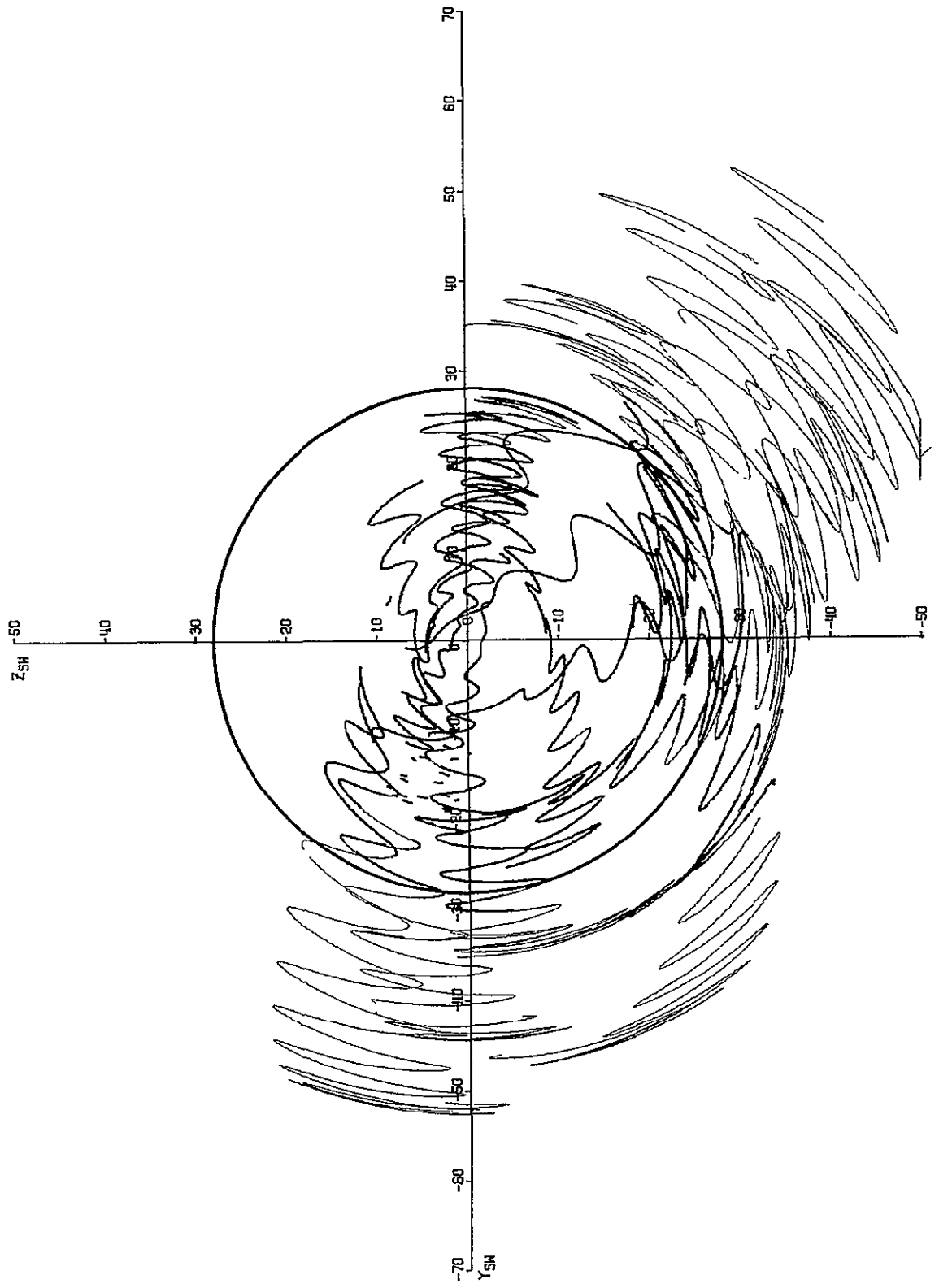

Figure 14

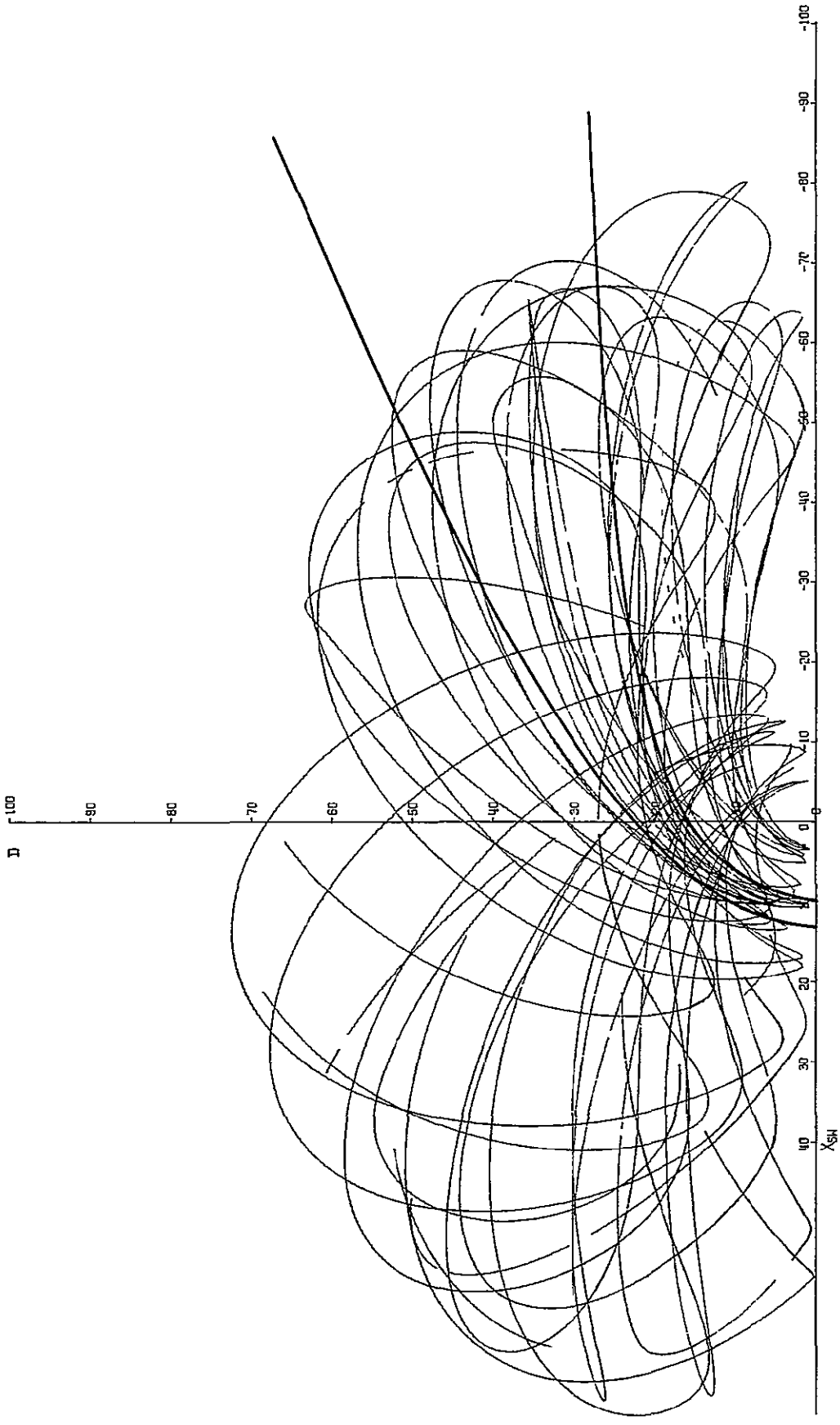
-100
-90
-80
-70
-60
-50
-40
-30
-20
-10
0
10
20
30
40
X_{SM}
100
90
80
70
60
50
40
30
20
10
0
n

Figure 15a

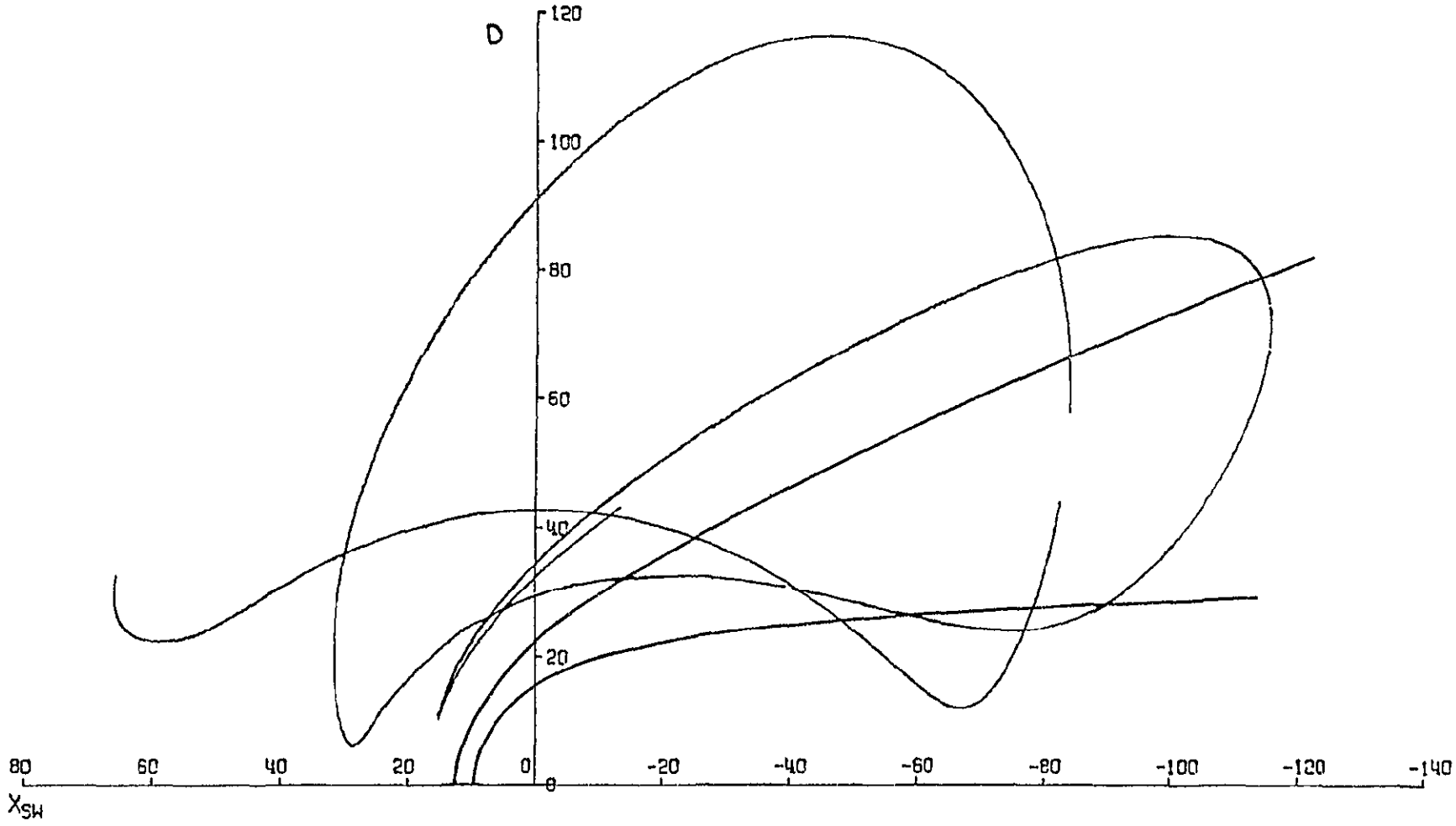

Figure 15b

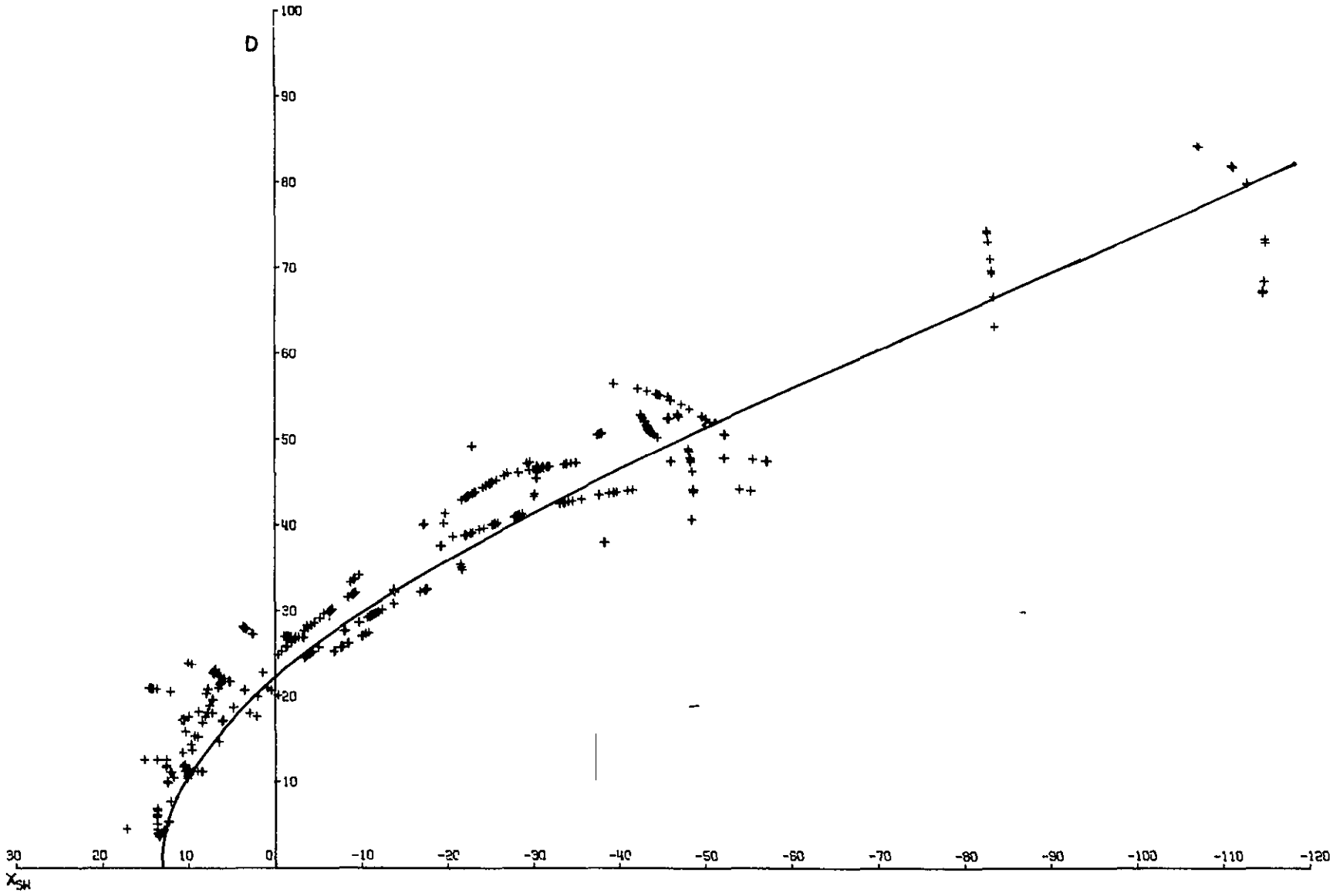
D
100
90
80
70
60
50
40
30
20
10
30
20
10
0
-10
-20
-30
-40
-50
-60
-70
-80
-90
-100
-110
-120
X_{SW}

Figure 16

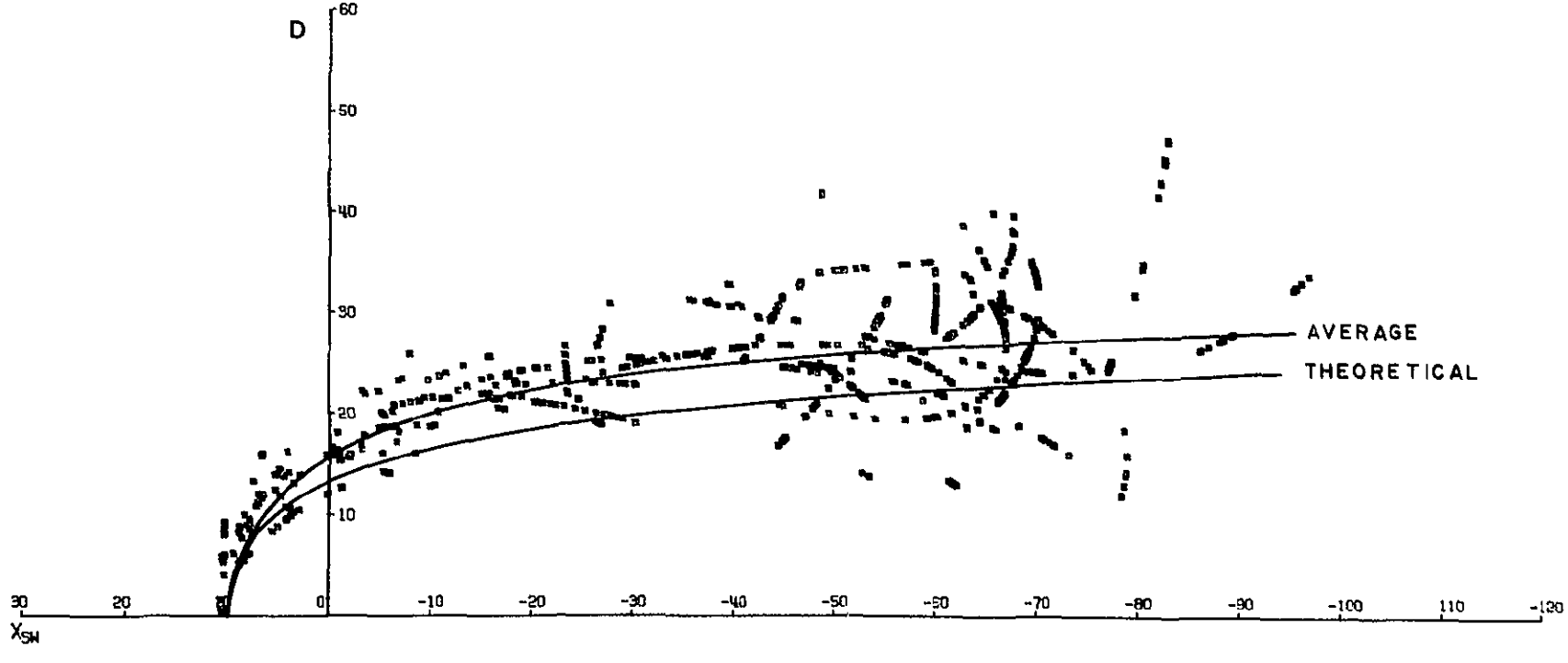
D
60
50
40
30
20
10
AVERAGE
THEORETICAL
30
20
0
-10
-20
-30
-40
-50
-60
-70
-80
-90
-100
110
-120
X_{SW}

Figure 17

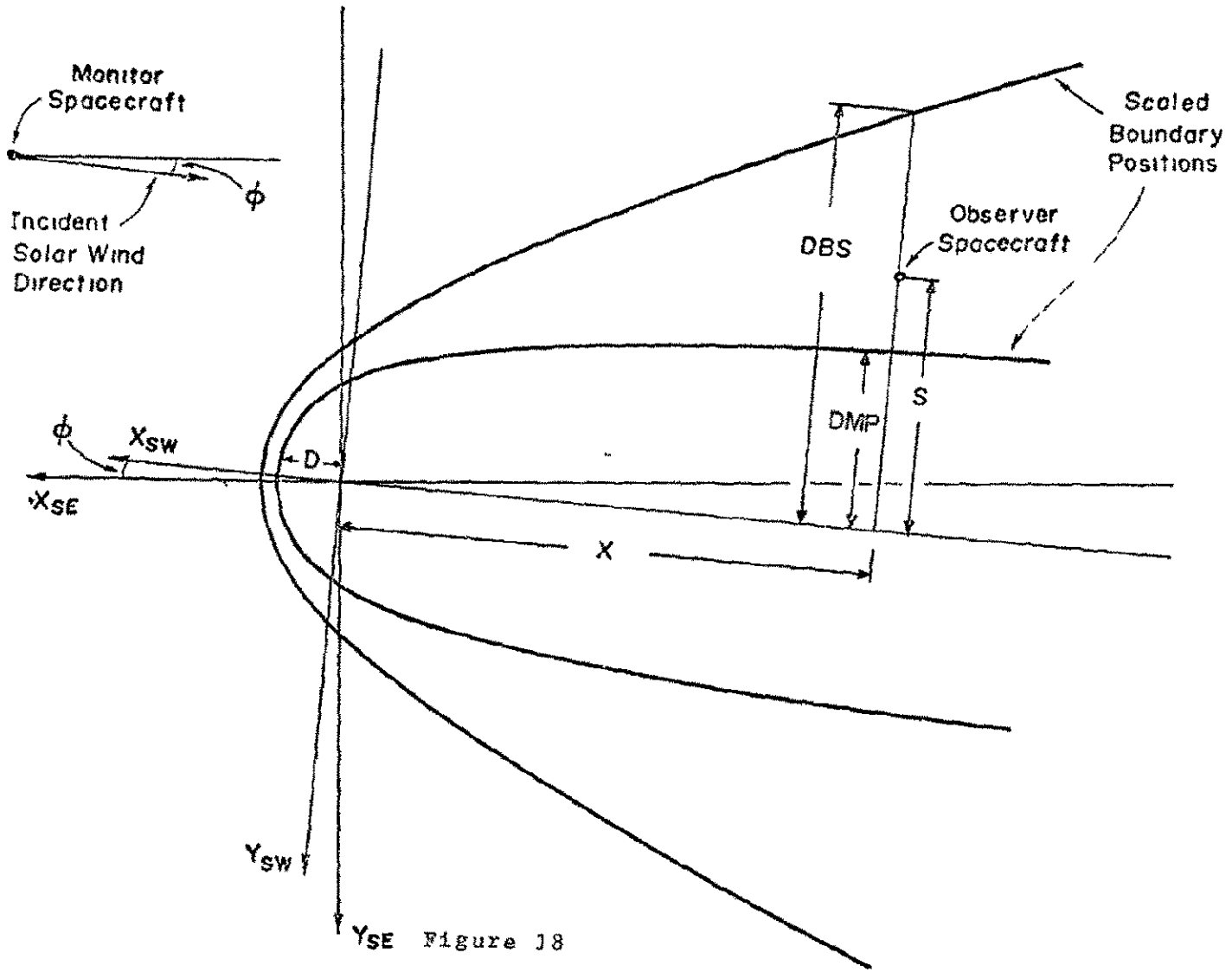
Monitor
Spacecraft
Incident
Solar Wind
Direction
ϕ
Scaled
Boundary
Positions
DBS
Observer
Spacecraft
DMP
S
ϕ
XSW
D
XSE
X
YSW
YSE

Figure 18

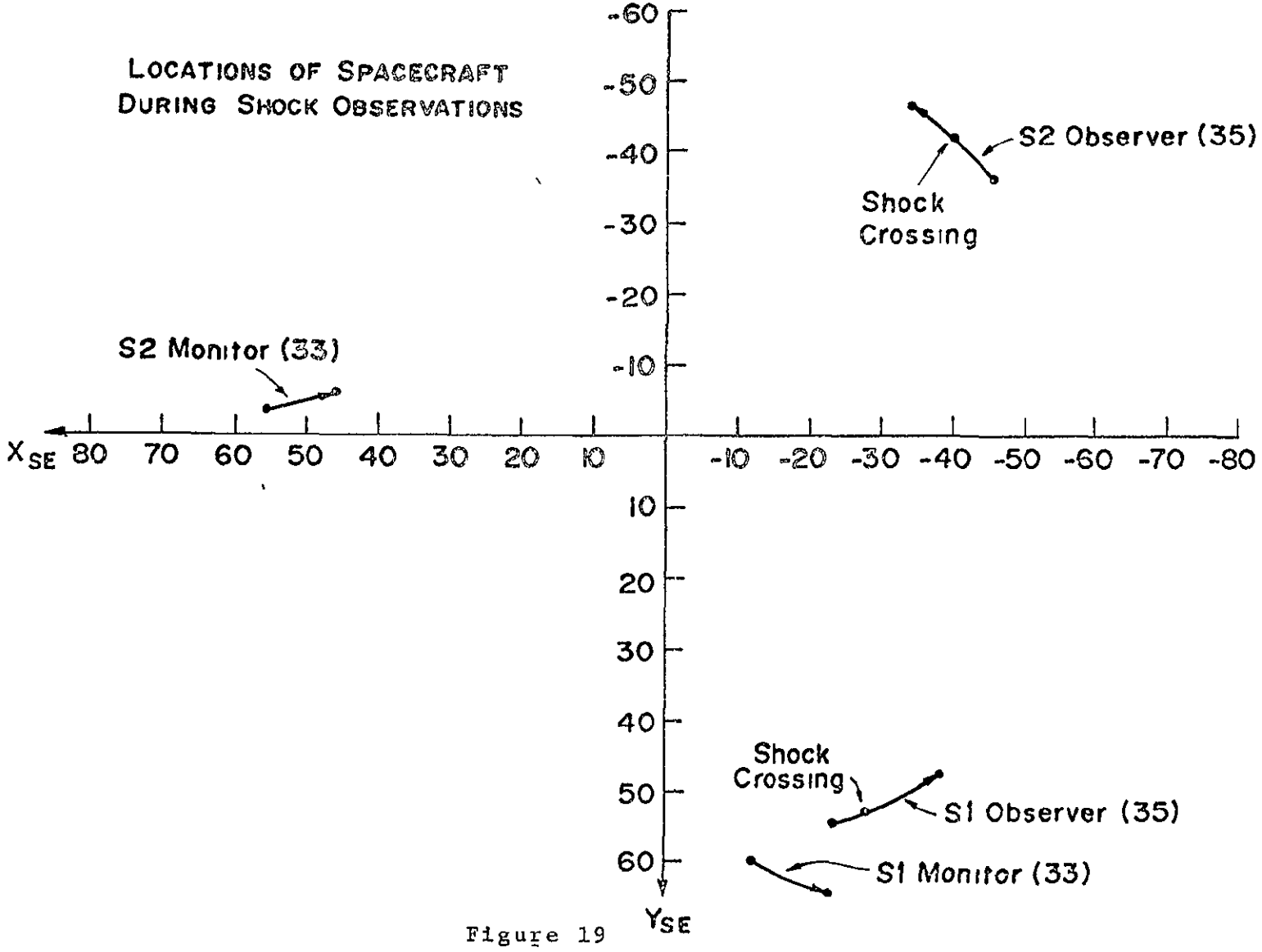
LOCATIONS OF SPACECRAFT
DURING SHOCK OBSERVATIONS
S2 Observer (35)
Shock
Crossing
S2 Monitor (33)
Shock
Crossing
S1 Observer (35)
S1 Monitor (33)
X_{SE}
Y_{SE}
80 70 60 50 40 30 20 10 -10 -20 -30 -40 -50 -60 -70 -80
-60 -50 -40 -30 -20 -10 10 20 30 40 50 60

Figure 19

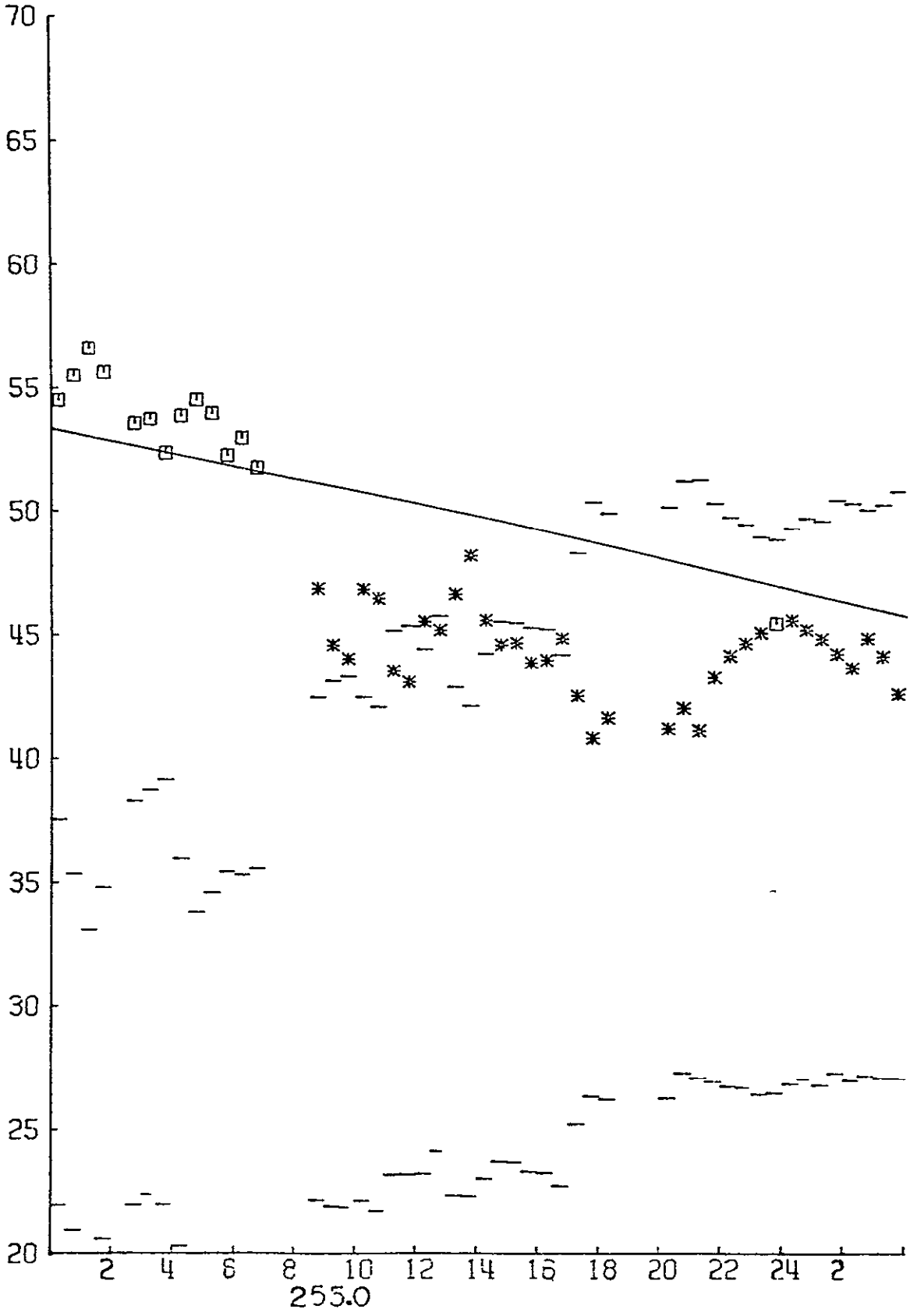

Figure 20

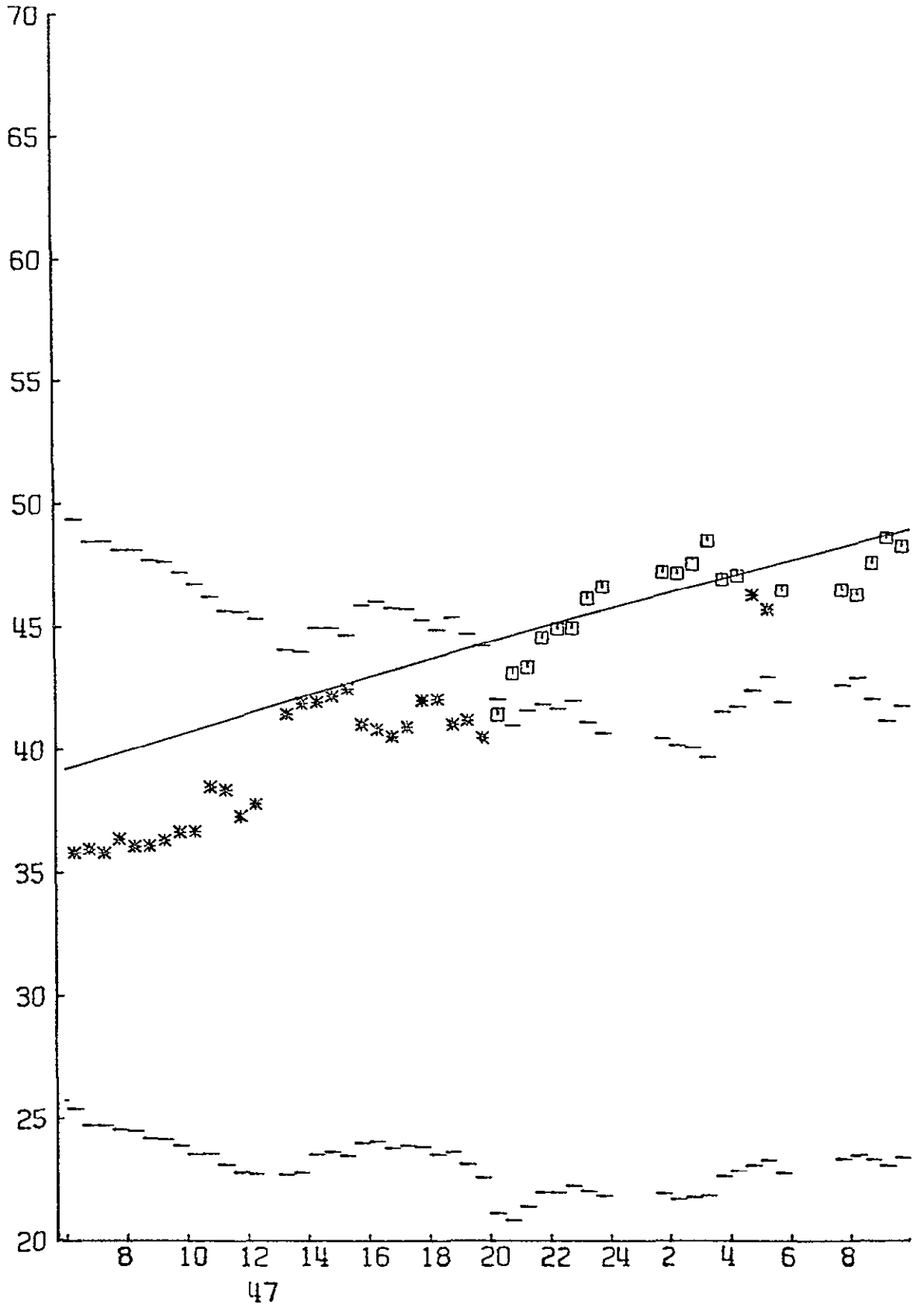

Figure 21

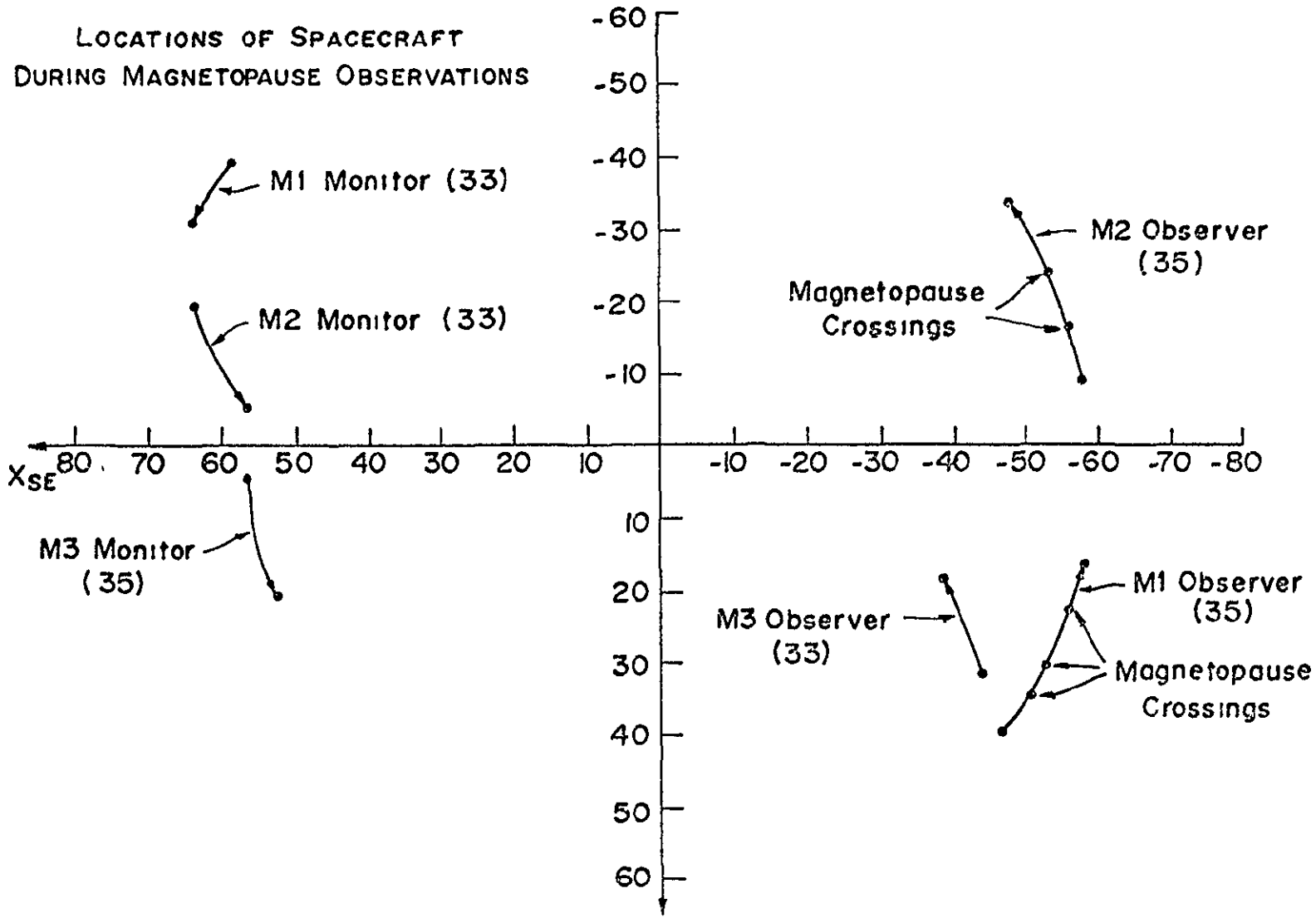
LOCATIONS OF SPACECRAFT
DURING MAGNETOPAUSE OBSERVATIONS
M1 Monitor (33)
M2 Monitor (33)
M3 Monitor
(35)
M2 Observer
(35)
Magnetopause
Crossings
M3 Observer
(33)
M1 Observer
(35)
Magnetopause
Crossings
-60
-50
-40
-30
-20
-10
10
20
30
40
50
60
80 70 60 50 40 30 20 10
-10 -20 -30 -40 -50 -60 -70 -80
X_{SE}
Y_{SE}

Figure 22

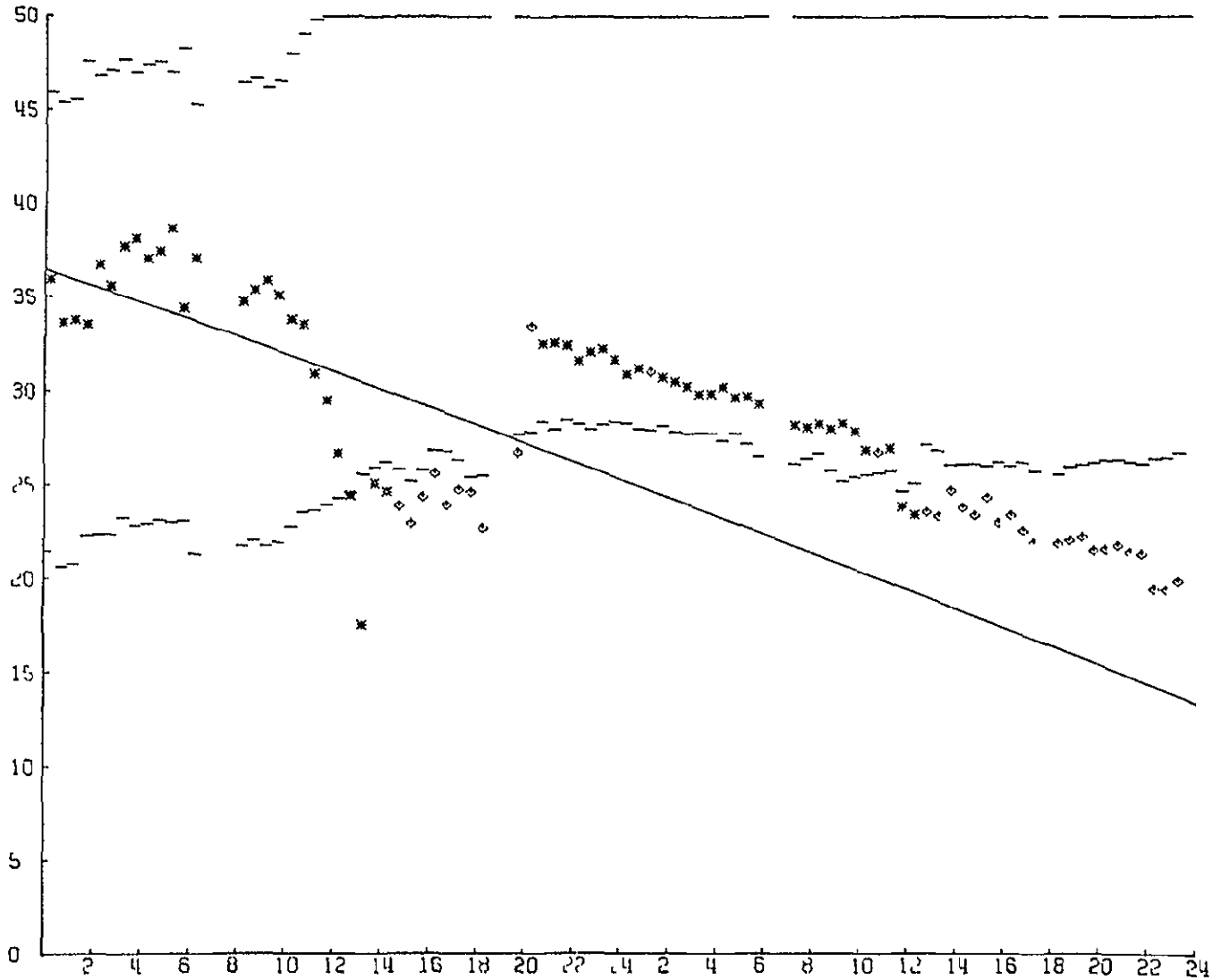
50
45
40
35
30
25
20
15
10
5
0
2 4 6 8 10 12 14 16 18 20 22 24 2 4 6 8 10 12 14 16 18 20 22 24
41
42

Figure 23

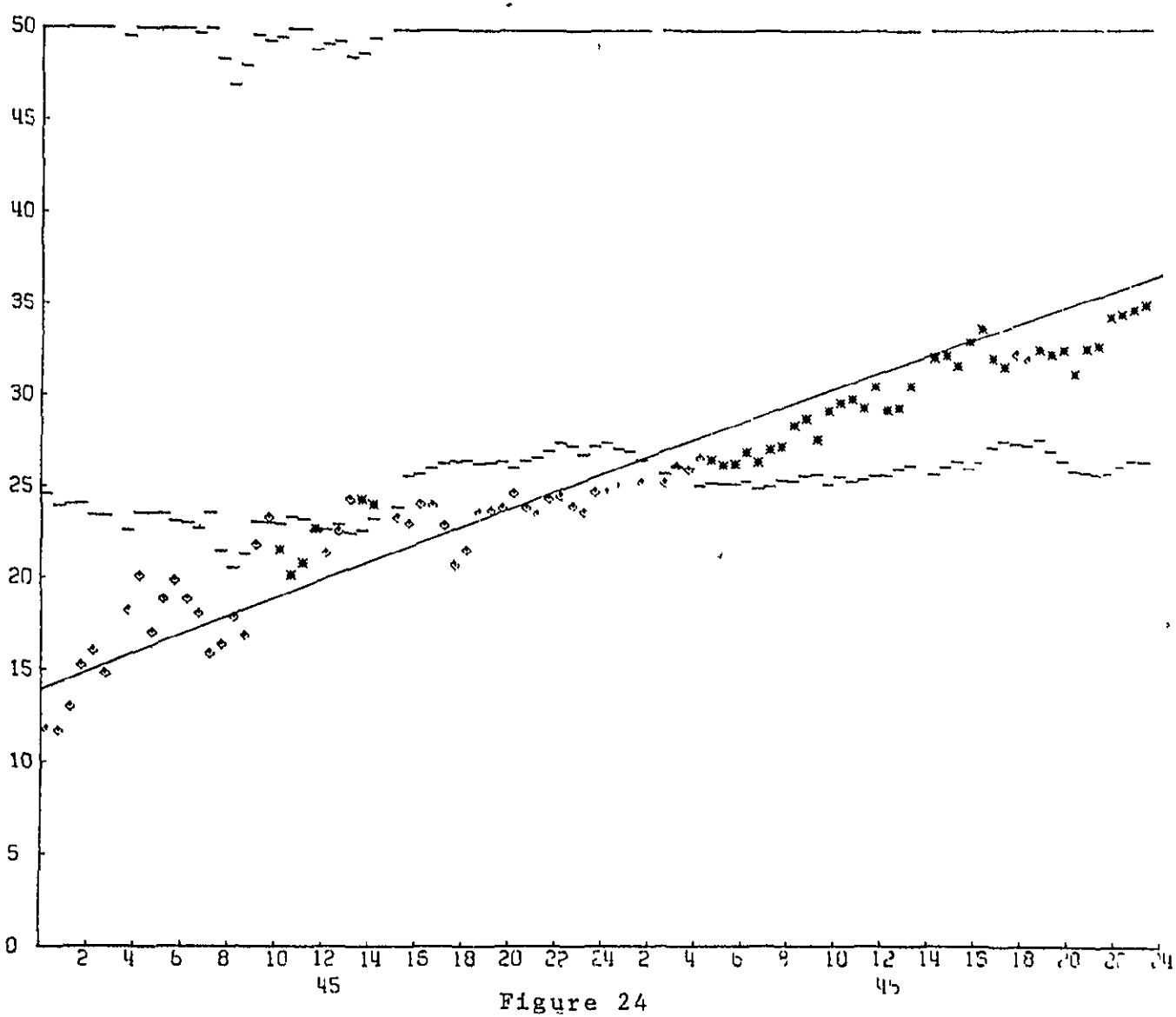
50
45
40
35
30
25
20
15
10
5
0
2 4 6 8 10 12 14 16 18 20 22 24 2 4 6 8 10 12 14 16 18 20 22 24
45
45

Figure 24

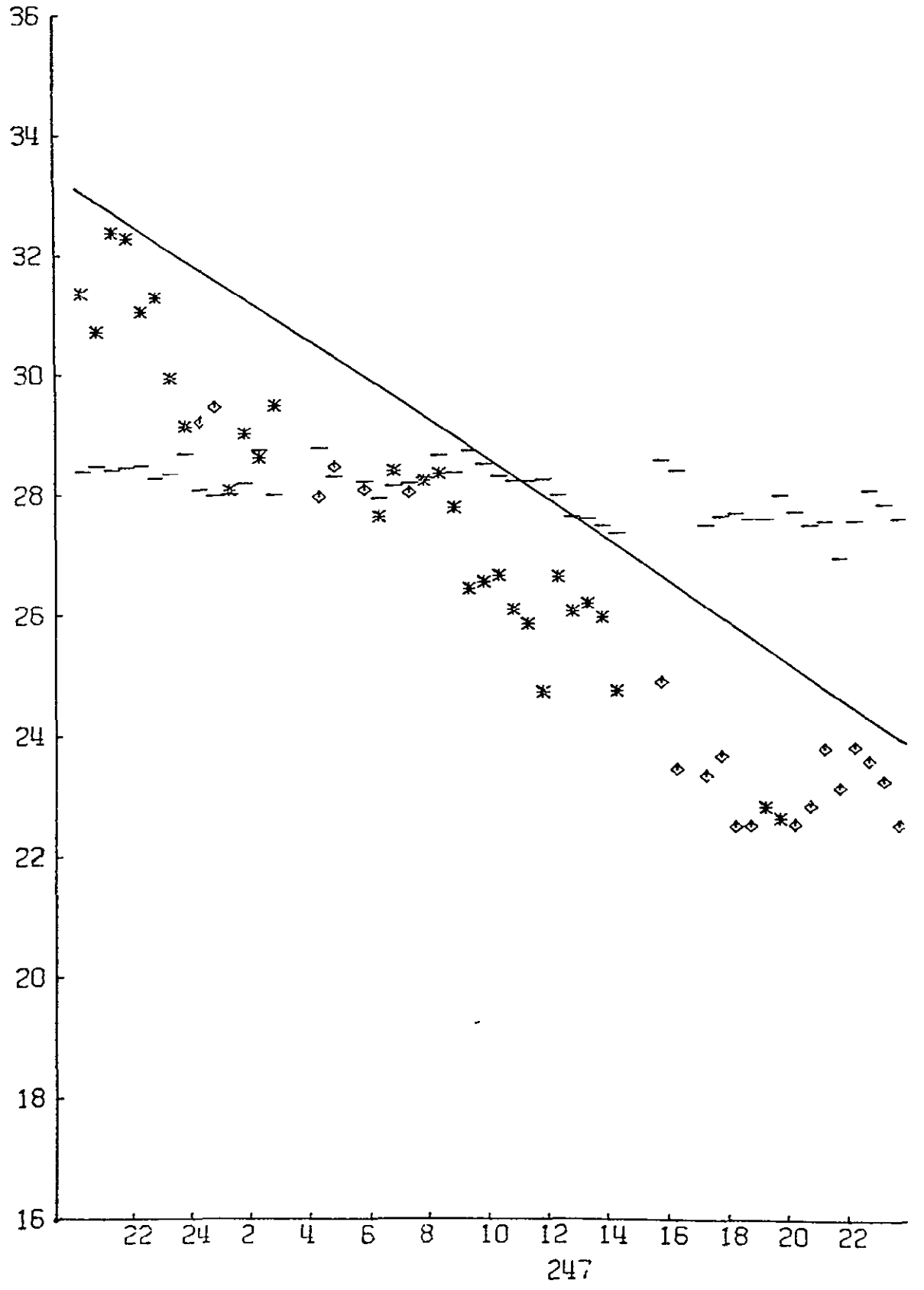

Figure 25

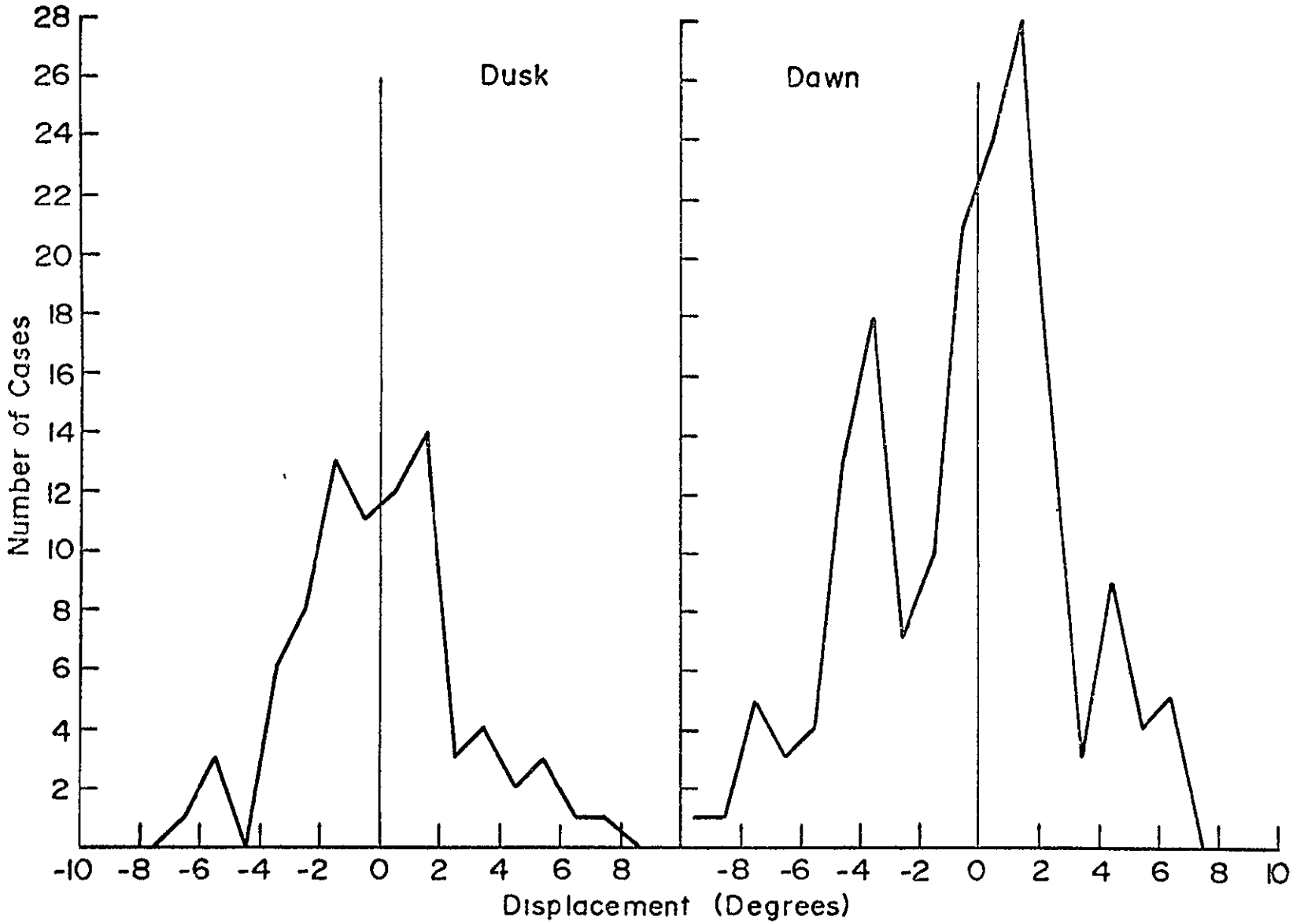
Dusk
Dawn
Number of Cases
28
26
24
22
20
18
16
14
12
10
8
6
4
2
-10 -8 -6 -4 -2 0 2 4 6 8
-8 -6 -4 -2 0 2 4 6 8 10
Displacement (Degrees)

Figure 26

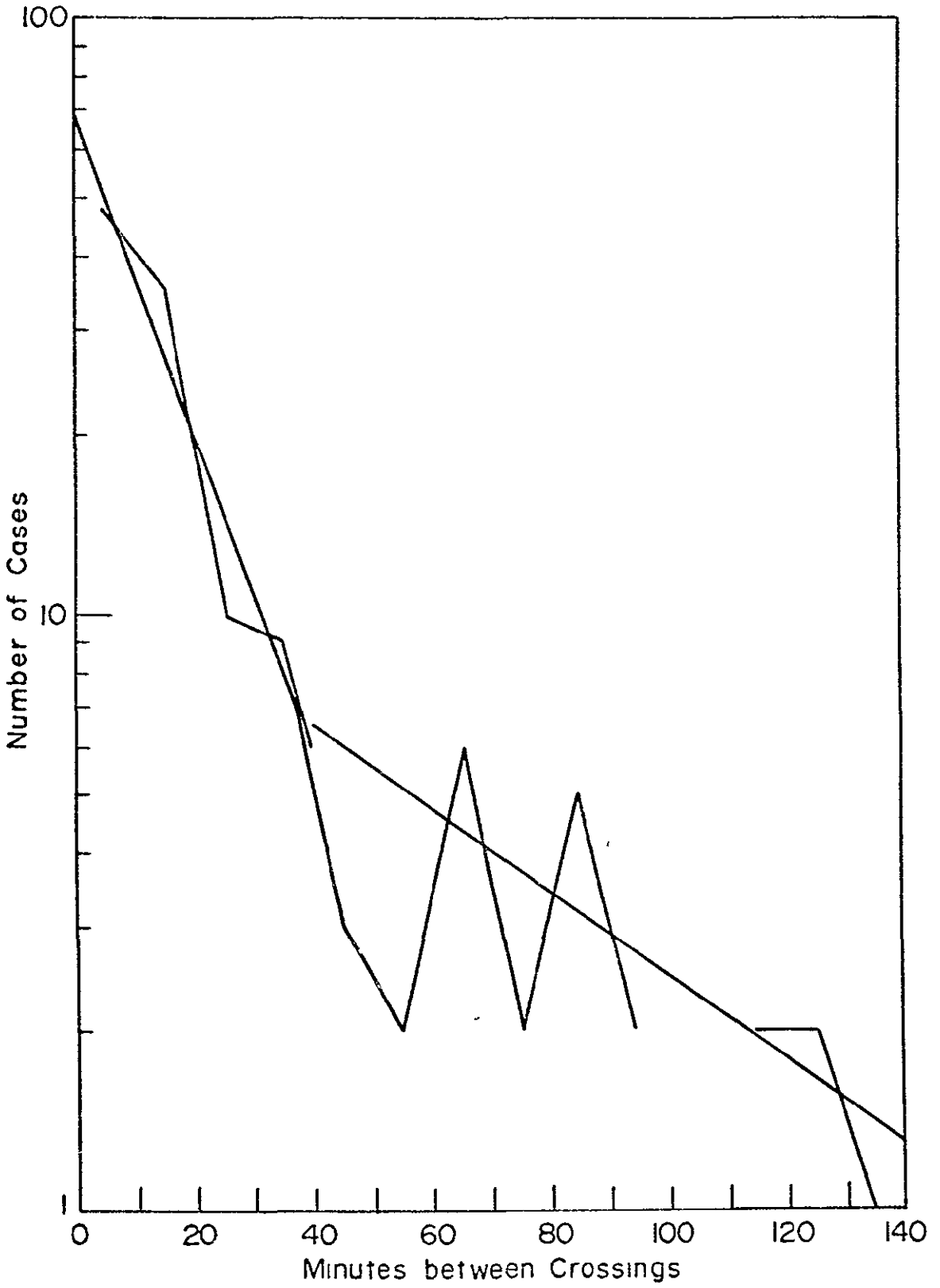
100
10
1
Number of Cases
0
20
40
60
80
100
120
140
Minutes between Crossings

Figure 27a

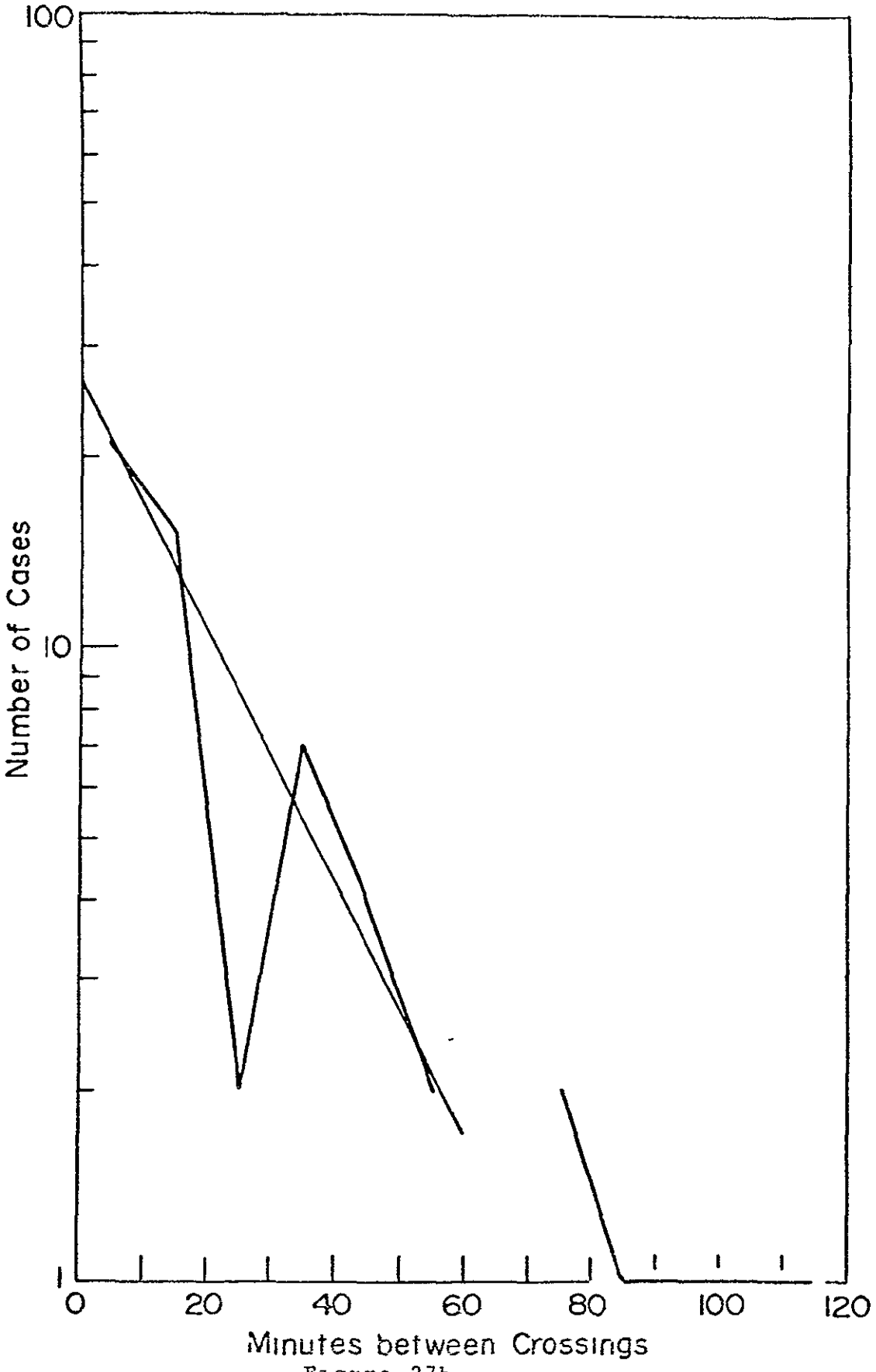
100
10
1
Number of Cases
0
20
40
60
80
100
120
Minutes between Crossings

Figure 27b

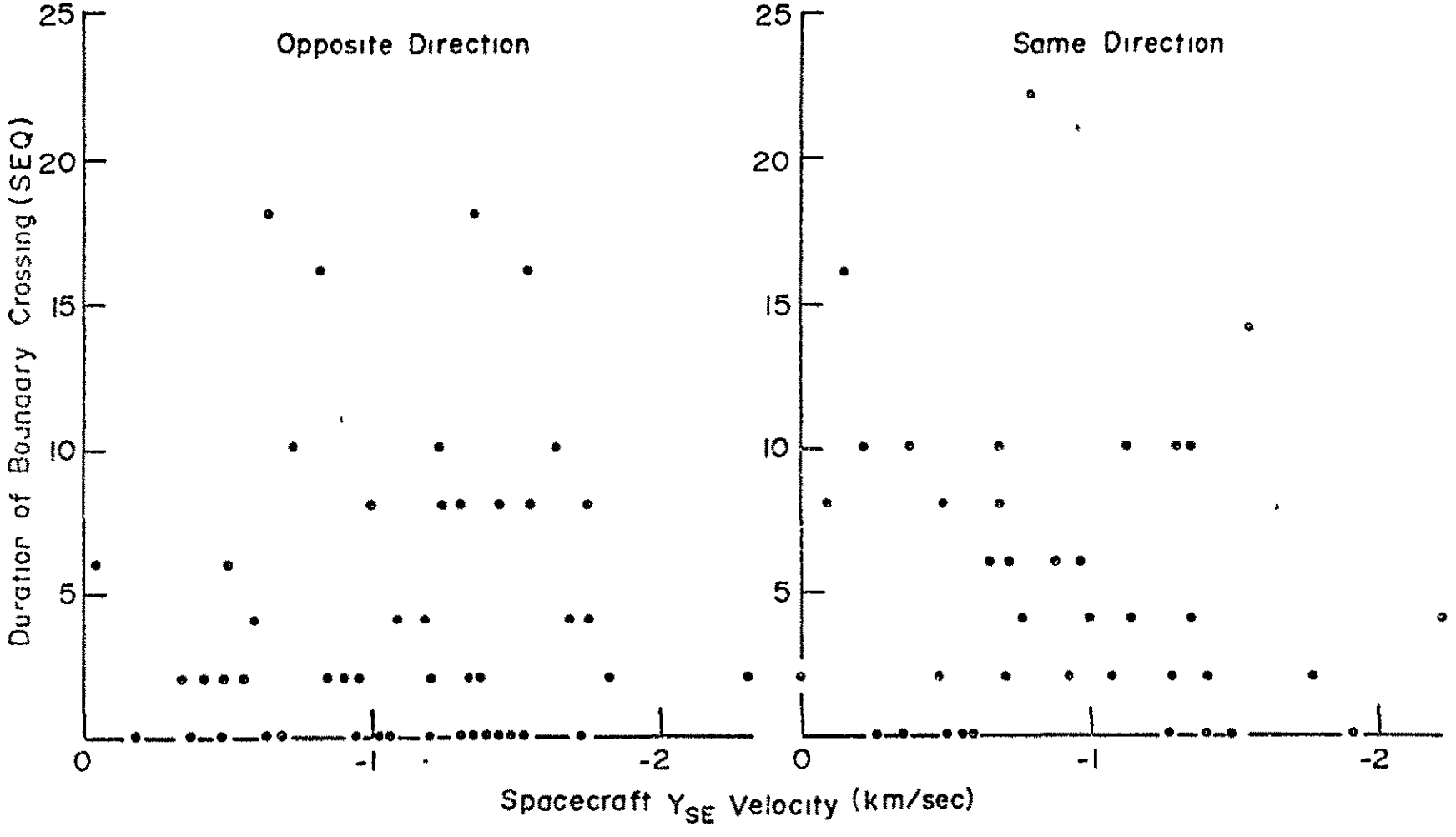
Opposite Direction
Same Direction
Duration of Boundary Crossing (SEQ)
25
20
15
10
5
0
-1
-2
Spacecraft Y_{SE} Velocity (km/sec)

Figure 28

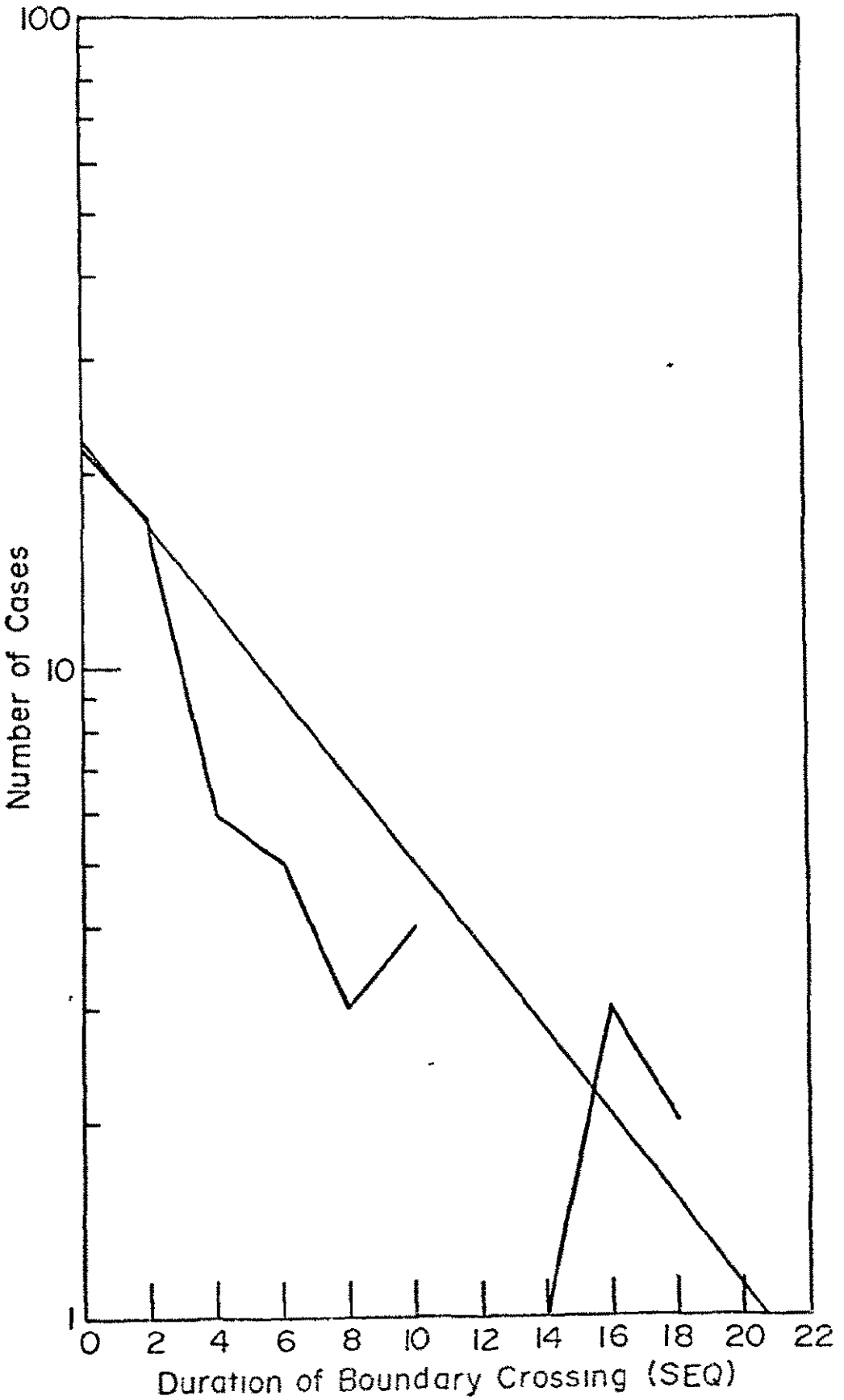
100
10
1
Number of Cases
0
2
4
6
8
10
12
14
16
18
20
22
Duration of Boundary Crossing (SEQ)

Figure 29a

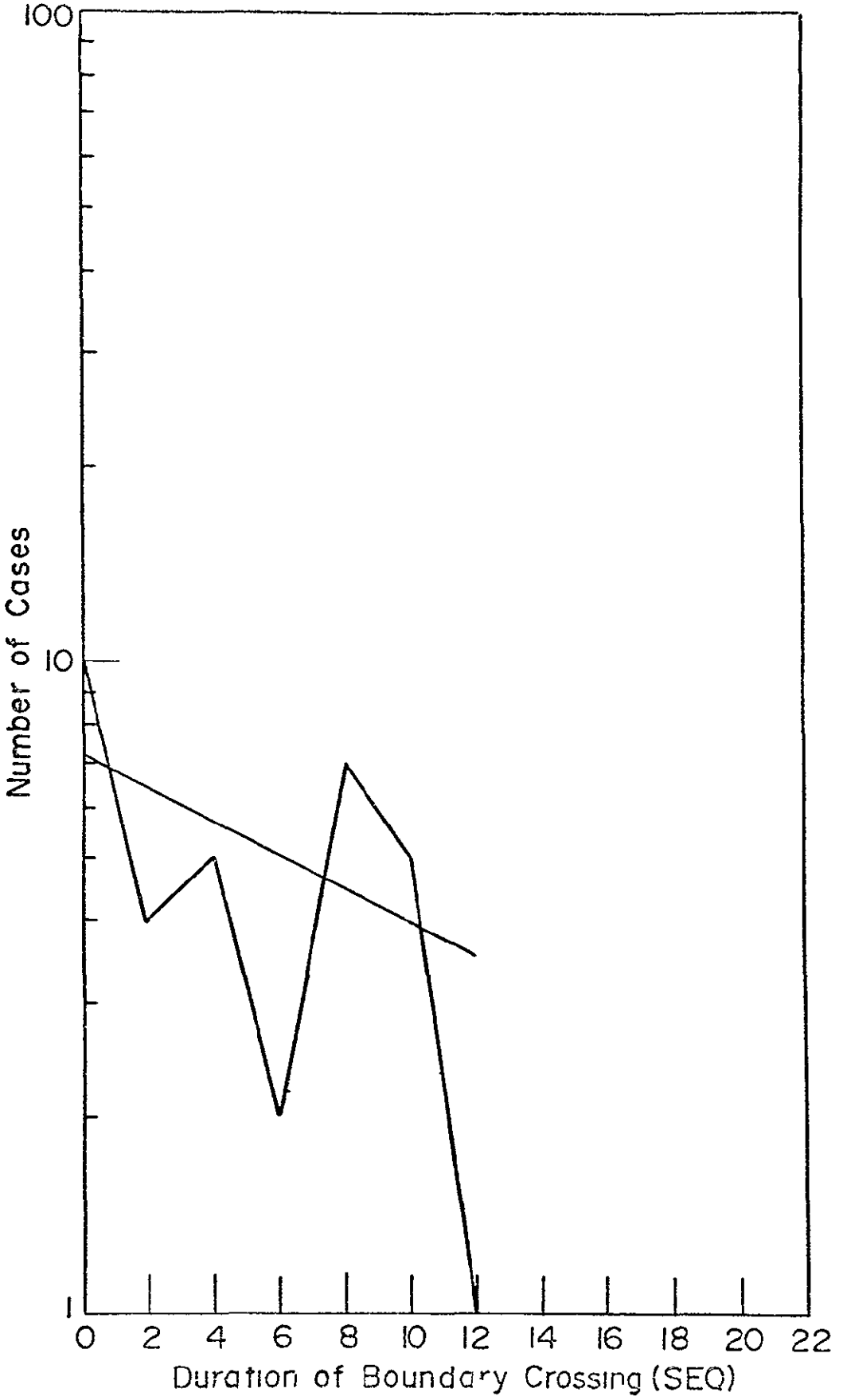
100
10
1
Number of Cases
0
2
4
6
8
10
12
14
16
18
20
22
Duration of Boundary Crossing (SEQ)

Figure 29b

BOUNDARY MOTION MODEL

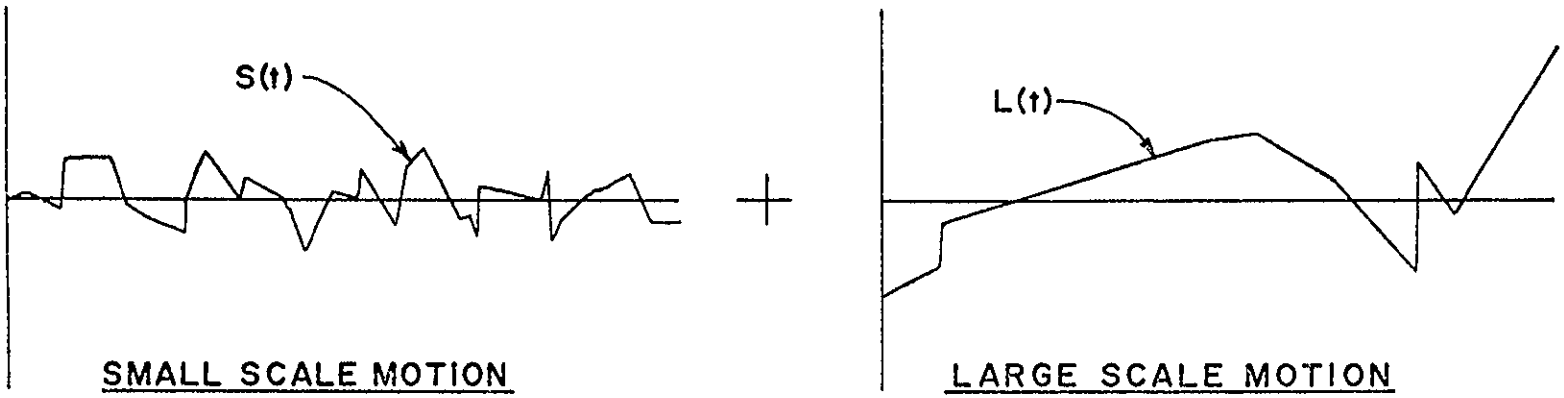

SMALL SCALE MOTION

LARGE SCALE MOTION

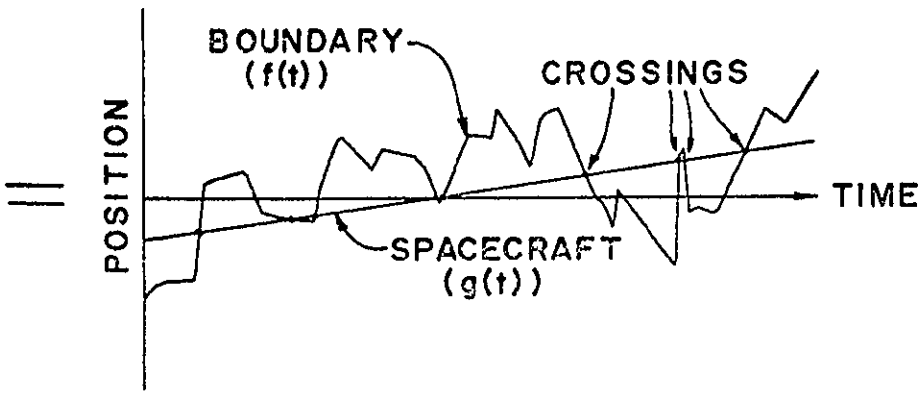

TOTAL MOTION Figure 30

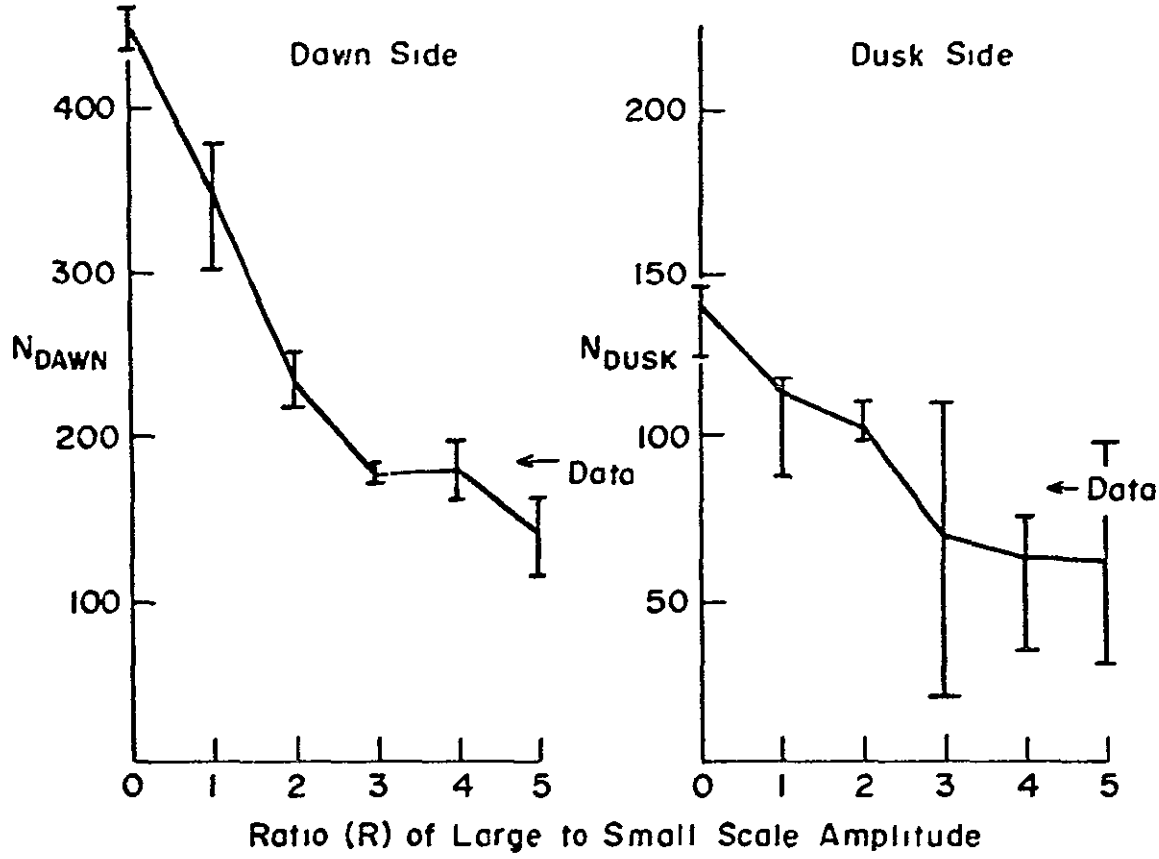
Down Side
Dusk Side
400
300
200
100
200
150
100
50
N_{DAWN}
N_{DUSK}
Data
Data
0 1 2 3 4 5
0 1 2 3 4 5
Ratio (R) of Large to Small Scale Amplitude

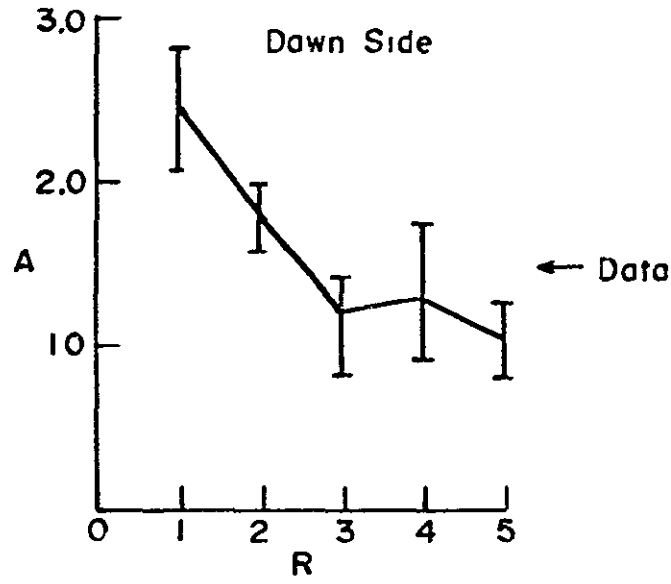
3.0
2.0
1.0
A
Down Side
Data
0 1 2 3 4 5
R

Figure 31

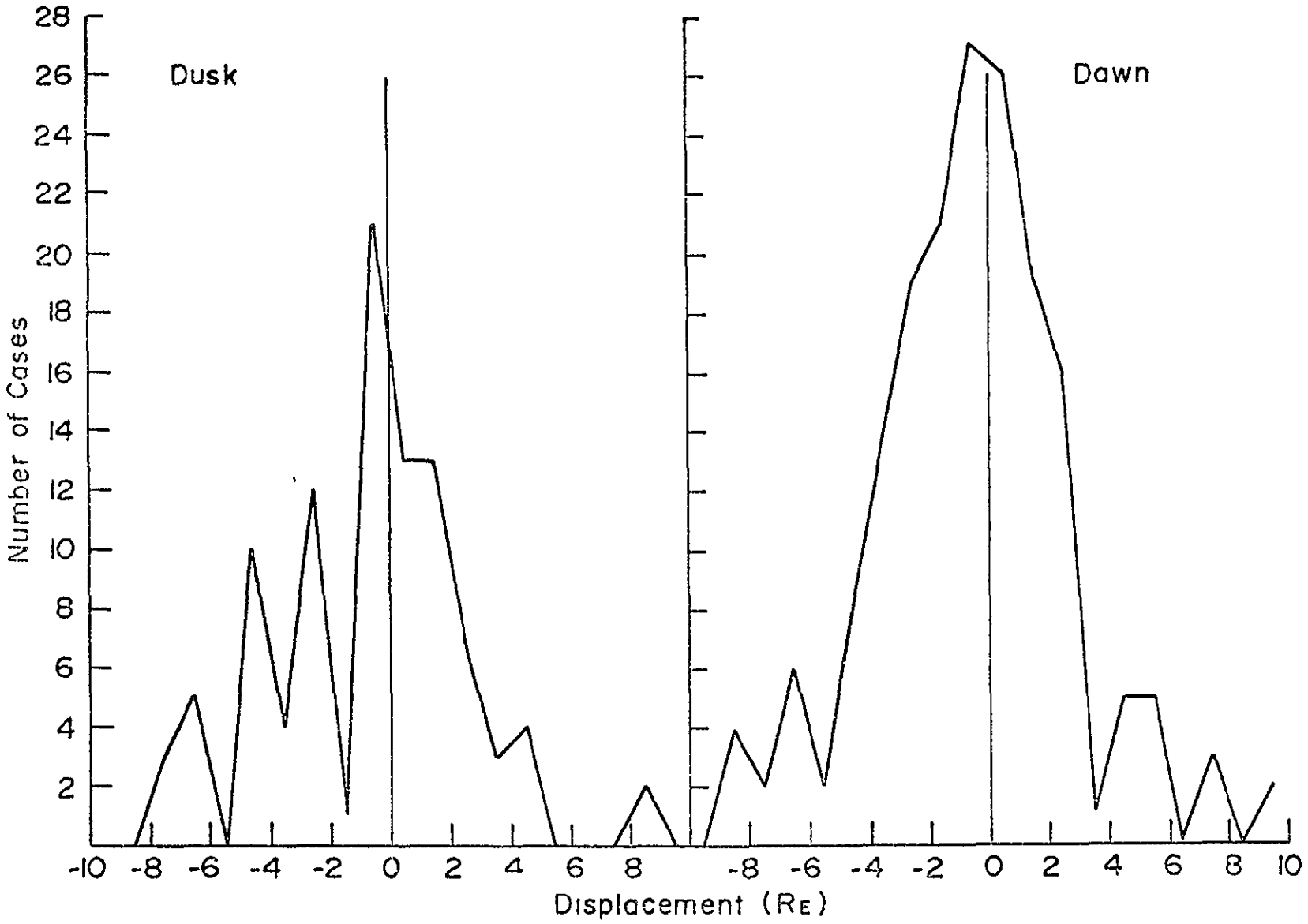
Dusk
Dawn
Number of Cases
28
26
24
22
20
18
16
14
12
10
8
6
4
2
-10 -8 -6 -4 -2 0 2 4 6 8
-8 -6 -4 -2 0 2 4 6 8 10
Displacement (RE)

Figure 32

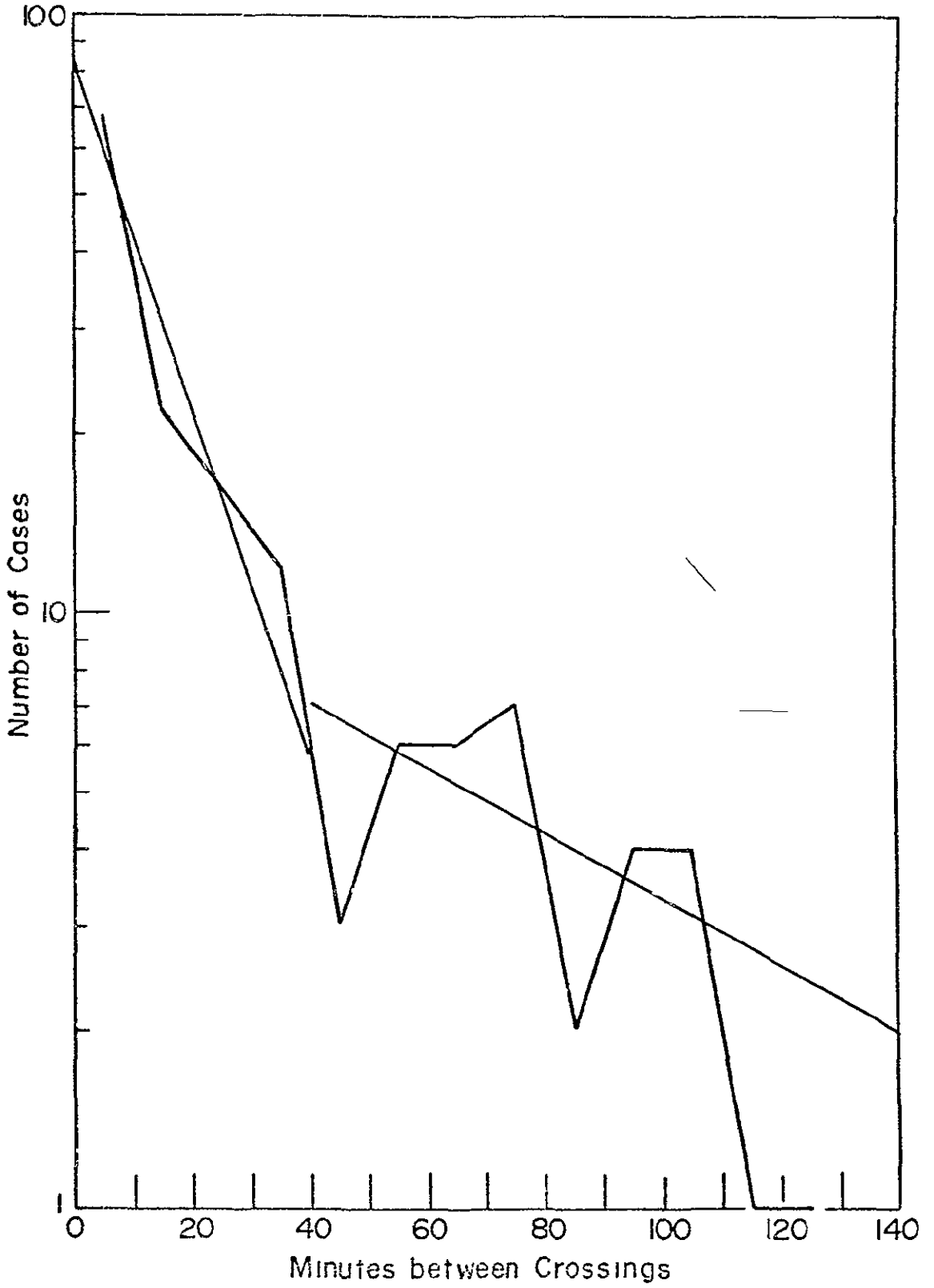
100
10
1
Number of Cases
0
20
40
60
80
100
120
140
Minutes between Crossings

Figure 33a

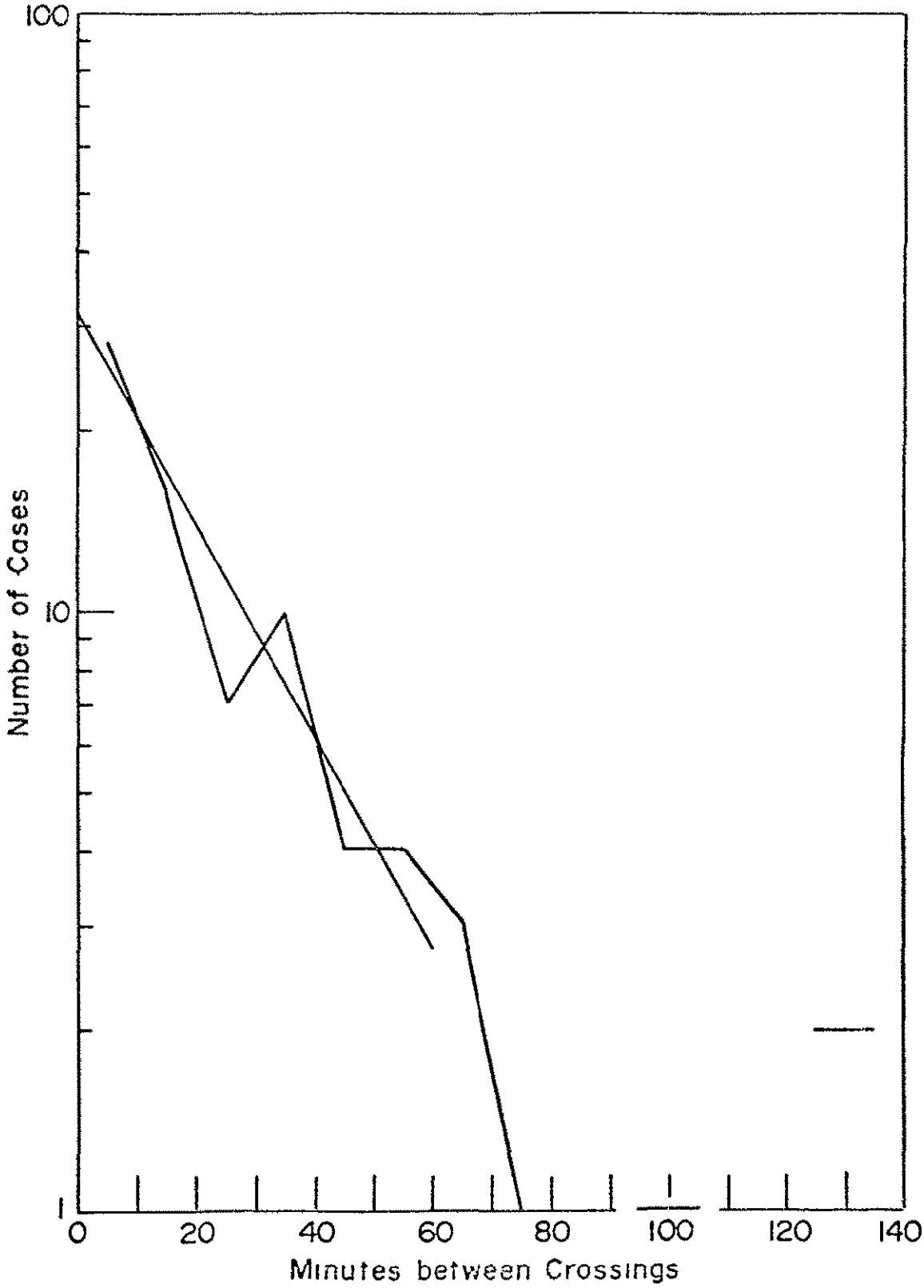
100
10
1
Number of Cases
0
20
40
60
80
100
120
140
Minutes between Crossings

Figure 33b

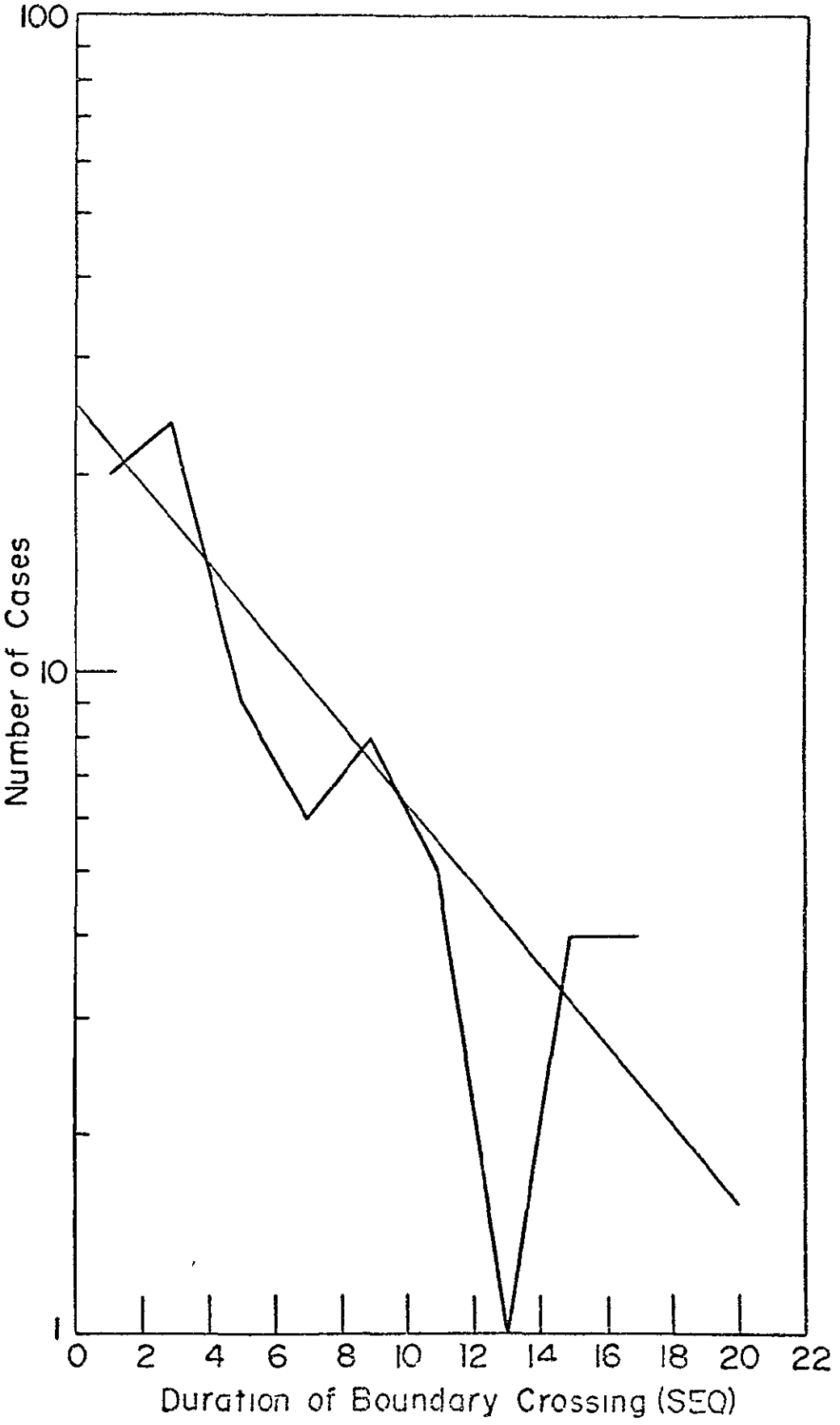
100
10
1
Number of Cases
0
2
4
6
8
10
12
14
16
18
20
22
Duration of Boundary Crossing (SEQ)

Figure 34a

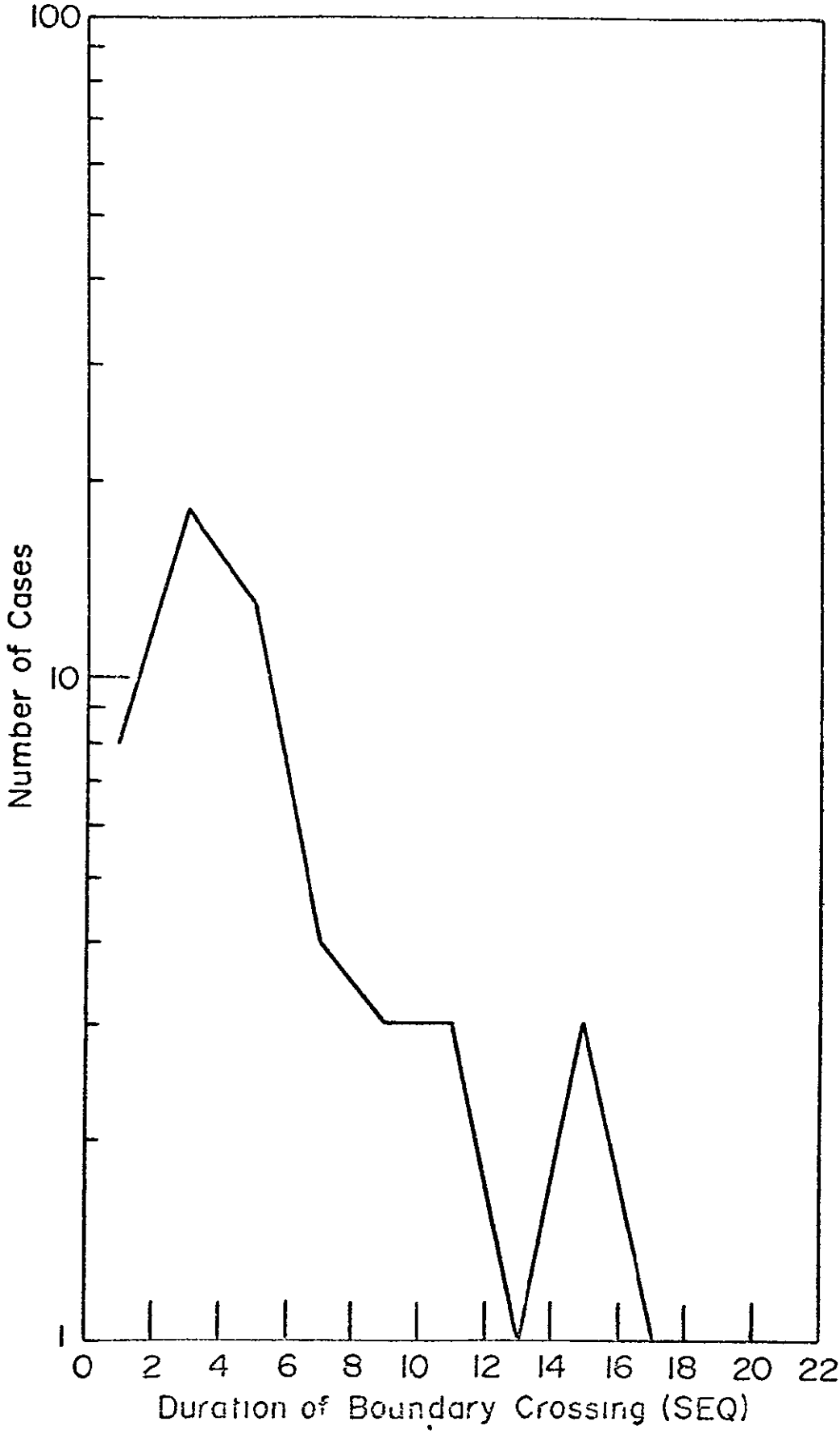
100
10
1
Number of Cases
0
2
4
6
8
10
12
14
16
18
20
22
Duration of Boundary Crossing (SEQ)

Figure 34b

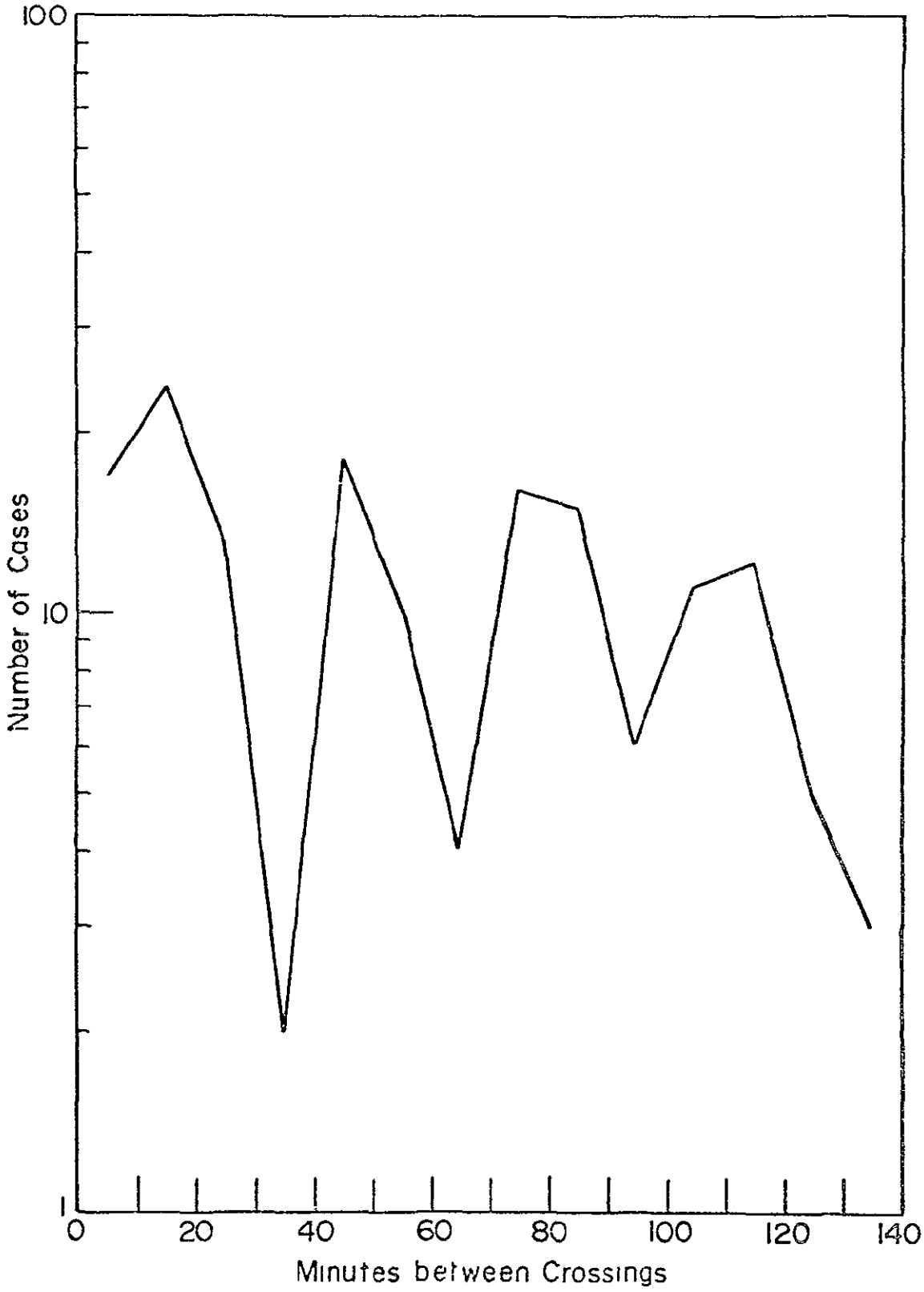
100
10
1
Number of Cases
0
20
40
60
80
100
120
140
Minutes between Crossings

Figure 35

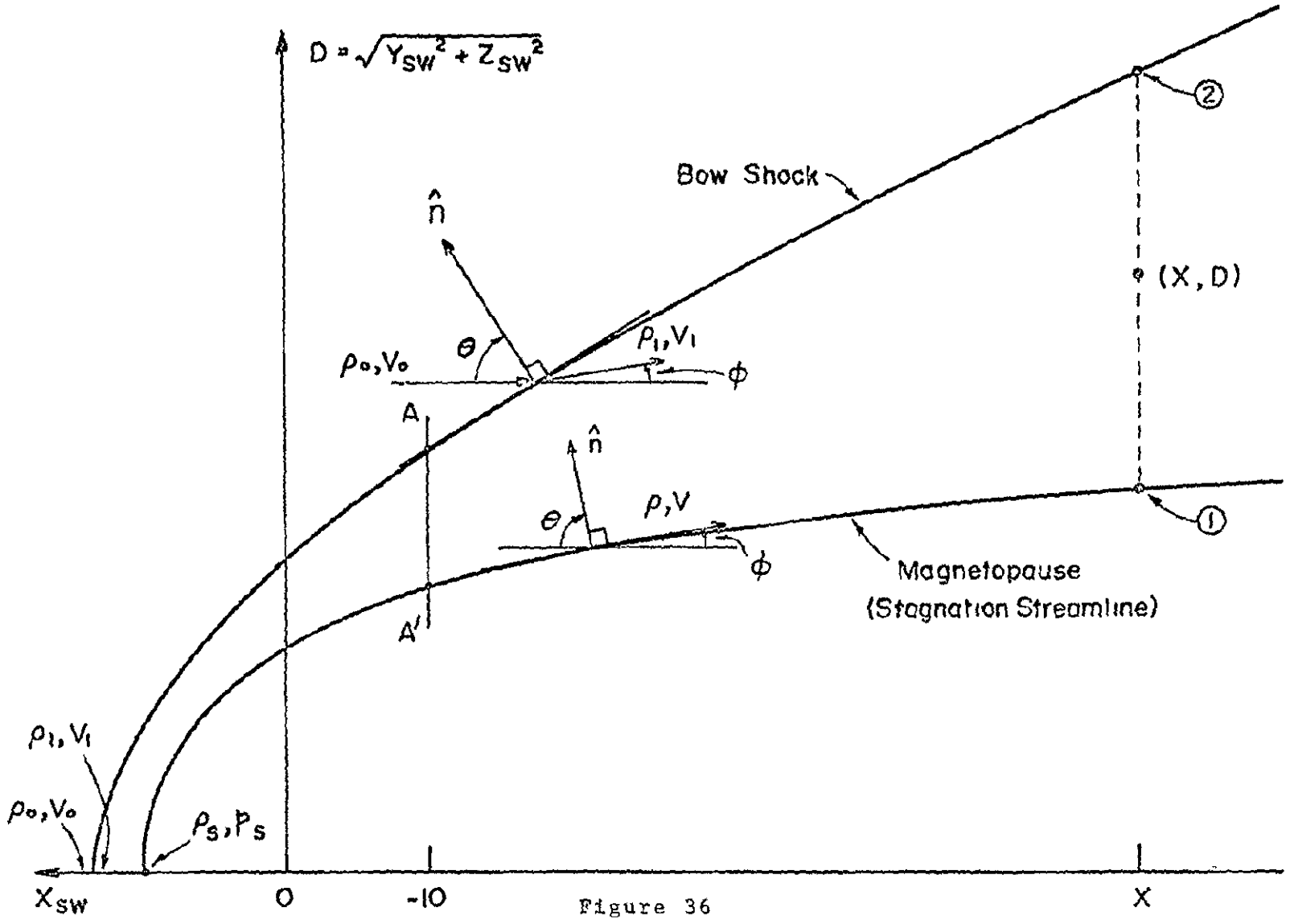
$D = \sqrt{Y_{SW}^2 + Z_{SW}^2}$
Bow Shock
$\hat{n}$
(X, D)
ρ_1, V_1
ρ_0, V_0
θ
ϕ
A
$\hat{n}$
ρ, V
θ
ϕ
A'
Magnetopause
(Stagnation Streamline)
ρ_1, V_1
ρ_0, V_0
ρ_s, P_s
X_{SW}
0
-10
X

Figure 36

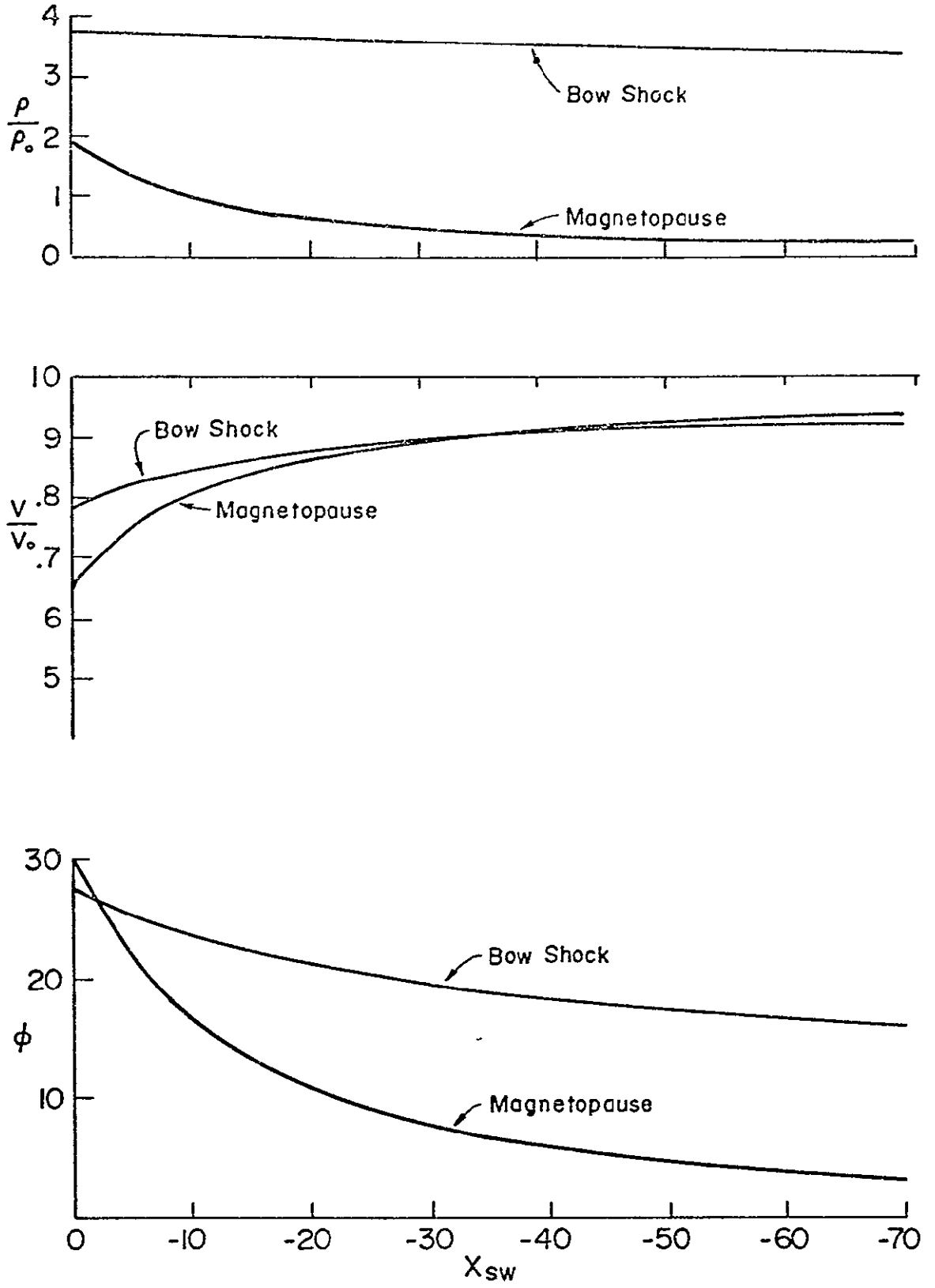
4
3
ρ/ρ₀ 2
1
0
Bow Shock
Magnetopause
10
9
V/V₀ .8
.7
6
5
Bow Shock
Magnetopause
30
20
ϕ
10
Bow Shock
Magnetopause
0
-10
-20
-30
-40
-50
-60
-70
Xsw

Figure 37

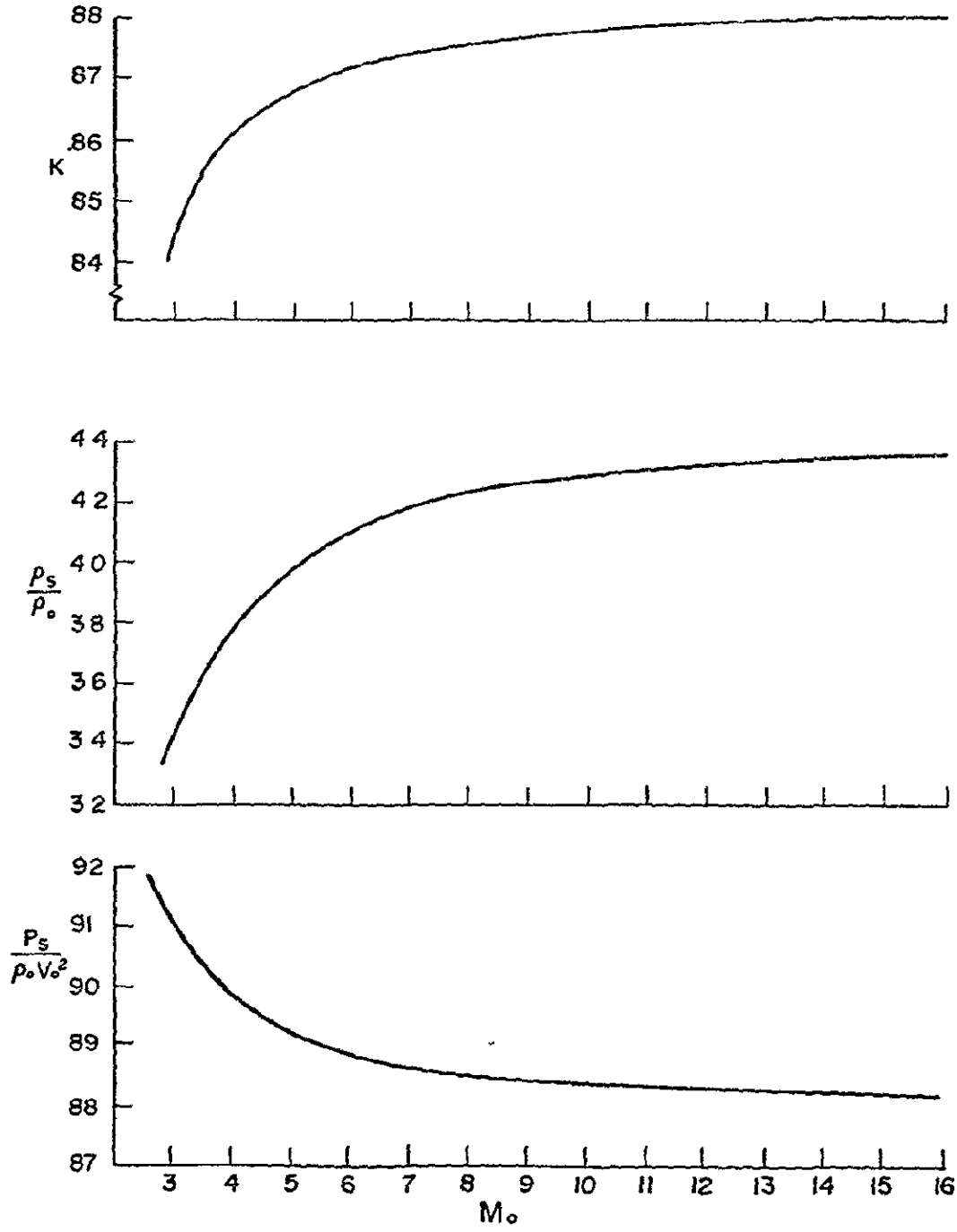
88
87
86
K
85
84
44
42
40
$\frac{p_s}{p_o}$
38
36
34
32
92
91
$\frac{P_s}{\rho_o V_o^2}$
90
89
88
87
3
4
5
6
7
8
9
10
11
12
13
14
15
16
M_o

Figure 38

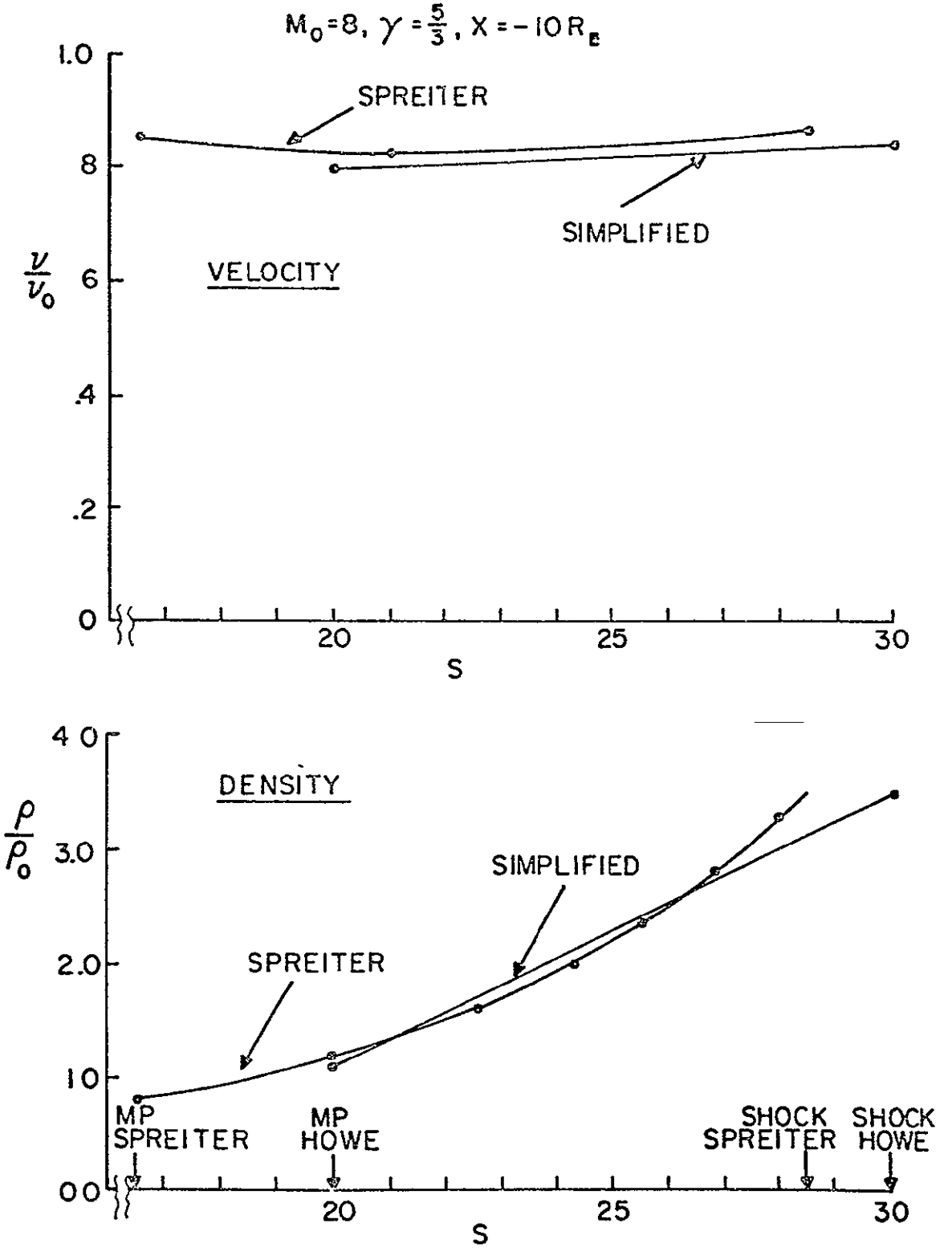
$M_0=8,\ \gamma=\frac{5}{3},\ X=-10R_E$
1.0
8
6
4
2
0
SPREITER
SIMPLIFIED
$\frac{v}{v_0}$
VELOCITY
20
25
30
S
4 0
3.0
2.0
10
00
DENSITY
$\frac{\rho}{\rho_0}$
SIMPLIFIED
SPREITER
MP SPREITER
MP HOWE
SHOCK SPREITER
SHOCK HOWE
20
25
30
S

Figure 39

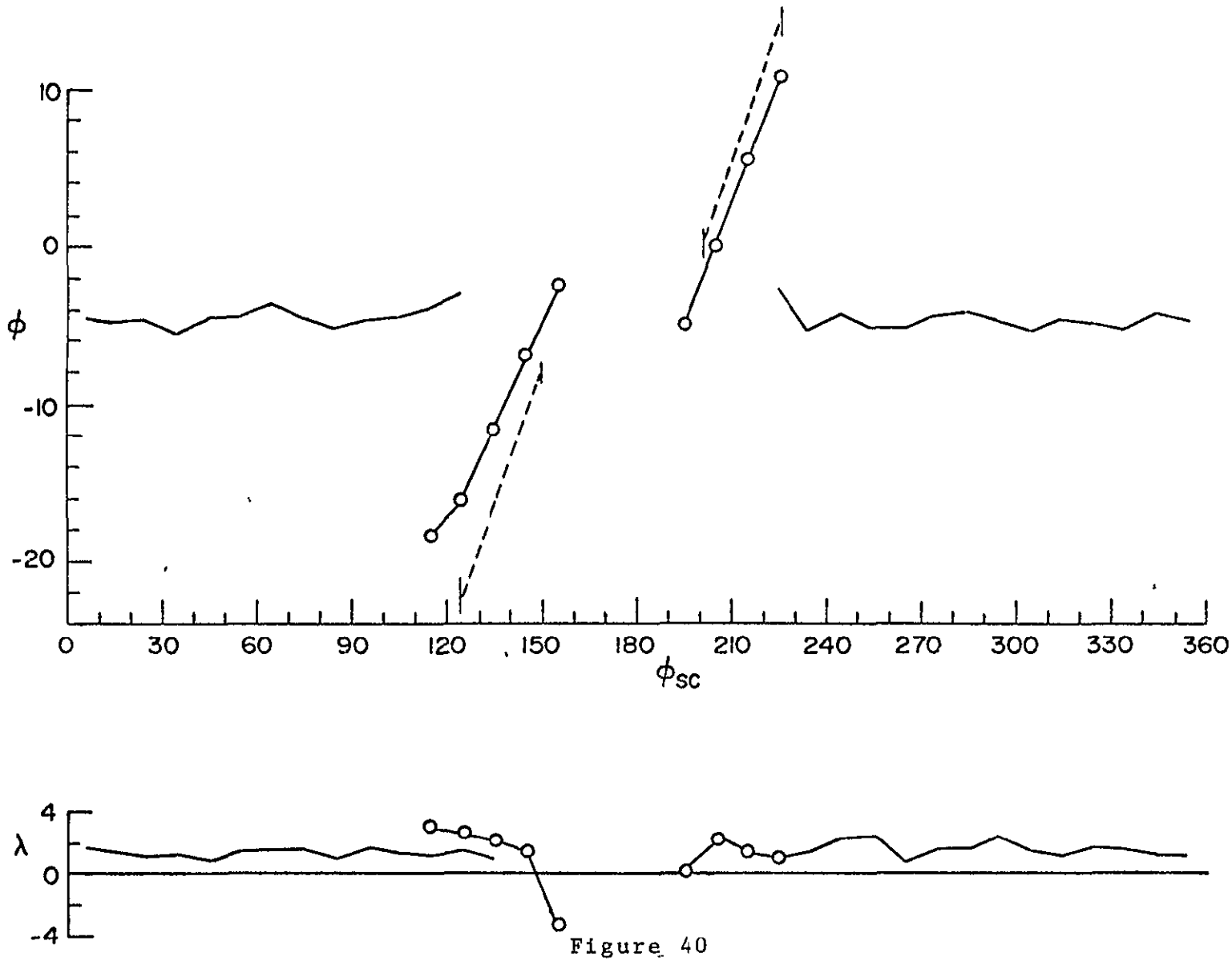

Figure 40

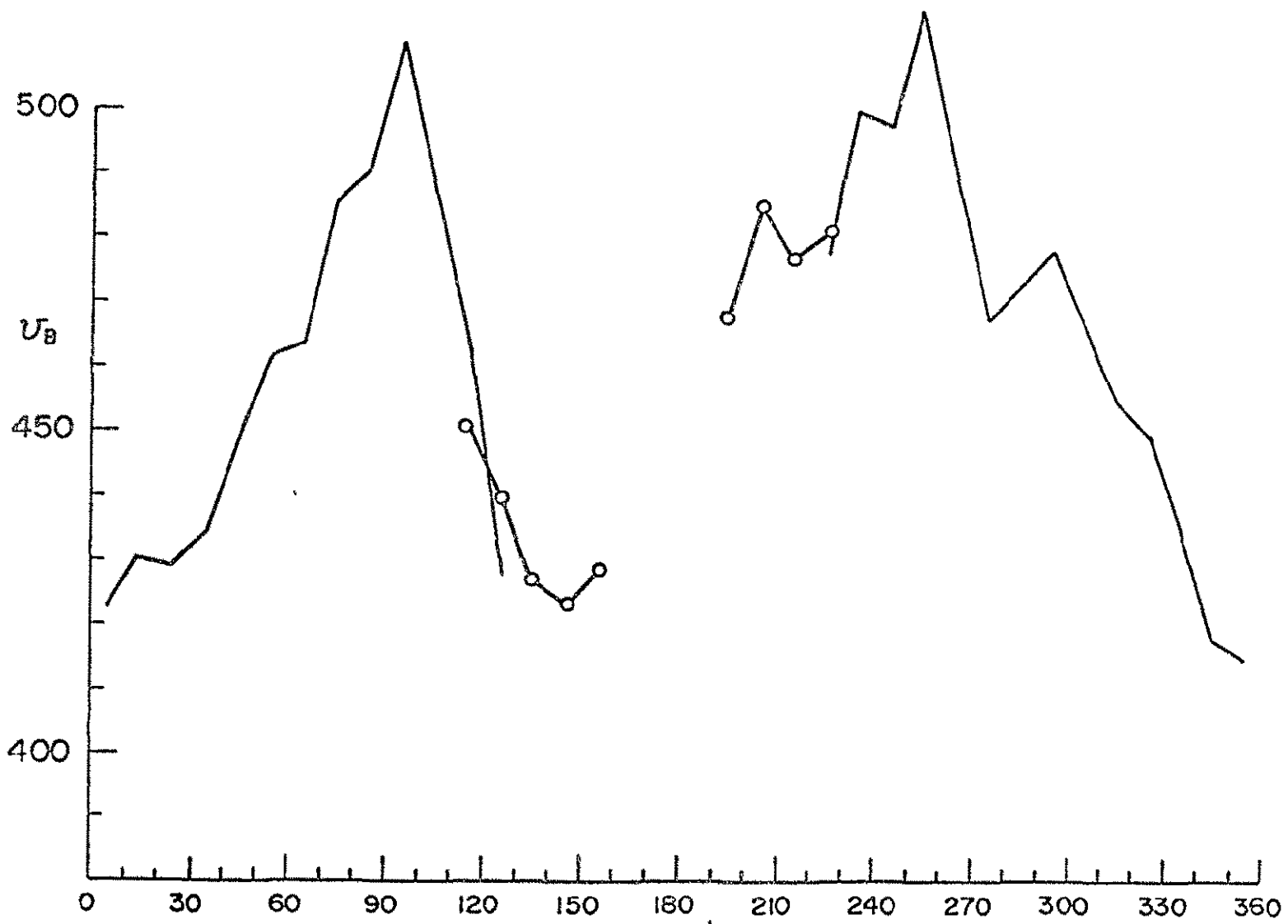
500
U_B
450
400
0
30
60
90
120
150
180
210
240
270
300
330
360
ϕ_{SC}

Figure 41

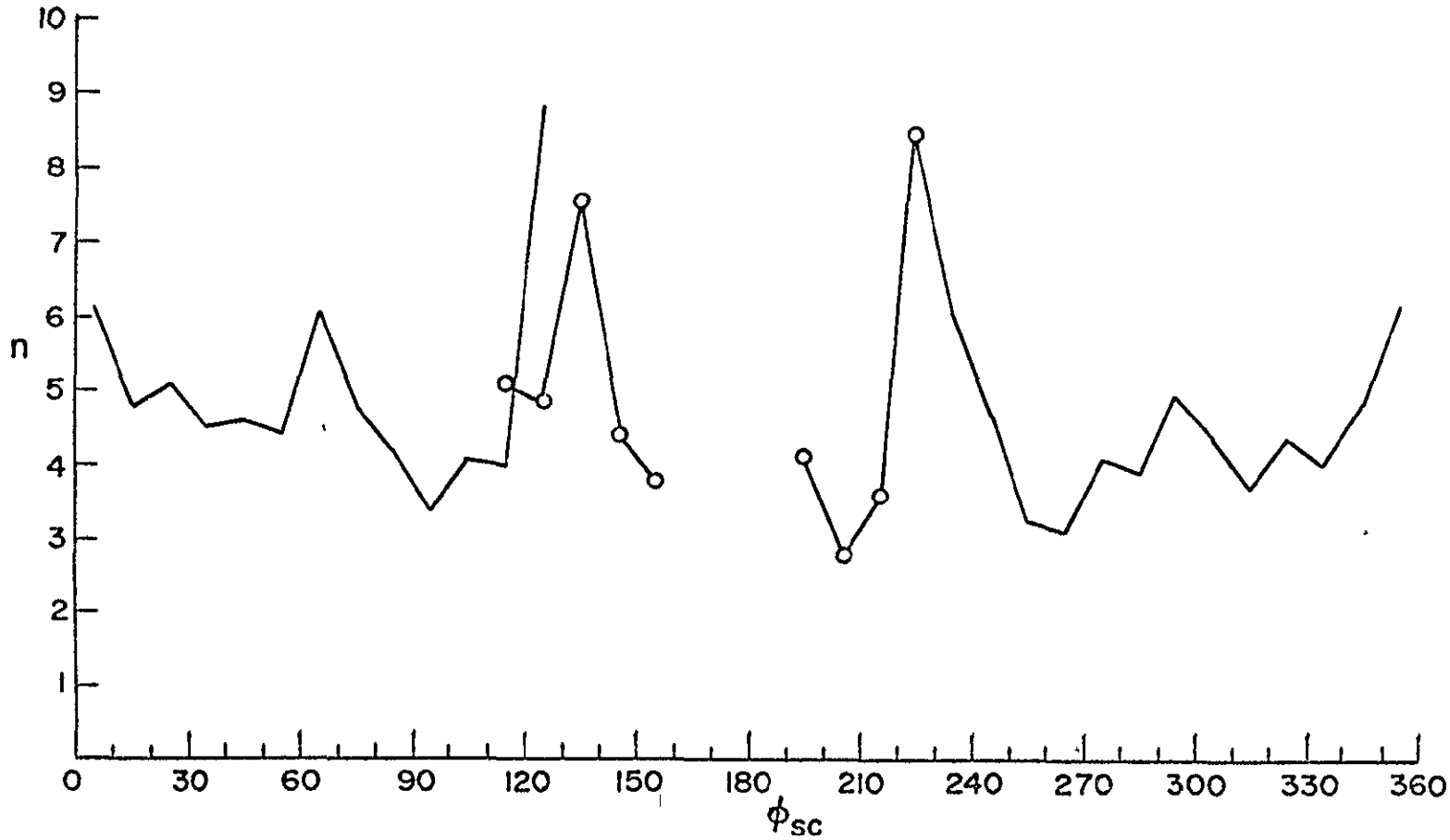
10
9
8
7
6
5
4
3
2
1
n
0
30
60
90
120
150
180
210
240
270
300
330
360
ϕ_{sc}

Figure 42

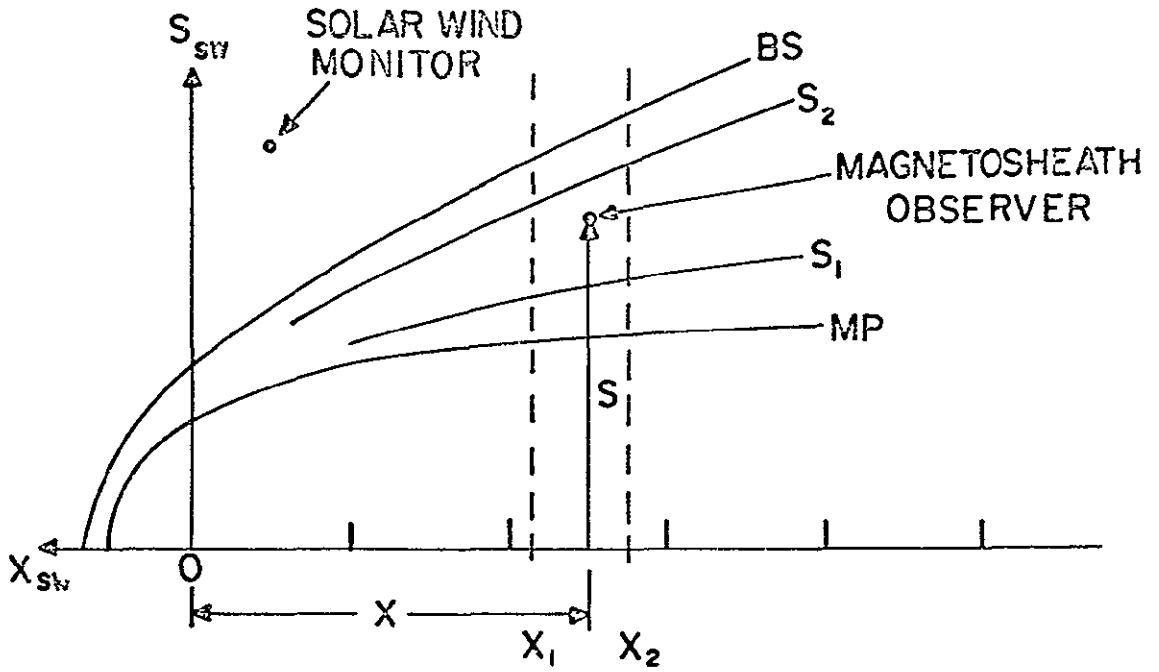
S_sw
SOLAR WIND MONITOR
BS
S_2
MAGNETOSHEATH OBSERVER
S_1
MP
S
X_sw
0
X
X_1
X_2

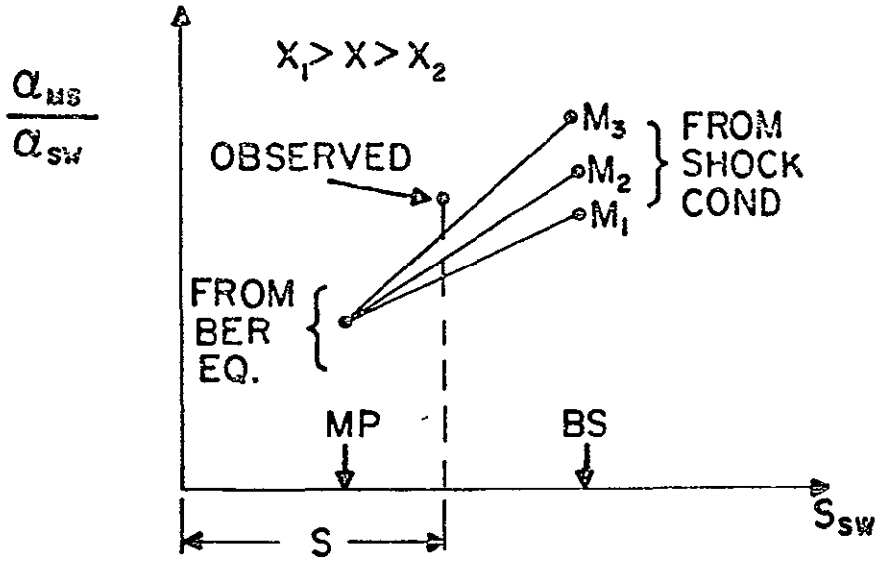
α_MS / α_SW
X_1 > X > X_2
OBSERVED
M_3
M_2
M_1
FROM SHOCK COND
FROM BER EQ.
MP
BS
S
S_SW

Figure 43

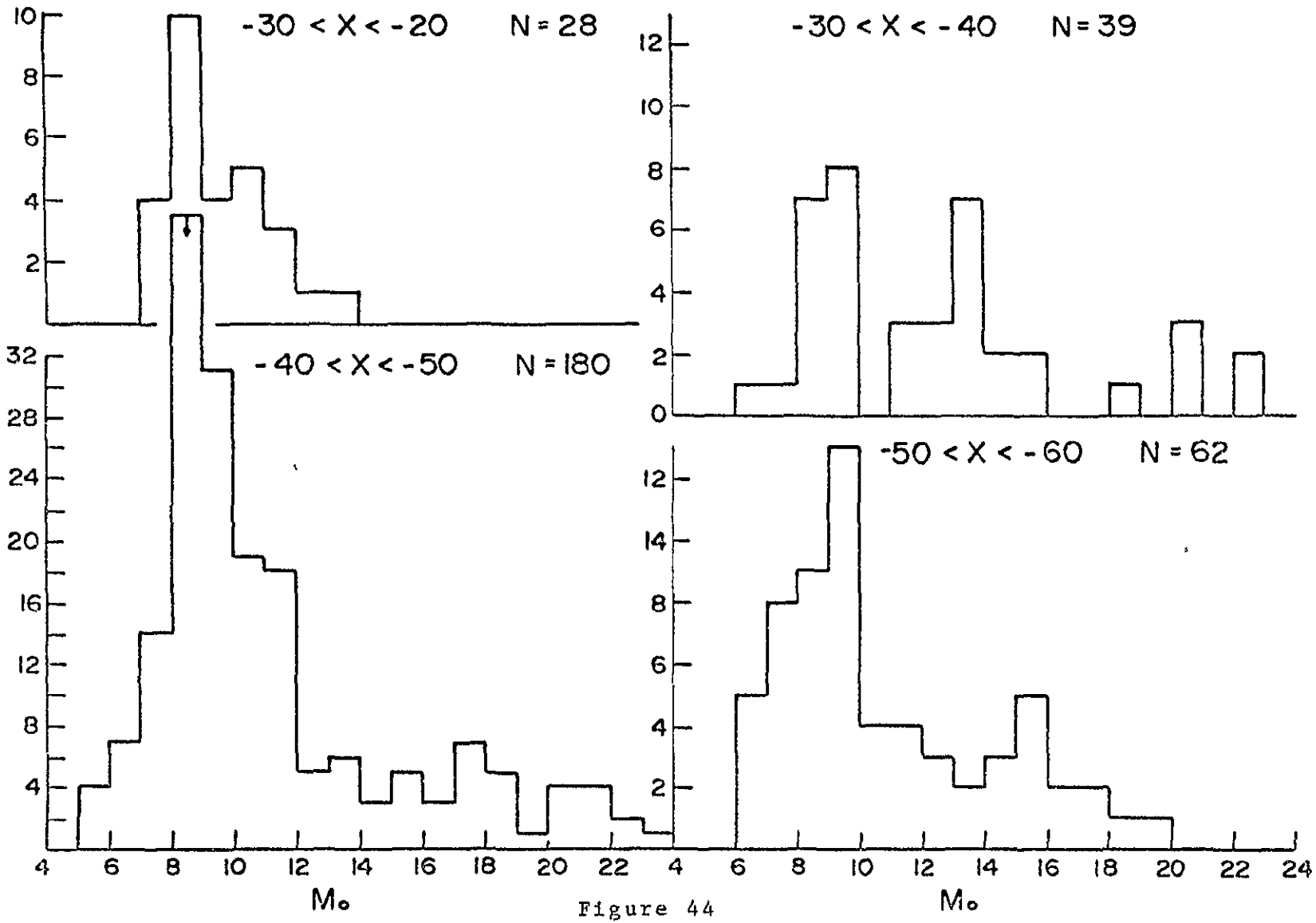

Figure 44

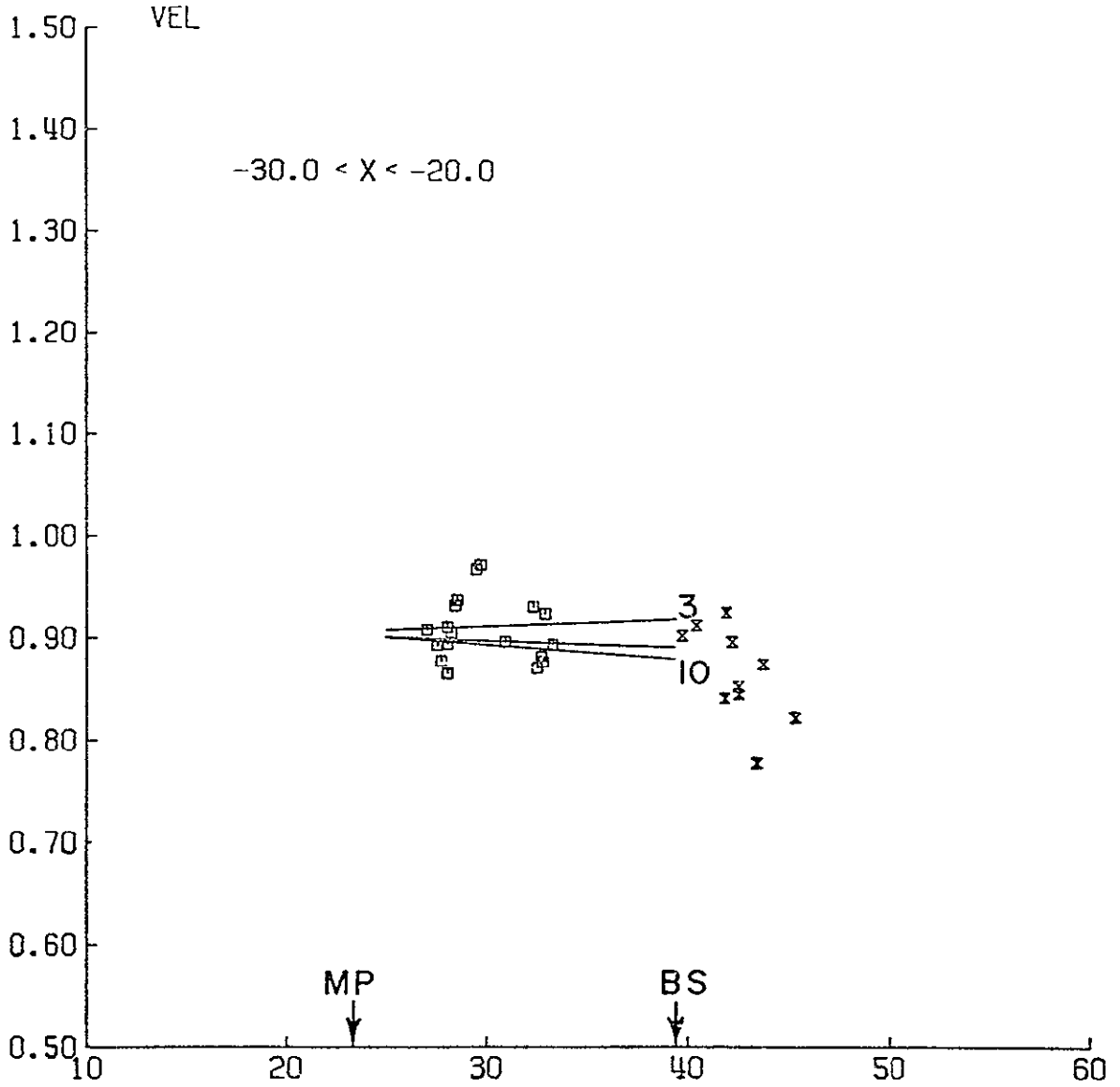
VEL
-30.0 < X < -20.0
1.50
1.40
1.30
1.20
1.10
1.00
0.90
0.80
0.70
0.60
0.50
3
10
MP
BS
10
20
30
40
50
60

Figure 45a

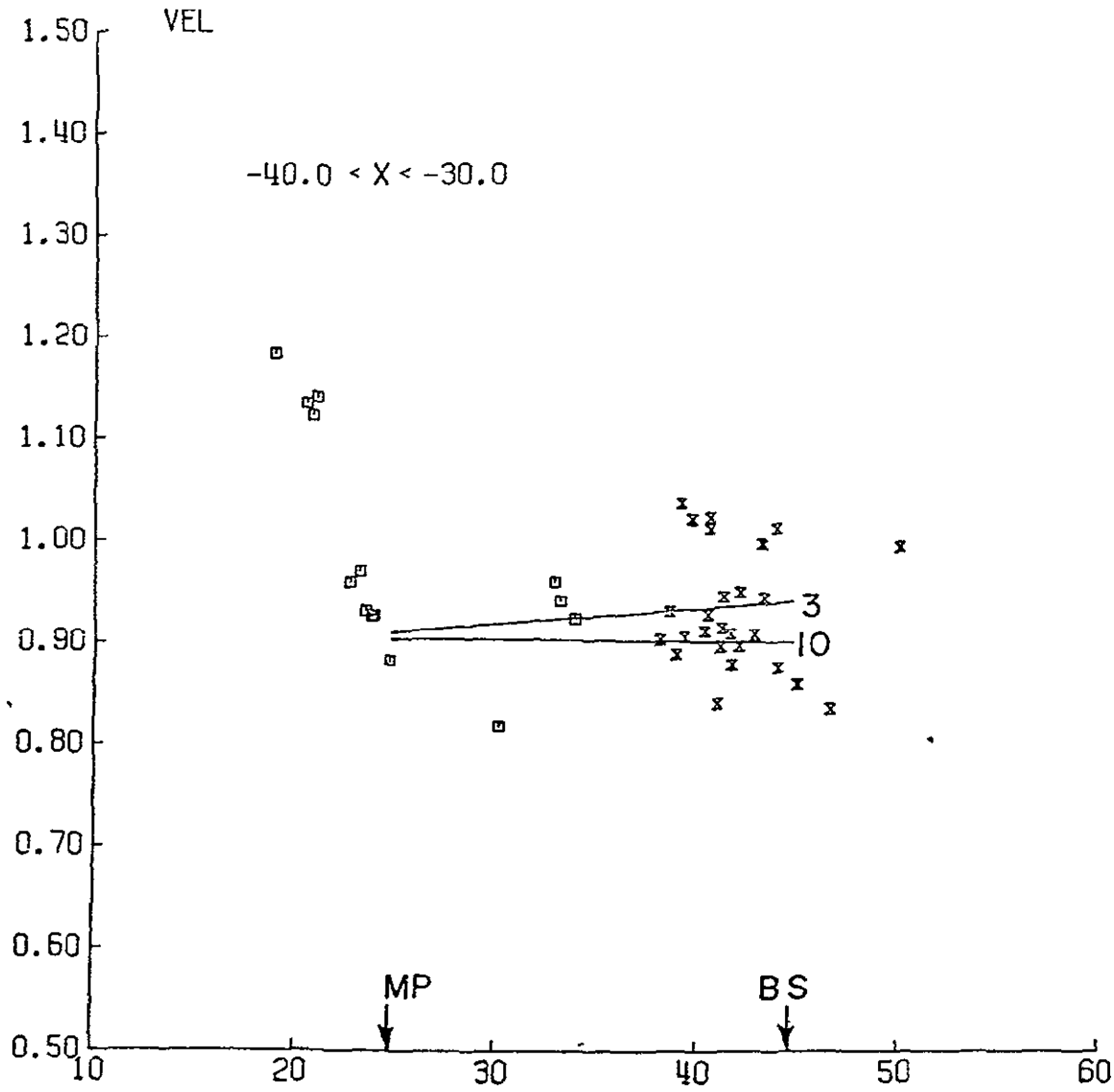
VEL
-40.0 < X < -30.0
1.50
1.40
1.30
1.20
1.10
1.00
0.90
0.80
0.70
0.60
0.50
10
20
30
40
50
60
MP
BS
3
10

Figure 45b

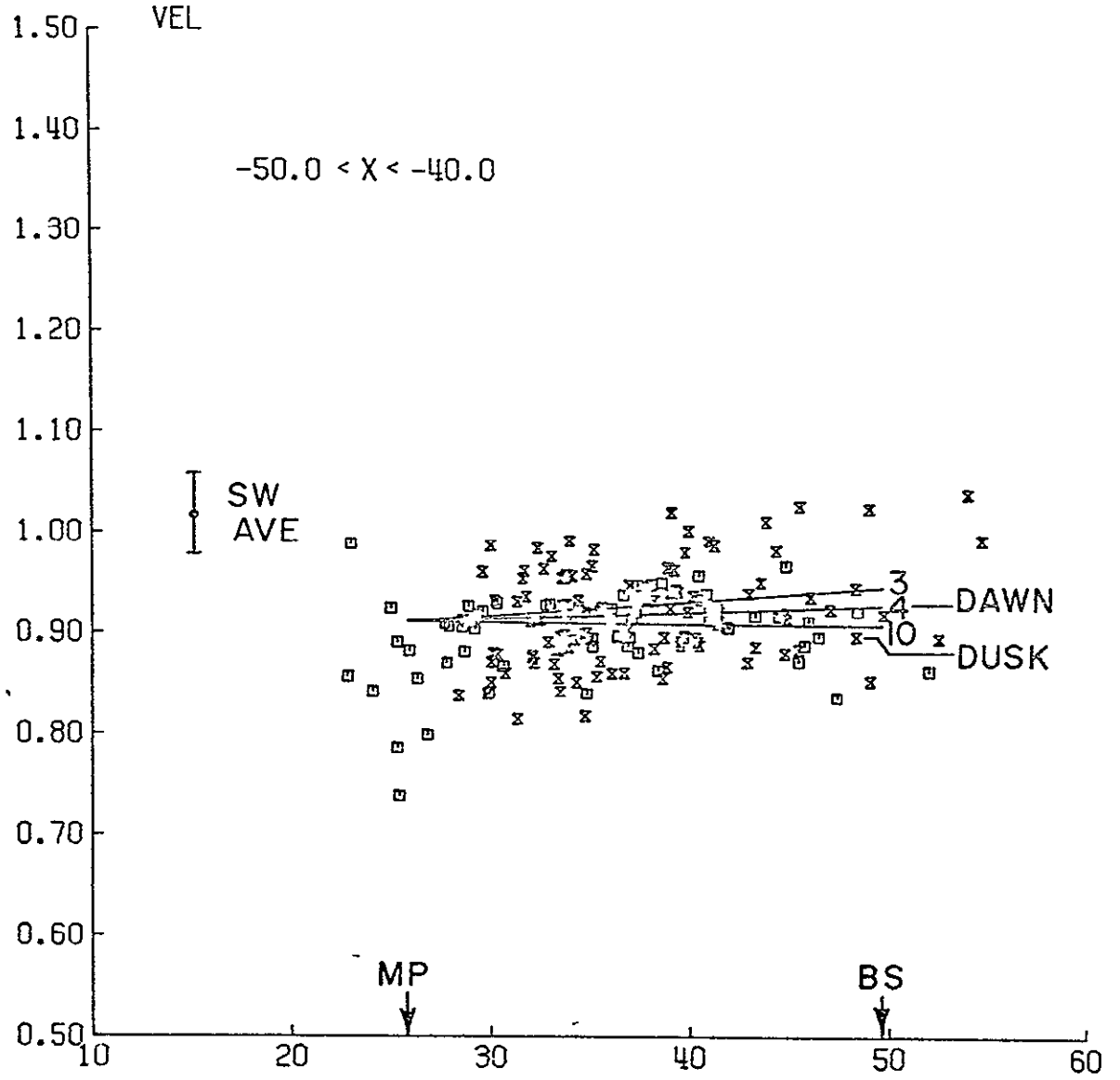
VEL
1.50
1.40
1.30
1.20
1.10
1.00
0.90
0.80
0.70
0.60
0.50
-50.0 < X < -40.0
SW
AVE
3
4
10
DAWN
DUSK
MP
BS
10
20
30
40
50
60

Figure 45c

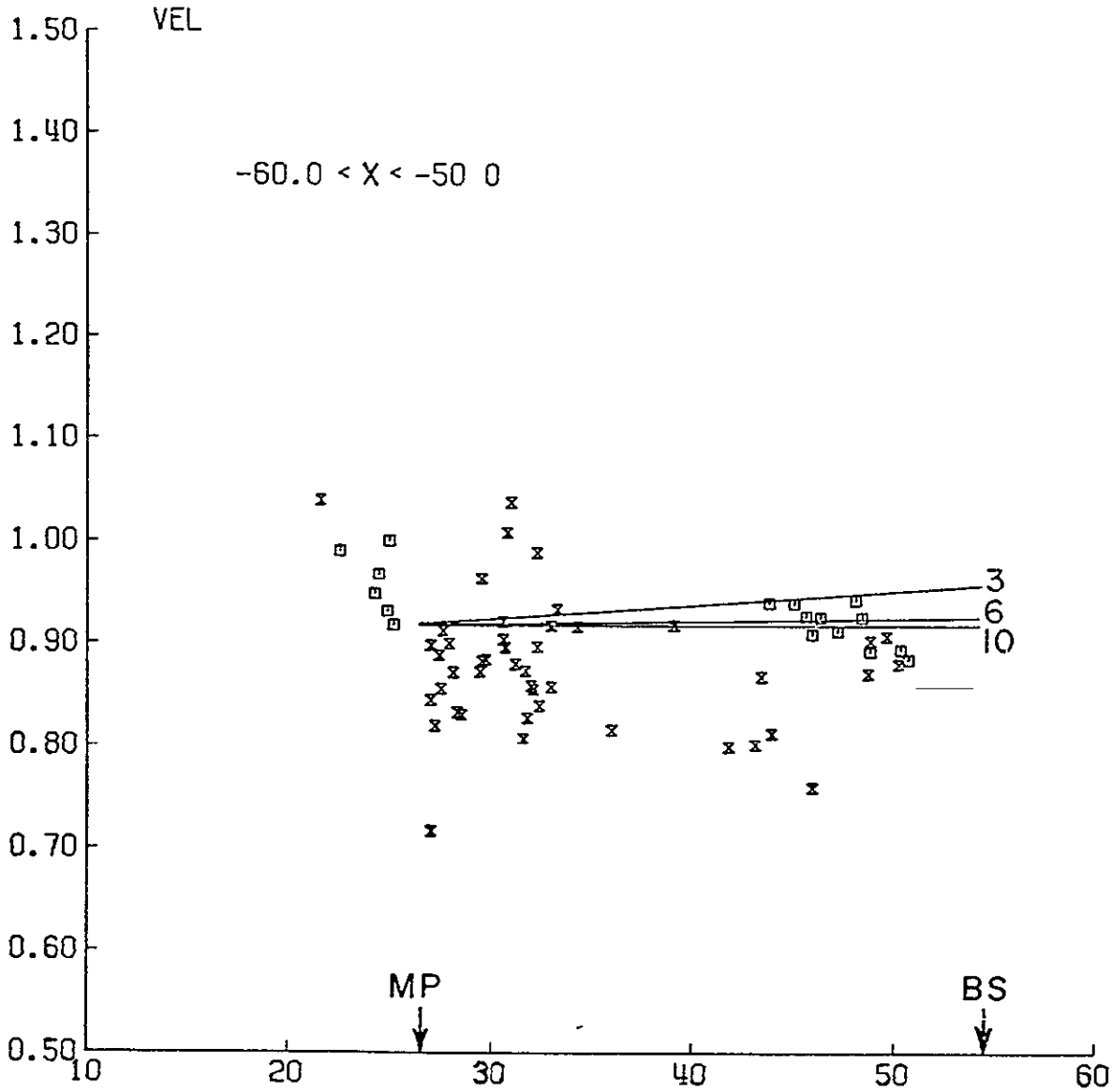
VEL
-60.0 < X < -50 0
1.50
1.40
1.30
1.20
1.10
1.00
0.90
0.80
0.70
0.60
0.50
10
20
30
40
50
60
MP
BS
3
6
10

Figure 45a

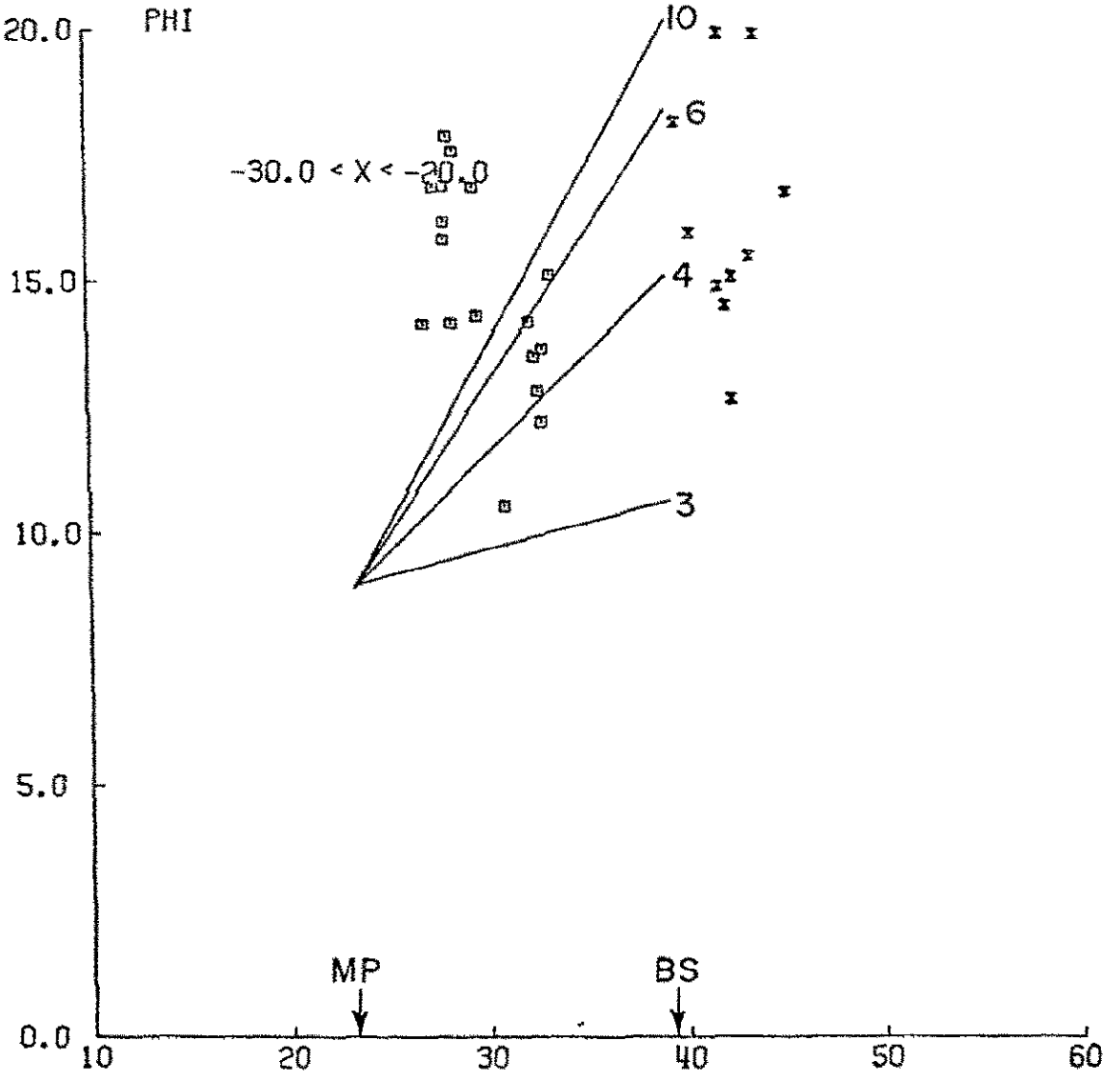

Figure 46a

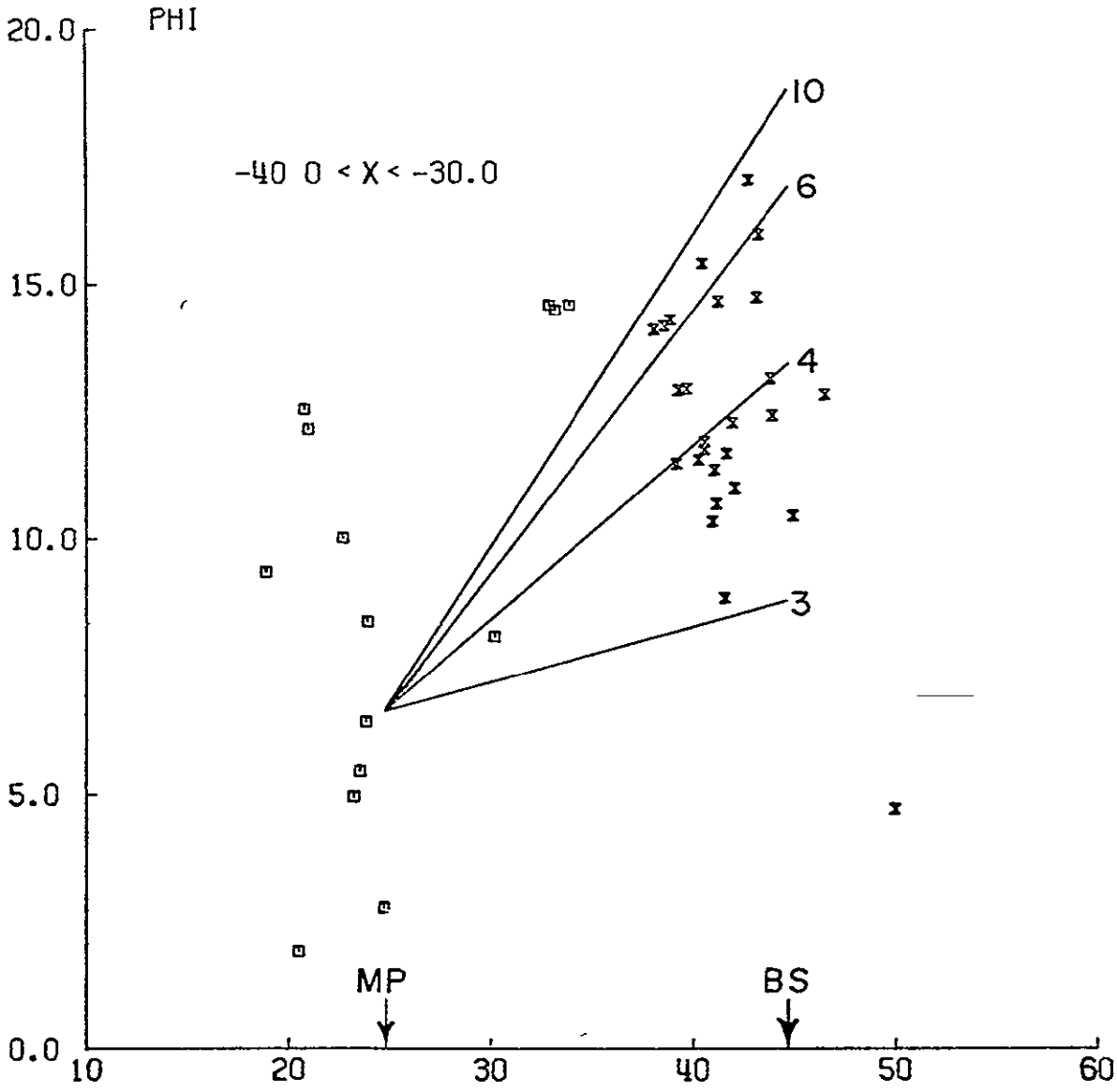

Figure 46b

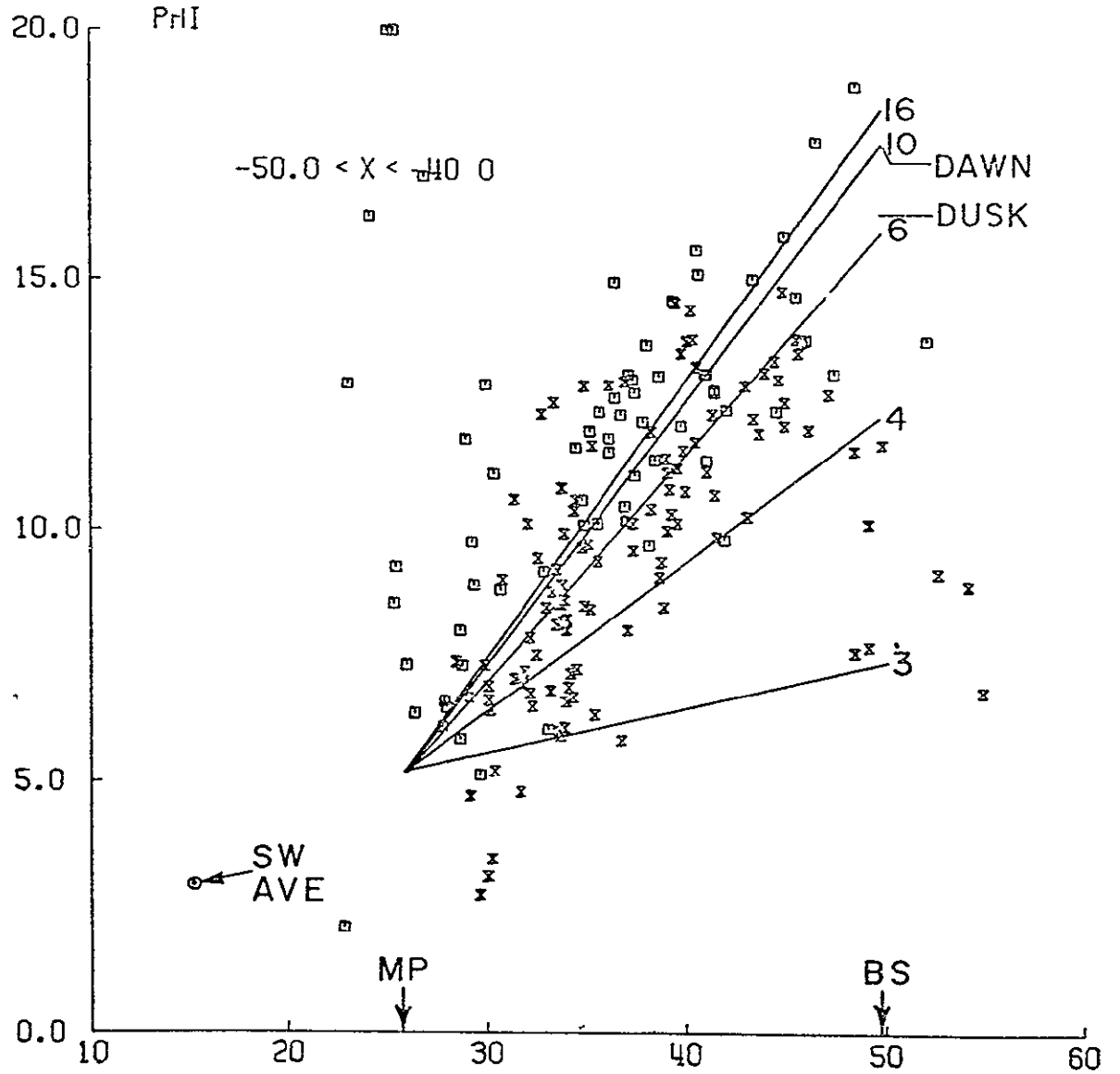
PHI
20.0
15.0
10.0
5.0
0.0
10
20
30
40
50
60
-50.0 < X < -40.0
16
10
DAWN
DUSK
6
4
3
SW
AVE
MP
BS

Figure 46c

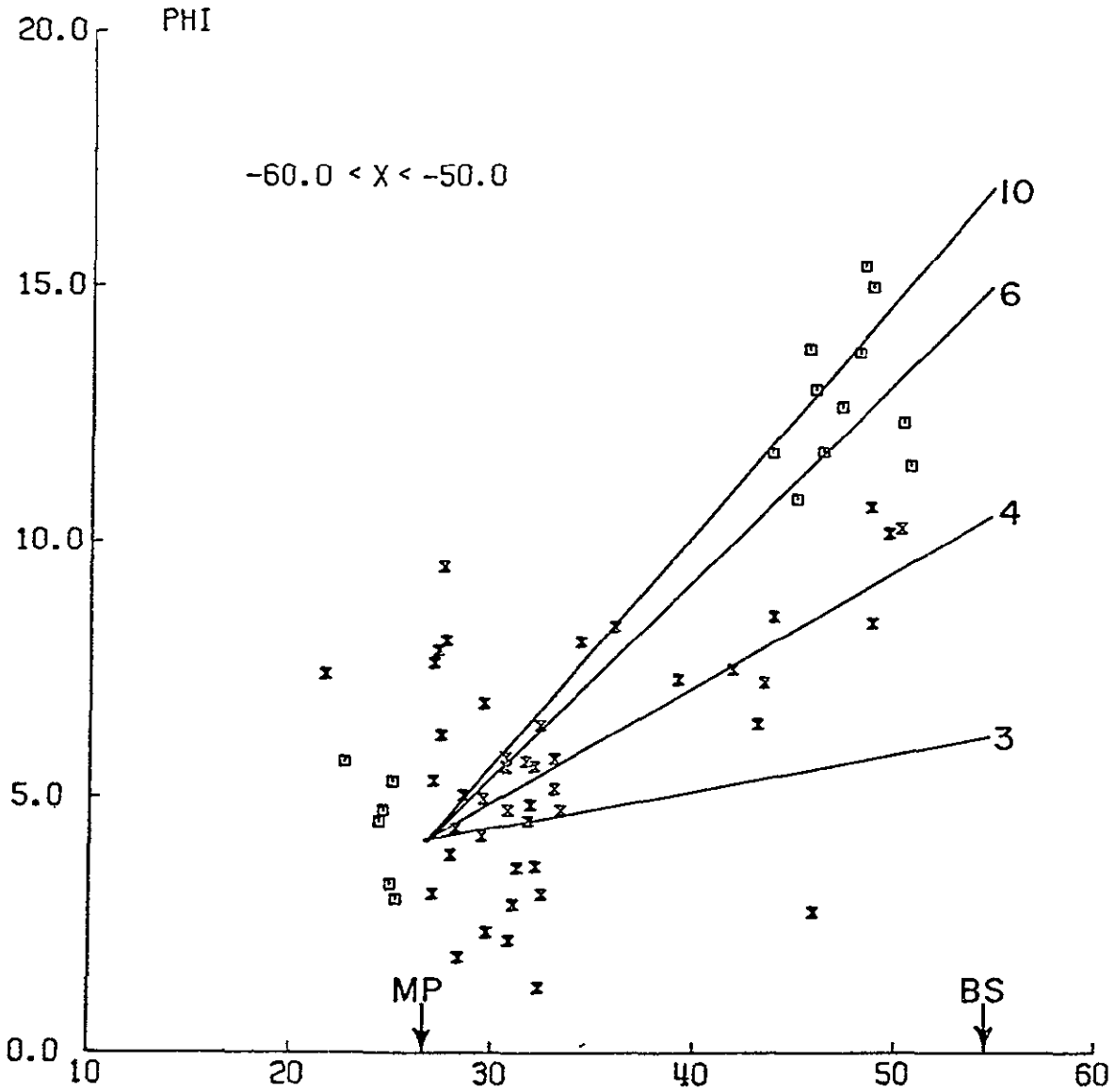

Figure 46d

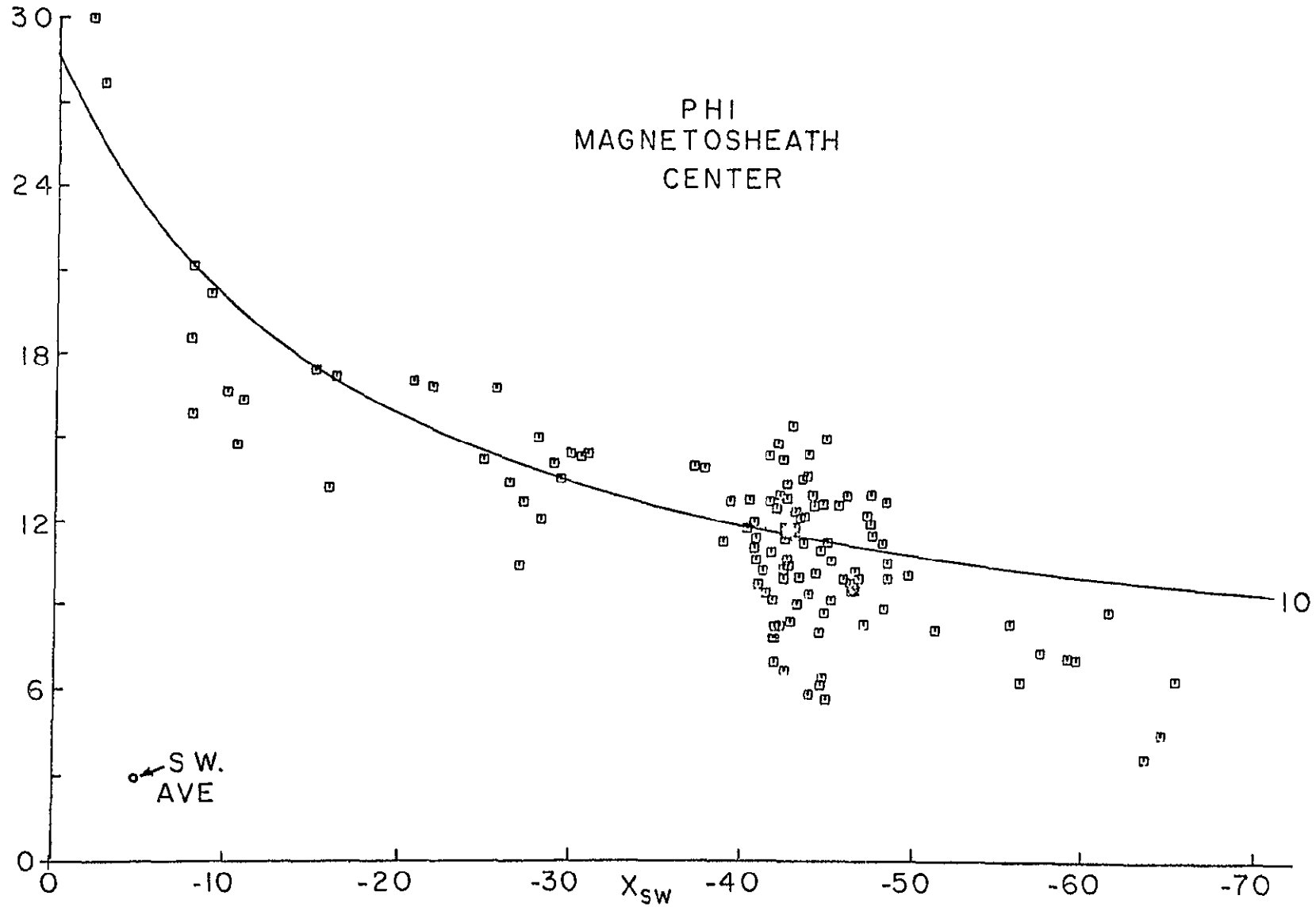
PHI
MAGNETOSHEATH
CENTER
30
24
18
12
6
0
0
-10
-20
-30
-40
-50
-60
-70
X_{SW}
10
S W.
AVE

Figure 47

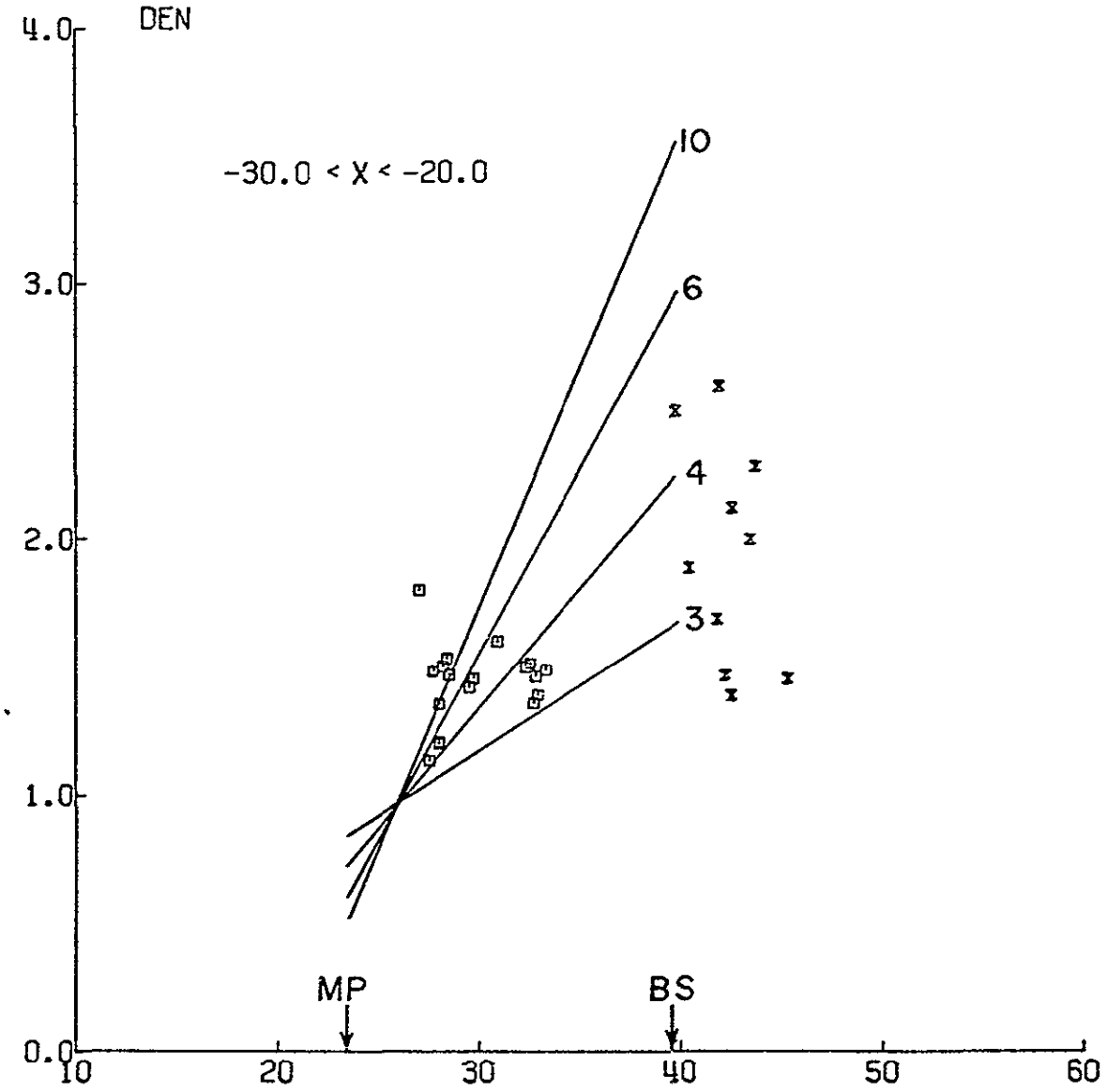

Figure 48a

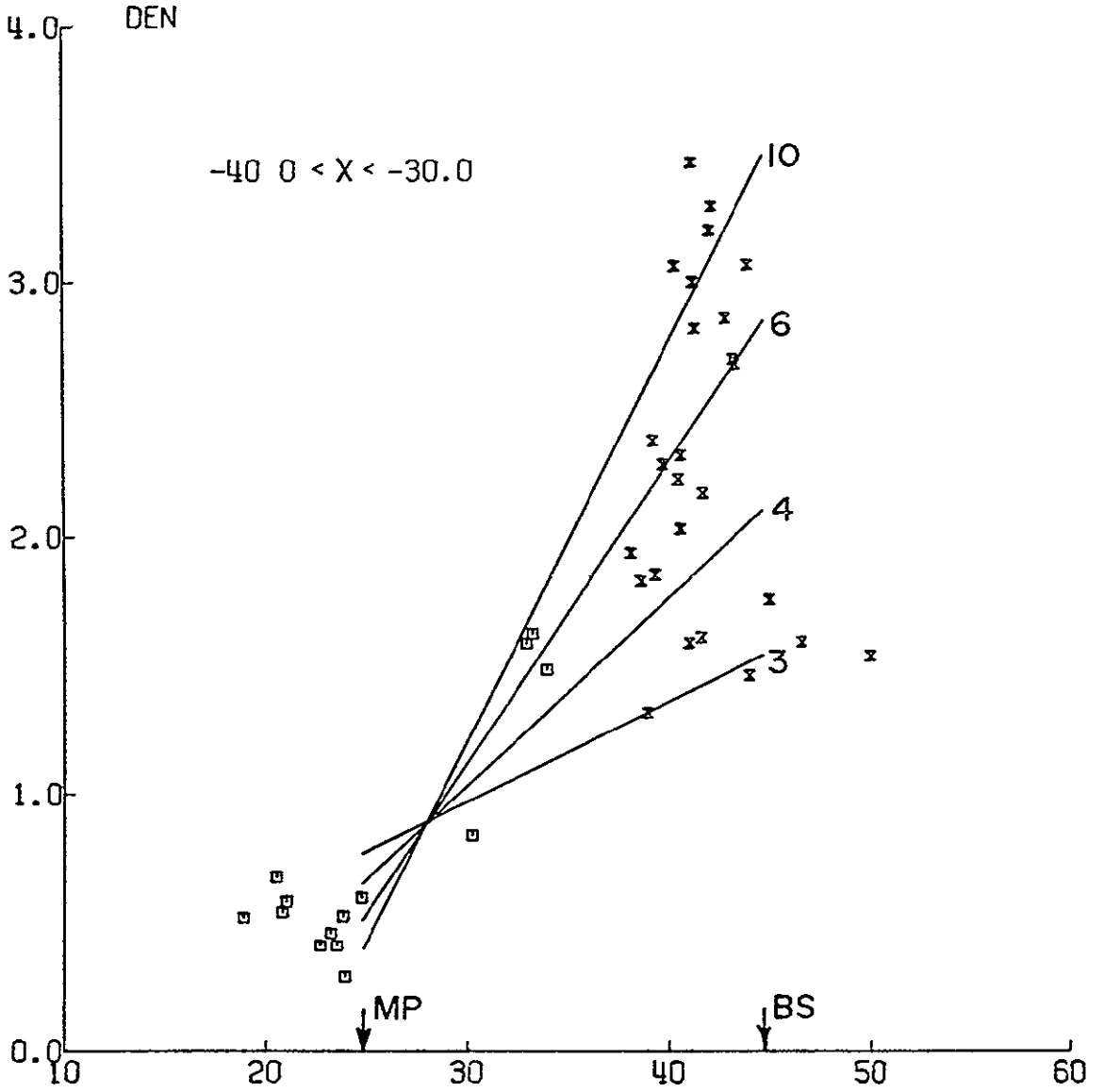

Figure 48b

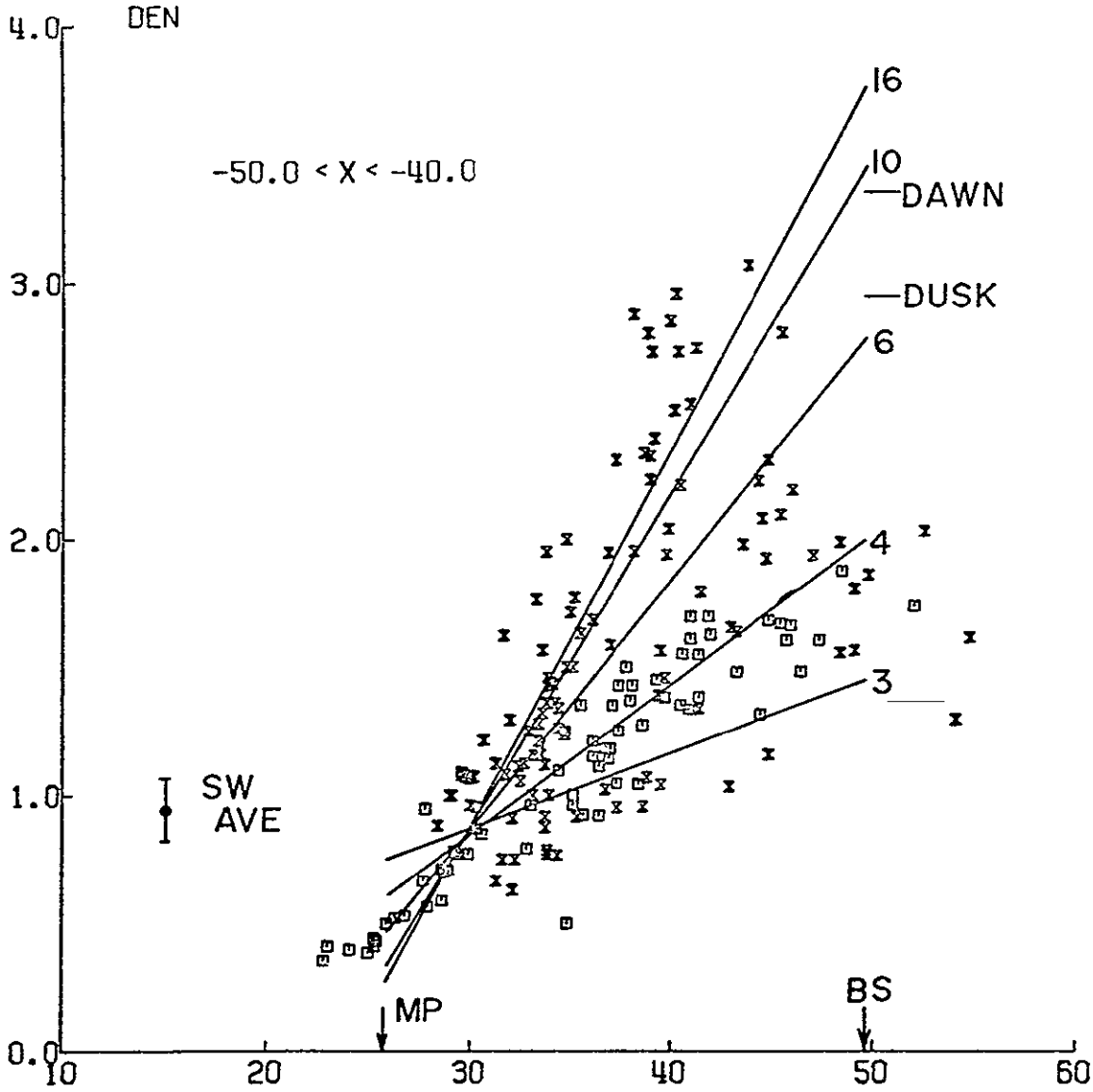
DEN
4.0
3.0
2.0
1.0
0.0
-50.0 < X < -40.0
16
10
DAWN
DUSK
6
4
3
SW
AVE
MP
BS
10
20
30
40
50
60

Figure 48c

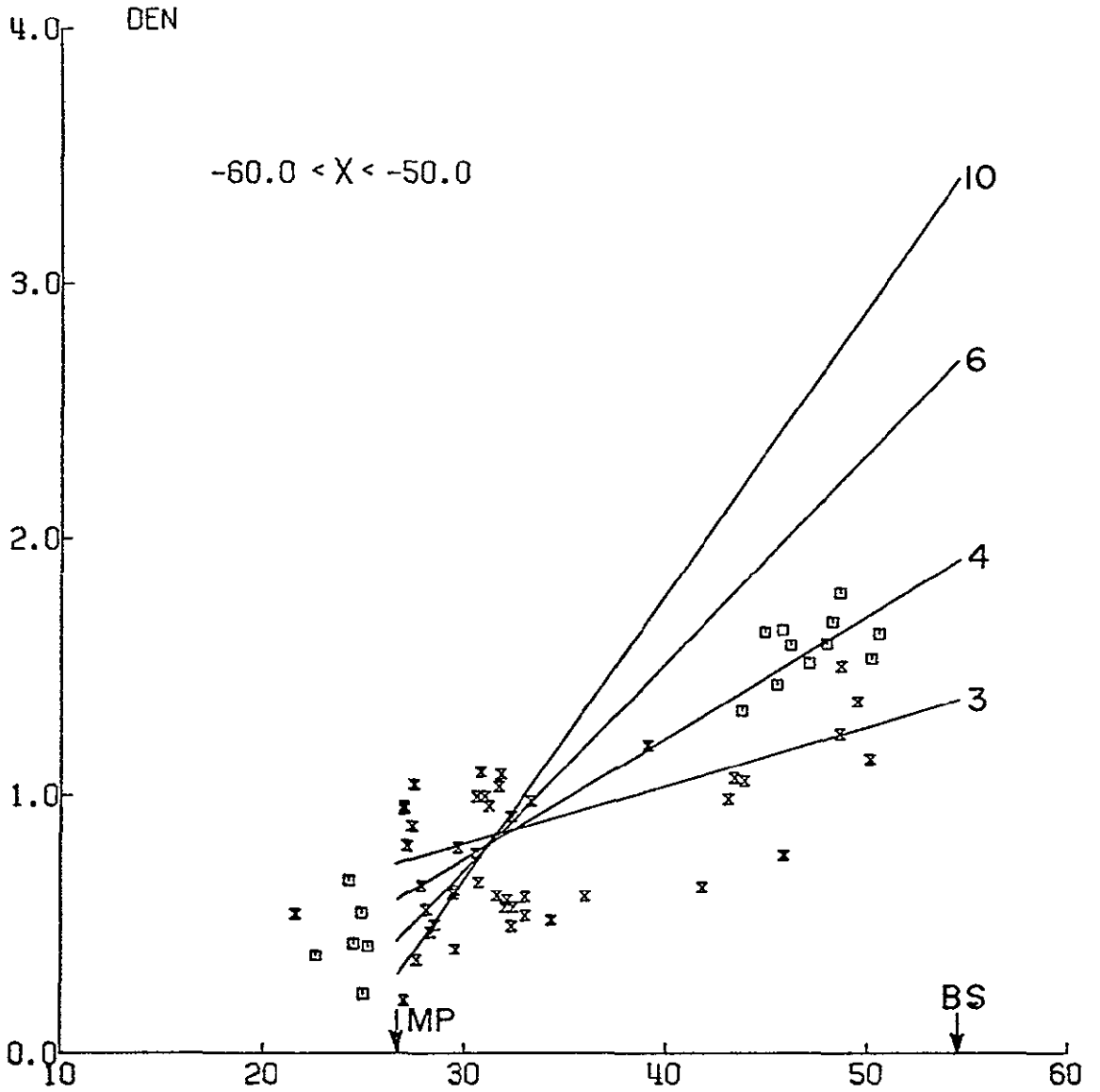

Figure 48d

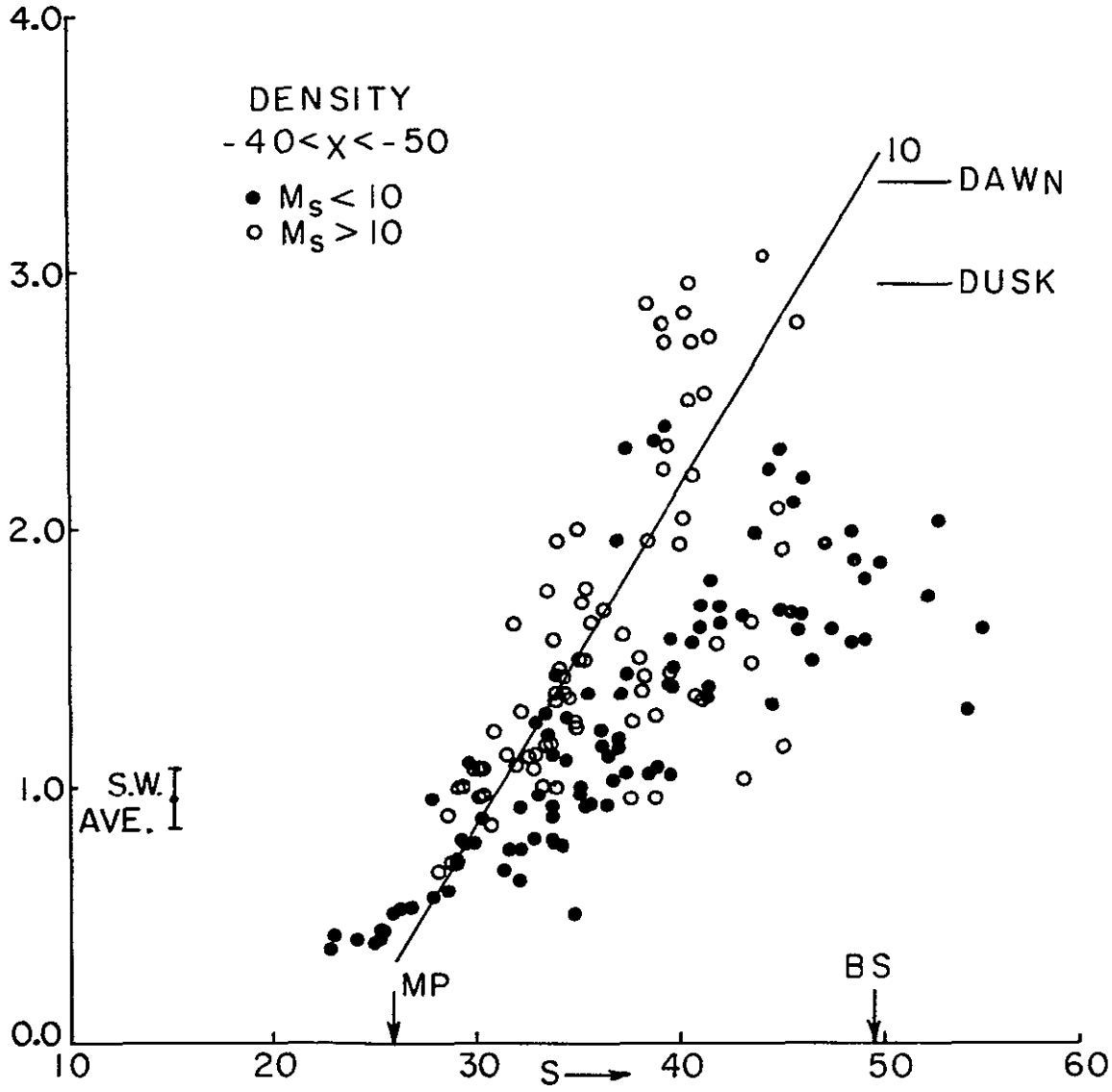
4.0
3.0
2.0
1.0
0.0
DENSITY
-40<X<-50
• Ms<10
o Ms>10
10
DAWN
DUSK
S.W.
AVE.
MP
BS
10
20
30
S
40
50
60

Figure 49

BIBLIOGRAPHY

Anderson, K A , J.H Binsack, and D H Fairfield, Hydromagnetic disturbances of 3 - 5 minute period on the magnetopause and their relation to bow shock spikes, J Geophys Res., 73, 2371, 1968

Argo, H V , J.R. Asbridge, S.J Bame, A.J. Hundhausen, and I B Strong, Observations of solar wind plasma changes across the bow shock, J Geophys Res , 72, 1989, 1967.

Asbridge, J.R., S J. Bame, and I B Strong, Outward flow of protons from the earth's bow shock, J Geophys. Res , 73, 5777, 1968

Atkinson, G and T. Watanabe, Surface waves on the magnetospheric boundary as a possible origin of long period geomagnetic micropulsations, Earth and Planetary Sci Letters, 1, 89, 1966

Aubry, M P., M G Kivelson, and C T Russell, Motion and structure of the magnetopause, J. Geophys Res , 76, 1673, 1971.

Aubry, M P , C.T Russell, and M G Kivelson, Inward motion of the magnetopause before a substorm, J Geophys Res , 75, 7018, 1970

Axford, W I , The interaction between the solar wind and the earth's magnetosphere, J Geophys Res , 67, 3791, 1962

Axford, W I., Viscous interaction between the solar wind and the earth's magnetosphere, Planetary Space Sci , 12, 45, 1964

Axford, W.I., Solar-wind interaction with the magnetosphere fluid dynamic aspects, in The Solar Wind, edited by R J Mackin, Jr and M Neugebauer, JPL Tech Rept. No. 32-630, 1966

Axford, W.I. and C O Hines, A unifying theory of high-latitude geophysical phenomena and geomagnetic storms, Can J Phys , 39, 1433, 1961.

Axford, W I., H E Petschek, and G L Siscoe, Tail of the magnetosphere, J Geophys Res , 70, 1231, 1965

Bader, M , Preliminary Explorer 12 data on protons below 20 kev, J Geophys. Res , 67, 5007, 1962.

Bame, S.J , J.R. Asbridge, A J Hundhausen, and I B Strong, Solar wind and magnetosheath observations during the January 13-14, 1967 geomagnetic storm, J Geophys Res , 73, 5761, 1968

Bavassano, B , F Mariani, U Villante, and N Ness, Multiple earth bow shock crossings at large geocentric distances, G.S F C. Preprint X-690-71-42, 1971

Beard, D B , The interaction of the terrestrial magnetic field with the solar corpuscular radiation, J Geophys Res , 65, 3559, 1960

Behannon, K W , Mapping of the earth's bow shock and magnetic tail by Explorer 33, J Geophys Res , 73, 907, 1968.

Behannon, K W , Geometry of the geomagnetic tail, J Geophys Res , 75, 743, 1970.

Biermann, L , Komentenschweife und solare korpuskularstrahlung, Zs f Astrophys , 29, 274, 1951.

Biermann, L., The solar wind and the interplanetary medium, in Space Astrophysics, edited by W S Liller, p 150, McGraw-Hill, New York, 1961

Binsack, J.H , Plasma studies with the IMP-2 satellite, Ph.D Thesis, M I T., 1966.

Binsack, J.H and V M Vasyliunas, Simultaneous IMP-2 and OGO-1 observations of bow shock compression, J. Geophys. Res., 73, 429, 1968.

Bonetti, A., H S Bridge, A J Lazarus, B. Rossi, and F Scherb, Explorer 10 plasma measurements, J Geophys Res , 68, 4017, 1963

Bridge, H.S , C Dilworth, A J. Lazarus, E F Lyon, B. Rossi, and F Scherb, Direct observations of the interplanetary plasma, J Phys Soc Japan, Suppl. 17, 553, 1962

Bridge, H S , C Dilworth, B. Rossi, F Scherb, and E F Lyon, An instrument for the investigation of interplanetary plasma, J Geophys Res , 65, 3053, 1960

Bridge, H , A Egidi, A Lazarus, E Lyon, and L Jacobson, Preliminary results of plasma measurements on IMP-A, Space Research, 5, 969, 1965

Burlaga, L F and K W Ogilvie, Observations of the magnetosheath-solar wind boundary, J Geophys. Res , 73, 6167, 1968.

Cahill, L J , The geomagnetic field, in Space Physics, edited by D P. Le Galley and A. Rosen, 327, 1964.

Cahill, L J and Amazeen, P.G , The boundary of the geomagnetic field, J Geophys. Res , 68, 1835, 1963

Cahill, L J and V.L Patel, The boundary of the geomagnetic field, August to November, 1961, Planetary Space Sci., 15, 997, 1967.

Cassen, P. and J. Szabo, The viscous magnetopause, Planetary Space Sci , 18, 349, 1970.

Chao, J K , Interplanetary collisionless shock waves, M I T. Report CSR TR-70-3, 1970

Chapman, S., Solar Plasma, Geomagnetism, and Aurora, Gordon and Breach, New York and London, 1964

Chapman, S and V C A Ferraro, A new theory of magnetic storms, Nature, 126, 129, 1930

Coleman, P.J , Characteristics of the region of interaction between the interplanetary plasma and the geomagnetic field Pioneer 5, J Geophys Res , 69, 3051, 1964

Coleman, P J , Tangential drag on the geomagnetic cavity, Cosmical Elec , 1, 145, 1970

Coleman, P J , C P Sonett, D.L. Judge, and E J Smith, Some preliminary results of the Pioneer 5 magnetometer experiment, J Geophys Res , 65, 1856, 1960

Cummings, W D and P J. Coleman, Magnetic fields in the magnetopause and vicinity at synchronous altitude, J Geophys Res , 73, 5699, 1968

Davies, C.M , The boundary layer between a cold plasma and a confined magnetic field when the plasma is not normally incident on the boundary, Planetary Space Sci , 16, 1249, 1968

Davies, C M., The structure of the magnetopause, Planetary Space Sci , 17, 333, 1969

Dessler, A J and R D Juday, Configuration of auroral radiation in space, Planetary Space Sci , 13, 63, 1965

Dryer, M , Solar wind interactions - hypersonic analogue, Cosmical Elec , 1, 115, 1970

Dryer, M , Comparison of experimental and gasdynamic fluid parameter jumps across the earth's bow shock, J Geophys Res , 76, 1070, 1971

Dryer, M and G R Heckman, On the hypersonic analogue as applied to planetary interaction with solar plasma, Planetary Space Sci , 15, 515, 1967

Egidi, A , V Formisano, F Palmiotto, P Saraceno, and G Moreno, Solar wind and location of shock front and magnetopause at the 1969 solar maximum, J. Geophys Res , 75, 6999, 1970

Eviatar, A and R A. Wolf, Transfer processes in the magnetopause, J. Geophys. Res , 73, 5561, 1968

Fairfield, D H , The ordered magnetic field of the magnetosheath, J Geophys. Res , 72, 5865, 1967

Fairfield, D H , Simultaneous measurements on three satellites and the observation of the geomagnetic tail at 1000 R_E, J Geophys Res , 73, 6179, 1968

Fairfield, D H and N F Ness, Magnetic field measurements with the IMP-2 satellite, J Geophys Res , 72, 2379, 1967.

Faye-Petersen, R and G Heckman, Viscous magnetospheric boundary layer, Annls. Geophys , 24, 347, 1968

Fejer, J A , Hydromagnetic stability at a fluid velocity discontinuity between compressible fluids, Phys Fluids, 7, 499, 1964.

Freeman, J W , The morphology of the electron distribution in the outer radiation zone and near the magnetospheric boundary as observed by Explorer 12, J Geophys Res , 69, 1691, 1964.

Freeman, J.W , L D Kavanagh, and L.J Cahill, An observation of transient variations in the magnetospheric boundary position, J Geophys Res , 72, 2040, 1967

Freeman, J.W , J A Van Allen, and L J. Cahill, Explorer 12 observations of the magnetospheric boundary and the associated solar plasma on September 13, 1961, J Geophys. Res , 68, 2121, 1963

Freeman, J.W , C S Warren, and J J Maguire, Plasma flow directions at the magnetopause on January 13 and 14, 1967, J Geophys Res , 73, 5719, 1968.

Gosling, J T , J R Asbridge, S J Bame, and I B Strong, Vela 2 measurements of the magnetopause and bow shock positions, J Geophys Res., 72, 101, 1967

Greenstadt, E W , I M. Green, G.T. Inouye, A J Hundhausen, S J. Bame, and I B Strong, Correlated magnetic field and plasma observations of the earth's bow shock, J Geophys Res., 73, 51, 1968 See also the following three references

Greenstadt, E W , I M Green, G.T. Inouye, D S. Colburn, J H Binsack, and E.F. Lyon, Dual satellite observations of earth's bow shock I the thick pulsation shock, Cosmical Elec , 1, 160, 1970

Greenstadt, E W , I.M Green, G.T Inouye, D.S Colburn, J H Binsack, and E.F Lyon, Dual satellite observations of earth's bow shock II field aligned upstream waves, Cosmical Elec., 1, 279, 1970

Greenstadt, E W , I M Green, G T Inouye, D S Colburn, J H. Binsack, and E.F Lyon, Dual satellite observations of earth's bow shock III field determined shock structure, Cosmical Elec., 1, 316, 1970

Heppner, J P , N F Ness, C S Scearce, and T.L Skillman, Explorer 10 magnetic field measurements, J Geophys. Res , 68, 1, 1963

Heppner, J.P., N.F Ness, T L Skillman, and C S. Scearce, Magnetic field measurements with the Explorer 10 satellite, J Phys Soc. Japan, Suppl 17, 546, 1962.

Heppner, J.P , M Sugiura, T L. Skillman, B G Ledley, and M Campbell, OGO-A magnetic field observations, J. Geophys. Res , 72, 5417, 1967

Herron, T.J., An average geomagnetic power spectrum for the period range 4.5 to 12,900 seconds, J Geophys Res., 72, 759, 1967.

Holzer, R.E , M.G. McLeod, and E J Smith, Preliminary results from the OGO-1 search coil magnetometer boundary positions and magnetic noise spectra, J Geophys. Res , 71, 1481, 1966.

Howe, H C , Pioneer 6 plasma measurements in the magnetosheath, J Geophys Res , 75, 2429, 1970

Hundhausen, A J , S J Bame, and J R Asbridge, Plasma flow pattern in the earth's magnetosheath, J Geophys Res , 74, 2799, 1969

_____, Initial results from the first Interplanetary Monitoring Platform (IMP-1), I G Bull , 84, 1, 1964.

Intriligator, D S , J H Wolfe, D D McKibbin, and H R Collard, Preliminary comparison of solar wind plasma observations in the geomagnetospheric wake at 1000 and 500 earth radii, Planetary Space Sci., 17, 321, 1969

Johnson, F.S , The gross character of the geomagnetic field in the solar wind, J Geophys Res , 65, 3049, 1960

Karlson, E T , On the equilibrium of the magnetopause, J. Geophys Res , 75, 2438, 1970

Kaufmann, R L , Shock observations with the Explorer 12 magnetometer, J. Geophys Res., 72, 2323, 1967

Kaufmann, R L , J.T Horng, and A Wolfe, Large-amplitude hydromagnetic waves in the inner magnetosheath, J Geophys Res , 75, 4666, 1970

Kaufmann, R L and A Konradi, Explorer 12 magnetopause observations ,large-scale nonuniform motion, J Geophys Res , 74, 3609, 1969

Kellogg, P J , Flow of plasma around the earth, J. Geophys Res., 67, 3805, 1962.

Konradi, A and R L Kaufmann, Evidence for rapid motion of the outer boundary of the magnetosphere, J Geophys Res , 70, 1627, 1965.

Lerche, I , Validity of the hydromagnetic approach in discussing instability of the magnetospheric boundary, J Geophys Res , 71, 2365, 1966

Lerche, I , On the boundary layer between a warm, streaming plasma and a confined field, J Geophys Res , 72, 5295, 1967

Levy, R H , H E Petschek, and G L Siscoe, Aerodynamic aspects of the magnetospheric flow, AIAA Journal, 2, 2065, 1964

Lyon, E F., A study of the interplanetary plasma, Ph D Thesis, M I T , 1966

Lyon, E., A Egidi, G Pizzella, H Bridge, J. Binsack, R Baker, and R Butler, Plasma measurements on Explorer 33 (I) interplanetary region, Space Res , 8, 99, 1968

McClay, J F and H.R Radoski, Hydromagnetic propagation in a theta-model geomagnetic tail, J Geophys Res , 72, 4525, 1967

McKenzie, J F , Hydromagnetic oscillations of the geomagnetic tail and plasma sheet, J Geophys Res , 75, 5331, 1970

Mariani, F and N.F Ness, Observations of the geomagnetic tail at 500 earth radii by Pioneer 8, J Geophys Res , 74, 5633, 1969.

Mead, G D and D B. Beard, Shape of the geomagnetic field-solar wind boundary, J. Geophys. Res , 69, 1169, 1964

Meng, C I., Variations of the magnetopause position with substorm activity, J. Geophys Res , 75, 3252, 1970

Mihalov, J D , D.S Colburn, R G Currie, and C.P. Sonett, Configuration and reconnection of the geomagnetic tail, J. Geophys. Res , 73, 943, 1968

Mihalov, J.D , D S Colburn, and C.P. Sonett, Observations of magnetopause geometry and waves at the lunar distance, Planetary Space Sci , 18, 239, 1970

Mihalov, J D., C.P Sonett, and J H Wolfe, MHD Rankine-Hugoniot equations applied to earth's bow shock, J Plasma Physics, 3, 449, 1969

Montgomery, M D., J.R Asbridge, and S.J Bame, Vela 4 plasma observations near the earth's bow shock, J. Geophys Res , 75, 1217, 1970

Ness, N F , The earth's magnetic tail, J. Geophys. Res , 70, 2989, 1965

Ness, N F., The geomagnetic tail, Rev Geophys , 7, 97, 1969

Ness, N.F., C.S. Scearce, and S C. Cantarano, Probable observation of the geomagnetic tail at 10^3 earth radii by Pioneer 7, J Geophys Res , 72, 3769, 1967.

Ness, N F , C S. Scearce, and J B. Seek, Initial results of the IMP-1 magnetic field experiment, J Geophys Res , 69, 3531, 1964

Ness, N F , C S Scearce, J B Seek, and J M Wilcox, A summary of results from the IMP-1 magnetic field experiment, Space Research, 6, 581, 1966

Neugebauer, M , Initial deceleration of solar wind positive ions in the earth's bow shock, J Geophys Res , 75, 717, 1970.

Neugebauer, M and C W. Snyder, Solar plasma experiment, Science, 138, 1095, 1962.

Neugebauer, M and C W. Snyder, Mariner 2 observations of the solar wind, 1, average properties, J. Geophys. Res , 71, 4469, 1966

Ogilvie, K W., L.F Burlaga, and T D Wilkerson, Plasma observations on Explorer 34, J Geophys. Res., 73, 6809, 1968

Olbert, S , Summary of experimental results from M.I.T. detector on IMP-1, in Physics of the Magnetosphere, D. Reidel Publishing Co., Holland, 1968

Parker, E N , Interaction of the solar wind with the geomagnetic field, Phys Fluids, 1, 171, 1958a

Parker, E N , Dynamics of the interplanetary gas and magnetic field, Astrophys. J., 128, 664, 1958b.

Parker, E N , Interplanetary Dynamical Processes, Interscience Publishers, New York, 1963

Parker, E N., Confinement of a magnetic field by a beam of ions, J Geophys Res , 72, 2315, 1967a

Parker, E N , Small-scale nonequilibrium of the magnetopause and its consequences, J Geophys Res , 72, 4365, 1967b.

Patel, V L , Low frequency hydromagnetic waves in the magnetosphere Explorer 12, Planetary Space Sci , 13, 485, 1965

Patel, V L , Long-period hydromagnetic waves in the magnetosphere Explorer 14, Space Research, 6, 758, 1966

Russell, C T., J V Olson, R E Holzer, and E J Smith, OGO-3 search coil magnetometer data correlated with the reported crossings of the magnetopause at 6 6 R_E by ATS 1, J Geophys Res , 73, 5769, 1968

Sen, A.K , Stability of the magnetospheric boundary, Planetary Space Sci , 13, 131, 1965

Siscoe, G L , Resonant compressional waves in the geomagnetic tail, J. Geophys Res , 74, 6482, 1969

Siscoe, G.L , L Davis, E.J Smith, P J Coleman, and D E Jones, Magnetic fluctuations in the magnetosheath Mariner 4, J Geophys Res , 72, 1, 1967.

Siscoe, G L., V Formisano, and A J Lazarus, Relation between geomagnetic sudden impulses and solar wind pressure changes - an experimental investigation, J Geophys Res , 73, 4869, 1968

Siscoe, G L., F L Scarf, D S. Intriligator, J H Wolfe, J.H Binsack, H S Bridge, and V M Vasyliunas, Evidence for a geomagnetic wake at 500 earth radii, J Geophys Res., 75, 5319, 1970

Skillman, T.L and M Sugiura, Magnetopause crossing of the geostationary satellite ATS 5 at 6 6 R_E, J Geophys Res , 76, 44, 1971

Smith, E J , P J Coleman, D L Judge, and C P Sonett, Characteristics of the extraterrestrial current system Explorer VI and Pioneer V, J Geophys Res , 65, 1858, 1960

Smith, E J and L Davis, Magnetic measurements in the earth's magnetosphere and magnetosheath Mariner 5, J Geophys Res , 75, 1233, 1970.

Snyder, C W , M Neugebauer, and U R Rao, The solar wind velocity and its correlation with cosmic-ray variations and with solar and geomagnetic activity, J Geophys Res , 68, 6361, 1963

Sonett, C P and I J Abrams, The distant geomagnetic field 3, disorder and shocks in the magnetopause, J. Geophys Res , 68, 1233, 1963

Sonett, C P , D L Judge, J M. Kelso, and A R Sims, A radial rocket survey of the distant geomagnetic field, J Geophys Res , 65, 55, 1960

Sonnerup, B U and L J Cahill, Magnetopause structure and attitude from Explorer 12 observations, J. Geophys Res , 72, 171, 1967

Sonnerup, B U and L.J Cahill, Explorer 12 observations of the magnetopause current layer, J. Geophys Res , 73, 1757, 1968

Southwood, D J , The hydromagnetic stability of the magnetospheric boundary, Planetary Space Sci , 16, 587, 1968.

Spreiter, J R and A Y Alksne, Comparison of theoretical predictions of the flow and magnetic fields exterior to the magnetosphere with the observations of Pioneer 6, Planetary Space Sci., 16, 971, 1968

Spreiter, J.R and A Y Alksne, Effect of neutral sheet currents on the shape and magnetic field of the magnetosphere tail, Planetary Space Sci , 17, 233, 1969a

Spreiter, J R. and A Y Alksne, Plasma flow around the magnetosphere, Rev Geophys , 7, 11, 1969b.

Spreiter, J R. and W P Jones, On the effect of a weak interplanetary magnetic field on the interaction between the solar wind and the geomagnetic field, J Geophys Res , 68, 3555, 1963

Spreiter, J R., A L Summers, and A Y. Alksne, Hydromagnetic flow around the magnetosphere, Planetary Space Sci , 14, 223, 1966

Sugiura, M , T L Skillman, B G Ledley, and J.B Heppner, Propagation of the sudden commencement of July 8, 1966, to the magnetotail, J Geophys Res., 73, 6699, 1968

Talwar, S.P , Hydromagnetic stability of the magnetospheric boundary, J Geophys Res , 69, 2707, 1964.

Turner, J., An examination of magnetohydrodynamic discontinuities in the solar wind and an investigation of their origin, Ph D Thesis, M I T , 1971

Vasyliunas, V.M , A survey of low-energy electrons in the evening sector of the magnetosphere with OGO 1 and OGO 3, J. Geophys Res., 73, 2839, 1968a

Vasyliunas, V M , Low-energy electrons on the day side of the magnetosphere, J. Geophys Res., 73, 7519, 1968b

Vasyliunas, V M , Deep space plasma measurements, in Methods of Experimental Physics, Volume 9B (Plasma Physics), ed R H Lovberg, Academic Press, New York, 1971

Walters, G.K , Effect of oblique interplanetary magnetic field on shape and behavior of the magnetosphere, J Geophys Res , 69, 1769, 1964

Wolfe, J H and D.S. Intriligator, The solar wind interaction with the geomagnetic field, Space Sci Rev , 10, 511, 1970

Wolfe, J H. and D D McKibbin, Pioneer 6 observations of a steady-state magnetosheath, Planetary Space Sci , 16, 953, 1968

Wolfe, J H. and R W. Silva, Explorer 14 plasma probe observations during the October 7, 1962, geomagnetic disturbance, J Geophys Res , 70, 3575, 1965

Wolfe, J.H., R W Silva, D D McKibbin, and R H Mason, Preliminary observations of a geomagnetospheric wake at 1000 earth radii, J Geophys Res , 72, 4577, 1967

Wolfe, J H , R W Silva, and M A Myers, Observations of the solar wind during the flight of IMP-A, J Geophys. Res , 71, 1319, 1966

BIOGRAPHICAL NOTE

The author was born on [redacted] in [redacted] He graduated from Point Loma High School, San Diego, in June, 1962 He received his Bachelor of Science degree in Engineering Physics, with Academic Distinction, from the University of California, Berkeley in June, 1966 He is a member of Phi Beta Kappa and Tau Beta Pi

In September, 1966, he began studies leading to the Doctorate degree in physics at M.I T During the first four years of his studies at M I T , he was a National Science Foundation Fellow. He has published the following paper "Pioneer 6 plasma measurements in the magnetosheath", J. Geophys. Res , 75, 2429, 1970